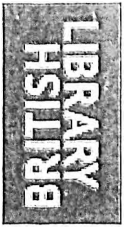THE ROLE OF NITROGEN IN THE

HOT WORKING OF NIOBIUM MICROALLOYED STEELS

by

Cesar Jose Janampa Ramos, B.Eng.,Dip.Met., M.Met.

To the Memory of my Father

SUMMARY

A detailed and critical survey of the Chemical and Physical
metallurgy principles of the hot working of niobium microalloyed
steels has been carried out emphasizing the role of nitrogen.

A series of steels of different nitrogen and niobium contents
were initially given a single pass rolling to study the recrystalliza-
tion kinetics. Subsequently two pass rolling schedules with a
roughing pass to recrystallize the austenite followed by a finishing
pass at a series of low temperatures were applied and slabs were
then held for different times before quenching.

The recrystallization kinetics after the second pass were
studied by quantitative metallography and precipitation kinetics were
followed by chemical analysis of electrolytically extracted pre-
cipitates. Accurate lattice parameters of the extracted carbonitrides
were determined by X-ray Diffraction to obtain their composition and
size. Those observations were complemented by limited Electron
Microscopy and free N analysis.

A thermodynamic model was developed to predict carbonitride
composition and solution temperatures. This is based on published
solubility data and involves the assumption of ideal solution in
the carbonitride, as information about the non-ideal characteristics
of the solution of niobium carbides and nitrides is not available.
Results obtained were compared with published observations on Re-
heating and with the present results on precipitation. Good agree-
ment was obtained with solution temperatures but it is clear that
the thermodynamic data is not comprehensive enough for the model to

predict closely the observed carbonitride composition which becomes N rich at high temperatures. The effect of Mn and Si were also considered and it was found that Mn had a greater effect than Si on the solution temperature.

On reheating all the experimental steels, grain coarsening occurred below the solution temperatures as a result of abnormal grain growth. The roughing pass at $1100^{o}C$ caused the recrystallization to produce austenite grain sizes of 50 - 70µm in all the steels and resulted in a significant fraction of carbonitride precipitation. After finishing, recrystallization was increasingly retarded with increasing N or Nb contents. In the former case this was attributed to the refinement of the precipitate size and in the latter case by the increase in volume fraction of precipitates.

Room temperature properties of air cooled slabs were found to be relatively poor as a result of the coarse (15µm) ferrite grain size after the two pass schedules.

C O N T E N T S

INTRODUCTION

Increased world needs for structural steels with high strength, toughness, formability, weldability and at competitive prices, led to the development of High Strength Low Alloy (H.S.L.A.) steels in the 1960's.

H.S.L.A. steels are basically low carbon-manganese steel containing microalloyed additions of Nb, V and Ti singly or in combinations up to 0.1% maximum. They are used as plates, bars, sheets and sections in the hot-rolled, cold-rolled and heat treated conditions by the construction, energy and transport industry.

The introduction of Controlled Rolling two decades ago has contributed enormously to the improved mechanical properties of these materials, particularly in the case of Nb microalloyed steels, where sound metallurgical principles were applied for its development. In spite of this, research programmes are being carried out to improve the understanding of the science and technology of these steels, to maximize their mechanical properties and to minimize their costs.

One of the areas in which information is rather poor concerns the role of nitrogen during the Controlled Rolling of Nb microalloyed steels. The presence of N in steel was first demonstrated in the late 19th century, when Allen (1879) determined, by wet chemical methods, contents of 0.005% to 0.015% N which are within the range for most air melted steels today. This variation in nitrogen content depends on the steelmaking route as was shown by the surveys carried out by

Speith and Von Ende (1959) and Kuhn and Detrez (1962). They concluded that the highest N contents are normally associated with processes where there is extensive contact between the molten metal and the atmosphere. The nitrogen content of steels made by the Bessemer and Electric Arc processes is about 0.006-0.010% compared with about 0.002-0.008% in the BOS or Open Hearth Steels.

Although the solubility of N in pure Fe at $1600^{o}C$ and 1 atm pressure is reported to be 0.045%, which could be increased or decreased by other elements in the steel, in practice the solubility is much less, Wright (1962). The explanation for this is a kinetic one since it is necessary for N_2 in the atmosphere to dissociate before it can be incorporated into the melt as N.

In certain grades of steel where the N content is deliberately increased (Cottrell, 1975), nitrogen additions are made using cracked ammonia, calcium cyanide , or manganese nitride, which overcome the kinetic problems associated with the dissociation of molecular nitrogen.

Nitrogen is well known to form a number of nitrides with Fe, Si, Mn and of course with Aℓ, Ti V and Nb. Before the use of Aℓ or Ti, V and Nb, the presence of N was considered to be very detrimental to the mechanical properties of the steel and in fact it was shown that the soluble or free nitrogen increases the strength but decreases the ductility and toughness. Low and Gensamer in 1944, have shown that the yield phenomena and the strain aging in low carbon steels are due to the segregation of free nitrogen and carbon to dislocations forming atmospheres of interstitials and anchoring the dislocations. This is not desirable in certain cold working operations, such as in deep-drawing, because of the appearance of surface markings or

"stretcher strains." The additions of Aℓ or Ti, V and Nb take part of the interstitials out of solution in the form of stable nitrides and carbides, which have a very important influence on grain size control and precipitation on the normalized and hot rolled condition. However in the case of Nb microalloyed steels it is not well known if the interactions between these particles and the microstructure; grain boundaries, subgrain boundaries or lattice defects, to give grain refinement and precipitation hardening, are due to the carbides or nitrides or carbonitrides of Nb and which are the mechanisms.

In this context this project aims to contribute to the understanding of the role of nitrogen during controlled rolling of Nb microalloyed steels.

The hot working principles of Nb microalloyed steels are given in Chapter 1, where the processing variables of controlled rolling are described as well as the new trends and types of products available. The chemical principles are discussed critically in Chapter 2 where the thermodynamic aspects have received special attention, and the basis for a thermodynamic model to calculate the solution temperatures of niobium carbonitride are established. The physical metallurgy of controlled rolling is given in Chapter 3, where the available data on recrystallization kinetics is carefully reviewed. Chapter 4 describes the experimental procedure while in Chapter 5 a thermodynamic model has been proposed and evaluated with other workers results. The experimental results of this project are given in Chapter 6.   The discussion of results, emphasizing the role N and the interaction with the microstructure have been given in Chapter 7. The Conclusions and Recommendations are given in Chapter 8. The computer programs used in this project are listed in the Appendix, as well as examples of calculations.

C H A P T E R   1

HOT WORKING OF NIOBIUM MICROALLOYED STEEL

1.1. Introduction

Controlled Rolling is a hot working operation through which the properties of a microalloyed steel are improved up to an equivalent or greater level than those of a more highly alloyed or heat treated steel. This is achieved by a careful control of the rolling process in order to refine the ferrite grains.

The advantage of grain refinement had been pointed out in the 1920's by Arrowsmith (1924) and Hanemann and Lucke (1925) but it was not until the experiences of World War II, when improvements in weldability and fracture resistance were needed, that refinement of the microstructure by Al-killing, normalizing and increments in the Mn/C ratio were adopted to meet these requirements.

In 1960 a hot-rolled high strength Nb bearing steel was pro- duced by Great Lake Steel in the U.S.A., for the first time, and to avoid deterioration in toughness, the application of Controlled Rolling to these steels started to be systematically studied by several organizations, BISRA in the U.K. being one of the most active.

Morrison and Woodhead (1963), Morrison (1963) and Webster and Woodhead (1964) confirmed the beneficial effects of small additions of Nb in the control of ferrite grain size and on precipitation hardening, giving improved mechanical properties in the heat treated condition.

In the hot rolled condition, Duckworth et al (1965) showed

that with a carbon content below 0.1% plus small niobium additions coupled with low finishing temperatures and heavy deformation, the yield strength could be increased to 550 MN/m^2 with a reasonable toughness. Phillips and Chapman (1966), Irani et al (1967) and Jones and Rothwell (1968) turned their attention to controlled rolling itself for the first time. They showed that Nb retarded recrystallization enabling the deformation of austenite to be carried out in a non-recrystallizing region, so that transformation from deformed austenite produced a fine ferrite grain structure and that an improper rolling schedule tended to cause a mixed grain structure. However, because their experiments were carried out in a laboratory bar mill and the only measure of controlled rolling was the finishing temperature, their results lacked overall agreement. Further research on the microstructural behaviour made it clear that Controlled Rolling did not need to cease in the γ region but could be extended into the $\gamma + \alpha$ field in order to enhance both strength and toughness, Little et al (1974) and Coleman et al (1974).

Now, modern Controlled Rolling can be established to consist of: (i) an appropriate selection of chemical composition, (ii) a proper slab-reheating temperature, (iii) γ-grain refinement by deformation in the recrystallization region, (iv) deformation of γ in the non-recrystallization region, (v) deformation in the $\gamma + \alpha$ two-phase region, and (vi) controlled cooling.

In this chapter, the processing of Niobium Microalloyed Steels will be outlined from the steelmaking to the finished product condition. Due to the variety of metallurgical reactions which occur during these stages they are bound to have effects on the evolution of the final microstructure and so on the final

mechanical properties.

1.2. Steelmaking

Today the majority of microalloyed steels are made using the BOS process, a minor tonnage by the Electric Arc Furnace route and still a minor tonnage using the Open-Hearth Furnace. The microalloying additions are made in the ladle before it is $\sim$ 1/3 full, to ensure homogeneity. One of the advantages of using Nb is that it enables semi-killed steels to be produced, Pickering and Gladman, (1963). But because of the soundness of internal quality and weldability, fully Al killed or Si deoxidised steels have become predominant.

The nitrogen level in this case will depend on their time of contact with the air, as mentioned before, as well as on the nitrogen content of the raw materials. Normally the N content in these steels varies from 0.004 to 0.007% for both routes being slightly higher for the steel made through the Electric Arc process. Higher levels of nitrogen in these steels $\sim$ 0.02% are obtained by additions of Mn-N alloys added also in the ladle.

On the other hand, techniques such as desulphurization of hot metal, vacuum degassing, ladle refining and inclusion shape control by REM or calcium, have made rapid progress largely improving the ductility of controlled rolled Nb steel and the resistance to hydrogen induced cracking, Nakai et al (1979).

1.3. Casting

Most microalloyed steels, either semi killed or killed are

ingot cast. The solidification microstructures have been inadequately studied, however, there are some indications that niobium acts like titanium, Wallace (1973), to refine columnar dendrite structures, Heikkinen and Packwood (1977) and to modify weld metal microstructures Bernard (1977), Jesseman (1977) and Kirkwood (1981). These inter-actions will depend on the temperature of casting. The higher the casting temperature the larger the columnar crystals and vice versa, the lower the casting temperature the smaller the columnar crystals or equiaxed grains will be formed at the core of the ingot, which then has good rolling properties.

The progress in the technology for continuous casting has widened the range of applicable steel grades. Niobium steels, including X - 70 grade for pipelines and other materials with plate thickness up to $\sim$ 50mm are now being manufactured by continuous casting.

1.4. Reheating

This is a very important variable in the hot working of microalloyed steels where the composition, temperature and time of reheating will determine the initial austenite grain size as well as fix the proportion of the microalloying additions available for precipitation.

For Nb microalloyed steels specifically there is a large amount of information dealing with the behaviour of austenite as a function of reheating temperature and composition. Among others Cordea (1970), McCutcheon (1974), Tanaka (1977b), Cuddy (1980) and Santella (1982) have shown agreement between their measurements. Representative results are given in Figs. 1.1.a 1.1.b. & 1.1.c. From these

figures it can be seen that for reheating temperatures of 1050-1300°C the variation of the austenite grain sizes are between 50 to 450μm depending on the composition and time of reheating. The higher the Nb content and the shorter the times of reheating, the smaller the prior austenite grain size. Incidentially, there are very few studies on the influence of time of reheating, most of the data given are for 1 hour reheating, which compared with practical situations is short. However, Miller (1951) and Gladman and Pickering (1967) indicated that the grain coarsening is a function of the holding time at temperature and the rate controlling factor is the thermally activated coalescence of precipitate particles, see Chapter 3, Section 3.2.6.

Also, according to Ohtani et al (1981) when rapid heating rates are used, such as occur in the induction treatment of plate or pipe and with the continuous annealing of sheets, the austenite grain sizes may be much finer, specially at short times and high temperatures, more than 1175°C.

The influence of N was not found by Gladman and Pickering (1967) to be clear but the tendency of their high N steels was to show higher grain coarsening temperatures than the steels with lower nitrogen.

Likewise, in industry beneficial effects have been demonstrated of a reduced austenitization temperature, ∿ 1150°C, improving the mechanical properties due to a smaller ferrite grain and shortening the process time, Hannukainen and Heikkinen (1974) and Heedman and Sjöstrom (1978).

But despite the proven benefits, there exists considerable opposition to the use of lower reheating temperatures in connection

with controlled rolling because not all the mills work fulltime
on controlled rolling but also have normal rolling which uses high
reheating temperatures $\sim 1250^{\circ}C$. Also, the reheating temperature
should exceed a minimum critical temperature otherwise the Nb $C_x N_y$
will remain undissolved and the beneficial effects coming from sub-
sequent precipitation will be lost.

1.5. Controlled Rolling

1.5.1. Introduction

The term Controlled Rolling refers to an optimized reheating
and hot rolling process of low-carbon austenite at low temperatures
in relation to those typical of conventional rolling. The aim is
to refine the ferrite/pearlite structures more than by normalizing
in order to improve the strength and toughness of the steel. However,
the above definition strictly applies only to rolling of plates or
large sections because the finishing temperatures in conventional
rolling for strip or small sections are very low as standard
practice.

Due to the relation between γ and α microstructures, refinement
of the α structure can be achieved partly through γ grain refinement
by repeated recrystallization, but this does not proceed indefinitely
and reaches a certain limit, Sekine and Maruyama (1973). For this
reason recrystallization of austenite must be avoided, once a
reasonably small grain size has been obtained. In commercial
practice this is achieved by using microalloying additions of
Nb, V or Ti on their own or in combination. Niobium has been shown
to be most effective suppressing the static recrystallization of γ
during finishing. This implies that subsequent rolling passes will

then be cumulative in continuing to flatten these grains to extremely small lateral dimensions prior to the eventual transformation. During this stage, deformation bands are also introduced in the elongated unrecrystallized austenite, from which ferrite/pearlite grains will nucleate as well as on γ grain boundaries, giving even finer room temperature microstructures.

From the viewpoint of austenite recrystallization and grain growth, controlled rolling can be divided into four stages as can be seen in Fig. 1.2 and which will be described next.

1.5.2. Stages of Controlled Rolling

Stage 1 - Comprises high temperature deformation usually about $1000^{o}C$ followed by austenite recrystallization in a matter of seconds. Subsequent grain growth, due to the lack of second phase particles, brings about coarse recrystallized austenite grains, which will transform to a relatively coarse ferrite and upper bainite structure.

Stage 2 - Covers the range 950 to $1000^{o}C$, where the austenite recrystallizes completely and minimal grain growth occurs. This could lead to a ferrite grain refinement as in case (a). Discontinuous coarsening after full recrystallization or partial recrystallization also may take place resulting in mixed structures as in cases (b) and (c) respectively. In these situations the γ grains will transform again into mixed structures of fine ferrite and bainite.

Stage 3 - Deformation at around $900^{o}C$, where the γ recrystallization is retarded for normal inter pass periods of 10-15 s. Therefore subsequent passes are cumulative in the sense that the austenite

grains become more and more"pancaked"in shape with the additional
introduction of deformation bands, Kozasu et al (1977). The trans-
formation into ferrite occurs by nucleation at grain interiors,
deformation bands, as well as at grain boundaries, therefore very
fine ferrite grains $\sim$ 5 - 10 μm are obtained.

Stage 4 - Involves rolling below Ar_3, that is deformation
of austenite-ferrite mixtures. In this case the α becomes strain
hardened and may develop a dislocation substructure as well as
texture, giving higher strength, via substructural strengthening,
but with poorer impact properties, Tanaka et al (1977a).

In general, the temperature ranges of these stages will vary
mainly with steel composition and in particular with the additions
of Nb, C and N.

1.5.3. Industrial Practice

Controlled Rolling in industry is seen as three operation
processes. Roughing, Hold Period and Finishing.

(i)   Roughing - This is carried out at $\sim$ 75 - 100°C below the
reheating temperature. The minimum reheating temperature conceivable,
at least for Nb steels, is 1100°C. Therefore this operation is carried
out above 1000°C, stage 1. The amount of predeformation depends on the
gauge of the final product since at least 50% reduction is usually
aimed for during finishing, irrespective of section size.

(ii)   Hold Period - This would correspond to stage 2 in the previous
description, where no rolling is carried out in order to minimize
bainite structures on transformation. This is between 950 to 1000°C.
The microstructural changes taking place during the hold period are
very important, since they determine the overall refinement of the

- 9 -

austenite microstructure which is achieved in controlled rolling.
In some mills the stock is transferred to another table to cool
down to ~ 900°C while the next ingot is roughed.

(iii)   Finishing - This does not usually start until the stock
temperature has fallen below 900°C. The finishing operation can
be carried out at temperatures of stages 3 and 4, where for normal
inter-pass periods of 10 to 15 seconds, recrystallization is completely
non-existent. One might expect that the accumulated driving force
from several passes should in the end be sufficient to initiate
static recrystallization, but the rapidly decreasing temperature
during finishing and the reduction in driving force due to inter-
pass recovery seem to effectively eliminate this.

(iv)   Cooling - The final properties of the hot-rolled products
are directly related to conditions of transformation from austenite
to ferrite and to the precipitation reactions taking place during
and after transformation. The usual medium for cooling is the air
but in order to increase the yield strength, especially for thick
plates, it is necessary to use water or choosing the right chemistry
such as more than 1.5% Mn or Mo, B in order to increase the rate of
nucleation of the ferrite in the γ grains by decreasing the trans-
formation temperature.

1.6. Post Rolling Treatments

Heat treatment may follow rolling and in such cases niobium
acts as grain refiner and toughener, De Ardo et al (1981). The
grain refining effects may be enhanced by proper control of the
prior rolling practice as described by Gondoh and Osuka (1981) and
Baumgardt et al (1981).

Recent more novel developments include simultaneous rolling and either intercritical or supercritical "normalizing" treatments, such as the Sumitomo High Toughness, SHT process described by Takechi et al(1977).

1.7. Properties and Applications

The different properties obtainable in microalloyed steels are given in Figure 1.3.

Reference should be made to Baumgardt et al (1981) for details of properties and applications of microalloyed steels. These authors summarize the properties and applications of these steels as: Structural Steels, Shipbuilding Steels, Cryogenic Steels and steels for elevated temperature, see Table 1.1.

CHAPTER 2

CHEMICAL METALLURGY

2.1. Introduction

In the design and manufacture of Nb microalloyed steels, a close control on the chemistry of the process is essential. Processing these steels involves energy changes and hence the study of thermodynamics is extremely valuable to understand. these processes. The rates at which these changes occur are very variable so that a knowledge of chemical kinetics is important to control the metallurgical reactions taking place.

Therefore in this Chapter, the interrelation and effects of alloying elements, the thermodynamics of Nb $C_x N_y$ formation and their precipitation kinetics will be considered.

2.2. Alloying Elements and the Periodic Table

Most of the elements found in a steel are located in blocks d and p.family of the transition metals in the Periodic Table, Table 2.1.

Perhaps one of the most important characteristics of the transition metals is their ability to fit small atoms such as H, B, C and N into the interstices of their lattices with classical examples of C and N in Fe, Nb, V and Ti forming carbides and nitrides. These are called interstitial compounds where the smaller atoms are deposited in the interstitial voids or holes

between the bigger atoms.

There are two types of voids in the b.c.c. structures, the larger ones being the tetrahedral holes, existing between two edge and two central atoms in the structure which together form a tetra-hedron. The octahedral holes, smaller type, occupy the centres of the faces and the $< 001 >$ edges of the body-centred cube with the surrounding atoms at the corners of a flattened octahedron. See Figs. 2.1.a and 2.1.b.

The f.c.c. structures although more closely packed, have larger holes than the b.c.c. structures and they are at the centres of the cube edges surrounded by six atoms in the form of an octagon, and so are referred to as octahedral holes. There are also smaller voids surrounded by a tetrahedron of four atoms and these are called tetrahedral holes. See Figs.2.2.a and 2.2.b. In Table 2.2. the size of the largest spheres fitting interstices in b.c.c. and f.c.c. structures is given.

A further feature of the transition elements is their tendency to form non-stoichiometric compounds. According to Lee (1979) this can be explained by considering their more common structural defects.

2.3. Base Steel Composition

In many cases the steel composition to which microalloying elements are added, corresponds to the BS4360, 968. This structural steel contains basically $\leq 0.2\%C$, $\leq 0.08\%N$, $\leq 1.60\%Mn$, $\leq 0.55\%Si$ or $\leq 0.025\%Al$, plus impurities such as sulphur and phosphorous which are kept below 0.02%.

These steels after conventional hot rolling have yield strengths of ~ 350 MN/m^2 and I.T.T. (27 Joules) of $-20^{\circ}C$. The

contribution of the given chemistry in these properties will be briefly outlined, in terms of their effects on solid solution, precipitation, grain size and transformation temperature.

A very small amount of carbon and nitrogen will go into solution interstitially in α - Fe, where they will occupy not the larger tetrahedral holes but the smaller octahedral ones producing great lattice distortion, as shown in Table 2.2. The effects of N will be reviewed with more detail in Section 2.3.2. On the other hand manganese, silicon and aluminium would form substitutional solid solution in accord with the Hume-Rothery Law (1944), where their difference in atomic radius from iron is less than 15%, see Table 2.2. But this will happen only if Mn, Si and Al are in excess after combining with S, 0; 0 and 0, N respectively.

Most of the C will exist as Fe_3C cementite, due to the low solubility of C in α $\sim$ 100 times less than in γ at $723^\circ C$, see Table 2.3. For the nitrogen level given, probably Al, Si or Fe will form very small amounts of nitrides.

The austenite grain size on reheating is controlled by Al N or Al_2O_3 particles up to $\sim 1050^\circ C$ by inhibiting grain growth. These relatively small austenite grains will subsequently produce smaller ferrite grains.

The transformation temperature, Ar_3 is decreased by carbon and manganese and increased by Si. On decreasing the Ar_3, the rate of α nucleation increases and so finer α grains are produced.

2.3.1. Microalloy Additions

The influence of Nb, V and Ti on the structural steels reviewed in the previous section is large, especially of Nb after

controlled rolling. These steels coded as BS4360, 1501, 968 have yield strengths of $\sim$ 550 MN/m^2 and ITT (27 Joules) of -20°C. The role of each element will be considered next.

2.3.1.1. <u>Niobium</u>

Among the elements contained in microalloyed steels Niobium has the greatest difference in atomic size in relation to the Fe, see Table 2.2. The order of size is Nb > Ti > Al > V > Si > Mn > Fe > C > N. According to this scale it is expected that Nb will generate the highest lattice distortion, when substituting Fe atoms in austenite, which would be an effective barrier to dislocations, sub and grain boundary movement.

Alternatively, Abrahamson and Blakeney (1960) have suggested that niobium has more powerful effects than vanadium on delaying the recrystallization of α - Fe, due to its electronic structure as shown in Figure 2.3. Consequently, the same could be indicated for γ - Fe because phase transformation does not affect electronic structures.

In addition, niobium is a strong carbide former and niobium carbide will be formed in preference to iron carbide. There is also more evidence that niobium will combine strongly with nitrogen and this is quite likely to occur because thermodynamically, as will be seen later, the enthalpy of formation of niobium nitride is more negative than niobium carbide at all temperatures.

These reasons indicate that the delayed recrystallization of γ at stage 3 during controlled rolling could be due to: electronic effects, lattice distortion and Nb $C_x N_y$ precipitation which would

hinder the migration of subgrain boundaries, delaying the nucleation and growth of new grains. This will be seen with more detail in Chapter 3.

2.3.1.2. Vanadium

Vanadium in proportion to its percentage, $\sim$ 0.15%, produces moderate precipitation strengthening and relatively weak grain refinement. Nitrogen enhances its effect. Precipitation strengthening with vanadium can be combined with niobium grain refinement for large strengthening effects. Compared with Nb or Ti the more rapid recrystallization of vanadium steels during hot working, results in a less textured product. Also V has greater solubility compared with Nb and Ti and after normalizing even heavy gauge plate, considerable precipitation strengthening can be obtained especially if sufficient N is also present.

2.3.1.3. Titanium

Titanium also gives strong precipitation strengthening but moderate grain refinement characteristics at $\sim$ 0.015%. At identical strength levels of Nb steels, the toughness of Ti steels is lower. A great advantage of Ti is in sulphide-shape control, through which uniform properties in the longitudinal transverse and thickness direction of cold formed Ti steels are achieved. Ti is also a very strong nitride former so that if the Ti/(C + N) ratio is sufficiently high, an interstitial-free steel results.

2.3.2. The Role of Nitrogen

As well as carbon, nitrogen is an interstitial element with

an atomic radius smaller than C, as can be seen in Table 2.2. Also
N atoms occupy the smaller octahedral interstices in α-iron because
it is more favourable to the release of strain.

The solubility of N in γ and α is much greater than
C as can be seen in Table 2.3 and Fig.2.4, but as in the case of C,
its solubility in α is smaller than its content. It is also reason-
able to assume, in the absence of other nitride forming elements, that
a great volume fraction of iron nitride can be obtained. In fact
this will happen in a two stage process, with a b.c. tetragonal α''
phase, $Fe_{16}N_2$, as the intermediate precipitate, forming as discs
on $\{100\}_\alpha$ matrix planes both homogeneously and on dislocations.
Above about 200^0C this transitional nitride is replaced by the
ordered f.c.c. γ', Fe_4N, which forms as platelets with $\{112\}_\gamma,//\{210\}_\alpha$.
This is one of the few phase changes which have been observed in steels
at such a low temperature and has a great significance in the hardening
and embrittling effects. Related with this, the strain ageing
phenomena is believed to be due to the interstitial nitrogen mainly
because of the greater solubility of N, than C in Fe.

Again, as for C, as N is increased the yield strength of the
steel increases but the toughness decreases. In the presence of other
strong nitride elements, N can be added up to 0.02% to improve the
toughness and cold working properties. Also N is an austenite
stabilizer and the γ-phase field is expanded over wider compositional
limits but its range is cut short by compound formation. This
expansion underlines the whole of the heat treatment of steels by
allowing formation of a homogeneous solid solution austenite con-
taining up to 2wt%C or 2wt%N. The solid solution strengthening
obtained by C and N are the highest obtainable. N is more useful

in this respect as it has less tendency to cause intergranular cracking
as has been shown in stainless steels where concentrations up to
0.25% are used and give double the proof stress of a Cr-Ni austenitic
steel, Honeycombe (1981).

In commercial low carbon steels, nitrogen is usually
combined with aluminium, or present in too low a concentration
$\sim$ 0.006% to be the reason for embrittlement or low toughness.
However, added in the right proportions in V and Ti microalloyed
steels, it has been proved to be of great benefit, due to their
more stable and less soluble nitrides, in controlling grain growth
during reheating and in giving greater precipitation hardening on
transformation, Honeycombe (1981), Woodhead (1980) and Leduc (1980).

2.4.   Compound Formation
2.4.1.   Introduction

Among transition metals the formation of oxides, sulphides,
carbides and nitrides is fairly common. In the first transition
series every element forms at least one carbide and nitride, in
the second and third transition series, carbide and nitride
formation is restricted mainly to elements from groups three to
seven, Goldschmidt (1967). Niobium in particular shows a strong
tendency to form carbides and nitrides but relatively little tendency
to form oxides, sulphides or solid solutions of these compounds. In
this regard it behaves similarly to vanadium but differently from
titanium which does not form carbides until all oxygen, nitrogen

and sulphur have been formed by initial additions of Ti, Meyer
et al (1977).

In general from all compounds formed between transition
metal atoms and light elements such as H, B, C, N and O, only
carbides and nitrides are closely related in crystal structure
types, phase relationships, bonding characteristics, electric
and magnetic properties. This can be understood considering the
similarities of electron structures, size and electronegativity
of nitrogen and carbon atoms. However the basic difference between
C and N is the additional electron of N which is reflected in their
transition metal compounds. Because of this additional electron,
the general properties of the fifth-group nitrides are often more
similar to those of the sixth-group carbides than to the fifth-
group carbides.

On the other hand, it is now well known that carbides
and nitrides are not stoichiometric phases mainly caused by anion
vacancy or metal excess. The composition range for each binary
phase is extensive and all its properties depend on the non metal-
to-metal ratio and the vacancy concentration, which could be present
up to 50 at % on the non-metal lattice sites and to lesser concentra-
tions on metal-atom lattice sites. In certain cases, even at
stoichiometric ratios, appreciable vacancy concentrations can exist
on both sub-lattices.

In this section only the most relevant compounds formed
during the processing of niobium microalloyed steels will be reviewed.

2.4.2. The Fe-Nb System

Nb and Fe are completely miscible in the liquid. The equilibrium diagram for this system is well established, see Fig. 2.5 The important feature of this diagram is the existence of a γ loop which limits the existence of this phase to alloys containing less than 0.83% niobium (0.50 at %). Niobium is an α stabilizer but additions of up to 0.10 and 0.20% lower the A_3 temperature. This means that the γ loop displays a minimum similar to that observed in the Fe-Cr and Fe-V systems and so small Nb additions will act as a γ stabilizer. This means that the transformation temperature will be decreased and so the hardenability will be increased as has been reported by De Ardo et al (1981). However, Shams (1982) suggests that Nb increases the hardenability by delaying the kinetics of transformation resulting in lower transformation temperature especially at faster cooling rates.

Maximum hardenability is achieved if high reheating temperature and very low C contents are used. The technological implications will be seen in Chapter 3 when considering the γ/α relationships.

2.4.3. The Nb-C System

This system has been studied extensively in the last 30 years, Storms and Krikorian (1960). The most recent and reliable diagram was given by Storms et al (1969) and is shown in Fig. 2.6.

The features of this phase diagram, at the lowest temperature indicated, $1500^{o}C$, are retained to lower temperatures of interest for the general precipitation reactions in steels.

There are three solid solution, single phase regions α, β, γ, which are summarized is Table 2.4.

The γ phase is the only phase found in microalloyed steels. However, an Nb_2C phase was also detected in steels having high Nb/C ratios, Schaab and Langerscheid (1972).

At room temperature the range of homogeneity of the γ phase has been shown to be from 0.70 to 0.98, Storms (1969), and owing to its strong covalent nature assures no change to this composition range for temperatures up to $1700^{o}C$. This range of possible carbon contents has led to the adoption of the symbol NbC_x to describe the γ phase, with x being equal to the mole ratio of C to Nb.

In the pure Nb-C system the carbide $NbC_{0.98}$ has been found in equilibrium with graphite. This suggests that the carbides precipitated in a low carbon steel are bound to be even more defective.

Alternatively, the lattice parameter of NbC_x has been shown by Storms and Krikorian (1960) to be a strong function of x, as represented in Figure 2.7. Pure stoichiometric NbC has a lattice parameter of $4.470\overset{o}{A}$ and the lattice parameter decreases with decreasing x up to $4.43\overset{o}{A}$ at $NbC_{0.7}$. This clearly suggests that the vacancy concentration in the γ phase has also a very strong

influence on the lattice parameter.

2.4.4. The Nb-N System

This system is very complex and experimentally it has been found to be difficult to establish the relationships accurately, Toth (1971). The crystal structures reported in the latest review made by Politis and Rejman (1978) showed the characteristics given in Fig. 2.8. and detailed in Table 2.5.

The wide variety of crystal structures exhibited in the composition range of 40-50 atomic % of nitrogen suggests a possible complexity of the phases when precipitated in steels. With the compositions present in microalloy steels, only some phases will precipitate. These will depend on the thermomechanical conditions, but mainly on their N/Nb and N/C ratios. So far only in steels with N/C > 1 were the pure nitrides δ^1 and ε phases found with compositions very close to stoichiometry, mainly as δ^1 - $NbN_{0.95}$ and ε - $NbN_{0.92 - 1.0}$, Goldshteyn et al (1973) and Mori et al (1964b).

2.4.5. The Nb-C-N System

The niobium carbides and nitrides are so similar structurally that large intersolubilities prevail, almost as extensively as between their carbide/carbide and nitride/nitride pairs. Extensive studies were carried out by Duwez and Odell (1950), Brauer and Lesser (1959) and Bittner et al (1963). They have measured accurate lattice parameters for a variety of NbC_xN_y compositions.

The difference between those studies is that Duwez and Odell did not take into account the amount of vacancies to obtain their

intersolubility diagrams, Fig. 2.9.   As a result their data shows
slight positive deviation from linearity.   In fact the NbC and NbN
system is a ternary system of NbC, NbN and Vacancies.   Brauer and
Lesser (1959) have studied the Nb-C-N system most extensively and in
particular, have estimated the wide ranges of stability of the cubic
carbonitride phase.   In Fig. 2.10 is shown a line drawing of a model
constructed by plotting their data as the ratios C/Nb, N/Nb and
Vacancies/Nb on a ternary axis and the lattice parameter on the
vertical axis.   In this figure it can be observed that the composition
of niobium carbonitride can be represented by NbC_xN_y where x = mole
ratio of C/Nb, y = mole ratio of N/Nb and 1 - (x + y) = mole ratio
of vacancies.   From this Figure also, it can be deduced that the lattice
parameters of the carbonitride will be strongly influenced by both the
nitrogen and vacancy concentrations, reducing the lattice parameter
of pure NbC.   Fig. 2.11 is another useful representation of the data
of Brauer and Lesser (1959).

However Storms and Krikorian (1960) point out that the inter-
pretation of lattice parameter measurements will be difficult unless
the vacancy concentration in the carbonitride can be assessed.

In practical terms the compositions of the $Nb\ C_x\ N_y$ found in
microalloyed steels have also been studied in detail by several
workers.   All of them have shown a direct relationship between the
composition of the carbonitride and the composition of the steel,
specifically the N/C ratio, Fig. 2.12.   The larger this ratio the
more nitrogen rich was the $Nb\ C_x\ N_y$, Meyer et al (1977), Aronsson and
Jonsson-Holmquist (1970).

Mori et al (1965) and subsequent workers   have also shown
that the composition of the carbonitride in any given steel can depend

upon the thermal conditions under which they form. Imai and Masumoto (1961) and Santella (1981) have found that the Nb $C_x N_y$ contained more N if it formed at higher temperatures. De Ardo et al (1981) show unpublished results of Hoesch-Estel, Figure 2.13 which shows this and are similar to results for precipitation of vanadium carbonitride, Brown et al (1976) and Roberts et al (1981).

As mentioned in 2.4.1., the presence of other elements such as Ti, Al, V, which are strong nitride formers, will affect the Nb $C_x N_y$ composition, Ouchi et al (1981), as is shown in Fig. 2.14 especially for steels reheated at high temperatures.

2.5. Thermodynamics

2.5.1. Direct Solubility Product Determinations

As far as Nb C_x, Nb N_y and Nb $C_x N_y$ are concerned, there have been several determinations of their solubility products, K', in steels. The experimental procedures to obtain these equations were one of the following:

a) Extraction and chemical analysis of the precipitates from steel specimens after the desired thermal or thermomechanical treatment.

b) Equilibrium of Fe-Nb alloys in CH_4/H_2 and N_2/Ar gas mixtures at fixed carbon and nitrogen potentials and examination of the phase fields through metallography and X-ray analysis.

c) Hardness measurements on quenched and tempered steels and analysis of the data using precipitation hardening model to estimate solubility limits, and

d) Theoretical calculations using thermochemical data.

2.5.1.1. Solubility of Niobium Carbide in Austenite

There have been a number of experiments in the Fe-Nb-C system to determine the solubility of niobium carbide. All of them have been analysed on the basis of a solubility product defined as:

$$\log [\% \text{ Nb}] \ [\% \text{ C}]^X = A - \frac{B}{T} \qquad \cdots\cdots(2.1)$$

Where A, B and x have been determined experimentally or through thermo-dynamic analysis.

The carbide equilibrium in austenite is strictly repre-sented by:

$$[\text{Nb}] + x \ [\text{C}] \ \underset{\leftarrow}{\overset{\rightarrow}{}} \ \text{Nb C}_X \ (s) \qquad \cdots\cdots(2.2)$$
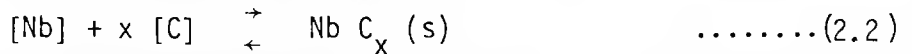
Where [ ] means: The component is in solution in austenite, the concentration of the component is in atom fraction and,

The standard state referred to is at infinite dilution in austenite.

In addition, the equilibrium constant for the carbide dissolution is given by:

$$K_c' = a_{\text{Nb}} \ a_C^x / a_{\text{NbC}_X} \qquad \cdots\cdots(2.3)$$

$$= \gamma_{\text{Nb}} \ \gamma_C^x \ [\text{Nb}] \ [\text{C}]^X \qquad \cdots\cdots(2.4)$$

Where: a = Raoultian activity, a_{NbC_X} assumed to be equal to unity

γ = Activity coefficients referred to the infinite dilution standard state.

There is considerable disagreement as to the exact value
of x to select, as an average representation of the carbide compo-
sition in a given temperature range of investigation. Earlier results
were put forward assuming perfect stoichiometry, x = 1, and an ideal
solution of the components in austenite, γ = 1. The stoichiometric
composition has never been shown conclusively due to the lack of
analysis of vacancies, nitrogen and oxygen.

However, as described in 2.4.2., in the austenite of low
carbon steels, the carbon activity is much less than that in carbon
rich niobium carbide, where the carbon activity equals that of
graphite. For these reasons and for the ones described in 2.4.3.,
the niobium carbide precipitated from low carbon austenite is bound
to be less than the stoichiometric value.

The solubility equations so far available are given in
Table 2.6. They are also plotted in Fig. 2.15 where the large scatter
of these results can be observed. Between the methods used to find
those equations, the equilibrium technique with appropriate gas
mixtures of H_2 - CH_4 is supposed to have the highest accuracy com-
pared with the other methods. However, the results of Smith (1962
and 1966), Johansen (1967) and Koyama et al (1971a and 1971b) show
a considerable disagreement. Nordberg and Aronsson (1968) have
discussed the above results in terms of the materials used which
contained high nitrogen levels, besides systematic errors. In
contrast, the results of Lakshmanan (1977) and Koyama et al (1971)
agree reasonably well.

In the method of isolation of precipitates, the results of
Mori et al (1968a) are the most comprehensive among the carbide
solubility data. Their solubility determinations agree well with
the results of Lakshmanan (1977) and Meyer (1966). However they
tend to be lower which could support their own conclusions that their

precipitates may have had small amounts of dissolved nitrogen. The
measurements of Nilsson   (1968), Reistad and Stchlstedt (1967)
and Wilson and Geiselman (1962) are less comprehensive and of limited
accuracy as admitted by the respective authors.

The hardness method, used by De Kazinczy et al (1963) to
obtain the solubility equation was recalculated and reinterpreted
by Nordberg and Aronsson, (1968). This was based on the fact that
the hardness of niobium containing steels increases linearly with l^{-1},
by an Orowan type mechanism, 'l' being the average distance between
particles of niobium carbide precipitated in ferrite. This corrected
the assumption of the de Kazinczy et al (1963), that the mechanism
was of the Mott-Nabarro type. Although solubility values obtained
through hardness measurements involve large uncertainties, they show
surprisingly good agreement with theory and the other determinations.

As far as the theoretical equations are concerned, the equations
obtained by Brown and Nordberg and Aronsson do not agree at all. The
differences in the thermochemical data values are not as large as their
final equations. The explanation for this great discrepancy, pointed
out by Lakshmanan (1977), is in Nordberg and Aronsson's incorrect
estimation for the free energy of solution of niobium in austenite
which makes their equation completely different from the trends, see
Fig. 2.15.

Nordberg and Aronsson (1968) reviewed some of the data of
Table 2.6 and found that the experimental solubility products agreed,
if the carbide was assumed to be $NbC_{0.87}$. The author agrees with
this and it is considered that the results of Mori et al are the most
reliable and representative equation of this group. The equations
of Lakshmanan and Koyama although agreeing with the results of Mori,
were obtained from pure samples which may not reflect their behaviour

when other impurities are present such as in a commercial steel. Later on in a specific section, the effects of alloying elements will be dealt with.

2.5.1.2. Solubility of Niobium Nitride in Austenite

Mori et al (1964 and 1968), Smith, R. P. (1962) and Narita and Koyama (1966), have made extensive studies to identify compounds in the Fe-Nb-N system. Their results are summarized in Table 2.7. which shows two facts. The compound precipitated in the pure Fe-Nb-N system is always of the hexagonal type ϵ or δ'. As far as their structure is concerned the ϵ phase is a pure stoichiometric NbN while the δ' phase has been found to be a carbonitride with substantial amounts of nitrogen.

The stoichiometric NbN-ϵ was found only in steels with an extremely low C content where the ratio N/C was greater than 1. This situation has never been reached in commercial low carbon steels.

Data from Hoogendoorn and Spanraft (1977) on solubility of their precipitates found an agreement with the solubility equations of Smith (1962) and Mori et al (1968), but their lattice parameter obtained of 4.46 $\overset{o}{A}$ does not indicate the precipitate to be pure niobium nitride, as will be seen later.

In Table 2.7 the solubility equations for niobium nitride in austenite, so far available, are given. They are also plotted in Figure 2.15.

From these data it is possible to conclude that pure stoichiometric NbN is not present in low carbon commercial steels at least in the experimental conditions of the above data. Also, they are much more stable than the NbC_x.

2.5.1.3. Solubility of Niobium Carbonitride in Austenite

As discussed in 2.4.5., most of the results show that the precipitates formed in equilibrium with austenite, may contain appreciable proportions of nitrogen. Mandry and Dornelas (1966) from measurements of the lattice parameter of electrolytically extracted precipitates concluded that their precipitate had a composition in the range $NbC_{0.87}$ - $NbC\ N_{0.83\ 0.14}$. Tests on strain-ageing behaviour indicated that the concentration of nitrogen in solid solution decreased during precipitation and therefore the later formula was considered to correspond more closely to the composition of their precipitates. Meyer (1966, 1967) on the other hand obtained precipitates corresponding to $Nb\ C_{0.9}\ N_{0.1}$ and $NbC_{0.65}\ N_{0.35}$, which correspond to an stoichiometric carbonitride. Mori et al (1964, 1965, 1968) who carried out the most detailed solubility determinations and precipitate identifications, obtained, like Mandry and Dornelas (1966), precipitates that contained slightly less than the stoichiometric proportion of carbon plus nitrogen, for example $NbC_{0.88}\ N_{0.08}$.

Analysis of the results of Mori et al, indicates that the degree of non-stoichiometry is greater at higher temperatures and the proportion of nitrogen in the precipitate is increased at higher temperatures. At very low N/C mole ratios in the steels, a carbonitride of fixed composition was observed.

Irvine, Pickering and Gladman (1967) determined the solubility relationship for a number of laboratory melted steels, using chemical analysis techniques for soluble and insoluble niobium, carbon and nitrogen. They considered the nitrogen content in terms of an equivalent carbon content, i.e. equal to (C + 12/14 N) because they did not find a marked tendency for niobium to form a separate

nitride phase. Besides, as described in 2.4.5. niobium carbide and niobium nitride are mutually soluble.

The solubility product equations for niobium carbonitride are given in Table 2.8 and Fig.2.16. From these results the formula NbC_xN_y with $x + y < 1$ seems to be the most approximate to real situations. There are available two more solubility equations for the niobium carbonitride, derived theoretically by Nordberg and Aronsson (1968) and Hudd et al (1971). Because of their importance in further thermodynamic calculations they will be considered in the next section.

2.5.2. Theoretical Calculations in the Fe-Nb-C-N System
2.5.2.1. Solubility of Nb $C_x N_y$ in Austenite

Nordberg and Aronsson (1968) and Hudd et al (1971) attempted calculations of carbonitride solubilities considering the following reaction:

$$[Nb] + x [C] + (1 - x) [N] \rightleftarrows Nb\, C_x\, N_{1-x} \qquad \dots\dots(2.5)$$
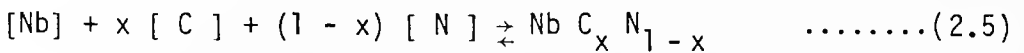
where the solubility product for this reaction is given by:

$$K'_{CN} = \frac{[Nb]\,[C]^x\,[N]^{(1-x)}}{Nb\,C_x\,N_{(1-x)}} \qquad \dots\dots(2.6)$$

Both treatments involved the following simplifying assumptions:

(i)   The precipitated carbonitride is stoichiometric and is of the composition $Nb\,C_x\,N_{1-x}$

(ii)   The carbonitride is a solution of the carbide NbC and the nitride ε - NbN and is made up of x moles of NbC and (1 - x) moles of NbN.

(iii)   The above solution is ideal and the effective activities

of the carbide and the nitride in the carbonitride are

equal to their respective concentrations and

(iv)   In addition to the free energies of formation of the

carbide and the nitride given by their respective

solubility products, only the entropy of mixing of the

two compounds needs to be taken into account.

Although Hudd et al (1971) pointed out dimensional inaccuracies

in the Nordberg and Aronsson equation, both followed the same principles

and claimed to have been in agreement with the results of Mandry and

Dornelas (1966), Meyer (1967) and Mori et al (1964).   Hudd et al's

equation, which is similar to Nordberg and Aronsson (1968), is given

by:

$$\log K'_{CN} = x \log K'_{C} + (1 - x) \log K'_{N} - \Delta S \qquad \ldots\ldots\ldots(2.7)$$

where: K'_{CN}, K'_{C} and K'_{N} = solubility products of $Nb\ C_x\ N_{(1-x)}$

NbC and NbN respectively.

x = atom fraction of carbon in the pre-

cipitatees at temperature T.

ΔS = entropy of mixing

= $- \{x \log x + (1 - x) \log (1 - x)\}$

However, both equations have a limitation, which arises from the

assumption that all precipitates are stoichiometric.

Lakshmanan (1977) analyzing most of the results given in Table 2.6

agreed with the initial assumption of Nordberg and Aronsson (1968), to

consider the most appropriate average carbide composition as $NbC_{0.87}$,

over the temperature range 1000-1250°C.   Also, referring to the

NbN phase diagram, Fig. 2.8 & Section 2.4.4., the δ-NbN$_x$ phase in the high temperature stable range, has the same crystal structure as the δ-NbC$_x$ phase and a lattice parameter, in this stable range, close to that of NbC$_{0.87}$. On this basis, two important conclusions were established:

(i)   The niobium carbonitride precipitated in steels is a defect compound of approximately fixed non-stoichiometry and its average composition could therefore be written as Nb C$_x$ N$_{0.87-x}$.

(ii)   The carbonitride is an ideal mixture of the non-stoichiometric metastable nitride δ - NbN$_{0.87}$ so that the activities of the carbide and the nitride in the carbonitride could be set equal to their concentrations x/0.87 and (0.87 - x)/0.87 respectively.

From these conclusions, equation (2.7) becomes:

$$\ell n \, K'_{C,N} = \frac{x}{0.87} \ \ell n \, K'_C + \frac{0.87 - x}{0.87} \ \ell n \, K'_N - \Delta S_m \qquad \ldots\ldots\ldots(2.8)$$

where: K'_{CN}, K'_C, K'_N are the solubility products of Nb C$_x$ N$_{(0.87 - x)}$, NbC$_{0.87}$ and NbN$_{0.87}$ respectively.

ΔS_m is the entropy of mixing of the carbide and nitride and is given by:

$$\Delta S_m = - \{ \frac{x}{0.87} \ \ell n \ \frac{x}{0.87} + \frac{(0.87 - x)}{0.87} \ \ell n \ \frac{0.87 - x}{0.87} \}$$

$$\ldots\ldots\ldots(2.9)$$

There are several determinations for the solubility product of NbC$_{0.87}$ but only one for NbN$_{0.87}$ which was obtained by Lakshmanan (1977) using the results of direct determinations, Mori et al (1965), for Nb (C,N)$_{0.87}$ along with his experimental results for NbC$_{0.87}$.

These estimated values of K'_N are given in Table 2.9.

2.5.2.2. Composition of Nb $C_x N_y$ in Austenite

Hudd et al (1971) attempted the calculation of the stoichio-metric Nb $C_x N_{1-x}$ composition, which led to a reasonable agreement with the results by then available. Lakshmanan (1977) assuming the fixed non-stoichiometric Nb $C_x N_{0.87-x}$ in equilibrium with austenite in the Fe-Nb-C-N system, Fig. 2.17 and applying the lever rule, put forward the following equations:

$$\frac{C_T - [C]}{Nb_T - \dfrac{x}{0.87}[Nb]} = \frac{\dfrac{x}{1.87} - C_T}{x/0.87 - Nb_T}{1.87} \qquad \ldots\ldots\ldots(2.10)$$

and

$$\frac{N_T - [N]}{Nb_T - \dfrac{(0.87-x)}{0.87}[Nb]} = \frac{\dfrac{(0.87-x)}{1.87} - N_T}{(0.87-x)/0.87 - Nb_T}{1.87} \qquad \ldots\ldots\ldots(2.11)$$

where: Nb_T, N_T, C_T = Total content of Nb, N, C in mol fractions.

[Nb], [N], [C] = Amount of soluble Nb, N, C in austenite in mol fractions

x = atom fraction of C in the precipitate

On the other hand, through the ideality assumption, the solubility products for the reactions representing the formation of $NbC_{0.87}$ and $NbN_{0.87}$ in the Fe-Nb-N-C system can be written as:

$$K'_C = \frac{[Nb][C]^{0.87}}{x/0.87} \qquad \ldots\ldots\ldots(2.12)$$

$$K'_N = \frac{[Nb][N]^{0.87}}{(0.87-x)/0.87} \qquad \ldots\ldots\ldots(2.13)$$

With these four equations (2.10) to (2.13) the four unknowns x, [C] [N] and [Nb] should be solved. However, the proportion of phases obtained with the lever rule in a quaternary system, appear not to change linearly with composition and equations (2.10) and (2.11) could not be valid. In Chapter 5 alternative equations are given.

2.5.2.3. Free Energy of Nb $C_x N_y$ Formations

The free energy of formation of Nb $C_x N_{0.87-x}$, assuming ideal solution, can be expressed as:

$$\Delta G_T^O = RT \left\{ \frac{x}{0.87} \ln K'_C + \frac{(0.87 - x)}{0.87} \ln K'_N - \Delta S_m \right\}$$

........(2.14)

where: K'_C, K'_N = Solubility products for the formation of

$NbC_{0.87}$ and $NbN_{0.87}$ respectively.

ΔS_m = The entropy of mixing given in equation (2.9)

2.5.3. Interactions of Alloying Elements with Niobium, Carbon and Nitrogen

The effects of alloying elements on the niobium carbonitride in equilibrium with austenite can be evaluated through the Wagner thermo-dynamic interaction parameters. This is expressed as $\varepsilon^M_{Nb,C,N}$.

Considering the reactions for the formation of Nb C_x and Nb N_y in a multi-component austenite:

$$[Nb] + x [C] \overset{K_C}{\underset{}{\rightleftharpoons}} Nb C_x \qquad \qquad ....(2.15)$$

$$[Nb] + y [N] \overset{K_N}{\underset{}{\rightleftharpoons}} Nb N_y \qquad \qquad ....(2.16)$$

The respective equilibrium constants will be given by:

$$K_C = \frac{a_{NbC_x}}{a_{Nb} \cdot a_C^x} \qquad \ldots\ldots\ldots (2.17)$$

$$K_N = \frac{a_{NbN_y}}{a_{Nb} \cdot a_N^y} \qquad \ldots\ldots\ldots (2.18)$$

The Henrian activities, considering the standard state at infinite dilution, are given by the Wagner formalism as:

$$\ln a_{Nb} = \ln X_{Nb}^\gamma + \sum_{i=1}^n \epsilon_{Nb}^M \cdot X_{Mi}^\gamma \qquad \ldots\ldots\ldots (2.19)$$

$$\ln a_C = \ln X_C^\gamma + \sum_{i=1}^n \epsilon_C^M \cdot X_{Mi}^\gamma \qquad \ldots\ldots\ldots (2.20)$$

$$\ln a_N = \ln X_N^\gamma + \sum_{i=1}^n \epsilon_N^M \cdot X_{Mi}^\gamma \qquad \ldots\ldots\ldots (2.21)$$

The solubility products $K_C^1 = 1/K_C$ and $K_N^1 = 1/K_N$ for the carbide and nitride reactions are therefore given by:

$$\ln K_C' = \ln [Nb][C]^X + \sum_{i=1}^n (\epsilon_{Nb}^{Mi} + \epsilon_C^{Mi})[Mi] \qquad \ldots\ldots\ldots (2.22)$$

$$\ln K_N' = \ln [Nb][N]^X + \sum_{i=1}^n (\epsilon_{Nb}^{Mi} + \epsilon_N^{Mi})[Mi] \qquad \ldots\ldots\ldots (2.23)$$

Experimental work, has been carried out by Koyama et al (1971a) and (1971b), where the effects of Mn, Si, Cr and Ni on the solubilities of NbC_x and NbN_y have been considered. Their results are given in Table 2.10.

The interaction coefficients ε_C^M and ε_N^M have recently been measured by a number of investigators and are summarized in Table 2.11

Using the solubility equations of Koyama and the interaction coefficients ε_C^M and ε_N^M, Lakshmanan (1977) evaluated independently the interaction coefficients for Nb, ε_{Nb}^{Mi} through equations (2.22 - 2.23) and his values are given in Table 2.12.

Therefore the carbonitride equilibrium in a multicomponent austenite can be predicted by substituting the activities defined by equations, (2.19 - 2.21) for the concentrations [Nb] [C] and [N] in equations (2.12 - 2.13) and proceeding as for the quaternary Fe-Nb-C-N.

This calculation has also been carried out and the results shown in Chapter 5.

2.6. Precipitation of $Nb\,C_x\,N_y$

2.6.1. Introduction

The formation of precipitates can be divided into three stages: (i) the formation of the nuclei; (ii) the growth of this nuclei; and (iii) the coarsening of the precipitate without change in its volume fraction.

Stage (i) happens in two basic ways. It can form at internal lattice defects such as: dislocations, stacking faults, incoherent twin boundaries, subgrain boundaries, interphase boundaries, grain boundaries and impurity particles. This is known as heterogeneous nucleation, where the formation of the precipitates are made easier by lattice defects. The second way of nucleation is the spontaneous formation of nuclei through composition fluctuations of the solute. This occurs in the matrix with considerable difficulty, Reed Hill (1964).

Stage (ii) reduces the supersaturation and so decreases the nucleation rate. The possible limiting factors considered are the rate at which atoms are brought to or removed from the interface by diffusion, and the rate at which they cross the interface.

Stage (iii) also known as Ostwald ripening process by which the larger particles grow at the expense of the smaller ones, with the growth kinetics controlled by diffusion.

In the next sections the formation stages of $Nb\ C_x\ N_y$, the rate controlling factors, the kinetics of precipitation, their crystallography, distribution and morphologies will be reviewed.

2.6.2. Nucleation of $Nb\ C_x\ N_y$

During controlled rolling of Nb microalloyed steels the nucleation of $Nb\ C_x\ N_y$ is likely to happen mainly through hetero-geneous nucleation on the lattice defects.

On the other hand the homogeneous formation of a particle is accompanied by a free energy change which can be expressed as:

$$\Delta G = -\Delta G_V + \Delta G_S + \Delta G_\epsilon \qquad \ldots\ldots\ldots(2.24)$$

where: ΔG_V = free energy associated with the formation of the volume of $Nb\ C_x\ N_y$

ΔG_S = precipitate - matrix interface energy

ΔG_ϵ = strain energy arising from the formation of the particle.

For a spherical embryo of radius r, eq. (2.24) becomes:

$$\Delta G = \frac{4}{3}\ \pi\ r^3\ (\Delta G_V + \Delta G_\epsilon) + 4\ \pi\ r^2\ \Delta G_S \qquad \ldots\ldots\ldots(2.25)$$

The condition for existence of the embryo is that the critical radius r^* should be given by:

$$r^* = \frac{2\ \Delta G_S}{-\ (\Delta G_V + \Delta G_\varepsilon)} \qquad\qquad \dots\dots\dots(2.26)$$

and so the critical energy of formation ΔG^* is expressed as:

$$\Delta G^* = \frac{16\ \pi\ \Delta G_S^{\,3}}{3\ (\Delta G_V + \Delta G_\varepsilon)^2} \qquad\qquad \dots\dots\dots(2.27)$$

The rate of nucleation $\overset{o}{N}_V$ is proportional to exp $(-\ \Delta G^*/KT)$, where K is the Boltzmann constant, T the absolute temperature.

The rate of heterogeneous nucleation is also proportional to exp $(-\ \Delta G^*/KT)$ but the magnitude of ΔG^* is lower due to the reduction in ΔG_S and ΔG_ε in eq. (2.25) caused by the interaction of the defects and the critical nucleus.

The crystal structures of the matrix and the precipitate must also be considered, because quite different structures and hence energies of the interface ΔG_S will arise from this factor. There are three cases: (i) coherent nucleation will occur if the crystal structures and lattice parameters of both phases are very similar; (ii) semicoherent nucleation will happen if the precipitate and matrix are related in such a way that an interface can be built from well-defined defects; and (iii) noncoherent nucleation will occur if both structures are so different that the interface has a structure similar to that of a high-angle grain boundary.

2.6.2.1. Nucleation on Grain Boundaries

These are effective in increasing $\dot{N}$, the rate of nucleation, since part of the boundary area is eliminated and this energy is available to reduce the ΔG_s term in eq. (2.25).

2.6.2.2. Nucleation on Dislocations

Cahn (1970) suggested that dislocations with a large Burger's Vector are more effective than those with a small one to decrease ΔG^*.

2.6.2.3. Nucleation on Vacancies

Vacancies can increase the diffusion rate of solute atoms and therefore increase the rate of nucleation. Also vacancies can become an integral part of the nucleus and therefore reduce the nucleation barrier to precipitate formation, Martin (1980).

2.6.3. Rate Controlling Factors for Precipitation

The formation of precipitates normally exhibits sigmoidal kinetic curves which can be approximated by the Johnson-Mehl equation, Reed Hill (1964):

$$Xp = 1 - \exp(-k\ t^n) \qquad \ldots\ldots\ldots(2.28)$$

where: Xp = fraction of precipitates formed

k = constant which includes the nucleation and growth rate

n = constant

t = reaction time

The nucleation rate is controlled by solute supersaturation while the growth rate is controlled by both, the diffusion coefficient and the solute supersaturation. On the other hand during controlled rolling these factors

will depend on the working variables such as reheating temperature
and time, deformation temperature, amount of deformation, interpass
and holding times and cooling rates.

2.6.3.1. Diffusion Coefficients

There are several estimates for the diffusion coefficients
of carbon, nitrogen and niobium in the ferrite and austenite. Although there
is a large scatter of those results, the typical values for the inter-
stitial and substitutional atoms in α-Fe and in γ-Fe show that there
is a difference of several orders of magnitude between them, see
Table 2.13. Carbon and nitrogen in this case will diffuse $\sim$ 3 to 4
orders of magnitude faster than niobium. Also from this Table it
can be established that at a particular temperature, diffusion of
both substitutional and interstitial solute occurs much more rapidly
in ferrite than in austenite. This is because γ-iron is a close-
packed structure whereas α-iron is more loosely packed, Honeycombe
(1981). This makes it respond more readily to thermal activation
and allows easier passage through the structure of vacancies and
associated solute atoms. In all cases, the activation energy Q
is less for a particular element diffusing in α-iron, than it is for
the same element diffusing in γ-iron.

In Fig. 2.18, the interdiffusion coefficients of Nb in austenite
are shown in various iron-based alloys obtained by Kurokawa et al
(1981). They indicate that the interdiffusion coefficients of Nb in
austenite is not strongly influenced by the composition of the solid
solution matrix and the coefficient for Nb is somewhat higher than
the coefficient for self diffusion of iron.

2.6.3.2. Supersaturation

It will depend basically on the composition of the steel, solubility temperature and working temperature in order to reach the level for precipitation. Supersaturation is defined as the ratio of concentrations C_{su}/C_e, where C_{su} = solute concent. of a particular (supersaturated) alloy and C_e = equilibrium solubility of the solute at the precipitating temperature.

Gladman et al (1977) Cohen and Hansen (1979) have defined a critical supersaturation ratio using Irvine et al's (1967) solubility product equation as:

$$\text{Critical Supersat.} = \frac{[Nb]\ [C + 12/14N]\ \text{solution}}{Nb\ (C,N)\ \text{solubility product at roll temp}}$$

$$\dots\dots(2.29)$$

They proposed that the condition necessary for an effective precipitation-recrystallization interaction is that the precipitation precedes austenite recrystallization, i.e. a sufficient Nb, C, N supersaturation at the rolling temperature is required so that strain induced precipitation will occur rapidly. On the basis of single pass rolling experiments Cohen and Hansen (1979) concluded that the critical supersaturation ratio was between 5 and 7.5. A value of 7.7 in a six pass rolling schedule was obtained by Chilton and Roberts (1980).

On the other hand Keown and Wilson (1981) have introduced a new method to establish the supersaturation level. This is called the Lines of Equal Solubility which are diagrams constructed from the solubility products of the considered precipitating species. According to the authors this diagram can be used to predict the order of

precipitation between two phases which will be given by the location of the steel composition with respect to these lines. However, as recognised by the same authors, due to the complexity of the situation, the interpretation of these diagrams becomes fairly speculative, especially during controlled rolling.

Wadsworth et al (1976) found that the degree of supersaturation will be higher the closer the composition of the steel is to the stoichiometric ratio Nb/C. In Fig. 2.19 it is shown that at stoichiometric values the wt% of niobium carbide available for precipitation is maximum and this is even greater if the compound is the stoichiometric NbC.

2.6.4. Kinetics of Nb C_x N_y Precipitation in Austenite

The kinetics of Nb C_x N_y precipitation during controlled rolling is a function of several factors such as steel composition and reheating temperature which will determine the degree of supersaturation; temperature of rolling which will determine the stability of phases, diffusion and activation energies; amount of deformation which will create or increase the lattice defects or nucleation sites; strain rate which will increase the density of lattice defects; interpass times and holding times.

The techniques used to follow the precipitation kinetics of Nb C_x N_y include chemical analysis, X-ray diffraction, quantitative electron microscopy, electrical resistivity, hardness testing and flow curves of specimens tested with single and multipass rolling, hot compression and hot torsion.

The precipitation which has been studied in these experiments is the strain-induced precipitation which occurs during and/or after

deformation. The exceptions are the work carried out by Jonas and Weiss (1979) and Akben et al (1981), who determined the dynamic precipitation which accompanies deformation.

In Fig.(2.20) and (2.21) and Table 2.14, all the $NbC_x N_y$ precipitation kinetics data available so far are given. From these the following can be concluded:

(i) Precipitation of $Nb C_x N_y$ appear to occur as early as $\sim 1100^o C$ as shown by the results of Davenport et al (1977) and Ouchi et al (1977).

(ii) Most of the results appear to follow C-curve kinetics with the nose of the curve located between 900 and $950^o C$ especially the ones of Watanabe et al (1977), Ouchi et al (1977), Hansen et al (1980) and Yamamoto et al (1981).

(iii) Below $900^o C$ the precipitation becomes slower following the pattern of the C curve. Results of Le Bon et al (1973 and 1975) and Watanabe et al (1977) show this.

(iv) In general the precipitation kinetics become sluggish as the amount of deformation decreases becoming about 2 to 3 orders of magnitude slower at $\sim 900^o C$ between a heavily deformed and non-deformed austenite, as shown by the results of Hoogendoorn et al (1977), Le Bon et al (1973 and 1975), Jizaimarn et al (1974), Watanabe et al (1977) Simoneau et al (1978) and Weiss and Jonas (1979).

The reasons for having slow kinetics of precipitation above $1100^o C$ and below $900^o C$ have been indicated by Davenport et al (1977) to be due to two effects: the first one related with the reduction of solute supersaturation as the temperature increases. The second one related with the change in deformation structures of austenite

$\sim 1100^O$C, where the structure will contain few sites for strain

induced precipitation due to its dynamically recrystallized state.

At low temperatures, between 800-900,the slower rate for precipitation

is considered to be due to the decrease in the diffusion rate of

Nb, C and N.

In addition,   the scatter of these results shown in Figs.

(2.20) and (2.21) is thought to be due to several other differences,

such as the base chemical composition, solution treatment conditions,

strain rate, deformation method and perhaps, the most important of

all, the technique of precipitation analysis.

It has been reported by Watanabe et al (1977) that by increasing

the amount of nitrogen from 0.006 to 0.010% the precipitation rate

increased between 850 to 925^OC. In the same way the presence of

Mo appears to shift the C curve to lower temperatures and shorter times.

However an increase in the Mn level from 0.42 to 1.9% shifts the

C-curve to longer times, Akben et al (1981).

2.6.5. Crystallographic Aspects

There are two important cases to consider in the nucleation of

Nb $C_x N_y$ precipitates. These are the orientation relationship that

exists between crystal structure of the precipitate and that of the

matrix and the degree of lattice matching between the matrix and

the precipitate.

The orientation relationship between the precipitate Nb $C_x N_y$

and the matrix γ or α has been provided by Honeycombe (1976),

Davenport et al (1975), Froes et al (1967) and Baker and Nutting (1959).

They propose that the Nb $C_x N_y$ precipitates in the f.c.c. lattice

austenite with a parallel orientation as:

$$\{100\}_{Nb\,C_x\,N_y} \quad || \quad \{100\}_{\gamma}$$

$$<010>_{Nb\,C_x\,N_y} \quad || \quad <010>_{\gamma}$$

And the precipitation in ferrite with a Baker-Nutting orientation:

$$\{100\}_{Nb\,C_x\,N_y} \quad || \quad \{100\}_{\alpha}$$

$$<011>_{Nb\,C_x\,N_y} \quad || \quad <010>_{\alpha}$$

These two orientations are illustrated through the use of the
appropriate metal-atom octahedra given by Jack and Jack (1973)
Fig. 2.22.

These orientation relationships should help to identify the
precipitates which were precipitated in γ or in α.. However, the
orientation relationship of the precipitates found in austenite,
on transformation to ferrite will be given by the Kurdjumov-Sachs

orientation relationship:

$$\{111\}_{\gamma} \quad || \quad \{110\}_{\alpha}$$

$$<110>_{\gamma} \quad || \quad <111>_{\alpha}$$

With respect to the degree of lattice matching the same
Fig. 2.22, can be used to calculate % increase in matrix lattice
parameter that would be required to bring the two lattices into
coincidence at the matrix-precipitate interface. This can be carried
out using the equation:

$$\% \text{ Mismatch} = \frac{L_p - L_m}{L_m} \times 100 \qquad \dots\dots\dots(2.30)$$

where: Lp = length of octahedron of the precipitate

    Lm = length of octahedron of the matrix

A more realistic calculation, to obtain the % of Mismatch would be using the lattice parameters of the precipitate and the matrix at the working temperatures. Lattice parameter measurements of γ and α as a function of temperature have been carried out by several workers with very good agreement. The results of Goldschmidt (1962) are plotted in Fig. (2.23).In the case of Nb C_x N_y there are very few results and they vary according with the precipitate composition. In Fig. (2.24),the results of Elliot and Kempter (1958) are plotted for Nb $C_{0.884}$. In Table 2.15 is given the results of these calculations.

2.6.6. Typical Distributions, Sizes and Morphologies of

Nb C_x N_y Precipitates

Santella (1981) has shown that in the case of recrystallized austenite, Nb C_x N_y forms almost exclusively on grain boundaries as is the case for precipitation in casting.

However in the case of non-recrystallized austenite the precipitates have been shown on what was once a grain or subgrain boundary in the prior austenite, Mangonon and Heitmann (1977), Davenport et al (1975), Irvine and Baker (1979) and Hansen et al (1980),as well as on deformation bands, Tanaka (1981).

Precipitation distribution in the ferrite is related to the nature of the austenite-to-ferrite transformation. If the precipitates were formed during transformation, then they will have the interphase distribution where the final microstructure consists of numerous sheets

of precipitates, where each sheet denotes the location of the inter-
phase boundary during the course of the transformation, Gray and
Yeo (1968), Davenport et al (1975) and Freeman (1977).

When the precipitation occurs in the ferrite after transformation,
the precipitate has a more uniform distribution, Gray and Yeo (1968).

Most of these precipitates have a cuboidal shape. However,
observations through the STEM 400, complemented by microanalysis, other
shapes of Nb rich precipitates have been observed, see Chapter 6.

Typical sizes of Nb $C_x N_y$ precipitated particles are shown in
Fig. (2.25). It has been reported that particles of $\sim$ 5 nm or less
are effective in hindering the migration of subgrain boundaries and so
delay recrystallization. From this figure it can be seen that at
950°C the frequency of particles below 5 nm are higher at a short
annealing time while rapidly coarsened at this temperature compared
with the slow coarsening rate at 850°C, which is expected as a result of
slower diffusion of Nb, C and N.

C H A P T E R   3

PHYSICAL METALLURGY

3.1. Introduction

The Physical Metallurgy principles for the controlled rolling
of niobium microalloyed steels are the same as for the general case
of hot working operations. The physical mechanisms concerned are:
work hardening, dynamic recovery and recrystallization, static recovery
and recrystallization, grain growth and austenite-ferrite transforma-
tion characteristics. Their interaction with the rolling variables
such as reheating temperatures, strains, strain rates and rolling
temperatures will determine the flow stress of the material and the
working forces required which eventually will establish the structure
and properties of the steel.

In this context, the interaction of the rolling variables with
the microstructure will be reviewed, emphasizing static recrystalliza-
tion, as this is one of the most important microstructual changes to be
controlled in order to obtain the best metallurgical and economic
benefits.

3.2. Structural Changes

In the hot and warm working ranges of controlled rolling > 0.5 Tm,
two types of restoration process take place, recovery and recrystalliza-
tion which can occur dynamically or statically and this could be
followed by grain growth.

3.2.1. Dynamic Recovery

During hot deformation of austenite, there is concurrent work hardening and dynamic restoration, the balance of which determines strength. The flow stress initially rises with the strain as a result of work-hardening and recovery; dislocation density rises and a sub-grain structure tends to develop, Sellars and Whiteman (1979), see Fig. (3.1.) In this case, however, dynamic recovery is relatively slow, the subgrain boundaries are not very well formed and therefore sufficient strain energy is stored to nucleate dynamic recrystallization, when a critical strain, ε_c, is reached. Dynamic recovery is further retarded by niobium in solution as indicated by the increase in flow stress with increase in niobium content, Migaud (1980) and Everett et al (1980).

3.2.2. Dynamic Recrystallization

As mentioned in the previous section, due to the sluggish dynamic recovery of austenite, the subgrain boundaries are ill-formed so that at some critical strain, ε_c, sufficient stored energy is available to initiate recrystallization. Recrystallization proceeds with strain (and time) and is complete for the first time when steady state is reached. Repeated recrystallization takes place each time ε_c is attained in previously recrystallized material, and the re-crystallization kinetics lead to the characteristic shape of the stress-strain curves, shown in Fig. (3.2.),   Luton and Sellars (1969).

The dynamic-softening process is thermally activated, giving a dependence of stress σ, on strain rate, $\dot{\varepsilon}$, and temperature, T, which in this case can be described in terms of the Zener-Hollomon para-meter Z :

$$Z = \dot{\varepsilon} \exp (Q_{def}/RT) \qquad \ldots\ldots(3.1)$$

where: Q_{def} = activation energy for deformation in mild

steels $\sim$ 312 KJ/mol, Hughes et al (1974)

R = gas constant

The dependence of stress under hot working conditions is:

$$Z = A \exp \beta \sigma \qquad \ldots\ldots\ldots(3.2)$$

Where A and β are constants for a given strain, or in steady state.

During steady state, the recrystallized grains remain almost equiaxed and of constant size as a result of the repeated recrystallization. The recrystallized grain size has been found to be a unique function of Z or σ_s defined as:

$$d_{rex}^{-n} \ \alpha \ \log Z \quad \text{McQueen (1968)} \qquad \ldots\ldots(3.3)$$

$$\text{or} \quad d_{rex}^{-n} \ \alpha \ \sigma_s \quad \text{Twiss R.J. (1977)} \qquad \ldots\ldots(3.4)$$

where: d_{rex} = dynamically recrystallized grain size

n = constant < 1 found $\sim$ 0.67 for mild

steels, Twiss, R. J. (1977).

σ_s = stress to the steady state

However, the structures developed by dynamic restoration are thermodynamically unstable and when held at a given temperature they are modified by the static restoration process.

When Nb was added to a low carbon steel drastic changes in the flow curves were detected among others, by Stewart (1977), Petkovic et al (1977), Jonas and Weiss (1979), Luton et al (1980) Meyer and Gobiller (1980) and Maehara et al (1981).

Representative curves are given in Fig. (3.3) where the critical strain, ε_c, to obtain dynamic softening is plotted vs. Nb and Ti content at several strain rates. It is observed that the higher the Nb content the higher the ε_c will be for a given temperature and strain rate. This effect is much less pronounced in the case of Ti containing steels.

Summarizing them from the results available, the addition of Nb increases the flow stress, the strain to maximum stress and the critical strain for the onset of dynamic recrystallization. Thus in the case of controlled rolling of plates, where high strain rates are achieved, it is unlikely that the criticial strain will be reached, which means also that it will be impossible to refine the γ-grain through dynamic recrystallization. Instead, grain refinement must be achieved by static recrystallization.

When microalloyed steels are deformed at relatively low strain rates and temperatures where dynamic precipitation can occur, this has a further retarding effect on dynamic recrystallization. This re-tardation has been used by Jonas and co-workers to examine the effect of composition and other variables on the kinetics of dynamic pre-cipitation.

3.2.3. Static Recovery

This softening mechanism is observed for small strains, less than that for static recrystallization, this accounts for the removal of only a fraction of strain hardening. The sub-boundaries become sharper and the dislocation density within subgrains is reduced with relatively little change in size or shape, Jonas et al (1969).
Luton et al (1980) found that Nb retards static recovery in the same

way as it retards dynamic recovery.

3.2.4. Static Recrystallization

During holding at temperature following deformation this
process proceeds in a similar way to that in cold worked material.
Nucleation sites for new grains are predominantly triple junctions
of grain boundaries and nucleation within grains is very small,
Kozasu et al (1971). The distribution of nuclei is highly localized
and inhomogeneous; while some grain boundaries give rise to numerous
nuclei, there are boundaries where nuclei are completely absent,
Kozasu et al (1971). The progress of recrystallization after nuc-
leation consists essentially of the migration of the recrystallizing
front into deformed matrix. The rate of recrystallization in these
steels and other materials is determined by the stored energy, the
density of favourable nucleation sites and the temperature. The
stored energy increases with increasing strain rate and decreasing
temperature of deformation and is strongly dependent on strain. All
these factors therefore increase the recrystallization rate, Morrison
(1972), Djaic and Jonas (1973). As nucleation takes place preferen-
tially at grain boundaries, the density of favourable nucleation
sites increases with decrease in grain size, leading to more rapid
recrystallization in finer grained materials, Barraclough (1974).

Temperature plays two important roles in influencing re-
crystallization after deformation at constant strain rate. Whereas
decreasing the holding temperature decreases the rate of recrystalli-
sation, decreasing the temperature of deformation increases the
stored energy at a given strain and therefore tends to increase the
rate of recrystallization, Sellars (1978).

Apart from the temperature of holding, the variables which increase recrystallization rate also decrease the recrystallised grain size, Glover and Sellars (1972). The lack of effect of temperature is, however, often masked by the occurrence of grain growth after recrystallization is complete as this is a strongly temperature dependent process, Sellars (1978).

3.2.5. Metadynamic Recrystallization

This is present at large strains, greater than ε_c, and well into the steady state region, see Fig. (3.1). It is influenced by the same factors as the static recrystallization, but after a steady state deformation the stored energy is no longer dependent on strain and the dynamically recrystallized grain size is independent of the original grain size. The important variables are the strain rate and temperature of deformation and the temperature of holding, Glover and Sellars (1972), Barraclough (1974). The grain size produced by this process is larger than that produced by dynamic recrystallization because of the lack of repeated nucleation, Sellars (1978). The difference from the static recrystallization is in the absence of the incubation period, presumably because the softening occurs by continued migration of regions of boundary at nuclei formed dynamically.

3.2.6. Grain Growth

It is now generally recognized that in a completely recrystallised metal, the driving force for grain growth lies in the surface energy of the grain boundaries. As the grains grow in size and their numbers decrease, the grain boundary area diminishes and the total surface energy is lowered. The greater the curvature of the boundary the

greater the diffusion of atoms from the convex to the concave grains and so the faster the movement of the crystal boundary, Reed-Hill (1964). This is called "normal" grain coarsening, or normal grain growth, when there is no barrier to the grain boundary migration.

In plain carbon steels, the dependence of the austenite grain size d on the austenitizing temperature is given by the relationship proposed by Feltham (1957):

$$d^2 = d_0^2 + K_0 t \ \exp \ (-Q/RT) \qquad \cdots\cdots (3.5)$$

where: d = average grain size at time t

d_0 = average grain size at time t = 0

K_0 = constant

t = coarsening time

Q = apparent activation energy

It has been established that in steels solute atoms will delay normal grain coarsening whereas second phase particles may suppress it.

Gladman (1966) has shown that for an effective pinning of grain boundaries, a given volume fraction of particles should have a maximum size, r_{crit}, above which it will lose its pinning effect. He showed that:

$$r_{crit} = \frac{6 \ \bar{R}_0 \ f}{\pi \ (1.5 - 2 \ Z^{-1})} \qquad \cdots\cdots\cdots (3.6)$$

where: r_{crit} = maximum size of the particle that will effectively counteract the driving force for grain growth.

f = volume fraction of particles

$\bar{R}_0$ = matrix radius

$$Z = \text{inhomogeneity factor (ratio of the radii of}$$
$$\text{the growing grain and the matrix grains}$$
$$\sqrt{2} < Z < 2)$$

If $r > r_{crit}$ some grain boundaries will overcome the barriers and a process called abnormal grain coarsening or secondary recrystallization will take place. During abnormal grain growth the small primary grains are consumed by the large abnormal grains and the process continues until all the small, primary grains are replaced by the large grains which will then continue to grow by the normal process.

During the processing of niobium microallyed steels normal and abnormal grain growth could occur on reheating, which will depend mainly on the composition, Nb-C-N contents, temperature and time of reheating as discussed in Chapter 1. Normal grain growth again could occur during the holding period which will depend mainly on the composition and temperature of holding.

All the data so far published on this subject indicates that Nb retards dramatically normal and abnormal grain growth compared with a plain carbon steel. This is due to its affinity to form second phase particles with C and N as well as its relatively large atomic radius, 1.43 Å, which gives to Nb a characteristic solid solution effect. Fig. (3.4) shows the grain growth behaviour of austenite after rolling for a plain carbon, niobium and vanadium microalloyed steel.

3.3. Static Recrystallization of Austenite During Controlled Rolling

3.3.1. Avrami Law

A considerable volume of data concerning the isothermal static recrystallization kinetics of Nb-microalloyed austenite is available,

among others, Le Bon et al (1973, 1975), Roberts (1977), Ouchi et al (1977), Roberts and Ahlblom (1978), Cohen et al (1979) and Hansen et al (1980). The time dependence of recrystallized volume fraction (X) usually follows an Avrami Law as long as $X \leqslant 0.70$:

$$X = 1 - \exp(-Kt^n) \qquad \dots \dots (3.7)$$

where: X = fraction recrystallized in time, t

t = time for X recrystallization

n, K = constants

The values of the constants K and n for several microalloyed steels are presented in Table 3.1. The data refer to the temperature range for which recrystallization is sufficiently "slow", that reliable measurements can be performed on quenched specimens, Roberts (1980). The value of the Avrami exponent, n, is about 1; which is expected for reactions in which nucleation proceeds predominantly at pre-existing grain boundaries. For Nb-steels the recrystallization kinetics are such that the reaction goes to completion in the pause periods between roughing passes whereas it is significantly delayed during finish rolling as discussed in Chapter 1, Section 1.5.

3.3.2.   Conditions for Full Recrystallization

3.3.2.1. Strain and Temperature Dependence

As already mentioned, static recrystallization accompanying hot deformation does not occur under all conditions but is mainly strain and temperature dependent for a given composition. In Fig. (3.5) it is shown that the critical amount of reduction, R_{crit}, required for the completion of recrystallization in 3 sec. is very large compared with the R_{crit} for plain C steels. In the same way

the temperature dependence is substantially higher for the Nb steels
and a rapid increase of R_{crit} with decreasing deformation temperature
can be observed. The reasons for these effects are believed to be due
to solute and strain induced precipitation of niobium which will be
discussed in Section 3.3.3.

Extensive studies were carried out lately by Ouchi et al (1977)
and Tanaka et al (1976, 1977, 1980), using single pass rolling, in
order to define the recrystallization behaviour of niobium microalloyed
austenite. They concluded that this can be divided into three regions,
recovery, partial recrystallization and full recrystallization. The
full recrystallization region can be subdivided into static and dynamic,
these regions are shown in Fig. (3.6) . Studying this figure it can be
seen that in practice it would be difficult to roll in the re-
crystallization region, since R_{crit} is very large. Consequently
rolling passes would be carried out in the recovery region or at most
in the partial recrystallization region. However, these curves were
obtained from samples quenched after only three seconds following
rolling, which compared with the interpass times in practice, are
three or four times shorter. On this basis, these limiting tempera-
tures given in Fig. (3.6) would be somewhat lower.

Tanaka (1981) indicates that if the initial rolling passes
are made in the recovery region huge grains are formed locally, due
to the strain induced grain boundary migration, which persist through
the whole course of rolling. These transform into upper bainite
and/or coarse ferrite grains giving poor toughness. On the other
hand if reduction is carried out in the partial recrystallization
region, recrystallization increases in volume fraction, with an
increasing number of passes, eventually reaching complete recrystallisa-
tion.

3.3.2.2. Composition Dependence

From metallographic observations carried out by Irvine et al (1970), Oakwood et al (1977), Ouchi et al (1977), Brown et al (1977) and Cuddy (1981) it has been found that the addition of Nb increases the recrystallization stop temperature, RST, defined as the temperature below which static recrystallization does not take place at normal inter-pass rolling times $\sim$ 15 seconds. This increment ranges from $\sim$ 900°C for a C-Mn-Si steel, up to $\sim$ 1050°C for a C-Mn-Si-Nb steel with $\sim$ 0.06% Nb at fixed deformation conditions. This effect becomes larger the greater the Nb content as shown in Fig. (3.7)

Si, Mn, Ni, Cr, Cu, V and Mo have also been found to increase the RST for a given time or retard the recrystallization rate for a given temperature, due to a substitutional solid solution effect but Nb showed the greatest effect of them all, Maehara et al (1980), see Fig. (3.8).

3.3.2.3. Quantitative Relationships

Sellars and Whiteman (1979) and Sellars (1980) attempted for the first time to quantify the effects of rolling variables on the recrystallization behaviour of austenite, in mild and Nb micro-alloyed steels.

From the data available Sellars (1980) put forward the following relationship for 50% recrystallization above 1000°C

$$t_{0.5} = 2.52 \times 10^{-19} \cdot d_o^2 \cdot \varepsilon^{-4} \cdot \exp \frac{Q_{rex}}{RT} \qquad \ldots\ldots\ldots (3.8)$$

for: $\varepsilon < \varepsilon_c$ and T > 1004°C

where: $t_{0.5}$ = time in secs for 50% recrystallization

d_o = initial austenite grain size obtained after reheating μm.

ε = equivalent tensile strain.

Q_{rex} = activation energy for recrystallization = 325,000 Joules

R = gas constant, Joules

T = temperature ^oK.

According to this equation, recrystallization in Nb steels is delayed about an order of magnitude compared with mild steels, which agrees with results in practice for the temperature range indicated. Note the large effect of the prior austenite grain size and strain for a given rolling temperature.

3.3.3. Delayed Recrystallization

3.3.3.1. Mechanisms

Whereas above $\sim 1000^oC$ the recrystallization of Nb micro-alloyed austenite is ~ 1 order of magnitude slower than for a plain C steel, at lower temperatures $\sim 900^oC$ recrystallization is more delayed ~ 3 to 4 orders of magnitude as can be seen in Fig. (3.9) and (3.10).

The retardation mechanisms have been discussed by many investigators and attributed to:

(i) Strain induced precipitation of fine Nb $C_x N_y$. Supported by Irani et al (1967), Jones and Rothwell (1968), Davenport et al (1975, 1977, 1980), Sekine and Maruyama (1976), Priestner et al (1968), Le Bon et al (1975), Watanabe et al (1977), Davenport and Dimicco (1980) and Hansen et al (1980), to mention a few.

(ii) Solute-drag effect. Supported among others by Le Bon et al (1973), Coladas et al (1977), Lamberigts and Greday (1977), Jonas and Weiss (1979) and Luton et al (1980).

(iii) The combined effects of solute Nb and precipitation of fine
$Nb\ C_x\ N_y$. Supported by Lamberigts and Greday (1977), Coladas (1977),
Jonas and Weiss (1979) and Yamamoto et al (1981).

The original hypothesis, based on electron metallography was
that Nb acted to suppress static recrystallization by precipitating
on the cell walls of the unrecrystallized austenite, therefore keeping
the structure from being able to form viable nuclei for subsequent
recrystallization, Jones and Rothwell (1968), Davenport et al (1975,
1977) and others.

Recently Coladas et al (1977), Jonas et al (1979), Akben et al
(1981) Luton et al (1980) and Yamamoto et al (1981) have suggested that
it is Nb in solution which retards recrystallization and it does this
by slowing down the rate of static recovery and so delaying the onset
of recrystallization. X-ray diffraction analysis carried out by
Yamamoto et al (1981), suggests that this retarding effect results
from the interaction between dislocation and lattice distortion by
solute atom. Both onset and progress of recrystallization are sub-
stantially delayed as soon as strain induced precipitation begins.

3.3.3.2. Kinetics of Static Recrystallization

Experimental data for the recrystallization kinetics is
abundant. Most of the data available has been plotted in Figs. (3.11) and (3.12
and the experimental details given in Table 3.2.

The general trends for all these data are:
(i)   From $\sim 1100^{o}C$, the lower the rolling temperature down to
$900^{o}C$, the longer the times for static recrystallization to take place.
The data of Davenport et al (1977) differs from the rest, at this range,
in the sense that the recrystallization of their 0.08% C, 0.02%N and
0.09% Nb steel is stopped rapidly at $\sim 1080^{o}C$.

(ii)   Below 900°c the recrystallization kinetics decreases even further with decreasing temperature for most of the data except in the cases of Le Bon et al (1973, 1975), Lamberigts and Greday (1977) and Roberts (1980) which show a reduced extent of retardation.   The results of Le Bon particularly are different at 850°C which show $\sim$ 1 order of magnitude faster recrystallization rate compared at 900°C

(iii)   As far as the strain applied is concerned, it can be deduced that the larger the strain applied, the shorter the times to start recrystallization above 900°C at similar compositions.   This is shown by the results of Cohen et al (1979), ε = 0.80 compared with Yamamoto et al (1981), ε = 0.69.   Also the results of Hansen et al (1980) ε = 0.80 compared with Lamberigts et al (1979), ε = 0.41 confirm this.   At $\sim$ 850°C this effect is less pronounced.

(iv)   Although most of the data given in Table 3.2 were obtained from samples reheated above 1200°C the indications are that the higher the Nb content the longer the times for recrystallization will take as well as the higher the temperatures to start delaying recrystallization. Cohen et al (1979), Hansen et al (1980).   The results of Davenport et al (1977) could be explained through this effect.

(v)   The results of Hansen et al (1980), Hoogendoorn (1977) and Ouchi et al (1977) with similar chemical compositions, and thermo-mechanical treatments except for the strain rate, suggests that strain rate is not important to the kinetics of recrystallization if the results of Hansen et al and Ouchi are compared.   However the results of Hoogendoorn showing   much faster kinetics above 850°C could indicate the effects of Mn which in this case is lower $\sim$ 0.99%Mn compared with 1.35% Mn of the steels of Hansen and 1.41%Mn in the steel of Ouchi.

3.3.3.3. Quantitative Relationships

Sellars and Whiteman (1979) and Sellars (1980) also proposed equations of the time for 50% recrystallization in the lower range of temperatures, i.e. below 1000°C. From the data plotted in Fig. (3.13) Sellars (1980) put forward the following equations:

$$t_{0.5} = 5.94 \times 10^{-38} d_o^2 \varepsilon^{-4} \exp \frac{Q'_{rex}}{RT} \qquad \ldots\ldots\ldots(3.9)$$

where: $\varepsilon < \varepsilon_c$, $891 < T < 1004°C$ and $Q'_{rex} = 780,000$ Joules

and $$t_{0.5} = 9.24 \times 10^{-9} d_o^2 \varepsilon^{-4} \exp \frac{Q''_{rex}}{RT} \qquad \ldots\ldots\ldots(3.10)$$

where: $\varepsilon < \varepsilon_c$, $T < 891°C$ and $Q''_{rex} = 130,000$ Joules

All the variables in these equations have the same meanings as in eq. (3.8). Summarizing, these three equations predict about an order of magnitude slower recrystallization for a steel with ∿ 0.04% Nb compared with the C-Mn steels for temperatures greater than 1000°C. Below 1000°C a delay of ∿ 2½ orders of magnitude is obtained. As suggested by the authors these equations will predict at least the minimum times required for a given recrystallized fraction. However, more accurate relation-ships would have to include compositional variables mainly concerned with the influences of Nb, C and N on the recrystallization kinetics.

3.4.   Recrystallized and Non-Recrystallized Austenite Grain Size

3.4.1.   Recrystallized Austenite Grain Size

The grain size created as a result of static recrystallization, following any deformation step is a complex function of the deformation parameters, temperature, strain and strain rate. The effects of strain on the recrystallized grain size d_{rex} are shown in Fig. (3.14)

where, as   the strain increases the austenite recrystallized

grain size decreases rapidly. This is much stronger in a C-Mn steel

than for the Nb steels with the exception of the data of Le Bon et

al (1973, 1975) which shows a steeper strain dependence probably because

they were obtained at temperatures below $1000^{o}C$ where precipitation

and recrystallization take place together, Sellars (1981). On the

other hand the effects of strain rate and temperature of deformation Z,

on d_{rex}, were found insignificant, Roberts(1980), Weiss et al (1973)

which is consistent with its lack of influence on recrystallization

kinetics, Sellars (1981). Fig. (3.14)also indicates that the larger the

original reheated grain sizes, d_{o}, the larger the recrystallized grains

result.

Considering the effects of the different variables independent,

the following expression has been put forward by Sellars (1980):

$$d_{rex} = D^{1} \quad d_{o}^{0.67} \quad \varepsilon^{-0.67} \qquad \ldots\ldots\ldots(3.11)$$

for $\varepsilon < \varepsilon^{*}$ and $T > 950^{o}C$

where: D^{1} = constant which varies form 0.66 to $1.86\mu m^{0.33}$, but for

a 0.04% Nb steel it is expected a value of $0.9\mu m^{0.33}$

d_{o} = initial γ g.s.

ε = strain less than $\varepsilon^{*} \simeq \varepsilon_{c}$ for the range of grain

sizes found on reheating.

On the other hand Cuddy (1981) found a systematic decrease in

grain size with increase in strain rate and temperature of rolling

which agrees with the results of Machida et al (1980) and the latest

results of Katsumata et al (1982). Cuddy proposed the following

relationship:

$$d_{rex} = (\frac{623}{\sigma})^{0.29} \qquad \ldots\ldots\ldots(3.12)$$

where: σ = flow stress at the last roughing pass, defined

                as a function of strain, ϵ, and the Zener

                Hollomon parameter $\bar{Z}$.

Based on the change of interfacial area/volume (S_v) with strain,

Katsumata et al (1982) proposed the following relationship:

$$\frac{S_v}{mm^2/mm^3} = \frac{1000}{d_o} \left(0.429 \,(1-R) + 1.571/(1-R) \right) + (80 \cdot R - 24)$$

$$\dots\dots\dots(3.13)$$

where: d_o = initial grain size in μm

                R = fractional rolling reduction

For rolling reductions of 0.3 or more, they found good correlation

between grain size obtained after rolling at a constant temperature and

S_v, but at reductions below 0.3 the strain dependence was found to be

much lower than the one observed by Tanaka et al (1977).

        These apparently contradictory results would mean that further

systematic work needs to be done.

3.4.2. Non Recrystallized Austenite Grain Size

        Theoretically the austenite area/volume ratio should increase

as the strain increases and becomes elongated or "pancaked" in the

rolling direction, keeping the same volume. Cuddy (1981) proposed the

following relationship:

$$h = (1.17 - R)d \qquad \dots\dots\dots(3.14)$$

where: h = height of the elongated γ grain

                R = reduction $\geqslant$ 0.5 below the recrystalliza-

                    tion temperature.

                d = recrystallized grain defined in eq. (3.12)

From the previous equation (3.12), eq.(3.14) becomes:

$$h = (1.17 - R) (\frac{623}{\sigma})^{0.29} \qquad \ldots\ldots\ldots(3.15)$$

3.5. Transformation to Ferrite

In order to get very fine ferrite grain size it is necessary to have a maximum ferrite nucleation rate combined with a minimum grain growth during and after transformation. In this case it is achieved through control of composition, rolling schedule, precipitate distribution and cooling rate.

The principal nucleation sites are the γ grain boundaries, deformation bands, dislocations and dislocation sub-structures, twin boundaries and some second phase particles, Ouchi et al (1977), Kozasu et al (1977) and Walker et al (1978). Le Bon (1977) also suggested that ferrite can nucleate at the ferrite-unrecrystallized austenite interface.

A measurement of the nucleation rate is reflected by the variations in the transformation temperature Ar_3, therefore the effects of composition, rolling schedule, precipitate distribution and cooling rate on Ar_3 will be reviewed next.

3.5.1. Influence of Composition

A few quantitative data exists in the literature about the effects of the microalloying elements on the transformation temperature Ar_3 of these steels after controlled rolling, Ouchi et al (1981) using a thermal analyser developed for this purpose, and analyzing results of controlled rolling of 173 steels with 50% reduction in the non-recrystallization γ-region obtained the following, statistically

significant relationship:

$$Ar_3 \ (^{O}C) = 910-310\%C-80\%Mn-20\%Cu-15\%Cr-55\%Ni-80\%Mo + 0.35 \ (t-8)$$

Where:

........(3.16)

The alloying elements are in wt% and t is plate thickness in mm. They reported that the variation range of Si, P, S and Aℓ were so small that their statistical significance was negligible. As can be seen in this equation, C, Mn, Mo and Ni effectively lower the Ar_3 temperature with Cu and Cr showing less pronounced effect and surprisingly Nb or V do not give rise to any influence, Fig. (3.15). In these 173 steels the maximum N content was 0.009% and therefore appears to be insignificant as well, but earlier workers such as, Bose and Hawkes (1950), Taylor (1953), in mild steels containing much higher N contents found that N decreased the Ar_3 transformation temperature and increased the hardenability. However, Ballinger and Honeycombe (1980) are of the opinion that the presence of N in the Fe-C-V system, accelerates the $\gamma \rightarrow \alpha$ transformation, i.e. the Ar_3 is raised, but this could be due to the interaction of VN pinning the prior γ grain boundaries, because as will be seen later, smaller austenite grain sizes increase the Ar_3.

In spite of the above results where Nb shows no effect in the transformation temperature, the consistent results of obtaining acicular structures in the microalloyed steels suggest that its effects could be connected with the interaction of other elements such as manganese. Irvine et al (1963) found that 2% Mn increases the solubility of vanadium in γ by $\sim$ 100% and therefore decreased the Ar_3 temperature significantly. This could be the same effect in the case of Nb steels. Besides, Morrison (1963) comparing the

transformation characteristics of two steels with low and high Mn and similar Nb contents found that it increased the hardenability only of the steel with more than 1%Mn. Irvine et al (1963) also found considerable amounts of bainite formed in air cooled similar Nb free steels. But Gray (1974), and others showed that 0.05% Nb in solution can depress Ar_3 by $\sim 55^{o}C$ in a steel cooled at $\sim 5^{o}C/sec$. Shams (1982) concluded that Nb, a ferrite forming element, will significantly depress the Ar_3 temperature by retarding the kinetics of transformation. It enhances the formation of apolygonal ferrite or acicular structures but its interaction with C and N could reduce this effect. These findings suggest that the effect of Nb on Ar_3 is still not clear.

3.5.2. Influence of the Rolling Schedule

This includes reheating temperature, rolling temperature and deformation. The reheating temperature because it will fix the initial austenite grain size. The higher the reheating temperature the larger the γ grain and the lower the Ar_3 as can be seen in Fig. (3.16), Ouchi (1981). The rolling temperature and deformation because they will determine the γ size and morphology. At a given reduction the lower the temperature of rolling the higher the Ar_3 becomes. At a given rolling temperature the larger the reduction the higher the Ar_3 becomes. This has been explained by Kozasu et al (1977) and Ouchi et al (1981) as due to the steady increase of the austenite grain boundary area but more so due to the rapid increase of the deformation band density, when decreasing temperature of rolling and increasing deformation, which will increase then the nucleation rate of ferrite (Ouchi 1981). Both effects are shown clearly in Fig. (3.17) which agrees with previous results of Smith et al (1971) Priestner et al (1973) and Ouchi et al (1977).

3.5.3. Precipitate Distribution

Very little is known about the effects of Nb C_x N_y precipitates on Ar_3. Hoogendoorn (1977) found that the Ar_3 is increased as the amount of dissolved Nb decreased i.e. precipitate increasing.

3.5.4. Cooling Rate

The faster the cooling rate the lower the Ar_3 becomes, Ouchi et al (1981) and Shams (1982). This can be seen in Fig.(3.18) and the term included in equation (3.15) as plate thickness. In this figure for a particular steel, increasing the cooling rate from 0.4 to 1^0 C/sec there will be a drop in Ar_3 of $\sim 10^0$C.

3.5.5. Ferrite Grain Size Relationships

Although the ferrite grain size is one of the major structural parameters affecting the properties of hot rolled products, there is limited quantitative information to enable this to be related to the austenite structure produced at the end of stage 3 in controlled rolling. Fig.(3.19) shows a considerable scatter on the effects of the variables reviewed above, but the results available indicate that the final ferrite grain size, for a given composition depends on: the prior austenite grain size (more appropriate would be the height of the non-recrystallized γ grains), the % of reduction in stage 3, the finishing rolling temperature, also in stage 3 and the cooling rate. A relationship between the α g.s., the prior γ g.s. the rolling variables and cooling rate will be:

$$d_\alpha = f\ (d\gamma,\ \%R,\ FRT,\ \dot{T}) \qquad \dots\dots\dots(3.17)$$

where: $\qquad d_\alpha$ = ferrite grain size

$$d_\gamma \quad = \quad \text{austenite grain size (non rex.)}$$

$$\%R \quad = \quad \text{amount of reduction in stage 3}$$

$$FRT \quad = \quad \text{finish rolling temperature}$$

$$\dot{T} \quad = \quad \text{cooling rate}$$

Recently two relationships relating d_α to a recrystallized austenite g.s. d'_γ were produced for experimental low C-Mn steel.

$$d_\alpha = 11.7 + 0.14 \, d'_\gamma + 37.7 \times \dot{T}^{-\frac{1}{2}} \qquad \dots\dots(3.18)$$

for d'_γ = 20 to 100µm and $\dot{T}$ = 3.6 to 120°C/ min

and

$$d_\alpha = -0.16 + 0.07 \, d'_\gamma + 25.36 \, \dot{T}^{-\frac{1}{2}}$$

for d'_γ = 20 to 50µm and $\dot{T}$ = 2.0 to 9.0^{o}C/sec $\qquad \dots\dots(3.19)$

Equation (3.17) Allbones et al was derived after normalizing and equation (3.18), Janampa (1980) after single pass rolling at 1000°C giving different reductions from 5 to 35%.

However these relationships give large d_α sizes for a controlled rolled Nb microalloyed steel, which as already described depends on more variables.

Cuddy (1981) has shown that the final α grain size nucleated on heavily deformed austenite will follow the relation:

$$d_\alpha \cong \frac{1}{2} \, (1.17 - R) \, (\frac{623}{\sigma})^{0.29} \qquad \dots\dots(3.20)$$

where: d_α = ferrite grain size

   R = amount of reduction $\geqslant$ 0.5 below the recrystallization temperature.

   σ = flow stress in the last roughing pass

This suggests that the final ferrite grain size will depend only on two factors: the maximum flow stress during roughing, σ, and the total finished reduction R.

3.5.6. Structure - Composition - Mechanical Properties Relations

The ferrite grain size is a very important parameter to control in these steels since its refinement increases the yield strength and decreases the impact-transition-temperature. Many studies have helped to quantify the relationships between micro-structural and compositional parameters, Irvine et al (1970), Pickering (1977).

The yield stress of polycrystalline solids follows the Hall-Petch relation, Hall (1951):

$$\sigma_y = \sigma_0 + k_y \, d^{-\frac{1}{2}} \qquad \qquad \cdots\cdots\cdots(3.21)$$

$$= (\sigma_\ell + \sigma_{ss} + \sigma_d + \sigma_p + \sigma_t) + k_y \, d^{-\frac{1}{2}} \qquad \cdots\cdots\cdots(3.22)$$

where:
σ_0 = internal stress

k_y = constant

d = grain size

σ_0 is divided into several terms: lattice hardening σ_ℓ, solid solution hardening σ_{ss}, dislocation hardening σ_d, precipitation hardening σ_p and texture hardening σ_t. This last term σ_t, however, has been found to be quite small by Tanaka et al (1977).

In the same way the impact transition, ITT has been defined as:

$$ITT^oC = A (\sigma_\ell + \sigma_{ss} + \sigma_d + \sigma_p + \sigma_t) - k_y \, d^{-\frac{1}{2}} \qquad \cdots\cdots\cdots(3.23)$$

where A is a constant. In both cases d has a strong influence.

Relationships concerned with the chemical composition and rolling variables are also available in a few cases, and the ones given below are considered to be used most in industry in the U.K., Randerson (1981):

Yield Strength:

$$Y.S. \ (N/mm^2) = 571 - 0.31 \ FRT - 1.63 \ PG + 380 \ CEV \quad \ldots\ldots(3.24)$$
$$\pm \ 32 \ N/mm^2$$

where: FRT = End of Finishing Rolling Temperature, ^{o}C

PG = Plate gauge, mm

CEV = Carbon equivalent defined by Lloyds =
$$C + \frac{Mn}{6}$$

Ultimate Tensile Strength:

$$U.T.S. \ (N/mm^2) = 589 - 0.28. \ FRT - 0.95. \ PG + 541. \ CEV \ \ldots.. \ (3.25)$$
$$\pm \ 27N/mm^2$$

where: $CEV = (C + \dfrac{Mn}{10})$

Impact Transition Temperature:

$$I.T.T. \ (27J) = -197 + 0.185 \ SS - 847 \ RR - 37\%Mn - 682\%Al_{sol}$$
$$\pm \ 17^{o}C \qquad\qquad\qquad\qquad \ldots\ldots(3.26)$$

where: SS = Slab soaking temperature ^{o}C

RR = Reduction ratio

Al_{sol} = Aluminium in solution

The processing variables, such as the end of finishing rolling temperature FRT is also defined as:

$$FRT = 180 + 0.51 \; EHT + 3.1 \; PG + 0.44 \; (PG.RR)$$

$$........(3.27)$$

where: EHT = End of holding temperature, ^{o}C

PG = Plage gauge, mm

RR = Reduction ratio

$PG.RR$ = Holding thickness, mm.

C H A P T E R   4

EXPERIMENTAL TECHNIQUES

4.1. Introduction

The aim of the experimental work was to detect the influence of nitrogen on the recrystallization of austenite and Nb $C_x N_y$ precipitation kinetics, on the ferrite grain size and on the mechanical properties of hot rolled Nb microalloyed steels.

The main techniques used for this purpose were: quantitative metallography to obtain the recrystallization kinetics; electrolytic separation of the precipitates to identify and measure accurately their lattice parameters through X-ray diffraction; chemical analysis of the extracts to obtain the precipitation kinetics and composition of the precipitates; transmission electron microscopy of replicas and foils to locate the precipitates and obtain their size distribution; thermodynamic modelling to establish solubility of Nb C_x and Nb N_y as Nb $C_x N_y$, and mechanical testing. Fig. 4.1 gives the distribution of specimens obtained from the rolled slabs and used with these different techniques.

As in many metallurgical systems, the final state of these steels depends on their previous thermomechanical treatments, therefore the experimental techniques, from the steelmaking stage to mechanical testing, will be outlined sequentially. Fig. 4.2 shows the sequence of these experimental techniques.

4.2. Steelmaking

A Birlec Air Induction furnace of 70 Kg capacity with a silimanite lining was used to make the five experimental steels.

The basic charge for all these steels was essentially Armco iron plus additions of ferrosilicon to deoxidise the melt, ferro-niobium and niobium metal and manganese flakes of low and high nitrogen contents to adjust the final compositions which are given in Table 4.1. In the case of the steels with high niobium and high nitrogen levels, additional ferroniobium and Mn-N flakes were added into the ladle to make up for losses in the furnace of about 10 and 20% respectively. At $1560^{o}C$ the melt was chill cast into cast iron moulds of 76 x 76 x 600mm with an exothermic compound on top of them. The exothermic compound used was Fedex 50, of Foseco which basically contains FeO + Al. The reaction $3 FeO + 2 Al \rightarrow Al_2 O_3 + 3Fe$ releases heat which keeps the top of the ingot hot enough and minimizes piping.

After cutting off the top and bottom $\sim$ 40 mm to obtain sound ingots they were rolled down to slabs of 25.5 x 52 mm section*.

4.3. Reheating of Slabs

An electric furnace with a non scaling atmosphere, provided by an exothermic gas generator, was used to reheat the slabs in all cases. The gas composition was approximately 98% N_2, 2% (CO_2 + CO + H_2) which minimized scaling and decarburization.

On the other hand, the diffusion of N_2 into the samples at the temperatures and times experienced was not detectable and was neglected in the investigation of the effects of nitrogen on the γ recrystallization

---

* Rolling carried out at B.S.C. Laboratories, Hoyle Street, Sheffield.

- 74 -

and precipitation kinetics of Nb in the steels.

4.3.1. Reheating Temperature

After a detailed study of the available solubility equations and checking by prior austenite grain size measurements on samples reheated at several temperatures and times, it was concluded that the reheating temperature for steels 12, 97 and 99 should be 1200°C and for steels 22 and 23 should be 1300°C for complete solution of niobium.

4.3.2. Reheating Time

The same experiments designed to obtain the optimum reheating temperature showed that the reheating times should be 45 minutes for steels 12, 97 and 99 and 90 minutes for steels 22 and 23 for complete solution of Nb. These times are at the actual reheating temperatures. To reach these temperatures, it was necessary to give ∿ 15 additional minutes in the furnace.

4.4. Rolling

Hot rolling was carried out on a 2 - high reversible Hille 50 rolling mill, driven by a 20 H.P. motor. This mill is fully instrumented to obtain loads, speed and temperature measurements which are described later.

The main rolling schedule consisted of two pass rolling: roughing at 1100°C and finishing at one of the following temperatures: 1000, 950, 925, 900, 850 and 800°C. Following to the second pass, different annealing times were given at those rolling temperatures. For this a second electric furnace was used which was set at a slightly higher

temperature to obtain a rapid return to the given temperature of rolling. After annealing, the slabs received one of the following treatments:

(a) One end water quenching, in which one of the ends of the rolled slabs was quenched in a water tank with a steel mesh at a depth of 51 mm in the water while the slabs were kept vertical during cooling, by a specially designed strip touching only at two points at the air cooled end,

(b) air cooling, carried out on nails, and

(c) full iced brine quenching, where the full length of the rolled slab was ice brine quenched with some agitation. As will be seen later, most of the rolled slabs received this last treatment. The reduction level was kept constant at 33% and 25% for the roughing and finishing passes respectively.

This main rolling schedule was designed from the results obtained with a single pass and one end water quenching schedule, after studying the recrystallisation behaviour of steels 97 and 99. See Fig. 6.11 In this case the slabs were pre-rolled to finish at 12.7 mm after a further 25% reduction. The cooling rates obtained previously , Janampa (1980), were used to correlate with the grain sizes along the length of the one end water quenched slabs.

The lengths of the slabs used were: 100 mm for the one end water quenching experiments and 80 mm for the air cooled and fully ice brine quenched ones.

4.4.1. Load and Speed Recording

The rolling load was measured by means of two load cells of 25 tonnes capacity inserted between the end of the screwdown and the

chocks of the top roll. Each of these load cells is provided with a stabilised 6V supply and their output is fed to a U.V. recorder. Deflections, obtained in this way were measured and converted into loads with the aid of calibration charts.

The roll speed was measured using an aluminium disc, with eight equally spaced small holes drilled on a circle of 50 mm diameter. The disc is fitted to the undriven end of the bottom roll and has a lamp on one side and a photo cell on the other. The output of the photocell is fed to the U.V. recorder. From the distance between the peaks in the record, the peripheral roll speed can be calculated using the following expression:

$$v = \pi \ r \ s \ /4 \ d \qquad \qquad \dots\dots(4.1)$$

where
v = roll speed (mm/sec)

r = roll radius (mm)

s = chart speed (mm/sec)

d = peak separation (mm)

This peripherical speed was kept constant through all the experiments at 219 mm/s, which gave a strain rate of 4.20 sec^{-1}

4.4.2. Temperature Measurements

All the slabs were rolled with a thermocouple inserted from the side to a position midway along the length, width and thickness. The Chromel-Alumel thermocouples used were 1.5 mm in diameter, 'Pyrotenax' inconel sheathed and mineral insulated, connected to a fast response Telsec recorder. This unit allowed recording of the complete thermal history of the specimens i.e. reheating rate, reheating temperature of the sample, temperature change during

rolling and post treatments. The Telsec recorder was calibrated with a standardized voltmeter after every test which was carried out either using a cold junction or allowing for the equivalent mv of the room temperature. In most cases this temperature was $\sim 25^{o}C \equiv 1.01$ mv.

4.4.3. Temperature Distribution in the Slabs during Rolling

Due to the way of handling the slabs during rolling, both of their ends were bound to be at lower temperature than their middle part. Therefore it was necessary to know the length of the specimens with uniform temperature before, during and after rolling. This was achieved by two methods. The first one was using the data of load measurements from the U.V. recorder and the second one, rolling with two thermocouples at a time, one of them inserted midway along the length of the slab and the other one between the middle and the end. In the first method the U.V. recorder was operated at high chart speed, 50 cm/sec in order to obtain a wide load vs time records to correlate them with the length of the slabs. For this correlation, the loads were converted into mean flow stress using the computer program given by Leduc (1980), for which careful measurements of the width of the rolled slabs on both surfaces and mid thickness were carried out.

From this it was established that 1/5 of their final lengths at each end should be scrapped because they showed $\sim 30^{o}C$ drop compared with the temperature of the middle part.

4.4.4. Temperature Distribution in the Slab during Cooling

This was measured on the one end water quenched slabs as well as on the air cooled ones. From previous measurements,

- 78 -

Janampa (1980), it was possible to fit the temperature readings
of the middle part of the slab with the ones above and below it.
From this also, a cooling rate vs distance from the end quenched slabs
was obtained.

In the air cooled slabs the temperature was recorded until
it was about 200°C.

4.5. Metallography

As a first attempt to detect the influence of N on controlled
rolling of niobium microalloying steels, recrystallisation fractions
and grain size measurements were carried out on the prior austenite
and ferrite - pearlite structures. The techniques and methods for
these measurements will be outlined as follows:

4.5.1. Etching Technique
4.5.1.1. Prior Austenite Grain Boundaries

Several reagents were tried in order to show up the prior
austenite grain boundary and measure the grain size and recrystallized
fraction. The reagent: 0.25 gr. of sodium peroxide + 5 ml of con-
centrated teepol completed to 200 ml. with saturated picric acid gave
the best results, etching at ∿ 70°C for 4 to 6 minutes in total, with
a 2-minute interval to swab them with cotton soaked in concentrated
teepol to increase the wetting action of the etching solution.

4.5.1.2. Ferrite - Pearlite Structures

The etching solution was in this case the well known nital
2% at room temperature for 15-20 seconds.

4.5.2. Sampling Area

Volume fraction analysis and grain size measurements were carried out on 4 x 4 mm areas at the middle of 12.8 x 18 x 27 mm specimens. These were from the longitudinal section of the rolled slabs where the rolling temperature and/or cooling rate were known. This sampling area allowed counting of at least 600 points in both transversal and longitudinal directions using the Swift Point counting equipment and measuring of at least 2,000 grains of the largest recrystallized prior austenite grains (80μm) and not less than 40,000 grains of the biggest ferrite - pearlite grains obtained (∿20μm). In the case of the non-recrystallized prior austenite grains the measurements were made on a 5 x 5 mm area which allowed counting of enough points and measured at least 500 grains.

4.5.3. Volume Fraction Determinations

This can be done by point counting, lineal and areal analysis on the plane of polish. According to previous experience, T. Gladman and J. Woodhead (1960), the accuracy of a determination is mainly given by the number of observations and the method is not important as long as the density of observations is not too large. For point counting the optimum density corresponds to an average of one point per grain. Satisfying this condition the systematic point counting has a smaller deviation than either lineal or areal analysis with the same number of observations.

With this criterion, the fraction recrystallized of the prior austenite was determined through point counting in the longitudinal and transverse directions. The same technique was applied to determine the fraction of pearlite as well as acicular phases in the ferrite - pearlite structures.

4.5.3.1. Size of the Sample

The minimum number of points to count was calculated through the following relationship:

$$n = \frac{P(1-p)}{(\sigma^2)}$$

<div style="text-align:right">........(4.2)</div>

where
n = total number of points to count

P = proportion of the feature

σ = standard deviation

This is assuming the results conform to a Binominal distribution and when n is large (∿ 400) the Binominal distribution can be approximated by a Normal or Gaussian distribution with the same mean and standard deviation, for p = 0.02 to 0.98.

In this context n can be determined if a confidence limit is established. In this case it was assumed a 95% probability that the true value of p lay between p ± 1.96 x σ or p ± 2σ. For several values of p and assuming a standard deviation of 0.05, 600 points was considered the optimum number to cope with possible errors as well as to measure the greater number of specimens in a reasonable time.

4.5.3.2. Sources of Error and Corrections

The two main sources of error, grain boundary and phase identifications were dealt with as follows: For the prior austenite structure, providing the best etching was achieved and still some grain boundaries were not clear, then a closer inspection on the change of direction of the martensite plates indicated the position of a grain boundary. To differentiate a recrystallized from a non-recrystallized prior austenite grain, it was assumed that recrystallized grains were the ones which showed roughly polygonal shapes and were not

bigger than the size calculated through Eq. (3.10), see Appendix 1
For the ferrite - pearlite structures, after over etching, all the
grain boundaries were shown and the identification of acicular from
polygonal ferrite was achieved through measurements on the longitudinal
and transverse directions, and in the same way as in the case of
prior austenite grains.

4.5.4. Grain Size Measurements

Ideally, a grain size in three dimensions given its shape and
way of assembly, would be necessary to correlate the grain size and the
mechanical or physical properties of the material, since most of these
properties involve all three dimensions.

In practice, the grain size is represented by a single parameter
which in the case of uniform grains can be related to the true size,
and with non-uniform grains such as the partially recrystallized prior
austenite grains, further measurements on two directions were necessary.

The grain size measurements in this case were carried out
through the mean linear intercept method, $\bar{L}$, which is the average
distance between grain boundaries along a line placed at random on the
sampling area. Eight lines with fifty grains per line were counted
in each longitudinal and transversal directions, using an optical
microscope with a micrometer stage. The other two methods, comparison
with standards and the mean intersected area were considered not
adequate for the purposes of this work.

For the cases when partially recrystallized and acicular
structures were present, the grain size was determined by counting
the grains in a given length of line L, differentiating the recrystall-
ized from the non-recrystallized and the polygonal from the acicular
grains. They were calculated using the following relationships:

$$gs._{rex,\ polyg} = \frac{\chi \cdot L}{N_{rex,\ polyg}} \qquad \dots\dots(4.3)$$

$$gs._{non\ rex,\ acic} = \frac{(1 - \chi) \cdot L}{N_{non\ rex,\ acic}} \qquad \dots\dots(4.4)$$

where: χ = fraction recrystallized or polygonal

L = length of line of measurements

N = number of rex/non rex or polyg./non polygonal

grains.

N and χ were both measured in the same line, through a double traverse technique and the average of the calculated grains sizes was reported.

In each case, these measurements were carried out in both longitudinal and transverse directions.

4.5.4.1. Size of the Sample

As in the case of Volume Fraction Determination in order to have a reasonable accuracy with the minimum time, it was necessary to know the minimum number of grains to count. This was calculated through the relationship derived by Pereira da Silva in 1966:

$$RE\ (\bar{L}) = RE\ (N_L) = K/\sqrt{N_T} \qquad \dots\dots(4.5)$$

where: RE = relative error

$\bar{L}$ = mean linear intercept

K = 0.65 ± 0.02

N_T = number of grains measured

N_L = number of grains per unit length

This equation has been shown to agree closely to practice considering the frequency distribution of linear intercepts are essentially normal distributions.

From this equation, the total number of grains required to give a chosen relative error can be calculated as shown in Table 4.2 from which the lower the relative error the larger the number of grains it would have been necessary to count. In this case 400 grains were counted in both prior austenite and ferrite - pearlite structures.

To give a RE $(\bar{L})$ = 0.033. The 95% confidence limits in this case will be given by:

$$95\% \text{ CL } (\bar{L}) = \bar{L} \pm 2 \times \text{RE } (\bar{L}) \qquad \ldots\ldots\ldots \quad (4.6)$$

4.5.4.2. Sources of Error and Corrections

The sources of error and corrections in this case are similar to the ones described in 4.5.3.2. due to the use of the volume fraction of polygonal/acicular and recrystallized/non

recrystallized grains to obtain the grain sizes. The same applies
in the case of the ferrite/pearlite structures where to get the true
ferrite grain size it had to be corrected for the volume fraction
of pearlite and calculated through an equation similar to (4.4)

4.6. Hardness Measurements

These measurements were carried out on water quenched and air
cooled specimens using the Vickers Pyramid Hardness Testing machine
according with BS 427 - Part 1, 1961, in the 30 Kg load range. About
eight to ten measurements were carried out for each specimen and their
average reported.

4.7. Precipitates Separation

As described in Appendix 2 it was considered that the electrolytic
methods of separation were superior to the chemical methods and
between them the sodium citrate cell was adopted.

The extraction cells consisted of a D.C. supply with three
channels to which the specimens were attached as anodes and stainless
steel plates as cathodes. These specimens $\sim$ 3-5 by 9-11 by 40-45 mm,
were previously ground up to 600# emery paper, washed in 6N HCl for
a few minutes, dried with methanol and weighed with a precision of
tenths of a milligram. The cathodes were surrounded by porous pots to
hold any iron which plated out and fell off. See Figure 4.3

The electrolyte solution consisted of an aqueous solution of
5% sodium citrate and 2% potassium bromide. Its volume was over
700 mls to compensate for evaporation and saturation and in this way
improve the dissolution performance. The levels of solution in the
porous pots were kept $\sim$ 2 cm below that for the rest of the cell.

The reason is that, during extraction the catholyte becomes increasingly alkaline due to the H_2 evolution and consequently the remaining hydroxil ions are likely to diffuse out of the porous pots and precipitate Fe $(OH)_3$ on the extracts which is not desirable. Then, this low volume of catholyte solution avoids this, favouring the diffusion of electrolyte solution into the porous pots.

The initial current density applied in every case was 0.05 amps/cm^2. The time of extraction varied between 15 - 20 hours to dissolve 20 - 25 grams of sample.

After dissolution, the extracts were washed in hot with 6N HCL to dissolve any iron compounds remaining. Centrifuged/ separated/washed/centrifuged several times until a clear solution was obtained. Then transferred into a glass beaker washed in H_2O plus methanol to speed up the drying stage. The dried extracts were weighed with high precision and stored in a desiccator.

Several pitfalls can occur using this extraction technique. The electrolyte must be rigorously stirred to ensure that the precipitates do not adhere to the specimen creating local polariza- tion and pitting. The catholyte level gradually increases which can enhance the diffusion of hydroxil ions into the anolyte. Regularly some of this catholyte should be siphoned out to counteract this. The surface area of the specimen decreases during extraction so the current passing through should be reduced to maintain the current density constant.

4.8. X-Ray Analysis

The particles extracted electrolytically were studied using the X-ray Diffractometer instead of the Debye Scherrer camera in

order to obtain not only the identification and accurate lattice parameter of the phases present but also to measure their particle size.

4.8.1. Identification of Phases

These were carried out scanning the low Bragg angles at 1 degree 2θ per minute, from 20 to 120 degrees. Using the J.C.P.D.S. Powder Diffraction Files and Index, the peaks obtained were identified. In most of the cases only the peaks of the Nb C_x N_y were detected, however, in a few of them the peaks of Fe_3 Cl and BrK were detected.

A Co radiation was chosen for this in order to minimize fluorescence of the sample. An emission power of 40KV and 28 mA were the set conditions.

4.8.2. Accurate Lattice Parameter Measurements

This implies the accurate determination of the interplanar spacing 'd'. At large Bragg angles θ^o is very sensitive to small changes in 'd'. Therefore this can be shown considering the Bragg equation for diffraction:

$$n\lambda = 2 d \ \text{Sin} \ \theta \qquad \dots\dots\dots(4.7)$$

where

$$n = \text{Integer}$$
$$\lambda = \text{Wavelength of irradiating X-rays}$$
$$d = \text{Interplanar spacing}$$
$$\theta = \text{Bragg angle}$$

Differentiating this equation:

$$\frac{n\lambda}{2d} = \frac{\Delta d}{\Delta \theta} \ \text{Cos} \ \theta \qquad \dots\dots\dots(4.8)$$

Combining (4.7) and (4.8):

$$\frac{\Delta d}{\Delta \Theta} = \frac{Sin \ \Theta}{Cos \ \Theta} = tan \ \Theta$$

$$\Delta d = \Delta \Theta \ tan \ \Theta \qquad \qquad \dots \dots (4.9)$$

As Θ tends to 90°, tan Θ tends to infinity. Thus a small change in 'd', at high values of Θ, produces a large change in Θ. Therefore the accurate lattice parameter measurements were carried out scanning the peaks between 100 to 160 degrees.

Resolution rather than intensity was important in these measurements and consequently, a small receiving slit (0.2mm) was used.

The Diffractometer was aligned to within $\frac{1}{2}$ minute using a silver standard. The angular positions of at least three peaks were determined by scanning at rates such as $1/4^{o}$/minute, $1/8^{o}$/minute and step scanning 0.05^{o}/10 minutes. The slow rates were used in the case of samples with small volume fraction of precipitates where the peaks at faster rates showed too much background noise.

The lines used were:

h	k	l	d
4	0	0	1.1170
3	3	1	1.0250
4	2	0	0.9994
4	2	2	0.9124

The lattice parameter was determined for each line where the peaks of $K_{\alpha 1}$ and $K_{\alpha 2}$ were resolvable. The accurate value of 'a' was obtained by extrapolation using a least square fit and plotting

against $\cos^2 \Theta$. A weighting factor was adopted to compensate for the 'a' values of $K_{\alpha 2}$. Usually the use of tan Θ is accepted for this, with the $K_{\alpha 1}$ value given twice the value of $K_{\alpha 2}$. A computer program was written for this purpose, see Appendix 3.

4.8.3. Particle Size Determination

It is possible to determine particle size through X-ray Diffraction when the crystal sizes are less than about 10^{-5} cm = 1000Å, which cause line broadening and its extent is related to the particle size through the Scherrer formula, Cullity (1967):

$$B = \frac{K \quad \lambda}{D \quad \text{Cos } \Theta} \qquad \dots \dots (4.10)$$

where: B = broadening of diffraction line measured
at half its maximum intensity (radius)

K = shape factor, 0.7 - 1.7, generally used as 0.9

λ = wavelength of irradiating X-rays

D = average diameter of particle

But B refers only to the extra breadth or broadening due to particle size effect alone. This means that B is essentially zero when the particle size exceeds 1000 Å. They are related through the Warren relationship, Cullity (1967):

$$\dots \dots (4.11)$$
$$B^2 = B_M^2 - B_S^2$$

where: B_M = is the measured breadth at half maximum
intensity of the sample under investigation
which has less than 1000 Å particle size.

B_S = is the measured breadth, at half maximum
intensity of a standard more than 1000 Å
particle size.

This is true assuming that the diffraction line has the shape of a Gaussian Distribution.

Corrections for instrumental broadening have to be considered in order to have a pure diffraction profile from the sample. Therefore, allowances for α_1 and α_2 broadening effects have to be taken into account. There is a relationship between d^1/B_{So} (or d^1/B_{Mo}) and B_S/B_{So} (or B_M/B_{Mo}) for different types of line profiles where:

d^1 = angular separation of α_1 and α_2

B_{So} = unresolved line breadth of the coarse powder profile

B_{Mo} = unresolved line breadth of the fine powder profile.

The relationship for the Gaussian case is shown in Fig. 4.4.

Therefore to determine the particle size, d^1 has to be calculated through the relation:

$$d^1 = |\Theta_2 - \Theta_1| = \frac{(\lambda_2 - \lambda_1)}{\lambda_{av}} \cdot 360 \cdot \tan \Theta_{av} \cdot 2 \qquad \ldots\ldots(4.12)$$

where: $\Theta_2 - \Theta_1$ = are in $^\circ 2\Theta$

Θ_{av} = is in $^\circ \Theta$

From the profiles B_{So} and B_{Mo}, coarse and fine powders, are measured and from Fig. 4.5 using $d^1|B_{So}$ and $d^1|B_{Mo}$, B_S and B_M can be found. These values now can be used in Eq. (4.11) and the result in Eq. (4.10) to obtain the particle size. Pure niobium carbonitride annealed at $1300^\circ C$ for 3 hours was used as standard coarse particles.

4.9. Chemical Analysis

The residues after extraction and X-ray examination were analysed for C, N, Nb, S, Si, Mn and Fe. The procedure followed for each element is described below.

4.9.1. Carbon and Sulphur Analysis

This was carried out simultaneously using the Leco CS-244 C & S determinator. In this case the powder is combusted in a flowing oxygen stream and the products of combustion i.e. CO_2 and SO_2 from the sample are measured by infra red detectors. The detector output is amplified, integrated, linearised and displayed directly as a percentage of C & S. The amount of residue used was 0.010gr plus 1 gr addition of a standard of known C & S content plus a flux which helped in the melting of the mixture.

4.9.2. Nitrogen Analysis

The nitrogen analysis in the residues was carried out using the Leco TC - 36 nitrogen and oxygen determinator. Here the sample is fused in a graphite crucible in an electrode furnace and helium, the carrier gas, transfers the released oxygen and nitrogen to the detector for measurement by thermal conductivity. The detector output is amplified, integrated, linearised and displayed directly in parts per million (ppm) of nitrogen and oxygen. In this case the readings for oxygen are not of use due to the nature of the sample.

4.9.3. Mobile Nitrogen Analysis

The equipment used in this case was the Polaron Mobile Nitrogen Analyzer CA700, which relies on the release and measurement of interstitial nitrogen by heating steel turnings of millings at selected temperature, in this case $400^{\circ}C$, in a stream of high purity hydrogen. The free nitrogen in these conditions is released from the steel as ammonia which is monitored continuously using an ammonium ion selective electrode. The content of Free N is obtained

using the calibration graph for this equipment to convert the mv reading into ug/ml and using the following equation:

$$\% \text{ Free Nitrogen} = (a - b) \times c \times 10^{-4}$$

where   a = final concentration of solution for sample (ug/ml)

b = final concentration of solution for blank (ug/ml)

c = final volume of solution after absorption period (ml).

4.9.4. Nb, Mn, Fe and Si

Nb, Mn and Fe were analysed using the Atomic Absorption Spectrophotometer. The methods used for each element are described by Thomerson (1971) and Whiteside-Milner (1981).

Si, was analysed through the gravimetric method described in BS Handbook No. 19 (1970).

For all these analyses 10 mg of residue was used with some duplicate analysis.

4.10. Electron Microscopy

To complement the information obtained through X-ray diffraction specifically to detect precipitation of Nb C_x N_y, during the roughing stages, direct examination of the precipitate particles was carried out using thin foils. For this, the specimens had to be machined down to 3mm ϕ rods.

Due to the complexity of the matrix, martensite and bainite structures, the particles had to be directly illuminated using dark field technique to identify them from the often heavily dislocated background.

The size distributions of the Nb C_x N_y particles were measured

for some slabs using carbon extraction replicas. These were prepared by polishing specimens following standard techniques, etching for 20 seconds in 2% nital, applying in vacuum the layer of carbon, scratching transversal and longitudinal lines 3mm apart across on this surface, etching again for 60 - 90 seconds in 10% nital to float the replicas in distilled water and collect them in copper grids. They were observed in the TEM 301 and photographs taken. The negatives were printed on special thin photographic paper and the particles measured using the Zeiss Particle Size Analyzer TCZ 3. Around 500 particles were measured in each case. In some cases it was necessary to use the STEM 400 to differentiate cuboid particles through microanalysis.

4.11. Mechanical Properties

Tensile and Charpy V-notch impact tests were carried out following the standards BS 18: Part 2: 1971 and BS 131: Part 2: 1972 respectively.

The specimens for these tests were obtained from air cooled slabs of steels, 97, 99, 22 and 23 as shown in Fig. 4.5. The thermo-mechanical treatments for these steels were carried out following rolling schedules 2, reheating at 1200°C (steels 97 and 99) 1300°C (steels 22 and 23) for 45 and 90 minutes respectively; rolling at 1100 and 900°C with 33 and 25% reduction, then air cooled.

C H A P T E R   5

THERMODYNAMIC MODEL

5.1. Introduction

This model was developed in order to cover the lack of a consistent
solubility product equation for niobium carbonitrides, incorporating the
principles of mutual solid solubility of niobium carbides with niobium
nitrides as well as their nonstoichiometric structures.

The principles of the model as well as its mathematical solution
are described with some detail. The solution temperatures, T_s, and
the $Nb C_x N_y$ composition variation for steels 97, 99, 22 and 23 are
predicted, as a function of temperature. To assess the versatility
of the model the experimental steel compositions of Mori et al (1968)
and Hoesch-Estel (1981) were input and these results compared with
their experimental ones. The model predictions and the experimental
results are critically examined, recognizing the limitations of the
model as well as of practical results.

The influence of Mn and Si have also been evaluated through
the use of the few interaction parameters available ε_C^{Mi}, ε_N^{Mi}
and calculating the ε_{Nb}^{Mi} from Koyama et al (1971a,b) equations.

5.2. Fundamentals of the Model

As reviewed extensively in Chapter 2, niobium carbide and
niobium nitride have been well recognised to have defect structures.
Both nitrides and carbides exist over a wide range of compositions
and appreciable vacancy concentration can exist on the non-metal lattice

sites. Most of the experimental data suggest that the nonstoichio-
metry ratio or (C + N)/Nb atom ratio lies around 0.87, therefore its
average composition can be written as $Nb\ C_x\ N_{(0.87\ -\ x)}$.

On the other hand, the carbonitride $Nb\ C_x\ N_{(0.87\ -\ x)}$ is assumed
as an ideal mixture of δ-$NbC_{0.87}$ and δ-$NbN_{0.87}$ so that their activities
in the carbonitride could be set equal to their concentrations x /0.87
and $(0.87 - x)/0.87$.

The Free Energy of formation for the carbonitride varies
linearly with x from the pure carbide to the pure nitride. The entropy
of mixing of C + N in the carbonitride is taken into account but their
enthalpy of mixing in the carbonitride and their entropy of mixing in
the matrix are both assumed to be zero because they are probably insig-
nificant, Hudd et al (1971).

Therefore, through a mass balance in the system Fe-Nb-C-N given
in Fig. 2.17, the following equations are proposed:

$$C_T\ =\ (1 - \emptyset)\ [C] + \emptyset\ \frac{x}{1 + x + y} \qquad \ldots\ldots(5.1)$$

$$N_T\ =\ (1 - \emptyset)\ [N] + \emptyset\ \frac{y}{1 + x + y} \qquad \ldots\ldots(5.2)$$

$$Nb_T\ =\ (1 - \emptyset)\ [Nb] + \emptyset\ \frac{1}{1 + x + y} \qquad \ldots\ldots(5.3)$$

where: C_T, N_T and Nb_T are the total carbon, nitrogen and niobium

[C]   [N]   [Nb] are in solution in austenite

$\emptyset$, mol fraction of precipitate

x, C/Nb atom ratio

y, N/Nb atom ratio

From the previous assumption for x + y = 0.87 and eliminating $\emptyset$, the

following equations are obtained:

$$\frac{C_T - [C]}{Nb_T - [Nb]} = \frac{\frac{x}{1.87} - [C]}{\frac{1}{1.87} - [Nb]} \qquad \dots\dots\dots(5.4)$$

$$\frac{N_T - [N]}{Nb_T - [Nb]} = \frac{\frac{(0.87 - x)}{1.87} - [N]}{\frac{1}{1.87} - [Nb]} \qquad \dots\dots\dots(5.5)$$

Similar equations were proposed by Lakshmanan (1977), but unfortunately they were not correct.

To solve the unknowns [C], [N], [Nb] and x, two more equations relating these four variables are necessary. The solubility products, for the $NbC_{0.87}$ and $NbN_{0.87}$ formation, under the ideality assumption can be written as:

$$K_C' = \frac{[Nb] [C]^{0.87}}{x/0.87} \qquad \dots\dots\dots(5.6)$$

$$K_N' = \frac{[Nb] [N]^{0.87}}{(0.87 - x)/0.87} \qquad \dots\dots\dots(5.7)$$

where: $x/0.87$ and $(0.87 - x)/0.87$ represent the activity term for the $Nb\,C_x$ and $Nb\,N_{(0.87 - x)}$ respectively, given by their concentrations.

The solubility product $K'_{C,N}$ and the Free Energy of formation, ΔG^o_T for the reaction:

$$[Nb] + x [C] + (0.87 - x) [N] \rightleftharpoons Nb\,C_x\,N_{(0.87-x)} \qquad \dots\dots\dots(5.8)$$
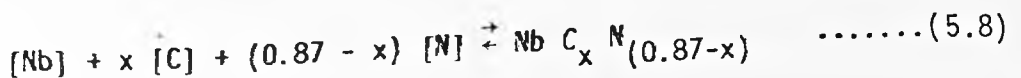
will be given by Eq. (2.8) and (2.14) given in Chapter 2.

Therefore using equations (5.4) to (5.7) or (5.4) and (5.5) with (2.8) they were solved graphically and through an iterative method which is described next.

5.3. Mathematical Solution

Equations (5.4) to (5.7) were reduced to two by substitutions to get them as a function of [Nb] and x, the C/Nb atom ratio. A computer program was written to solve these two equations through iteration, using the C05NAF Fortran subroutine of the NAG library given by Powell (1968). This subroutine finds the solution of N non linear equations in the form:

$$\underline{R} (\underline{X}) = \underline{0}, \text{ where } \underline{X} = (x_1, x_2, x_3 \ldots x_N)^T \quad \ldots\ldots\ldots(5.9)$$

This is a hybrid technique which combines the Newton and steepest descent methods in such a way as to give a steady progress and a fast rate of convergence. For further details the reader is referred to the files of the NAG library - zeros of one or more transcendental equations. The main program is given in Appendix 4.

The values for K'_C and K'_N were taken as the ones given by Mori et al (1968) and Lakshmanan (1977). To find the effects of Mn and Si, K''_C and K''_N were calculated using the interaction parameters for C and N given in Table 2.11 and for Nb calculating from Koyama et al's (1971a,b) equations, given in Table 2.10.

5.4. Results and Discussion

5.4.1. The Fe-Nb-C-N System

Along with the calculations of soluble C, N, Nb and x, the C/Nb atom ratio, the Nb $C_x N_{(0.87-x)}$ volume fraction, composition

and Free Energy of formation are also calculated as a function of temperature, for steels 97, 99, 22 and 23. These results are given in Table 5.1, and plotted in Figs. 5.1 a,b,c, 5.2, 5.3 and 5.4. The reasons for having values above the solution temperatures are due to the method used to solve the equations A = B and C = D, where the residuals of A - B and C - D are attempted to tend to zero with a precision set in this case to 10^{-14}. For these equations the CO5NAF subroutine will always find a solution regardless of the total imputs of carbon, nitrogen, and niobium, TC, TN and TNb respectively. Therefore as observed graphically these values are only valid up to the solution temperatures.

In order to compare the model predictions for Nb C_x $N_{(0.87-x)}$ composition as a function of temperature, with practical results, the steel compositions given by Mori et al (1968) and Hoesch-Estel (1981) where imput into the model and the results given as the mole ratio of N/(C + N) in the carbonitride, are plotted as broken lines in Figs. 5.5, 5.6 and 5.7.

The solubility temperatures and the niobium carbonitride compositions obtained as a function of temperature will be discussed in detail.

5.4.1.1. Solution Temperatures

The solubility temperatures, T_s, obtained from the model for steels 97, 99, 22 and 23 are: 1133, 1160, 1235 & 1315° respectively which are obtained from the intercept of the total contents in C, N and Nb lines with their curves of solubility, as a function of temperature or the intercept of the volume fraction lines with the temperature axis, indicating total dissolution, see Figs. 5.1 and 5.3.

These results compared with the ones obtained using the last five authors' equations in Table 5.2, which consider Nb, C and N, are in fair agreement, except for the results obtained with Mandry and Dornelas (1966) and Yamamoto et al's (1981) equations, which predict the lowest and highest T_s respectively than the average T_s obtained with the other equations and the model. On the other hand the predictions for steel 23 differ considerably. Although most of the equations predict a Ts more than $1300^{\circ}C$, this would be $\sim 1325^{\circ}C$ as deduced from experimental results. Through accurate chemical analysis of extracts it was found $\sim 5\%$ of the total Nb content was undissolved when reheated at $1300^{\circ}C$ for 90 minutes. This means that the predictions of Mandry and Dornelas, Meyer and Yamamoto et als' equations can be discarded, considering only the predictions of Irvine et al and Mori et al.

As far as steels of Hoesch-Estel are concerned, the T_s temperatures calculated through those last five equations, the model and their experimental results are compared in Table 5.3. There can be seen the very close agreement between the model predictions and the T_s obtained experimentally, especially for steels HE1 and HE5. Irvine et al's and Yamamoto et al's equations prediction are the next closest ones to the model predictions and experimental results. The T_s for steel HE4, predicted for most of the equations is greater than the one obtained experimentally which could suggest some experimental errors.

5.4.1.2. <u>Niobium Carbonitrides Compositions</u>

As observed in the experimental data given by Mori et al (1968) and Hoesch-Estel (1981) continuous lines in Figs. 5.5 , 5.6 and 5.7 respectively, the N/(C + N) mole ratio increases as the temperature

increases. According to Hoesch-Estel data this ratio increases rapidly near the solution temperature of the steel while according to Mori's data this increment is less pronounced.

As far as the model predictions are concerned, this agrees very well for steels CN1, CN5 and CN6, up to 1200°C while for steel CN3 the prediction is the opposite to the one found experimentally by Mori et al. In the case of Hoesch-Estel data a fair agreement is obtained with steels HE4 and HE5 also up to 1200°C, whereas with steels HE1, HE2 and HE3 the opposite trends to the ones obtained experimentally are predicted. In Figs. 5.5.a, 5.6.a and 5.7a the model predictions are drawn with broken lines.

Considering steels 97, 99, 22 and 23 of this project, the model predicts a decreasing N/(N + C) ratio as can be seen in Figure 5.2.

Under this situation a systematic investigation was carried out to correlate the steel compositions with these different behaviours in the N/(C + N) mole ratio predictions. It was found that the common factor for the steels for which the model predicts the right trends of that obtained experimentally, is in their Nb/(C + N) mole ratio more than 0.58. Less than this value the predictions are the opposite to those obtained experimentally. These ratios can be seen in Table 5.4 and compared in Figs. 5.2, 5.5.a, 5.6.a and 5.7.a.

Also from this correlation it would appear that the agreement is closer if this ratio lies around 0.6 as shown for steels CN1 and HE5 and less close if this ratio is greater than 1.0 as in the cases of steels CN6 and HE4. However, more data would be needed to make this correlation more precise.

This analysis on the other hand also shows that the model in

itself depends on the solubility product equations chosen and these could be applicable only to certain steel compositions, depending on their absolute contents in Nb, C, N as well as on their Nb/(C + N) mole ratios. The equations chosen for K_C' of Mori et al (1968) agrees reasonably well with the other equations available for K_C', whereas the K_N' chosen from Lakshmanan (1977) is the only one available for the nonstocihiometric Nb $N_{0.87}$ and has an enthalpy term greater than the other equations for NbN. Thus, the use of this relationship means a relatively greater amount of nitrides than carbides in the carbonitrides are dissolving as the temperature increases, which could be particularly sensitive the lower the Nb/(C + N) mole ratio in the steel.

Although the Nb/(C + N) mole ratio and their absolute contents of Nb C and N of a steel, will have a large influence on the composition of the carbonitrides, the disagreement between the model predictions and the experimental data, that is, N/(C + N) increasing as the temperature increases, regardless of the steel compositions, turned our attention to investigate the assumptions made earlier to establish the model.

i) The nonstoichiometry configuration of $NbC_{0.87}$ and $NbN_{0.87}$, assumed for simplicity may not be accurate. As reviewed in Chapter 2, the niobium nitrides tend to be less nonstoichiometric than the carbides which approximates to the carbonitrides. This means that the entropy change is not symmetric as assumed and will be greater for the nitride dissolving in the carbonitride than the carbide dissolving in it. This will offset the entropy change for solution in the matrix or lead to less sensitivity to temperature and proportionately give a greater effect than for the carbide. Besides the fixed nonstoichiometry of 0.87 for the carbonitride will be changing as the temperature increases due to the increased amount of vacancies, offsetting even more the entropy change.

ii)   Also, as the temperature increases, the activity of the carbides and nitrides will go towards ideality. That is in equations (5.6) and (5.7) the activity terms for the $NbC_{0.87}$ and $NbN_{0.87}$ would have to be expressed as a function of temperature for which a more complex function will be needed. That is:

$$K'_C = \frac{[C]^{0.87}[Nb]}{a_{NbC_{0.87}}} = f(T) \qquad \ldots\ldots(5.10)$$

$$K'_N = \frac{[N]^{0.87}[Nb]}{a_{NbN_{0.87}}} = f(T) \qquad \ldots\ldots(5.11)$$

(iii) The little evidence for $Ti\,C_x\,N_y$ suggests the tendency of separation between $Ti\,C_x$ and $Ti\,N_y$. In the Fe-Cr-Ni base steels are frequently found to be the two-phase Ti (C, N) and Ti (N, C), with lattice spacings mutually approaching but without solution having been attained. These two phases can be extracted from a steel at different C/N ratios and lattice spacing ranges. If this would be the case here, it could be reflecting positive deviation from Raoult's Law for the entropy of mixing of the $Nb\,C_x\,N_y$.

The above observations lead us to conclude that a lower temperature dependence term in the K'_N equation was needed. As this is not available for a nonstoichiometric nitride, the following trials were carried out:

Trial 1

Changing the temperature dependence of the nitride solubility product equation towards similarity with the carbide but keeping equivalent stability, i.e. the B term in the equation:

$$\log [Nb][N]^{0.87} = A + B/T = 4.41 - 10341./T \qquad \ldots\ldots(5.12)$$

was made equal to the of the carbide solubility product,

$$\log [Nb] [C]^{0.87} = A + B/T = 3.18 - 7700/T \qquad \ldots\ldots(5.13)$$

and a

new value for A was calculated to keep the same stability at $1150^{\circ}C$.
The results of this trial for steels 97 and 99 are given in Figs.
5.8 a.b.c. 5.9, 5.10, 5.11.   From these figures the following

features can be observed:

- The solution temperatures, Ts, are virtually unaffected
  because both are near $1150^{\circ}C$ which was chosen as for equal
  stability from eqs. (5.12) and (5.13).   If another tempera-
  ture had been chosen, for equal stability, the solution
  temperatures for these steels would have changed.

- The N/(N + C) ratio in $Nb\ C_x\ N_{(0.87-x)}$ now increases
  as the temperature is increased, which is in the same
  trend as found experimentally, given in Chapter 6, and
  in agreement with the results of Mori et al (1968) and
  Hoesch-Estel (1981).

  The same trial was carried out with the steels of Mori et al
and Hoesch-Estel and the predictions drawn in Figs. 5.5.b, 5.6.b and 5.7.b
with chain lines

  A very close agreement for all the steels CN and HE is now
obtained up to 50 - $100^{\circ}C$ below its solution temperature, where
sudden increase in the N/(C + N) ratio is observed experimentally
in steels HE but the model is not able to predict this.

  Thus these results then show the possibility that, regardless
of the steel composition, a nonstoichiometric ratio in the carbonitride
changing as a function of temperature, as well as a nonsymmetric entropy
of mixing between the $Nb\ C_x$ and $Nb\ N_y$, needs to be considered.   The
activity terms for $Nb\ C_x$ and $Nb\ N_y$ in equs. (5.10) (5.11) also would

have to be expressed as a function of temperature if a closer prediction to experimental results is to be obtained.

From the adjustment in the temperature dependence term for Trial 1 and considering the likely errors that could be involved in the determination of the solubility products, a second trial was carried out by increasing the stability of K'_N of Trial 1 as follows:

Trial 2

Maintaining the same temperature dependence as in Trial 1, but increasing the stability of the nitride 1.5 times i.e. the A term in eq. (5.12) was made x 1.5 lower than the previous value in Trial 1. In this case the same stability is kept at $872^{\circ}C$ compared with the original equation. The results of this Trial are given in Figs. 5.12. a.b.c, 5.13, 5.14 and 5.15.

From these figures the following features can be observed:

- The solution temperatures for both steels were increased by as much as $50^{\circ}C$ for steel 97 and $80^{\circ}C$ for steel 99 compared with the initial and Trial 1 predictions.

- The N/(N + C) ratio is very high for steel 99 keeping an amount nearly constant of 72% from $900^{\circ}C$ to its solution temperature, $1240^{\circ}C$. This ratio, for steel 97 however increases relatively more steeply from 48% at $900^{\circ}C$ to 56% at the solution temperature of $1180^{\circ}C$.

This trial was also carried out for the steels of Mori et al and Hoesch-Estel and the model predictions are the same as in Trial 1, except for the increased amounts of N in the carbonitrides.

In relatively small variations in the N/(C + N) ratio indicate that the errors likely to occur in the determination of the solubility products would not account for the experimentally observed variation of

N/(C + N) as a function of temperature. But this will only stress the greater entropy change for the nitride dissolving in the carbonitride making the carbonitrides less temperature sensitive as can be observed in Fig. 5.13 where the N/(C + N) is kept fairly constant for steel 99.

To further assess the effects on the entropy change, the log $K'_{C,N}$ vs 1/T is shown in Fig. 5.16 with the lines for several x values. On these lines the log $K'_{C,N}$ for steels 97, 99 and CN1 is plotted. From this it can be observed that these generated curves do not have a pronounced maximum and so a small variation in the entropy term, the maximum of these curves will be shifted dramatically changing consequently the proportions of C and N in the carbonitride as well as their solution temperatures. However this would not account as much for the sharp increase of N/(C + N) in the carbonitride closer to the solution temperature. Therefore to finally assess this sudden increase a third trial was carried out.

Trial 3

By assuming that dissolution occurs only with the $NbC_{0.87}$ at temperatures closer to the solution temperature, i.e. with the initial composition of steel 99, and the initial solubility product equations, the solution temperature, Ts and the C/Nb ratio, x, were obtained. Below Ts, $\sim 10°C$, the amount of N left to be dissolved was assumed to result from precipitates of pure $NbN_{0.87}$. The amount of Nb corresponding to this compound was subtracted from the total and the new composition was imput to calculate the new Ts and x keeping the C content constant. This procedure was repeated again three times and the results are given in Table 5.5. There it can be seen that the drastic change does not occur even with this artificial increase in the stability of the nitrides.

Although the limitations of the assumptions made in this model have been considered, the last two trials indicate that even with the extreme conditions, considering pure nitrides closer to the solution temperatures, the model does not predict a sharp increase in the N/(C + N) ratio as observed in the data of Hoesch-Estel. However from the solubility product equations available and previous comments on the lower temperature dependence of the carbonitrides it is difficult to believe this sharp increase. This could imply experimental errors which are understandable considering the difficulty in measuring small amounts of carbonitrides. Unfortunately this data has not been published by the authors and the technique they used to determine their results is not known. On the other hand, the results of Mori et al, obtained through accurate chemical analysis and lattice parameter measurements of extracts, do not show this sharp increase. Although their measurements did not go up to the solution temperatures of most of their steels, steel CN1 was closer and found to behave in a similar way to their other steels. An alternative explanation could be that possible clustering associated with positive deviation from ideality is eliminated cooperatively as temperature increases, leading to a more rapid increase in the N content in the carbonitrides when the final solution temperature is approached.

5.4.2. System Fe-Nb - C - N - Mn - Si

The effects of the alloying elements Mn and Si on the solubility temperature and composition of the Nb $C_x N_{(0.87 - x)}$ were evaluated with K''_C and K''_N calculated using the interaction parameters ε_C^{Mi} and ε_N^{Mi} given in Table 2.11, last entry. The interaction parameter for niobium, ε_{Nb}^{Mi}, however, is very scarce and the values calculated by

Lakshmanan (1977) for ε_{Nb}^{Si} and ε_{Nb}^{Mn} appear to be wrong. Therefore using the equations of Koyama et al, converted to mol fraction and natural logarithm, the interaction parameters given in Table 2.11, ε_{Nb}^{Si} and ε_{Nb}^{Mn} were calculated by averaging the values obtained from the carbides and nitrides equations of Koyama et al (1971a,b). And so the calculated values for the interaction parameters ε_{Nb}^{Si}, ε_{Nb}^{Mn} are:

$$\varepsilon_{Nb}^{Si} = 98.9 - \frac{185087.2}{T} \qquad \ldots\ldots\ldots(5.14)$$

$$\varepsilon_{Nb}^{Mn} = -182.9 + \frac{291186.1}{T} \qquad \ldots\ldots\ldots(5.15)$$

With these values ε_{Nb}^{Mi}, ε_{C}^{Mi}, ε_{N}^{Mi} corrected by nonstoichiometry and using the previous equation of Mori et al (1968) K'_C and Lakshmanan (1977) K'_N for the nonstoichiometric carbides and nitrides the following expressions were obtained:

$$K''_C = \exp(2.3026 \times (-0.200-7700/T) + (40.71 - \frac{70855.9}{T}) [Si] +$$

$$\ldots\ldots\ldots(5.16)$$

$$(\frac{286775.1}{T} - 182.9) [Mn])$$

$$K''_N = \exp(2.3026 \times (0.9717 - 10340.6/T) + (68.45 - \frac{134888.2}{T})[Si] +$$

$$\ldots\ldots\ldots(5.17)$$

$$(\frac{272916}{T} - 175.8) [Mn])$$

The quadratic terms in Mn were neglected due to its small effect. Concentrations given in mol fractions.

Using these two equations the effects of Mn and Si were calculated with the computer model described before.

The results are given in Tables 5.6 and 5.7 and Figs.5.17 and 5.18.

Note the relatively large effect of manganese on the solubility temperatures compared with silicon in steel 97. Manganese decreases the solubility temperature from $1133^{\circ}C$, predicted by the model when no additions of Mn or Si are considered, to $1100^{\circ}C$ when 1.3% Mn are added with no Si. Silicon increases the solubility temperature from $1133^{\circ}C$ to $1143^{\circ}C$ when 0.29% Si is added with no Mn. Therefore, the resultant solubility temperature for steel 97 decreases from $1133^{\circ}C$ to $1110^{\circ}C$ when its Mn and Si contents are taken into account. For steel 99, Ts decreases from $1160^{\circ}C$ to $1144^{\circ}C$ when their respective Si and Mn are considered.

From these results in steel 97, it is clear that Mn has an overall larger effect than Si, because it decreases the solubility temperatures of niobium carbonitrides by $\sim 25^{\circ}C$ for each 1wt% of Mn. This is consistent with the effects on the activities of C, N and Nb which are reduced by manganese, thus a higher concentration of Nb, C and N is required in solution to keep constant the equilibrium at a given temperature. This means that the solubility temperature will be lower.

Silicon on the other hand increases the solution temperature by increasing the activity of carbon. But this is offset by the reverse effect of Si on Nb and N which reduces their activity. Therefore the increased Ts is less than expected.

The agreement of these results with practical observations indicates the prospective usefulness of this model, to be tested with more complex systems such as stainless or tool steels.

CHAPTER   6

EXPERIMENTAL RESULTS

6.1.   Reheated Austenite Grain Size

6.1.1.   Influence of Temperature

The austenite grain size variations with reheating temperature
for 1 hour of steels 97, 99, 21 and 22 are given in Fig. 6.1.a. It
can be observed that the largest γ grain size for a given temperature
corresponds to steel 97 with the opposite effect shown by steel 22.
Abnormal grain growth occurs at ∿ 1110°C for steels 97 and 99 and at
∿ 1210°C for steel 22 and 1260°C for steel 23.

6.1.2.   Influence of Time

The results of the austenite grain size variations with
reheating time at 1100, 1200°C for steels 97, 99 and 1200, 1300°C for
steels 22 and 23 are shown in Fig. 6.2.a. At 1200°C, the variation of
γ g.s. with time is greater for steel 97 > 99 > 22 > 23. Abnormal
grain growth is shown for steels 97 and 99 after about 45 minutes
reheating at 1200°C, and for steels 22 and 23 this starts after
45 and 75 minutes respectively, on reheating at 1300°C. Abnormal
grain growth was not detected at 1100°C for steels 97 and 99 and at
1200°C for steels 22 and 23 for the times experienced. Typical
microstructures are shown in Figs. 6.1.b. and 6.2.b.

6.2.   Solution Temperatures

At the beginning of this project, in order to know the range
of reheating temperatures at which the NbC_xN_y is in solution in the

four steels, calculations of the solubility temperatures were carried
out using the available solubility equations gathered together in Tables
2.6, 2.7 and 2.8. The results are given in Table 5.2. Note the large
difference in solubility temperatures $\sim 230^{o}C$ for NbC_x, $\sim 56^{o}C$ for
NbN_y and $\sim 130^{o}C$ for NbC_xN_y, between all the calculated values.
Although the equations more often used are the ones of Nordberg and
Aronsson (1968) for carbides, method D4, Smith's (1966) for nitrides
and Irvine et al's for the Nb (C + 12/14N) phase, they would not be
representing the phases present in reality.

On the other hand the thermodynamic model proposed in the
previous Chapter predicts solution temperatures of $1133^{o}C$, $1160^{o}C$,
$1235^{o}C$ and $1315^{o}C$ for steels 97, 99, 22 and 23 respectively.

6.3. Rolling Schedules

Most of the experiments were carried out through a two pass
rolling schedule, derived from a single pass schedule to give rapid
and complete recrystallization after the first pass and slow or non
recrystallization after the second. Some specimens were one end quenched.
A schematic representation of these two schedules is given in
Figures 6.3 and 6.4.

6.3.1. Rolling Temperatures

Rolling temperatures were 1050, 1000, 950 and $900^{o}C$ for the
single pass rolling schedules of steels 97 and 99. In the case of
the two pass rolling schedules, $1100^{o}C$, was the first pass rolling
temperature for all the steels and 950, 925, 900, 850, $800^{o}C$ for
the second pass of steels 97 and 99. The second pass for steels
22 and 23 were at 1000, 950, 900 $850^{o}C$. The actual rolling tempera-
tures are given in Tables 6.1, 6.2 and 6.3.

6.3.2. Strains

These were kept constant in every case. The single pass rolling reduction was $\varepsilon = 0.33$ (25%), finishing as slabs of 12.8 mm thick. In the two pass schedule the strain was kept to $\varepsilon = 0.46$ (33%), for the first pass and $\varepsilon = 0.33$ (25%) for the second one, all of them finishing with slabs 12.8 mm thick. The true strains were calculated assuming a plane strain condition by:

$$\varepsilon = \frac{2}{\sqrt{3}} \ell n \frac{(100)}{(100 - R)} \qquad \ldots\ldots\ldots(6.1)$$

where R = % of reduction in thickness

6.3.3. Strain Rates

These were kept constant at 4.20 sec^{-1} in all the rolling conditions. This was calculated through the relationship given by Larke (1967) for strip rolling:

$$\frac{\cdot}{\varepsilon} = V\left(\frac{2}{D (ho - h_f)}\right)^{\frac{1}{2}} \varepsilon \qquad \ldots\ldots\ldots(6.2)$$

where: v = is the peripheral roll speed calculated through
           eq. (4.1) given in Chapter 4, 219mm/sec.

      D = roll diameter 139 mm

      ho = initial thickness

      h_f = final thickness

      ε = true strain calculated through eq. (6.1).

6.3.4. Cooling Rates $\overset{o}{T}$

Cooling rates were obtained in the one end water quenched slabs by following the cooling curve of the thermocouple inserted at the

middle of the slabs and by comparison with the cooling curves at other points of Aℓ- killed slabs of similar geometry, Janampa (1980 - Series I). They agreed closely as can be seen in Fig. 6.5. There-fore from Fig. 6.6, the cooling rate between $875^{0}C$ to $400^{0}C$ has been plotted against distance as shown in Fig. 6.7.

6.3.5. Temperature Distribution in the Slabs

Temperatures were measured directly at several points during rolling. These points and the difference in temperature obtained are given in Fig. 6.8. Note this difference in temperature between both ends of the slabs and their middle is as much as $30^{0}C$.

This difference in temperature was confirmed by load measure-ments and plotting the calculated mean flow stress, $\bar{\sigma}$, vs rolling temperature, Tc, as well as vs length, L, as shown in Fig. 6.9. From this Figure plotting the temperature vs length of the slab, Fig. 6.10 is obtained. Some of the data used to calculate the mean flow stress is given in Table 6.4. The computer program is given in Appendix 5.

From this, 1/5 of the length at each end of the rolled slab in the two pass rolling schedule, was scrapped, See Fig. 4.1.

6.4. Recrystallization Kinetics

6.4.1. Single Pass Rolling Schedule

Although Fig. 6.11 is not a complete diagram to establish the kinetics of recrystallization, it shows the recrystallized fraction vs rolling temperature for steels 97 and 99. Steel 99 shows a slower recrystallization kinetic especially at $1000^{0}C$ where this difference in fraction recrystallized is as much as 30%. In both steels the lower the rolling temperature the lower the recrystallized fraction,

becoming this, 0% at 900°C. Equivalent times of holding at each temperature were calculated using the temperature compensated time for recrystallization equation Whittaker, (1973), and from the cooling curves obtained from the temperature of rolling down to 875°C, the end quenching temperature. These equivalent times were 5s for 1050°C, 2s for 1000°C, 1.5s for 950°C and 0.5s for 900°C.

Steel 12 was found to behave similarly to steel 97.

6.4.2. Two Pass Rolling Schedules

6.4.2.1. Steels 97 and 99

The kinetics of recrystallization for these two steels rolled consecutively, are given in Fig. 6.12. They were found to follow the Avrami type relation as shown in Figs. 6.13 and 6.14, where the slopes of log ($\ln \dfrac{1}{(1 - x)}$) vs logt. can be 0.65 for steel 97 and 0.50 for steel 99 at all temperatures. Note the slower recrystallization kinetics for steel 99 at all temperatures tested especially at 900°C when this difference becomes about 1 order of magnitude. Both steels also show a decrease in the retardation of recrystallization rate at, $\sim$ 850°C, this being similar to that of 900°C. The temperature of the fastest full recrystallization for both steels is 950°C, taking 10^4 seconds for steel 97 and 10^5 seconds for steel 99. See Fig. 6.12. Further details are given in Table 6.3

6.4.2.2. Steels 22 and 23

Their kinetics of recrystallization are given in Fig . 6.15.   Also these steels follow the Avrami type relation shown

in Figs. 6.16 and 6.17. The slopes of the $\ln \left(\dfrac{1}{(1-x)}\right)$ vs time are $\sim$ 0.50 for both steels. Recrystallization in these steels is delayed from as high as $1000^{o}C$ being the slowest for steel 23, by $\sim$ 2 orders of magnitude compared with steel 22 to start recrystallization at $1000^{o}C$.

Full details of the rolling schedules are given in Table 6.3.

6.5. Austenite Grain Sizes

6.5.1. One Pass Schedule

Tables 6.1 and 6.2 show the ranges of recrystallized and non-recrstallized austenite grain sizes obtained in steels 97 and 99 with the general trend showing slightly smaller grains for steel 99.

After rolling at $1050^{o}C$, steel 97 showed 100% recrystallization and 68 μm γ grain size, whereas steel 99 showed 95% recrystallization and 65 μm. For both steels as the rolling temperature decreased the recrystallized fraction decreased and therefore the average grain size became larger. The sizes given, are the square root of the product of the transverse and longitudinal measurements, i.e. g.s. $= \sqrt{a \times b}$

6.5.2. Two Pass Schedule

6.5.2.1. Recrystallized Grain Size

The grain sizes obtained for steels 97, 99, 22 and 23 are given in Table 6.3. It can be observed that the recrystallized grains for steels 97 and 99 after rolling at $1100^{o}C$ and quenching immediately, varied from 65 to 75 μm with a tendency of smaller grains for steel 99. After the $1100^{o}C$ rolling, cooling down to $900^{o}C$ and quenching did not affect the recrystallized grain sizes for these steels.

For steels 22 and 23 however, the resultant recrystallized grains after the $1100^{o}C$ rolling were $\sim$ 70 μm for steel 22 and $\sim$ 50 μm for steel 23.

After the second pass, at different rolling temperatures and different times of annealing, recrystallized grain sizes of 35 to 45 μm were obtained for steel 97 and 30 to 40 μm for steel 99. For steels 22 and 23 the recrystallized grains after their second pass varied from 35 to 40 μm for steel 22 and from 28 to 32 μm for steel 23.

6.5.2.2. Non Recrystallized Grain Size

After the second pass, the non recrystallized austenite grain size average agreed closely to the one calculated at constant volume and under plain strain compression, from a cube reduced 25% in height and enlarged by the same amount in the rolling direction . This can be seen in Table 6.3.

6.6. Precipitation Kinetics

Initially an attempt was made to follow the precipitation kinetics of NbC_xN_y through Hardness measurements and Free Nitrogen Analysis. These and the results obtained through chemical analysis of electrolytically extracted residues are given.

6.6.1. Hardness Measurements

These were carried out in some water quenched and air cooled specimens of steels 97 and 99, after tempering for several lengths of time at $600^\circ C$. The plot of Hardness Hv_{30} vs tempering times at $600^\circ C$ are given in Figs. 6.18 and 6.19 for water quenched slabs. The hardness Hv_{30} , after 1 hour tempering at $600^\circ C$, vs the annealing times at $950^\circ C$, 900, 850 and $800^\circ C$ are given in Fig 6.20.. These results plotted in Figs. 6.18, 6.19 and 6.20, show a greater hardness for steel 99 at all treatments.

Hardness of the air cooled slabs after tempering at $600^\circ C$ is

shown in Figure 6.21 for both steels 97 and 99. For the annealing times given at 900°C, these specimens do not show any increase in hardness. The exceptions are the slabs immediately left to air cool after rolling at 1050°C and end quenching. Note in this case also the higher hardness of steel 99 in all cases.

6.6.2. Nitrogen Analysis

Both analysis of Free and Total Nitrogen contents in millings of steels 97 and 99 are given in Table 6.5. The values given are the average of at least duplicate analysis in each case. Note the large difference in the results obtained for the free Nitrogen content with the Polaron and Leco techniques.

6.6.3. Chemical Analysis of Electrolytically Extracted Particles

6.6.3.1. Niobium Contents

These are given in Tables 6.6 and 6.7 for steels 97, 99 and 22 and 23 respectively. Through atomic absorption and X-ray Diffractometry, Nb precipitates were detected immediately after the first pass at 1100°C in steels 99, 22 and 23. They were found to be as much as 20%, 22% and 34% of the totals respectively. In the case of steel 97 ∿ 10% of the total Nb was estimated through an X-ray fluorescence scan.

The weight fraction of Nb precipitated as a function of annealing times and several temperatures are shown in Figs. 6.22 and 6.23. Figs. 6.24, 6.25, 6.26 and 6.27 show the Avrami type relationship followed by precipitation obtained taking into account the early precipitation after roughing at 1100°C.

From Figs. 6.24 and 6.25, the fastest precipitation occurred at 900°C for both 97 and 99 steels which ended after ∿ 400s for steel 97 and after 60s for steel 99 at this temperature.

From Figs. 6.26 and 6.27 the fastest precipitation occurred at ∿ 950°C for steel 22 and at ∿ 975°C for steel 23 ending precipitation after ∿ 100 secs in both steels.

6.6.3.2. Nitrogen Contents

The general trend of the N content in the extracts for steels 97, 99, 22 and 23 is higher   in the extracts of slabs rolled at high temperatures. These results are given in Tables 6.6. and 6.7.

6.6.3.3. Carbon Contents

The results shown in Tables 6.6 and 6.7 do not correspond only to the C contents of the extracts but also to the cement in acetone used to bind the residue and used in the X-ray Diffractometer. Values up to 12% C might correspond to the Nb, $C_x N_y$ while the rest is due to this contamination.

6.6.3.4. Other Elements

As shown in Tables 6.6 and 6.7, Si is the major component in the extracts with more than 50% as SiO_2. Sulphur, iron and manganese were also detected in some of the extracts. X-ray fluorescence scans of the extracts showed the presence of high contents of Bromine and Potassium which came from the electrolytic solution. Trace elements such as Ti, Cr and Cu were also detected through this technique.

6.7. X-ray Diffractometry Analysis

All the extracted powders were fast scanned at $1°$ (2θ) per minute in order to detect other components than Nb $C_x N_y$. In some of them the presence of bromine, chlorine and iron were detected.

To measure the lattice parameters for steels 97 and 99 it was necessary to step scan at 0.05° (2θ) every 10 minutes. For steels 22 and 23 a slow scan of $\frac{1}{8}°$ (2θ)/minute was enough to clearly resolve the relevant peaks.

6.7.1. Lattice Parameter Measurements

The lattice parameter of most extracted residues are given in Tables 6.8 and 6.9 for steels 97, 99, 22 and 23. These show that the higher the rolling temperatures, the smaller the lattice parameter becomes as shown in Fig. 6.28.

The lattice parameter increases slightly as the time of annealing increases at a given temperature, as shown in Fig. 6.29.

The lattice parameter of the carbonitrides decreases as the N content in the steel increases. This is after rolling at $850^{o}C$ and 30s of annealing at this temperature. See Fig. 6.30.

The lattice parameter of the precipitates plotted vs   the Nb content in the steels shows the higher this content, the smaller its lattice parameter becomes. This is shown in Fig. 6.31 where the lattice parameter of the extracts from slabs rolled at 900 and $850^{o}C$ immediately quenched is plotted.

6.7.2. Particle Size

The average size of the carbonitrides obtained through equations (4.10), (4.11) and Fig. 4.4 are given in Tables 6.8 and 6.9.

6.7.3. Precipitates Composition

Due to the chemical contamination and presence of other compounds the results from the chemical analysis for C and N cannot be used to calculate the values of x and y in the Nb C_x N_y. But this can be carried out, using the ternary phase diagram of Nb, NbC, NbN obtained by Brauer and Lesser (1959) given in Figure 2.11, where the results of Mori et al (1968) are also plotted. From Mori's data, line P Q is generated. The measured lattice were located in this line PQ and the values of N/(C + N) are obtained.   From assumptions

made in Chapter 2 the ratio (N + C)/Nb was considered to be 0.87. Therefore with this data the composition of the carbonitrides was calculated and is given in Tables 6.8 and 6.9.

6.8. Electron Microscopy Observations

Replicas from steels rolled at $1100^{o}C$ and quenched immediately are shown in Fig. 6.32.a. Some bright field micrographs of foils are given in Fig. 6.32.b.

The size distribution of the carbonitrides in steel 23 obtained through replication and quantitative analysis in photographs obtained with the TEM 301 is shown in Fig. 6.33. Note, the sizes obtained through replication are smaller than the ones obtained through the X-ray diffraction method due to the selection between newly formed and undissolved coarse precipitates.

Some analysis of particles carried out in the STEM 400 are given in Table 6.10. Note the presence of not only cuboidal shape precipitates corresponding to niobium carbonitrides but also other shapes.

6.9. Austenite/Ferrite Relations

Ferrite grain sizes were obtained as a function of the prior austenite grain size, geometry, cooling rate, manganese and nitrogen contents. The main results are given in Tables 6.11 and 6.12 for the two pass schedule and in Tables 6.1 and 6.2 for the single pass.

6.9.1. Effect of the Prior γ Grain Size and Geometry

The single pass schedule is plotted in Fig. 6.34. This graph also includes the influence of the cooling rate on the α grain size. The smaller the γ grain size as well as the faster the cooling rate the smaller the α grain size.

6.9.2. Effect of Manganese Content

Steel 12 was cast in order to detect its influence on the ferrite grain size. This is shown in Table 6.13 and Fig. 6.35. The higher the Mn content the A3 transformation temperature decreases 'and so the smaller the α g.s.

6.10. Mechanical Properties

The Tensile and Charpy V-notch Test results are given in Tables 6.14-6.15 . The proof strength and the U.T.S. were calculated from the chart itself, the % of Elongation and % of Reduction in Area were measured directly on the specimens. The tensile results are the average of three specimens for each steel 97, 99, 22 and 23.

The Charpy V-notch Test results are plotted in Fig. 6.36 where the Impact Transition Temperature, I.T.T., is given at 27 Joules.

The higher the N the higher the Proof Strength and the U.T.S. The same occurs as the higher the Nb content becomes. The % of Elongation and Reduction in Area decreases as both the N and Nb increase

The I.T.T. increases as the N and Nb increase at about the same ferrite grain size. The upper shelf energy decreases as the N and Nb increase, See Fig. 6.36.

C H A P T E R   7

DISCUSSION OF EXPERIMENTAL RESULTS

7.1. Introduction

For discussion purposes the experimental results obtained in
this project have been divided into the following sections:
Reheating, where the solubility of Nb $C_x N_y$ and austenite grain
growth are considered; recrystallization of austenite; precipi-
tation of Nb $C_x N_y$ in austenite; interaction between recrystalliza-
tion of austenite and precipitation of Nb $C_x N_y$ and room temperature
microstructure and mechanical properties.

7.2. Reheating

7.2.1. Solubility of Niobium Carbonitrides

In Table 5.2 the solution temperatures T_s, for steels 97, 99,
22 and 23 are shown. These were calculated using the solubility
equations so far available for niobium carbides, nitrides and carboni-
trides as well as with the model proposed in Chapter 5.

As discussed in Chapters 2 and 5, according to theoretical
principles and experimental data available, in steels with low
nitrogen and relatively higher carbon contents or vice versa, the
precipitates formed will be non stoichiometric carbonitrides of low
or high N or C contents. The T_s for this phase has been found to be
higher than for the single phases of carbides and nitrides, thus the
assumptions of single phases present, for a given steel composition,

would be underestimating their solution temperatures.

Although for practical purposes, the solubility equation proposed by Irvine et al (1967) is often used, it would not be reflecting the real composition of the carbonitrides and would be overestimating T_s, especially at high Nb and high C contents but underestimating it at relatively high N contents. On the other hand, the T_s calculated with the model agrees very well with results in practice as already discussed in Chapter 5. Therefore the solution temperatures calculated with the model will be used as a reference in further discussions.

7.2.2. Austenite Grain Growth

The effects of the reheating temperature and time on the austenite grain size of steels 97, 99, 22 and 23 are shown in Figs.6.1.a and 6.2.a. There can be seen the presence of plateau regions of fairly uniform austenite grain sizes and the presence of rapid growth, which in the temperature ranges shown indicate a two stage growth.

Stage 1, of slow growth rate where the austenite grain size is fairly uniform because the temperature and time are lower than a critical temperature and time Tc and t_c respectively.

Stage 2, of rapid growth rate or abnormal grain growth above Tc and t_c, presenting an inhomogeneous microstructure.

These two stages of grain growth can be explained in terms of the theory of grain boundary pinning by precipitates proposed by Gladman (1966). As reviewed in Chapter 3, the austenite grain boundaries are pinned by precipitates as long as they are present in a sufficiently large number per unit volume, n_v, and have a radius

$r < r_{crit}$ at a given temperature and time. As the temperature increases, coarsening of the precipitates takes place with the diffusion of atoms from the small precipitates to the large ones and hence the tendency will be that the small particles will dissolve and the large ones will grow. This arises because of the Gibbs - Thomson effect, which requires that the concentration of solute in the matrix γ adjacent to a small particle to be higher than that in a region adjacent to a large particle. There is thus a diffusional flow of solute Nb, C and N in the matrix from small particles to the large ones and this flux is maintained by the progressive dissolution of the small particles. The net driving force for the reaction would be the decrease in the Nb C_x N_y/γ interfacial area and hence in the surface free energy.

Thus the total number of precipitates will decrease and at a certain critical temperature and time, when this number is too small as well as the radius of the remaining particles is greater than r_{crit} the grain boundaries are no longer effectively pinned and as a consequence stage 2 develops rapidly. It is suggested that this could be happening in certain areas, thermodynamically and kinetically favourable for the dissolution and coarsening of pre- cipitates hence for the grain boundary migration. Thus depending on the temperature and time abnormal grain growth would be taking place in these areas until a generalized grain coarsening develops. Beyond this point grain growth would continue normally.

As observed in Figs.6.1.a and 6.2.a the critical temperature and time would depend basically on the niobium content with small effects of their carbon and nitrogen contents, that is Tc and t_c for steels 23 > 22 > 99 = 97 for a given time and temperature

respectively. This would be because C and N are always in excess of the necessary amounts to combine all the Nb present in these microalloyed steels and thus a small variation in these contents will not affect Tc or t_c very much as shown by steels 97 and 99. On the other hand the effects of increasing Nb is shown clearly by steels 99, 22 and 23.

Tc and t_c, as shown in those figures, are related to their austenite grain sizes and so the greater the Tc and t_c for a given time and temperature respectively, the smaller the reheated austenite grain size is. Another observation in these figures is that if the solubility temperatures Ts calculated by the model are located, it will be observed that Tc is always less than Ts and grain coarsening would be taking place when at least 50% of the total niobium content has gone into solution. This is in agreement with most of the experimental observations on reheated austenite grain sizes, as shown in Figs. 1.1.a and 1.1.c and with the Gladman theory as discussed already.

The knowledge of Tc, t_c and Ts for a given steel would be very important for the design of the most convenient rolling schedules and to obtain the best combination of mechanical properties.

7.3. Static Recrystallization of Austenite

As reviewed in Chapter 3, nucleation of recrystallization takes place preferentially at grain boundaries so that the larger the grain boundary area, the larger the number of nucleation sites for recrystallisation becomes. The grain boundary area is increased by reduction in grain size or by increasing its number.

On the other hand, the rate of static recrystallization also depends on the strain, strain rate temperature of deformation and temperature of holding, which as described in the previous Chapter,

were kept constant except for the rolling temperatures and holding temperatures.

In order to keep constant the influence of the grain size on recrystallisation, a roughing pass, at 1100^oC was applied to reduce the large as-reheated austenite grains to a fairly uniform grain of $\sim$ 65, 56, 70 and 54 μm for steels 97, 99, 22 and 23 respectively. Therefore the static recrystallization kinetics observed for these steels given in Figs. 6.12 and 6.15 are only functions of their composition, temperatures of rolling and holding.

7.3.1. Microstructure

A typical non-recrystallized structure is shown in Fig. 7.1. where it can be observed that in addition to the pancaking of the austenite grains, the rolling process produces a number of deformation bands which are not uniformly distributed. This shows the heterogeneous nature of plastic deformation during rolling and indeed in several other deformation techniques.

A representative progress of recrystallization is illustrated in Fig. 7.2 a,b,c,d, where the grain boundary nucleation of re-crystallization can be observed as well as the highly non-uniform starting points. As recrystallization proceeds, many of the austenite grain boundaries remain unaffected as nucleation sites. The reasons for this are thought to be due to the non-uniform distribution of the stored energy as well as of the high angle sub-boundaries. In these figures the progressive consumption of the unrecrystallized areas as the recrystallization front migrates into the unrecrystallized regions is observed.

At 800^oC the start of recrystallization is slow enough to be preceded by ferrite nucleation, as shown in Fig. 7.3 for steels 97 and 99.

7.3.2. Recrystallization Kinetics

Figs. 6.12 and 6.15 show the influence of the holding temperature and time on the statically recrystallized fraction of austenite in steels 97, 99, 22 and 23. As can be seen in these figures the static recrystallization of austenite is more delayed in steel 99 than steel 97 and steel 23 considerable more delayed than steel 97, 99 and 22 at all temperatures. The main differences between all these steels are in their N and Nb contents, as can be seen in Table 4.1. Between steels 97 and 99 the other difference which could be important is in their manganese content 1.30 and 1.55% respectively, for which steel 12 with 1.69%Mn and 0.007%N was cast and its recrystallization kinetics measured. This was found to be very similar to steel 97 and confirms the results of Hansen et al (1980) and other workers who found that for the difference in Mn contents such as for steels 97, 99 and 12, Mn has a hardly noticeable influence on austenite recrystallization through solid solute effects. Maehara et al (1981) found in a 0.1%C, 0.3% Si steel that increasing manganese contents from 0.5% to 1.0% the time for 50% recrystallization was delayed $\sim$ 1 order of magnitude but above 1.0 wt%Mn up to 2.5% hardly any change was obtained, which again confirms our results.

Therefore the differences obtained in the recrystallization kinetics of steels 97 and 99 can be attributed to their differences in N contents, 0.006 and 0.015% respectively, which through precipitation of niobium carbonitrides rich in nitrogen would be more effectively delaying the recrystallization of austenite. On the other hand the differences between steels 99, 22 and 23 can be attributed to their difference in Nb contents, 0.03, 0.06 and 0.12 respectively, and thus to their greater volume fraction of pre-

cipitates.   These ideas will be discussed further in Section 7.5.

Figs 6.13 and 6.16 indicate that the kinetics of recrystalliza-
tion for these steels follow the Avrami law with a time exponent less
than 1. For steel 97 this would be about 0.65 and for steels 99,
22 and 23 it would be about 0.50. These results would indicate that
nitrogen would be decreasing the time dependence for recrystallization.

Comparing the nucleation times for these steels, they are
at about the same orders of magnitude but their growth rate becomes
much slower the higher their N and Nb contents become.

Going back to Fig. 6.12 where the temperature, time and
recrystallized fraction, TTR are shown, a particular reduced extent
of retardation is obtained for steels 97 and 99 below $900^{o}C$, this is
considered to be due to the increasing driving force for recrystalliza
tion as the temperature decreases and its interaction with precipitation.
This will be discussed further in Section 7.5.

7.3.3. Comparison with Available Data

As can be observed in Figs.3.11 and 3.12 most of the data
available for the recrystallization of austenite in Nb microalloyed
steels are plotted. In this context two characteristic behaviours
are observed: (i) a steady increase in time to start recrystallization
as the temperature decreases for almost all the steels with more than
0.04% Nb, (ii) a steady increase in time to start recrystallization
down to $900^{o}C$ but below this temperature the start of recrystallisation
becomes about the same time as at $900^{o}C$ for steels below 0.04%Nb
as shown by the data of Roberts, W. (1980), Lamberights et al (1977), Fig.3.11.b
or even faster as shown by the results of Le Bon et al (1973),
Fig. 3.12.b.

Steels 22 and 23 agree very well with the results included in (i) while steels 97 and 99 with the results in (ii). However the main difference between these data and the results of this project is that the former were obtained after single deformation through rolling or tension or torsion, implying a much larger, prior austenite grain size than is the latter, when as indicated in Section 7.3 and Chapter 6, the reheated austenite grain was refined by a roughing pass. This prior austenite grain refinement could have meant that the recrystallization kinetics for steels 97, 99, 22 and 23

be faster than all the data shown in these figures, but this did not happen. The simple explanation could be that although the nucleation of new grains could have been faster than the rest of the data available, the retardation of recrystallization in this case would have been much greater, because early precipitation occurred during roughing when also a large deformation of 33% ($\varepsilon = 0.46$) was applied.

From these figures it can also be suggested that, the experimental procedure would have had an influence on the results such as in the ones deformed and annealed at the same temperatures, at least for niobium contents below 0.04%. This is considered to be due to the increasing driving force for recrystallization as the deformation temperature decreases, compared with the constant driving force when deformed at high temperatures and annealed at different temperatures. In the case of the steels with > 0.04% Nb this effect would seem to be unnoticeable.

However, it should be clear from an overall analysis of these results that they are not in absolute agreement even if they were obtained from about the same Nb contents, and using the same conditions and techniques of deformation. The reasons for this are thought to be

due to their different levels of C, N or impurity levels such as P or S as well as due to the sometimes difficult metallography.

7.3.4. Model Predictions

As reviewed in Chapter 3, Sellars (1979) put forward equations to predict recrystallization. The calculated values for an initial austenite grain size of 65 and 200 μm are plotted in Figs. 3.11 and 3.12 as discontinuous lines. These predictions agree reasonably well with steel 97 below 900°C when the predictions are made for $d_o = 65\mu m$ which is the same as obtained after roughing in steel 97. However above 900°C Sellar's equations predict a much faster start of recrystallization than these experiments and some of the experimental results given in Fig. 3.11 and 3.12. But in general terms these equations would be predicting the appropriate orders of magnitude for recrystallization below 950°C. The disagreements with steels 99, 22 and 23 for $d_o \sim 65\mu m$ of this project and with some other results for $d_o \sim 200$ μm suggests that some compositional factor in Nb-C-N would be needed in these relationships to make them generally applicable.

7.4. Static Precipitation

As reviewed in Chapter 2, precipitation of niobium carbonitrides occur heterogeneously at internal lattice defects such as dislocations, stacking faults, incoherent twin boundaries, subgrain boundaries, grain boundaries and perhaps impurity particles.

This will depend basically on the composition of the steel, reheating temperature, amount of deformation, deformation temperature, inter pass and holding times and cooling rates which will control the

nucleation and growth rate of these particles.

In this work all the steels but one were reheated above their solution temperature. Steel 23 was the exception with $\sim$ 95% of its total Nb content in solution, i.e. 0.114% from 0.12%. The other variables have already been established in Section 7.3 and Chapter 6.

7.4.1. Precipitation after Rolling at 1100°C

As shown in Tables 6.6 and 6.7 niobium carbonitride precipitates were detected after rolling and quenching immediately at 1100°C. The measurements were through X-ray fluorescence, X-ray diffraction and analyzing through atomic absorption, electrolytically extracted residues, as described in Chapter 4.

Steel 23 showed the highest weight fraction of Nb $\sim$ 34% of its content in solution, followed by steel 22 - 22%, steel 99 - 20%. In steel 97 it was estimated to be $\sim$ 10%.

The reasons for this early precipitation can be attributed to the amount of deformation applied and composition of the steels. As far as the amount of deformation is concerned, ε = 0.46, (33% reduction), this is considered relatively high if the deformation applied per pass during roughing in industrial practice is taken into account. Although at this high temperature the lattice internal defects would have been swept away very rapidly by recrystallization, the grain boundary area becomes greatly increased. Therefore the nucleation sites for this early precipitation would be the grain boundaries and as can be seen in Figs. 6.32a & 7.4 this is the case. Similar results were obtained by Davenport et al (1977) and Hansen et al (1980) in recrystallized and unrecrystallized austenite.

As far as the composition is concerned, considering that the steels were reheated above their solution temperature, the supersaturation

increases with increase in the Nb content. That is considering that the critical supersaturation, C.S.S., can be defined as:

$$C.S.S. = \frac{[\,[Nb]\ [C]^x\ [N]^{(0.87-x)}\,]}{(\,[Nb]\ [C]^x\ [N]^{(0.87-x)}\,)} \qquad \ldots\ldots\ldots(7.1)$$

where: [ ] in solution at reheating temperatures

( ) in solution at rolling temperature, calculated

through the model at equilibrium. Chapter 5.

The C.S.S. at 1100°C for steels 97, 99, 22 and 23 would have been 1.45 1.98, 4.27 9.94. According to Cohen and Hansen (1979) this means that for steels 22 and 23, due to its level of supersaturation, precipitation could be expected as high as 1100°C even with no deformation. As reviewed in Chapter 2, as soon as deformation is applied precipitation is induced and will occur at short times. This could be equivalent to say that an artificial increase in the supersaturation ratios occurs and would explain the precipitates detected for steel 99 and 97 which with a C.S.S. at equilibrium of ~ 2.0 would have not been expected to give any precipitation at this high temperature.

On the other hand at this temperature also the diffusion rate of N, C and Nb is greater and so growth of these particles would be enhanced once nucleation had occurred.

In Fig. 7.5 is shown the weight per cent of Nb precipitates at different rolling temperatures for steel 99 and compared with that expected at equilibrium. The start of precipitation at 1100°C is very close to the equilibrium conditions but in general below it. At lower temperatures this is increased due to precipitation in non-recrystallized austenite. This will be discussed amply later on.

7.4.2. Composition of the Precipitates

In spite of the fact that the presence of Si, Fe, Mn, Ti, Cr, S, P. Br, Cl, K were detected in most of the electrolytic extracts, through X-ray fluorescent scans and wet chemical analysis, they are not expected to be in the niobium carbonitrides. Silicon would be forming: silica because it results from the deoxidation process during steelmaking, complex silicates formed with Fe and Mn in excess of Si and silicon rich compounds, assumed to be silicon nitrides, when analysed in replicas through microanalysis in the STEM400, which would confirm the results obtained by Long (1976) and Niltawach (1977) in similar steels. Manganese would also be expected to be as undissolved Mn S inclusions while Br, Cl and K forming salts from contamination during the electrolytic extraction. Chromium titanium and calcium detected in some of the residues and replicas are considered to be very low impurities in the steel picked up during steelmaking.

Thus, for these reasons the only essential elements present in the niobium carbonitrides are considered to be Nb, C and N. The proportions of these elements were calculated through lattice parameter measurements and using the lattice parameter composition diagram in the Nb-NbC-NbN system derived by Brauer and Lesser (1959), Fig. 2.11 The calculated compositions are given in Tables 6.8 and 6.9 where a fixed vacancy concentration of 0.13 was taken into account. This value as discussed in Chapter 2 agrees with most of the experimental results.

Considering that the lattice parameter measurements have a potential error of $\pm$ 0.002Å, the results obtained, plotted as N/(C + N) mole ratio Fig. 7.6 , indicate that at 1100°C the proportion of N in the carbonitride is higher than at lower temperatures. This is the same trend as obtained on reheating by Mori et al (1968) and Hoesch Estel (1982). This figure also compares the predictions of Trial 1

for steels 97 and 99, there can be seen that although the model gives a reasonable agreement for steel 97, it predicts a much greater effect of steel composition than is observed as shown by the one of steel 99. The discrepancies are similar to those discussed in Chapter 5 and cannot be attributed to non equilibrium composition of the precipitate particles because composition was shown to change very little with time as shown in Fig. 6.29.

As far as the variation of the lattice parameter of precipitates formed immediately after rolling with respect of the Nb contents, this decreases as the Nb content increases at a given temperature as shown in Fig.6.3.1. The lattice parameter measurements have been converted to the equivalent $N/(C + N)$ ratios and are shown as a function of Nb content for the steels of about the same N content in Fig. 7.7 . This indicates a general trend for the $N/(C + N)$ ratio to increase with increase in Nb which is the opposite trend to that predicted by the model shown as broken line at 900^oC. This opposing trend cannot be attributed to the Mn or Si contents because as shown in Tables 5.6 and 5.7 these elements have a small effect in the $N/(C + N)$ ratio. Similarly in Fig. 7.7 the experimental data for the effect of N in solution would indicate that with a higher volume fraction of precipitates, (i.e. with higher Nb content) the decreased N remaining in solution should have a smaller effect than predicted by the model but still in the same sense, therefore it must be concluded that the opposite trend observed experimentally arises because in the higher Nb steels the composition of precipitates found initially is richer in N than the equilibrium composition.

7.4.3. Precipitates Size and Distribution

Tables 6.8 and 6.9 show the average size of some of the

precipitates, obtained through X-ray diffraction line broadening.
From the few values obtained it can be observed that the precipitates
obtained after finishing at $\sim$ 950°C and 900°C are in agreement with
most of the results obtained through extraction replicas. In the case
of steel 23 this is fairly large due to the size average of fine
particles precipitated after rolling at 1100°C and coarse ones which were
not dissolved during reheating.

As already mentioned, the precipitates observed in replicas
immediately after rolling at 1100°C, were located mainly at grain
boundaries as shown in Figs. 6.32a & 7.4. This is considered to be due to
the lack of lattice defects at this temperature which were swept
away by recrystallization. At lower temperatures general precipitation
in the grains, randomly distributed rather than preferentially
on subgrain boundaries was observed.

The precipitate size frequency distribution was obtained for
steel 23 through extraction replicas, Fig. 6.33. Discriminating the
coarse non dissolved particles from those newly formed after rolling
there appears to be two peaks in the fine particles but this can not
simply be correlated with particles on grain boundaries or in the
matrix. In this figure it is also observed that the coarsening rate
of these precipitates at 850°C is slow, indicating its longer effective-
ness to retard recrystallization because $\sim$ 50% of the precipitates
present were $\sim$ 60Å after 5,400s of annealing at this temperature.

7.4.4. Kinetics of Precipitation

As observed in Figs. 6.24, 6.25, 6.26 and 6.27, the static pre-
cipitation kinetics were obtained for steels 97, 99, 22 and 23 after the
second pass rolling corrected for the precipitation occurred during
roughing. It was found that precipitation in these steels follows

the Avrami equation and from the results where more than one time was examined it appears that n = 0.65 in this equation gives a satisfactory fit. This slope is also satisfactory even when recrystallization starts before precipitation is complete, c.f. steels 97 at 950-900 and 99 at 850. Therefore a constant value on n = 0.65 has been assumed for all the other data.

From the plots given in Figs.6.24.a,6.25.a,6.26.a, 6.27.a; C Curves for the precipitation kinetics have been obtained, as shown in Figs.6.24.b., 6.25.b., 6.26.b., and 6.27.b. In these C curves the start (5%) of precipitation for steel 97 was found to be the slowest of all while for steel 23, the fastest at all temperatures. Precipitation is faster at ~ 900°C for steels 97 and 99 while at 950°C and ~ 975°C for steels 22 and 23 respectively.. On the other hand, because the n value is assumed constant the times for 50% precipitation show exactly the same trend as for 5% precipitation.

Comparing these results with the other results obtained in practice, our results show a much faster start of precipitation especially steels 99, 22 and 23. The data shown in Figs. 2.20 and 2.21 were already discussed in Chapter 2 from which the following conclusions can be drawn:

- Precipitation appears to occur as early as 1100°C.
- Precipitation in deformed austenite is ~ 2 to 3 orders of magnitude faster than in undeformed austenite.
- It shows a C curve with the nose of the curve between 900 and 950°C.
- The higher the Nb content the faster the precipitation becomes in the non-recrystallized and recrystallized austenite. The same effect has been found as the N increases. However, an increase in Mn from 0.42 to 1.9% the opposite effect was obtained.

These conclusions would indicate that the start of precipitation of steels 97, 99, 22 and 23 would have been expected to be much slower than most of the data available but they are not.

The main difference between the data available and the results in this project are that most of them were obtained from steels deformed once through rolling, torsion and compression and the niobium precipitated was analyzed through different methods, such as extraction replicas, hardness, microhardness, electrical resistivity, strain to the peak, chemical extraction and electrolytic extraction.

The kinetics of precipitation obtained for the steels in this project thus could have been influenced by the roughing pass at $1100^{\circ}C$, by increasing the number of nucleation sites through the precipitation occurring after the roughing pass. This coupled with the now much greater supersaturation, 14.5, 15.1, 15.5 and 16.1 for steels 97, 99, 22 and 23 respectively at $900^{\circ}C$, discounting for precipitation at $1100^{\circ}C$, would have led to this fast precipitation kinetics.

With respect to the different techniques of analysis and considering that these could be one of the major sources of discrepancy, the reliability of these techniques is discussed next.

The microhardness and resistivity methods introduced by Le Bon et al (1975) and Simoneau et al (1978) respectively, although they are based on bulk properties, they involve measurements on quenched and tempered phases implying that the results could be affected by other phenomena related to or accompanying the precipitation process. The Hot Compression test developed by Weiss and Jonas (1979) which involves again the bulk properties of the material and avoids complications of quenching and tempering, the detection of the start and finish of precipitation however seems to be arbitrary. The Hardness test by Amin and Pickering (1979), applied on the ferrite/pearlite structures, where it is necessary

to compensate for the grain size effect plus some other effects such as alloying elements has been found to be not sensitive enough to detect the progress of early precipitation. Transmission Electron Microscopy: Replicas applied by Hansen et al (1980) gives good results for the particle size distributions, but are not reliable with respect to the volume fraction of each size, because precipitates smaller than $20\overset{o}{A}$ cannot be detected in replicas. Besides it is not possible to differentiate the nature of the precipitates, Nb C_x or Nb N_y or Nb C_x N_y because the differences in their lattice parameters are outside the precision of the electron microscope which is $\pm 0.1 \overset{o}{A}$. And Electrolytic Extraction which with an accurate chemical method of analysis could be the most reliable of all, providing an appropriate solution and technique of separation are chosen.

Thus comparing the results obtained by the same technique, there is an agreement between the results for steel 97 and the ones of Hoogendorn et al, although they had 0.8 strain compared with 0.33 for steel 97, but which had a pre-precipitation stage, and would be compensating for the effect of low strain. The results of Watanabe et al, however are surprisingly slow, although their steels had a predeformation stage of three passes above 1090^oC, having a 25 μm. prior austenite grain size with a relatively high Nb content, 0.08%, would be expected to start precipitation earlier than the results obtained by Ouchi et al, Yamamoto et al or Le Bon et al, but this is not the case. The explanation could be found on their method of separation of the electrolytically extracted precipitates. It would appear that the filter used with pore size of 0.1 μm would have been too large and consequently some of their precipitates would have been lost resulting in a delayed detection of the start of precipitation.

- 137 -

On the other hand, the technique used in the present research, as described in Chapter 4, involved centrifuging rather than filtering which should have involved a minimum loss of particles and therefore an early detection of precipitates was possible. Also, the technique does not discriminate between particles in the grain boundaries or in the matrix and so the start for precipitation curve could well represent precipitation at grain boundaries for which the kinetics are faster than in the matrix, Hansen et al (1980).

Pre-existing boundary particles formed after roughing are considered to have only a minor influence because extraction replicas show an increased number of particles per unit area, with increasing time during precipitation indicating that the major contribution of volume fraction of precipitation detected in the electrolytic extraction method arises from nucleation and growth of new particles rather than continued growth of existing particles.

7.5. Interaction between Recrystallization and Precipitation

So far, as reviewed in Chapter 3, three mechanisms have been proposed for the recrystallization inhibition; a) solute-drag, b) strain induced precipitation and c) the combination of solute-drag plus strain induced precipitation. From the present results it is difficult to differentiate the solute drag effects due to the early precipitation detected at $\sim 1100^{o}C$ in all our experimental steels. However from convincing experiments carried out with C and N almost free steels by Luton et al (1980) and Yamamoto et al (1981), showed that Nb retarded γ recrystallization through solid solute effect by far more effectively than any other element commonly added to a microalloyed steel. As reviewed in Chapter 2 this has been suggested to be due to its largest atomic size as well as due to its

characteristic electronic structure which causes lattice distortion and increases the recrystallization temperature repectively.

But in microalloyed steels enough C and N will always be present to combine with Nb, which due to thermodynamic and kinetic conditions will always tend to form rapidly below $1000^{\circ}C$. Besides as shown by experimental results available, the larger the supersaturation defined by equation (7.1) as well as the larger the amount of deformation, the higher will be the temperature and also the shorter the time at which precipitation of carbonitrides will occur. These precipitates are not coherent, as suggested by several workers if the lattice mismatching of Nb $C_x N_y$ and γ, which is about 23%, is considered. This would be the case at all temperatures and directions as shown in Figs. 2.23 and 2.24 and Table 2.15.

But for an effective overall delay in recrystallization the volume fraction and size of precipitates will be of most importance. Hansen et al (1980) have discussed this interaction in terms of the driving force for recrystallization (F_R) and a retarding force (F_p) arising from precipitation. F_R has been defined as:

$$F_R \cong \frac{\mu b^2}{2} \Delta\rho \qquad\qquad \ldots\ldots\ldots(7.2)$$

where: μ = shear modulus ($\sim 7 \times 10^4$ MN /m^2 for steel)

b = Burgers vector ($\sim 2 \times 10^{-10}$ m)

$\Delta\rho$ = Change in dislocation density as the recrystallization front moves along $\sim 10^{16}/m^2$ for the hot rolled austenites involved.

This gives F_R = 14MN/m^2 which is considered to be in line with similar order of magnitude calculations.

On the other hand, if a random dispersion of spherical precipitates of radius r and volume fraction f are assumed, F_p was shown to be

negligibly small, Hansen et al (1980). However for preferential

precipitation on subgrain boundaries, F_p was found to have values

of similar order to F_R. F_p was defined as:

$$F_p = \frac{3}{2\pi} \frac{\gamma}{} \frac{f \, \bar{\ell}}{r^2} \qquad \qquad \ldots\ldots\ldots(7.3)$$

where: γ = interfacial energy per unit boundary area,

$\sim 0.7 - 0.8 \ J/m^2$ in austenite.

f = volume fraction

$\bar{\ell}$ = mean subgrain size

r = precipitate radius

Sellars (1982) suggested that the above equation can be considered
appropriate for preferential precipitation on grain boundaries before
matrix precipitation occurs, that is $\bar{\ell}$ can be replaced by $\bar{d}o$. Thus
considering the volume fractions computed in Chapter 5, the initial
grain size before finishing pass applied $\sim 58\mu m$ and particle radius of
$30\overset{o}{A}$ for steel 99 and at 900^oC, assuming about 20% of the volume
fraction, 1.5×10^{-4}, precipitated at the grain boundaries, $F_p = 75 \ MN/m^2$
which is ~ 5 times larger than F_R at 900^oC, and would explain the great
retardation effect of these precipitates on recrystallization. If the
volume fraction of precipitates on the grain boundaries is greater than
20% then F_p increases rapidly up to $370 \ MN/m^2$ when considered 100%.

In the case of precipitation occurring on subgrain boundaries,
calculating the mean subgrain size through the equation:

$$\log \frac{\sigma}{\Gamma} = 0.9 - \log \frac{t}{b} \qquad \qquad \ldots\ldots\ldots(7.4)$$

given by Twiss (1977)

where: σ = mean flow stress = 190MN/m^2 at 900°C, see Fig. 6.9

Γ = shear stress = $\mu/(1 - \nu)$, ν = 0.33

b = Burgers vector = $\sim 2 \times 10^{-10}$ m.

t = $\bar{\ell}$ = mean subgrain size

$\bar{\ell}$ = 0.874μm = 8.74 $\times$ 10^{-7}m

and replacing $\bar{\ell}$ in equation(7.3) assuming about 80% of the volume fraction precipitated on the subgrain boundaries, F_p = 4.45 MN/m^2 for a particle radius of 30Å. The smaller the precipitate in this case the larger the F_p becomes, for $\sim$ 10Å particle radius F_p = 50 MN/m^2.

These calculations indicate that with the observed sizes of precipitates the value of F_p is sufficiently large to retard recrystallization. But within the approximations made it is not possible to conclude that F_p is larger than F_R so that recrystallization would be entirely prevented. In fact the experimental observations for all steels show the occurrence of recrystallization after sufficient holding time.

Summarizing the results of the recrystallization and precipitation kinetics, the possible interactions between both solid solute effects and precipitation of niobium carbonitrides with recrystallization are shown in Fig. 7.8. Considering a low C-Mn steel with no Nb its recrystallization kinetics could be represented by the equation derived by Sellars (1980) drawn in broken lines. The solid solute retarding effects can be derived from the data given by Yamamoto et al (1981) and are shown by the chain lines. These solution effects were calculated assuming all the Nb is in solution and therefore they represent an absolute maximum. In practice 10 to 35% is precipitated after roughing and as further precipitation occurs after finishing the solute retarding effect is further diminished. Thus the retarding

effects of precipitates may be seen by comparing the observed R_s curves with a line that falls between the broken line and chain line, which would more nearly approach the former as temperature decreases.

In this figure it is also clearly shown that the start of recrystallization in niobium microalloyed steels is delayed at least $\sim$ 2 orders of magnitude at and below 950°C for all the steels. Increasing the N content the start of recrystallization is delayed even more because of the relatively smaller sizes of the precipitates as shown in Table 6.8 being the slowest at 900°C. Increasing the Nb content increases the volume fraction of precipitates after a given rolling treatment and therefore from eq. (7.3) it gives increasingly delayed recrystallization with increasing Nb contents.

The decreasing extent of retardation below 900°C observed for steels 97 and 99 can be attributed to the high values of F_R, resulting from the low temperature deformation, which means with low volume fractions of precipitates temperature has a greater effect on F_R than on F_p.

In all the steels at the highest temperatures examined recrystallization starts while precipitation is still proceeding. As F_p would be expected to increase during precipitation because of the increasing volume fraction of precipitates, this suggests that due to the relatively coarse precipitates found at high temperatures F_p is always somewhat less than F_R. In steel 97 this situation exists at all temperatures whereas in the other steels at lower temperatures precipitation is finished before recrystallization starts and in these cases precipitate coarsening could also play a role in reducing F_p.

7.6. Room Temperature Microstructure and Mechanical Properties

7.6.1. Room Temperature Microstructure

In the few experimental results obtained on air cooled slabs of steels 97 and 99, after a two pass rolling schedule and finished at 900°C, the variables found to exert an influence on the ferrite microstructure were: The size and geometry of the prior austenite, the cooling rate and composition, these last two directly affecting the transformation temperature Ar_3. As reviewed in Chapter 3, deformation bands as well as precipitate distribution will also affect the nucleation rate and growth of the ferrite, but in the present work, due to the schedules given, their influence was not detected. Thus the effects of the geometry and size of the austenite grains as well as of the transformation temperature on the ferrite grain size, will be discussed.

7.6.1.1. Austenite Grain Size and Geometry Effects

It is known that the ferrite grains will nucleate preferentially at grain boundaries as well as at deformation bands. Consequently for geometrical reasons, the larger the surface to volume ratio of the prior austenite, the greater the possibilities of nucleating more ferrite grains which on growth will impinge giving small ferrite grains. This is achieved when "pancaked" elongated austenite grains are obtained after deformation in the non-recrystallization region.

However in this case, due to the constant reduction 25% applied on finishing, the ferrite grains obtained were in the range of ∿ 16 µm which compared with the height of the prior γ grains gives an γ/α ratio of ∿ 1.8 for steels immediately air cooled after finishing.

The ratio γ/α in steels annealed for different times increased, as the time of annealing increased, from 1.8 to 3.0 for both steels 97 and 99, see Tables 6.11 and 6.12. This is considered to be due to the recrystallization taking place with the recrystallized γ grain diameter becoming larger than the non-recrystallized γ height, but with not a large increase in the average ferrite grain size. This ratio is in agreement with the results of Kozasu et al (1977) and Sekine and Maruyama (1976) who found it to be ~ 2.3. The ratio obtained also indicates that the nucleation of ferrite has occurred mainly on grain boundaries rather than on deformation bands. This is probably due to the relatively low deformation bands density induced by the 25% thickness reduction.

7.6.1.2. Transformation Temperature Effects

The transformation temperature was changed in these experiments mainly by composition and cooling rates. As far as the composition is concerned, the manganese content is considered to be the main factor which decreases the transformation temperature as demonstrated by steels 12, 99 and 97 with 1.69, 1.52 and 1.30% Mn and transformation temperatures of 715, 726 and 756 respectively. This is illustrated in Fig. 6.35. Although N and C in solution are well known elements that decrease the transformation temperature, in this case the N content of these steels does not correlate with the observed Ar_3. This is thought to be partially due to the precipitation of mainly niobium carbonitrides and possibly silicon nitrides which decreased this effect. This would confirm our observation in replicas through the STEM 400 of Si rich particles, assumed to be Si N based on the results obtained by Niltawach (1977) in similar steel compositions.

On the other hand the large effect of Mn would also be over-shadowing the remaining free N effects; 20, 55, 45, 40 ppm for steels 97, 99 22 and 23 respectively; after full precipitation. As fas as C is concerned because of the fairly constant content in these steels, no effects on Ar_3 were observed.

With respect to the cooling rates, it is also well known that the faster the cooling rate the lower the Ar_3 and thus the faster the nucleation rate of ferrite. In the results obtained with the one end water quenching technique given in Tables 6.1 and 6.2 the α grain sizes obtained at cooling rates of 2.4°C/sec are smaller for steel 99 than for steel 97 in the fully recrystallized as well as in the non-recrystallized prior austenite. Considering that in both cases the prior austenite grains were about the same for a given cooling rate these smaller ferrite grains in steel 99 are thought to be due to their differences in Mn and N contents. As shown before, Mn has a powerful effect on decreasing the transformation temperature and thus refining the α grains, despite the small differences in Mn content, 0.22% would have been enough. Nitrogen if uncombined has also strong effects on the Ar_3 and will decrease it in this case more in steel 99 than in steel 97 due to their difference in total and free nitrogen, 20 and 55 ppm respectively.

At lower cooling rates of $\sim$ 1.2°C/sec, the grain sizes obtained from the fully recrystallized of $\sim$65μm and the non-recrystallized austenites of $\sim$ 160 are the same but the α g.s. for steel 99 is smaller than for steel 97. The reasons for this coincidence in grain size arise from the balance between the effects of grain size and the effects of deformation, see Fig. 3.19. The smaller grain size of steel 99 is mainly attributed to its higher Mn content which reduces the Ar_3.

7.6.1.3. Acicular Structures

As can be seen in Fig. 6.34 , the volume fraction of acicular structures increases as the cooling rate increases, as well as the higher the N and Mn becomes, as shown by the results of steel 99. However, even at low cooling rates, the volume fraction of acicular structures is relatively high,even in the low N, steel 97. This is in agreement with the results of several other workers who found relatively large amounts of acicular structures in Nb microalloyed steels. This has been amply discussed in Chapter 3 and from the results available so far, it could be suggested that this is due to the interaction of the Nb and Mn contents decreasing the transformation temperature. On one hand,with high Mn,   > 1% increases the solubility of Nb in γ as shown in Chapter 5. This was also found experimentally by Irvine et al (1963) in V-steels which with 2%Mn, the solubility of V in γ was increased by 100%. This would lead to a major influence on decreasing the Ar_3. On the other hand,although niobium is a ferrite stabilizer, it would also have an influence on the kinetics of transformation as suggested by Shams (1982). Therefore Nb microalloyed steels in the normalized or rolled condition and with relatively small prior austenite grain size would always be expected to have some fraction of acicular structures, as shown by these results and Shams (1982), see Fig. 7.9.

7.6.2. Mechanical Properties

As established in Chapter 3,fine ferrite grains are the unique contributors for both strength and toughness of steels. This effect is clearly seen when calculations are made using any of the equations derived correlating the yield strength, Y.S. and Impact Transition Temperature, I.T.T.,with ferrite grain size, d. In this

case equations (3.21) and (3.23) given in Chapter 3, will be used for comparison purposes. They are:

$$\sigma_y = \sigma_0 + K_y \cdot d^{-\frac{1}{2}}$$

$$= (\sigma_\ell + \sigma_{ss} + \sigma_d + \sigma_\rho + \sigma_t) + K_y \cdot d^{-\frac{1}{2}} \qquad \ldots \ldots (7.5)$$

and

$$ITT = A \sigma_0 - K_y \cdot d^{-\frac{1}{2}}$$

$$= A (\sigma_\ell + \sigma_{ss} + \sigma_d + \sigma_p + \sigma_t) - K_y \cdot d^{-\frac{1}{2}} \qquad \ldots \ldots (7.6)$$

Morrison (1978) indicated that for a α grain size of 10 and 5μm their contribution towards the Y.S. are 180 and 250N/mm^2 and to the ITT -100 and -140 respectively. On this basis, considering the Y.S. of $\sim$ 450MN/m^2 normally obtained in controlled rolled plates with $\sim$ 7μm ferrite grain size and composition 0.1%C, 0.007%N, 0.03%Nb, 1.35%Mn and 0.30%Si, the effect of the ferrite grain size would account at least for $\sim$ 50% of that Y.S. with the other contributions such as solid solution σ_{ss}, precipitation in ferrite σ_p, dislocation σ_d, and texture σ_t, accounting for the remaining 50%.

On the other hand the ITT for that α grain size would be $\sim$ -140°C but because of the detrimental effects of the other contributors, the ITT is increased by $\sim$ 90° resulting in an ITT of - 50°C.

In this context the results obtained for the Proof Stress, Ultimate Tensile Strength, Elongation, Reduction in Area and the Impact Transition Temperatures will be discussed.

7.6.2.1. Proof Stress

Surprisingly none of the steels showed evidence of the yield point despite the fact that there is still N and C in solution. It appears possible that the presence of the acicular ferrite acts in a similar way to the martensite phase in dual phase steels, which produces local strain concentrations in the matrix so the sharp yield point is not observed.

The 0.2% proof stress of steels 97 and 99 is slightly lower by $\sim$ 7% than the expected Y.S. considered above. This is thought to be basically due to their relatively large ferrite grain sizes which are $\sim$ 15μm, see Table 6.14 . However the strength of steel 99 is slightly improved probably due to its $\sim$ three times larger volume fraction of acicular structure which increases the σ_d term in eq. (7.5) through the overall increment in dislocation density as well as the presence of fine subgrains, Pickering (1977).

In the case of steels 22 and 23, they have slightly higher proof stress $\sim$ 7% than the Y.S. given as standard and $\sim$ 14% higher than the proof stress of steels 97 and 99. This increased proof stress, in spite of their similar ferrite grain size to steels 97 and 99 which is twice the α g.s. given as the example is considered to be due to their increased precipitation hardening term, σ_p. It is expected that despite the faster precipitation kinetics in austenite with increasing Nb content, more Nb content will remain in solution on direct cooling after rolling to give an increased volume fraction of precipitation in ferrite. However the similar proof stress of steels 22 and 23, in spite of their difference in Nb content, can be explained to be due to the large volume fraction of acicular structure formed in steel 22, thus in the greater contribution of σ_d.

7.6.2.2. Elongation and Reduction in Area

In Table 6.14 it can be observed that the Elongation and Reduction in Area for steel 97 are slightly better than for steels 99, 22 and 23, these ones being about the same. This suggests that precipitation hardening and dislocation hardening due to acicular structures do not have much influence in these properties. Yet considering that they have similar grain sizes it could be thought that their slight difference in Mn and large difference in N contents could be the explanation of these results.

7.6.2.3. Impact Transition Temperature

As mentioned earlier in this section, σ_ℓ, σ_{ss}, σ_d, σ_p, σ_t all have detrimental effects on the ITT and only the reduction in ferrite grain size has beneficial effects on the impact properties. However, Morrison and Mintz (1976) suggested that the presence of fissures > 800μm deep, in steels finish rolled in the γ, $\gamma + \alpha$ and α region could improve the ITT, by forming ahead of the main crack thus relaxing the triaxial stress system. The origin of fissures are not clear yet but there is some evidence that they start at points where second phase particles, carbides, nitrides or non-metallic inclusions are situated.

The impact properties for all the experimental steels are rather poor, as shown in Table 6.15 and Figure 6.36 . The lowest ITT at 27 Joules was obtained for steels 97, -20°C and the highest for steel 23, $+52^\circ$C. Clearly the main reason for these high values is considered to be due to the relatively large α grain size. But as all of them have a similar α grain size, decreasing this would mean a proportionate decrease in the ITT by -35°C for all of them and the same relative positions would be maintained i.e. ITT for steels

23 > 22 > 99 > 97. From considerations given earlier in this section and assuming a $\sim 7\mu$m ferrite grain size for all these steels, taking into account the other main contributions such as σ_d and σ_p, their calculated ITT using eq. (7.6) would be -55, -18, 21 and 27°C. That is still not a good ITT for steels 22 and 23. On the other hand, Morrison (1978) and other workers have found that the presence of acicular structures has little effect on the ITT presumed to be due to the introduction of fissures. This means that the high ITT of these steels can be attributed to the increased σ_p and chemical composition.

Comparing steels 99, 22 and 23 which had about the same C, N, Mn, Si, S and P contents but increasing Nb contents i.e. 0.03, 0.06 and 0.12% correlates with increased ITT. As discussed earlier, it is probable that as the Nb content increases, the volume fraction of niobium carbonitrides available for precipitation in the ferrite will be higher, thus increasing σ_p and increasing the ITT.

However, in the case of steels 97 and 99 with the same Nb contents, the increased ITT for steel 99 is considered to be due to its N content. But this is not to say that niobium carbonitrides rich in N are more detrimental than niobium carbonitrides rich in C, but rather suggests that due to the excess in N after combining with Nb, it would have combined with Si and ~ 50 ppm was still free in steel 99 compared with 20 ppm in steel 97. Therefore the rise in the ITT of steel 99 is thought to be mainly due to the free nitrogen and silicon nitrides. This is in line with previous correlations as well as in resemblance to the deleterious effect of Al N found in aluminium killed steels.

CHAPTER 8

CONCLUSIONS

8.1. From this work the following can be concluded:

1. The austenite grain size of Nb microalloyed steels depends mainly on their Nb content, C and N having only a minor influence because their amounts are always greater than needed to combine the Nb normally present in these steels as carbonitrides. The greater the Nb content the smaller the reheated austenite grain size will be at a given temperature and time. Also the greater the Nb content the higher the critical temperature Tc, at which grain coarsening will take place.

2. Time of reheating becomes very important the higher the temperature at which the steel is held. This is because the coarsening of particles and hence the critical temperature at which grain growth will take place depend on time.

3. The solubility temperature of the carbonitrides will depend on the relative amounts of C and N in the steels. The higher the N content the higher the solution temperature for a given C and Nb content as predicted by the proposed thermodynamic model. Manganese will decrease this solution temperature by as much as $30^{o}C$ per $\sim 1.3\%$ Mn, whereas Si will increase the Ts by $\sim 12^{o}C$ per $\sim 0.3\%Si$. These contents are usually encountered in these steels.

4. The proposed thermodynamic model, although it assumes ideal solution in the carbonitrides, predicts the evolution of the carbonitrides composition as a function of temperature. This is in fair agreement with experimental results available and with this work even the conditions of precipitation may not reach equilibrium.

5. The composition of the carbonitrides is a non stoichiometric one, rich in N at high temperatures, as obtained through accurate lattice parameter measurements and predicted by the model. Its N content decreases as the temperature decreases to a certain level, which depends on the N/C ratio in the steel.

6. Precipitation of niobium carbonitrides has been detected as early as $1100^{o}C$ after a roughing pass, becoming faster the higher the N content. Increasing niobium also has the same effect. These precipitates were found to be located at grain boundaries.

7. The size of the precipitates rich in N has been found to be smaller than the ones rich in C.

8. Static precipitation after finish rolling at 1000 to $850^{o}C$ starts about 2 to 3 orders of magnitude earlier than static recrystallization and is randomly distributed through the grain. Thus, calculations of interaction forces predict a large retardation of recrystallization at all temperatures through precipitation locking of sub and grain boundary migration. The solid solute effect would be small compared with the effect of precipitation.

9. Recrystallization in the high N steel for a constant Nb and C

content has been found to be more retarded than in the low
N steel. This has been attributed to the greater effect
on the retarding force, F_p, by the smaller precipitates
obtained in the high N steel. Manganese variations of
1.3 to 1.5% Mn have been found not to have any significant
effect on the γ recrystallization kinetics.

.10. Increasing the Nb content increases the retardation of
recrystallization continuously as the temperature decreases
in contrast with steels of 0.03%Nb where a decreased
extent of retardation below $900^{o}C$ has been observed. This
has been attributed to the increased driving force for
recrystallization, F_R, even though the coarsening rate at
these temperatures would have been low.

.11. The mechanical properties obtained in these steels are not
as good as normally obtained in practice, due to the rolling
schedule given and thus to the resultant ferrite grain size.
As far as chemical composition is concerned, the higher
the Nb content the greater the volume fraction of precipitates
would be on the ferrite and therefore the larger the Y.S.
and the higher the ITT. This increased precipitation hardening
compensates the loss in strength due to the relatively large grains
whereas it adds detrimental effects to the ITT.

12. Although the ITT in steel 99 is not as good as in steel 97,
from its more delayed recrystallization kinetics it would
appear that the recrystallization retardation could have been
increased to higher temperatures. Therefore it would be
possible to carry out a greater number of passes during finishing,
without implying large forces or extra energy, in order to decrease
further the α grain size and obtain improved impact properties
in this cheaply alloyed steel...

8.2. Suggestions for further work.

1. The thermodynamic model proposed could be improved to give accurate predictions by determining experimentally whether:
   - the non-stoichiometric ratio in the carbonitride changes as a function of temperature.
   - a non-symmetric entropy of mixing between $Nb\ C_x$ and $Nb\ N_y$ occurs.
   - the activity terms of $Nb\ C_x$ and Nb_y in equations (5.6) and (5.7) vary as a function of temperature.

2. Precipitation and recrystallization interactions during roughing is an area where studies are not abundant. From the present work it would appear that to simulate controlled rolling closer to practice, multipass rolling schedule experiments must be considered.

3. Experiments with high N steels, giving more passes during finishing or larger reductions should be attempted in further experiments, taking advantage of their more retarded kinetics of recrystallization.

ACKNOWLEDGEMENTS

REFERENCES

Abrahamson, E.P. and Blakeney, B.S. (1960), Trans. Metall. Soc. AIME, 218, 1101.

Allbones, S.P., Lang, M.P. and Woodhead, J.H. (1979); Ferrite Grain Size in Low Carbon Steel, Final Year Report, Sheffield University.

Akben, M.G., Weiss, I. and Jonas, J. J. (1981), Acta Metallurgica, 29, 111.

Allen, A. H. (1879), J.I.S.I., 11, 480.

Amin, R. K. et al (1979), 'Hot Working and Forming Process' Eds. C. M. Sellars and G. J. Davies, The Metals Soc. London, p.27.

Argent, B. B. (1982), Private Communication.

Aronsson, B. (1969), Steel Strengthening Mechanisms, Zurich, Climax Molybdenum Co., p.77.

Aronsson, B. and Jonsson-Holmquist, B. (1970). Swedish Institute for Metal Research, Internal Report, Stockholm.

Arrowsmith, A. (1924), J.I.S.I. 110, 317.

Bain, E. and Paxton, H. (1961), Alloying Elements in Steel, A.S.M., 2nd Ed., Metals Park, Ohio, p.182

Baird, J. D. and Preston, R. R. (1973), 'Processing and Properties of Low Carbon Steels,' Metallurgical Society of AIME, N.Y., p.1.

Baird, J. D. and Preston, R. R. (1969), 'Hot Workability of Steel Conference,' I.S.I., London.

Baker, R. G. and Nutting, J. (1959), Precipitation Processes in
Steels, I.S.I. Special Report No. 64, London, p.1.

Balliger, N.K. and Honeycombe, R.W.K. (1980), Met. Trans. A.,
11A, 421.

Barraclough, D. R. (1974), Ph.D. Thesis, University of Sheffield, U.K.

Barrett, C. S. and Massalski, T. B., (1980), Structure of Metals,
3rd Ed., Pergamon Press, Chapters 3, 7, 8, 10, 13.

Baumgardt, H. et al (1981), 'Niobium 81   Int. Symposium', San
Francisco, in press.

Beiser, C. A. (1959), Preprint 138, Annual Convention ASM, Chicago.

Bernard, G. (1977), Microalloying 75, Union Carbide Co., N.Y., p.552

Birat, J. P. et al (1981), "Niobium 81', Int. Symposium, San
Francisco, in press.

Bittner, H. et al (1963), Mh. Chem., 94, 518.

Bose, B.N. and Hawkes, M. F. (1950), Trans. Am. Inst. Mining
Met. Eng., 188, 307.

Brauer and Lesser (1959), Z. Metallk. 50, 487.

Brown, E. L. et al (1977), The Hot Working of Austenite, J. Ballance,
edt. TMS-AIME, N.Y., p.250.

Brown, J. F. (1965), G.K.N. Group Res. Lab. Rep. No. 796

Brownrigg, A. and Boelen R. (1980), Metal Science, 14, 237

Bepari, M. M. A., (1981), Ph.D Thesis, Metallurgy Department
University of Sheffield. U.K.

Cahn, R. W., (1970), Physical Metallurgy, North-Holland, Chapters
4, 6 - 10, 19.

Chandra, T. et al (1981), Canadian Met. Quarterly, 20, 421.

Chilton, J. M. and Roberts, M. J. (1980a), Met. Trans., 11A, 1711.

Chilton, J. M. and Roberts, M. J. (1980b), 'Vanadium in High

      Strength Steel', Vanitec, London, p.11.

Christian, J. W. (1970), 'Physical Metallurgy,' Ed. by R. W. Cahn,

      Chap. 10.

Cohen, M. and Hansen, S. S. (1979), MiCon 78, ASTM STD 672, p.34.

Cohen, M. and Owen, W. S. (1977),   'Microalloying 75'

      Union Carbide Corp.,   N.Y. p.2.

Coladas, R. et al (1977), 'The Hot Deformation of Austenite,'

      J. Ballance Ed., TMS-AIME, N.Y., p.341.

Coleman, T. et al (1974), 'The Microstructure and Design of Alloys',

      The Metals Society, London, Vol. 1, p.70.

Cordea, J. N. (1970), 'Symposium on Low-Alloy High-Strength Steels',

      The Metallurgical Companies, Nuremburg, BRD, p.61.

Cottrell, A. (1975), 'An Introduction to Metallurgy,'

      Edward Arnold , p.246.

Cuddy, L. J. et al (1980), Met. Trans., 11A, 381.

Cuddy, L. J. (1981), Met. Trans., 12A, 1313

Cullity, B. D. (1967), Elements of X-ray Diffraction, 3rd Ed.,

      Addison-Wesley Publishing Co., London.

Darken, L. S. and Gurry, R. W. (1953), Physical Chemistry of

      Metals, McGraw-Hill Book Co., Inc., Metallurgy and

      Metallurgical Engineering Series, p.387/372.

Davenport, A. T. et al (1975), J. Metals, 27, 21.

Davenport, A. T. et al (1977), 'The Hot Deformation of Austenite',

      The Metallurgical Society of AIME, p.186.

Davenport, A. T. and Dimicco, D. K. (1980) 'Int. Conf. on Steel
        Rolling,' The Iron and Steel Inst. of Japan, Tokyo, p.1237.

DeArdo, A. J. et al (1981), 'Niobium 81', Int. Symposium, in press.

De Kazinczy et al (1963), Jernkont. Ann., $\underline{147}$, 408.

Duckworth, W. E. (1964), Iron and Steel, $\underline{37}$, 585.

Duckworth, W. E. et al, (1965), J.I.S.I., $\underline{203}$, 1108.

Djaic, R. A. P. and Jonas J. J. (1973), Metall. Trans., $\underline{4}$, 621.

Duwez, P. and Odell, F., (1950), J. Electrochemical Society, $\underline{97}$,
        (Part 10), 299

Elliott, R. P. (1965), 'Constitution of Binary Alloys,' First
        Supplement, McGraw-Hill Book Co., N.Y.

Elliott, R. P. and Kempter, C. P. (1958), J. Phys. Chem. $\underline{62}$, 630.

Everett et al (1980), 'Hot Working and Forming Processes,' Eds.
        C. M. Sellars and G. J. Davies, Metals Soc., London, p.16

Fast, J. D. (1976), Gases in Metals, The Macmillan Press Ltd.,
        Chapters I and II.

Feltham, P. (1957), Acta Met. $\underline{5}$, 97.

Freeman, S. (1971), 'Effect of Second Phase Particles on the
        Mechanical Properties of Steel, I.S.I. Special Publication
        No. 145, London,   p.152.

Froes, F. H. et al (1967), Acta Met., $\underline{15}$, 157.

Fukuda, M. et al (1977), 'Microalloying 75', Union Carbide Corpn.
        N.Y., p.136.

George, T. J. et al (1971), J. Aust. Inst. Metals, $\underline{16}$, 34.

Gladman, T. (1963), J.I.S.I., $\underline{201}$, 1044.

Gladman, T. (1966), Proc. Roy. Soc. A., $\underline{204}$, 298.

Gladman, T. et al (1977), 'Microalloying 75' Union Carbide Corp.N.Y. p.25.

Gladman, T. and Pickering, F. B. (1967), J.I.S.I. $\underline{205}$, 653.

Gladman, T. and Woodhead, J. H. (1960), J.I.S.I., $\underline{198}$, 189.

Glover, G. and Sellars, C. M. (1972), Metall. Trans. $\underline{3}$, 2271.

Goldschmidt, H. J. (1962),'Advances in X-ray Analysis' Vol. 5,

       Plenum Press, N.Y.,p.191.

Goldshteyn, M. I. et al (1973), Fiz. Metal. Metalloved, $\underline{36}$, No. 1, 222.

Gondoh, H. and Osuka, T. (1981), 'Niobium 81 Int. Symposium,'

       San Francisco, in press.

Grabke, H. J. et al (1975), Z. Metallkunde, $\underline{5}$, 286.

Gray, J. M. (1974), 'Heat Treatment 73', The Metals Society,

       London, p.19.

Gray, J. M. and Yeo, R. B. (1968), Transactions Quarterly AIME, $\underline{61}$.

Great Lakes Steel Corp. (1959), Mech. Eng., $\underline{81}$, 53.

Goldschmidt, H. J. (1967), Interstitial Alloys, Butterworths

       (London) Publishers, Chaps. 1 - 5 and 10.

Hall, E. O. (1951), Proc. Phys. Soc., $\underline{643}$, 747.

Hanemann, H. and Lucke, F. (1925), Stahleisen, $\underline{45}$, 1117.

Hannukainen, T. and Heikkinen, V. (1974), Scand. J. Metallurgy, $\underline{3}$, 158.

Hansen, S.S. et al (1980), Met. Trans. $\underline{11A}$, 387.

Heedman, P. and Sjöström, A. (1978), Hot Working Research Station

       Luleå, Report No. 78050.

Heikkinen, V. K. and Packwood, R. H. (1977), Scand. J. Metallurgy, $\underline{6}$, 170.

Helsop, J. and Petch, N. J. (1958), Philos. Mag., $\underline{3}$, 1128.

Hoesch-Estel, Dortmund, (1981), Unpublished results quoted by

       DeArdo et al (1981).

Honeycombe, R. W. K. (1976), Metall. Trans., $\underline{7A}$, 915.

Honeycombe, R. W. K. (1981), Steels, E. Arnold Publishers, Chapters

       1 - 4 and 9.

Hoogendorn, T. M. and Spanraft, M. J. (1977), 'Microalloying 75'
Union Carbide Corporation, N.Y. p.75.

Hudd, R. D. et al (1971), J.I.S.I., 209, 121.

Hume-Rothery, W. (1944), 'The Structure of Metals and Alloys,' The
Institute of Metals, London, 2nd ed.

Hume-Rothery, W. et al (1969), The Structure of Metals and Alloys,
5th Ed., The Metals and Metallurgy Trust, Chapters I to V.

Irani, J. J. et al, (1967), 'Strong Tough Structural Steels Proceed-
ings' The Iron and Steel Institute, London, p.135.

Imai, Y. and Shono, Y. (1966),'Tetsu -to-Hagane,', 52, 110.

Irvine, K. J. (1967), ibid, p.1.

Irvine, K. J. and Baker, R. G. (1979), Recrystallization in the
Development of Microstructure, Met. Sci., 13, 228.

Irvine, K. J. et al (1967), J.I.S.I., 205, 161.

Irvine, K. J. et al (1970), J.I.S.I., 208, 717

Jack, D. H. and Jack, K. H. (1973), Matls. Sci. and Eng., 11, 1.

Janampa, C. (1980), M.Met. Dissertation, Sheffield University
Chapters 3 - 5.

Jesseman, R. (1977), Microalloying 75',Union Carbide Corp., N.Y. p.578

Jizaimarn, J. et al (1974), Tetsu-to-Hagane, 60 , 177.

Johansen, T. H. et al (1967), Trans. Aime, 237, 1651.

Jonas, J. J. et al (1969), Met. Rev., 14, 1.

Jonas, J. J. and Weiss, I. (1979), Metal Science, 13, 238

Jones, J. D. and Rothwell, A. B. (1968), 'Deformation under Hot
Working Conditions,' I.S.I., London, p.78.

Kaspar, R. et al (1980), 'International Conference on Steel Rolling'
Vol. 2, I.S.I.J., Tokyo, p.1052

Katsumata, M. et al (1982), 'Thermomech. Process. of Micro-alloyed
Austenites, Eds. P. J. Wray and A. J. DeArdo, AIME,
Warrendale, in press.

Kawamura, K. (1958), Nippon Kinzoku, British Iron and Steel Institute
6650, Vol. 32 (2), 180.

Kazinsky, F. et al (1963), Jernkontorets Annaler, 147, 408.

Keown, S. R. and Wilson, W. G. (1981), 'Int. Conf. on Therm. Process
of Microalloy γ' Pittsburgh, in press.

Kirkwood, P. R. (1981), 'Niobium 81 Inst. Symp.' San Francisco, in press.

Koyama, S. et al (1971a), Jap. Inst. of Met., 35, 698.

Koyama, S. et al (1971b), Jap. Inst. of Met., Jl, 35, 1090.

Kozasu, I. et al (1971), Trans. Iron Steel Inst. Jpn., 11, 367.

Kozasu, I. et al (1977), 'Microalloying 75', Union Carbide Corp., N.Y., p.120.
Kubaschewski, O. (1982) 'Iron-Binary Phase Diagrams,' Springer-Verlag,
Berlin, p.71.

Kurokawa, S. et al (1981), 36th A.B.M. Annual Congress, Recife. Brazil.

Kuhn, V. and Detrez, P. (1962), Modern Casting, 27, p.469.

Lakshmanan, V. K. (1977), M.Met. Eng. Thesis, McMaster University,
Canada.

Lamberigts, M. and Greday, T. (1977) 'The Hot Deformation of Austenite'
J. Ballance, Editor, TMS-AIME, New York, p.286.

Le Bon, A. (1977), Microalloying 75', Union Carbide Corp., N.Y., p.90.

Le Bon, A. et al (1973), Revue de Metallurgie, 70, 577.

Le Bon, A. et al (1975), Metal Science, 9, 36.

Leduc, L. (1980), Ph.D thesis, Sheffield University, U.K.

Lee, J. D. (1979), Concise Inorganic Chemistry, 3rd Ed., Van

      Nostrand Reinhold, Chaps. 1 and 6.

Liljestrand, L. G. (1972), Scandanavian J. of Metallurgy, 1, 271.

Little, J. H. et al (1974), 'The Microstructure and Design of Alloys',

      The Metals Society, London, Vol. 1, p.80.

Low, J. R. and Gensamer, M. (1944), Trans. AIME, 158, 207.

Luton, M. J. et al (1980), Metals Transactions A, 11A, 411

Luton, M. J. and Sellars, C. M. (1969), Acta Met., 17, 1033.

Long, G. D. (1976) Ph.D. Thesis, Dept. of Chemistry, Sheffield University

      U.K.

Machida, M. et al (1980), 'International Conference in Steel Rolling'

      The Iron and Steel Inst. of Japan, Tokyo, 1980.

Maehara, Y. et al (1981), Tetsu-to-Hagane, 67, 138.

Mandry, P. and Dornelas, W. (1966), Comptes Rendus des Seances,

      263, 1118.

Mangonon, P. and Heitmann, W. E. (1977), 'Microalloying 75'

      Union Carbide Corp. N.Y., p.59.

Martin, J. W. (1980), Micromechanisms in particle-hardened alloys,

      Cambridge University Press, 1st Ed.

McCutcheon, D. B. (1974), 'Journee Internationale de Siderurgie'

      Paris, reprinted at the Revue de Metallurgie - Fevrier

      1976, p.143.

McLean, A. and Kay, D. A. R. (1977), 'Microalloying 75' Union

      Carbide Corp. N.Y., p.215.

McQueen, H. J. (1968), Journal of Metals, 20, 31.

McQueen, H. J. and Jonas, J. J. (1975), 'Plastic Deformation of

      Metals' R. J. Arsenault Ed., p.393

Meyer, L. (1966), Dissertation Clausihal Bergund Huettenmaennische

Meyer, L. (1967), Z. Metallkunde, $\underline{58}$, 334. BISI Trans. 6009

Meyer, L. et al (1977), 'Microalloying 75', Union Carbide Corp.
N.Y., p.153.

Meyer, L. and G. Robiller (1980) IRISO Int. Symp. on Rex. and
Grain Growth of Multi-phase and Particle-Containing
Materials', Eds. Hansen, Jones and Leffers, Riso
National Lab., Denmark, p.311.

Migaud, B. (1980), 'Hot Working and Forming Processes' Eds.
C. M. Sellars and G. J. Davies, Metals Soc. London, p.67

Milinskaya, I. N. and Tomlin, I. A. (1973), Akad Nauk SSSR Doklady
174, 135.

Miller, O. (1951), Trans. Amer. Soc. Metals, $\underline{43}$, 260.

Miroslava, V. M. and Tůma, H.(1973) Neve Hütte, $\underline{7}$, 430.

Moore, J. J. (1981), Chemical Metallurgy, 1st Ed., Butterworth & Co
Publishers, Chaps 1 - 3.

Morcinek, P. et al (1977),'Microalloying 75' Union Carbide Corpn.
N.Y., p.272.

Mori, T. et al (1963), Mem. Fac. Eng., Kyoto Univ., $\underline{25}$, 164.

Mori, T. et al (1964a), Tetsu-to-Hagane, $\underline{50}$, 911.

Mori, T. et al (1964b), 19th Committee on Reactions in Steelmaking,
Rep. No. 8022.

Mori, T. et al (1965), Tetsu-to-Hagane, $\underline{51}$, 2031.

Mori, T. et al (1968), Tetsu-to-Hagane, $\underline{54}$, 763.

Morrison, W. B. (1963), J.I.S.I., $\underline{201}$, 317.

Morrison, W. B. (1978), 'Hot Working Symposium' Swedish Institute for
Metals Research, Stockholm, preprint.

Morrison, W. B. (1972), J. Iron Steel Inst. $\underline{210}$, 618.

Morrison, W. and Mintz, B. (1976), 'Heat Treatment 76', The Metals
Society, London.

Morrison, W. and Preston, R. (1981), 'Niobium 81 Int. Symposium,' in press.

Morrison, W. B. and Woodhead, J. H. (1963), J.I.S.I., 201, 43.

Muller, T. L. F. (1967), Ph.D Thesis, Metallurgy Department,
        Sheffield University, U.K.

Nakai, Y. et al (1979), Kawasaki Steel Technical Report, 11, 1, p.44.

Narita, K. and S. Koyama, (1966), Jap. Inst. of Metals, Jl, 52, 292.

Nilsson, R. (1968), Private Communication to Nordberg and Aronsson,
        J.I.S.I., 206, 1263.

Niltawach, S. (1977), Ph.D Thesis, Metallurgy Department Sheffield
        University, U.K.

Nordberg, H. and Aronsson, B. (1968), J.I.S.I., 206, 1263.

Norin, T. M. (1963), Ship Structure Committee Special Report, SSC154.

Oakwood, T. G. et al (1976), 'The Hot Deformation of Austenite',
        The Metals Society of AIME, John Ballance Editor, Ohio, p.204.

Ohmori, Y. (1966), 'Nippon Kiusoku Gakkaishi', 30, 1164.

Ohtani, H. et al (1981), Lecture 5557, 101st I.S.I.J. Meeting, Tokyo
        Japan.

Ouchi, C. et al (1977), 'The Hot Deformation of Austenite', The
        Met. Society of AIME, J. Ballance Ed., Ohio, p.316.

Ouchi, C. et al (1981), to be published in Trans. Iron Steel Inst. Japan.

Pearson, W. B. (1972), The Crystal Chemistry and Physics of Metal
        and Alloys, Wiley Ed., N.Y., p.151.

Pehlke, R. D. and Elliott, J. F. (1960), Trans. AIME, 218, 1088.

Petch, N. J. (1953), J.I.S.I., 173, 25.

Petkovic, R. A. et al (1976), 'The Hot Working of Austenite,' Ed. J. Ballance, TMS-AIME, N.Y., p.68.

Pickering, F. B. (1977), 'Microalloying 75', Union Carbide Corp., N.Y., p.9.

Pickering, F. B. and Gladman, T. (1963), 'Metallurgical Developments in Carbon Steels', I.S.I. Special Report 81, London, p.10.

Phillips, R. and Chapman, J.A. (1966), J.I.S.I., 204, 615.

Politis, C. and Rejman, G. (1978), KFK - Ext. 6/78-1.

Powell, M.J.D. (1968), Harwell Report, AERE - R5947, H.M.S.O.

Priestner, R. et al (1968), J.I.S.I. 206, 1252.

Priestner, R. and Biring, M.S. (1973), Metals Science, 7, 60.

Pye Unicam Ltd., (1975), Atomic Absorption Methods, AA/5/, p.1227

Pereira da Silva, (1966), Ph. D. Thesis, Sheffield University, U.K.

Randerson   (1981), IST Course, invited lecture, Sheffield University

Reed Hill, R. E. (1964), Physical Metallurgy Principles, Van Nostrand Reinhold, Int. St. Ed.,Chapters 1 - 4, 8 - 11, 16.

Reistad, T. and Sehlstedt, P. (1967), Jernkont., 151, 950.

Roberts, W. (1977), Swedish Institute for Metals Research, Report No. 1211.

Roberts, W. (1980), Scandinavian Journal of Metallurgy, 9, 13.

Roberts, W. and Ahlblom, B. (1978), Swedish Institute for Metals Research, Report No. 1279.

Roberts, W. et al (1979), 'Hot Working and Forming Processes,' Eds. C. M. Sellars and G. J. Davies, Metals Society, London, p.38

Roberts, W. A. et al (1981), Vanadium Steels (Krakow), Vanitec, London, p.19.

Rollason, E. C. (1973), Metallurgy for Engineers, 4th Ed., Ed. Arnold, Chapters 9 and 10.

Rossard, C. (1968), Rev. Met., 65, 181.

Rossard, C. and Blain P., (1958), Rev. Met., 55, 573.

Santella, M. L. and DeArdo, A. J. (1982), 'Thermomechanical
    Processing of Microalloyed Austenite,' AIME, A. J. DeArdo
    Editor, in press.

Santella, M. L. (1981), Ph.D. Thesis, Department of Metallurgical
    and Materials Engineering, Pittsburgh University

Schenk, H. and Steinmetz, E. (1966), StahlEisen-Sonderberichte, 7, 27

Schwaab, P. and Langerscheid (1972), Prakt Metallogr. No. 2, p.67.

Sekine, H. and Maruyama, T. (1972), Tetsu-to-Hagane, 58, 1424

Sekine, H. and Maruyama, T. (1973), 'Proceedings, 3rd Int. Conf.
    on the Strength of Metals and Alloys, I.S.I. London, p.85.

Sekine, H. and Maruyama, T. (1974), 'The Microstructure and Design of
    Alloys,' The Metals Society, London, 1, 85.

Sekine, H. and Maruyama, T. (1976a), Trans. Iron & Steel Inst. of
    Japan, 16, 427.

Sekine, H. and Maruyama, T. (1976b), Seitetsu-Kenkyu, No. 289, p.43.

Sellars, C. M. (1978), Phil.Trans. R. Soc. London A., 288, 147

Sellars, C. M. (1979), 'Hot Working and Forming Processes,' Eds.
    C. M. Sellars and G. J. Davies, The Metals Society,
    London, p.3.

Sellars, C. M. (1980), '1st Risø Conf. on Rex. and Grain Growth of
    Multi Phase and Particle Cont. Materials, Roskilde, p.291.

Sellars, C. M. (1982), 'Deformation Process and Structure' ASM
    Seminars, St. Louis, in press.

Sellars, C. M. and Whiteman, J. A. (1979), Metal Science, 13, 187.

Shams, N. (1982), Ph.D Thesis, Sheffield University, U.K.

Simoneau, R. et al (1978), Metal Science, 12, 381.

Smith, R. P. (1962), Trans. AIME, 224, 190.

Smith, R. P. (1966), Trans. AIME, 236, 220.

Smith, W. F. (1981), Structure and Properties of Engineering Alloys,
        McGraw Hill, N.Y. p.155.

Speith, K. G. and Von Ende, H. (1959), Journal of Metals, 11, 333.

Srivastava, K. K. (1976), Ph.D. Transfer Report, Department of
        Metallurgy and Mat. Science., McMaster University.

Starratt, F. W. (1958), J.Metals   ., 10, 799.

Stewart, M. J. (1976), 'The Hot Deformation of Austenite,' J. Ballance
        Edit., TMS-AIME, N.Y., p.233.

Storms, E. K., (1967), The Refractory Carbides, Academic Press Inc.,
        (London) Ltd., Chapters V and XIII.

Storms, E. K. et al (1969), J. High-Temp. Sci., 1, 430.

Storms, E. K. and Krikorian, N. H. (1960), J. Phys., Chem., 64, 1747.

Tanaka, T. et al (1977a), 'Microalloying 75' Union Carbide Corp.
        N.Y., p.107.

Tanaka, T. et al (1977b), ibid, p.399

Tanaka, T. and Tabata, T. (1978), Tetsu-to-Hagane, 64, 1353.

Tanaka, T. (1981), International Metals Reviews, 26, 185.

Tanaka, T. (1980), 'Hot Deformation of Steels,' The Iron and Steel
        Institute of Japan, Tokyo, p.23.

Takechi et al (1981), 'Niobium 81' Int. Symposium, San Francisco,
        in press.

Taylor, A. (1953), 'Soft Magnetic Materials for Telecommunications,'
        Intersci. Pub., New York, 202

Tegart, W. McG. and Gittins, A. (1977), 'The Hot Deformation of Austenite,' The Metallurgical Society of AIME, N.Y., p.1.

Tennent, R. M. (1971), Science Data Book, Oliver and Boyd Publishers.

Thomerson, D. R., (1971), Spectrovision, 26, 13 -

Toth, L. E. (1971), Transition Metal Carbides and Nitrides, Academic Press, Inc. (London) Ltd., Chapters 1 - 5 and 8.

Twiss, R. J. (1977), 'Pure Appl. Geophys.' 115, 227.

Wada, T. et al (1971), Met. Trans., 2, 2199.

Wada, T. et al (1972a), Met. Trans., 3, 1657.

Wada, T. et al (1972b), Met. Trans., 3, 2865.

Wadsworth, J. et al (1976), Metal Science, 10, 342.

Wagner, C. (1952), Thermodynamics of Alloys, Addison-Wesley, Reading, Mass. U.S.A. Chapters 1 - 2.

Wallace, (1973), referred to in DeArdo et al's (1981) paper.

Watanable, H. et al (1977), 'The Hot Deformation of Austenite', The Metallurgical Society of AIME, J. Ballance Editor, p.140.

Webster, D. and Woodhead, J. H. (1964), J.I.S.I., 202, 987.

Weiss, I. and Jonas, J. J. (1979) Metal Transactions A, 10A, 831.

Whiteside, P. and Milner, B. (1981), Atomic Absorption Data Book, 4th Edition.

Williamson, G. K. and Smallman, R. E. (1953), Acta Crystallogr. 6, 361.

Wilson, J. L. and Geiselman, D. (1962), Union Carbide Tech. Report, R-62-15.

Woodhead, J. H. (1979), 'Vanadium 79' Conference, Chicago, Preprint.

Wright, J. A. (1962), Ph.D Thesis, Metallurgy Dept., Sheffield University
    U.K.

Wittaker, H. J. (1973), Ph.D Thesis, Metallurgy Dept., Sheffield University
    U.K.

Yamamoto, S. et al (1981), 'Int. Conf. on Process. of Microalloyed γ'
    Pittsburgh, in press.

Zidek, M. et al (1969a), Hutnicke Listy, 24, 98.

Zidek, M. et al (1969b), ibid. 24, 650

APPENDIX 1

Recrystallized Austenite Grain Size Calculations

They were carried out using the equation proposed by Sellars (1980)
for niobium microalloyed steels:

$$d_{rex} = D_x^1 d_o^{0.67} \varepsilon^{-0.67}$$

$$\text{For} \quad \varepsilon < \varepsilon^*, \quad T > 950^o C$$

where: D^1 = constant $\sim 0.9 \mu m^{0.33}$

d_o = prior austenite grain size in μm

ε = strain lower than the peak strain

After roughing at $1100^o C$ in all the steels full recrystallization was ob-
tained and the grain sizes obtained through measurements and calculations
are shown below:

Steel Code	Grain Sizes		$D^1 = 0.9$ Recrystallized Calculated	$D^1 = 1.1$ Rex. Calculated
	As reheated	Recrystallized Measured		
97	180	65	49	60
99	160	56	45	55
22	375	75	80	98
23	190	52	51	62

A good agreement is obtained when calculations are carried out using
$D^1 = 0.9$ for the high Nb steels while for the low Nb steels $D^1 = 1.1$
gives a better fit.

At 950°C, after the second pass and some time of annealing, re-crystallized grain sizes were considered if they were about the same or below the calculated ones when $D^1 = 1.1$.

Steel Code	Rex. Grain Sizes Calculated	Measured
97	38	40
99	34	35
22	38	41
23	33	32

APPENDIX 2

Theory of Niobium Carbonitrides Separation

There are mainly two methods to separate second phase particles from
the matrix: Chemical and Electrolytic dissolution. Chemical dissolu-
tion in the last few years has been rarely used for low alloy or
microalloyed steels, because the reagents, if they are strong enough
to produce sufficient residue in a reasonable time, also tend to
dissolve these precipitates. H_2 is evolved during matrix dissolution
and could react with the C or N of the residue to produce hydro-
carbons or ammonia. Highly concentrated solutions of HCL, HNO_3 and
$H_2 SO_4$ are used in the above cases as well as alcoholic iodine and
bromine solutions to avoid attack to the residue, but in those cases
extensive contamination of the residue takes place from the undissolved
matrix.
In general, electrolytic methods of extraction are superior to chemical
methods because:
-    matrix dissolution tends to be faster
-    the electrolytes are less reactive
-    to some extent, the rate of dissolution can be controlled by
     the current density
-    hydrogen is evolved at the cathodes, away from the residues.
Essentially, electrolytic methods of separation depend upon the less
noble character of the matrix relative to the carbonitride phases.
These methods have been reviewed comprehensively by Andrews and Hughes

(1966) for a variety of carbides, intermetallics and inclusions in low and high alloy steels.

The electrolyte used here consisted of an aqueous solution of 5% Sodium Citrade and 2% Potassium Bromide.

The role of the constituents of this solution can be separated as follows: the current is transported by the movement of potassium ions to the anode and hydrogen ions to the cathode. The dissolving iron from the matrix is completed by the Sodium Citrate.

The potassium ions arriving at the anode are also complexed by sodium citrate. These complexed potassium ions tend to overcome the polarization of the anode, i.e. the formation of local cathodic areas minimizing the pitting of the anode and possible decomposition of the carbides.

In recent years, the tendency is to use hydrochloric acid as the electrolytic solution, however if the temperature rises, there will be the danger of dissolving some of the niobium carbonitrides.

APPENDIX 3

```
 1) C ACCURATE LATTICE PARAMETER CALCULATIONS
 2)        DIMENSION X(8),Y(8),W(8),D(8)
 3)        REAL*8 ALFA1,ALFA2,TETA1,TETA2
 4)        WRITE (1,3)
 5)      3 FORMAT ('INPUT ALFA1,ALFA2')
 6)        READ (1,*) ALFA1,ALFA2
 7)        I=-1
 8)      9 WRITE (1,4)
 9)      4 FORMAT ('INPUT TETA1,TETA2,H,K,L')
10)        READ (1,*) TETA1,TETA2,H,K,L
11)        IF (TETA1.LT.0.)GO TO 10
12)        I=I+2
13)        II=I+1
14)        D(I)=ALFA1/(2*SIN((3.141592/360.)*TETA1))
15)        D(II)=ALFA2/(2*SIN((3.141592/360.)*TETA2))
16)        P=H**2+K**2+L**2
17)        Y(I)=D(I)*SQRT(P)
18)        Y(II)=D(II)*SQRT(P)
19)        X(I)=(COS((3.141592/360.)*TETA1))**2
20)        X(II)=(COS((3.141592/360.)*TETA2))**2
21)        W(I)=(SIN((3.141592/360.)*TETA1))/COS((3.141592/360.)*TETA1)
22)        W(II)=0.5*(SIN((3.142592/360.)*TETA2))/COS((3.141592/360.)*TETA2)
23)        WRITE (6,5) (Y(I),Y(II),X(I),X(II),W(I),W(II))
24)      5 FORMAT (5(F10.5,5X))
25)        GO TO 9
26)     10 N=I
27)        CALL LSQ (X,Y,W,N,A,B,VARA,VARB)
28)        WRITE (6,12) A,B,VARA,VARB
29)     12 FORMAT('A=',F10.5,5X,'B=',F10.5,'VAR A:',F10.5,5X,'VAR B:',F10.5)
30)        CALL EXIT
31)        END
32)        SUBROUTINE LSQ (X,Y,W,N,A,B,VARA,VARB)
33)        DIMENSION X(N),Y(N),W(N)
34)        REAL SWY,SWX,SWXY,SW,SWX2,SWY2
35)        SWY=0
36)        SWX=0
37)        SWXY=0
38)        SW=0
39)        SWX2=0
40)        SWY2=0
41)        DO 1 I=1,N
42)        SWY=SWY+W(I)*Y(I)
43)        SWX=SWX+W(I)*X(I)
44)        SWXY=SWXY+W(I)*X(I)*Y(I)
45)        SW=SW+W(I)
46)        SWX2=SWX2+W(I)*X(I)*X(I)
47)        SWY2=SWY2+W(I)*Y(I)*Y(I)
48)      1 CONTINUE
49)        B=(SWXY*SW-SWY*SWX)/(SWX2*SW-SWX*SWX)
50)        A=(SWY-B*SWX)/SW
51)        S2XY=(1./(N-2))*(SWY2-A*SWY-B*SWXY)
52)        VARB=S2XY/(SWX2-SWX*SWX/SW)
53)        VARA=(SWX2/SW)*VARB
54)        RETURN
55)        END
```

Instruction	Comments
	This Fortran IV porgram calculates lattice parameters for a cubic crystal, using X-ray Diffraction data.
5	Asks the $K_{\alpha 1}$, $K_{\alpha 2}$ radiation values. In this case Co radiation. ALFA1 = 1.78892, ALFA2 = 1.79278
9	Asks the θ_1, θ_2 angles as well as their respective h, k, 1 planes.
14 - 15	Calculates the 'd' spacings through the Bragg law equation.
17 - 18	Calculates the lattice parameter for each θ input.
19 - 20	Calculates the $\cos^2\theta$ for extrapolation purposes.
21 - 22	Calculates the weighting factors for the $K_{\alpha 1}$ $K_{\alpha 2}$ radiations.
32 - 53	Subroutine LSQ, standard least square fitting.

This Fortran IV program has been adapted to the requirements of the NAG Library CO5NAF subroutine to obtain the zeros of one or more Transcendental equations through iteration and applying the Newton steepest descent methods.

5 - 10

Identifies the real and integer variables needed using double precision.

12

Asks to input in mol fraction the total contents of Carbon, Nitrogen, Niobium, Iron, Silicon and Manganese.   0.0 should be input in the case that the effects of Mn or Si are not required to be evaluated.

15

Asks to input the terms of the solubility product equations. In this case Cl = 0.200, C2 = 7700, RN1 = 0.972, RN2 = - 10,340.6 from the equations of Mori et al (1968) and Lakshmanan (1977) converted into mol fractions.

13 - 25

Calculates the solubility product K''_C and K''_N taking into account the interactions of Mn and Si.

28 - 29

Calculates the solubility product K'_C and K'_N with no consideration of interactions of Si and Mn.

31

Asks an initial estimate of the position of a solution to start the iteration X(1) = atom fraction C/Nb varying from 0.00 to 0.87 and X(2) = mol fraction of Nb, varying from 0.0000 to the total Nb input. This has to be input for each temperature.

33

N, number of variables, in this case N = 2.

36

FTOL indicates the precision required to obtain the answers larger precisions than 10^{-14} lead to failure of the program.

39

MAXCAL No. of interactions to find the answer = 100

42,45

The CO5NAF requires that X(1) and X(2) to be of the same order of magnitude. Thus X(2) was multiplied and divided by 1000.

```
51)          S1=-(X(1)/.87)*DLOG( DABS( X(1)/.87) )
52)          S2=-((.87-X(1))/.87)*DLOG( DABS(.87-X(1))/.87)
53)          S=S1+S2
54)          G1=(X(1)/.87)*DLOG( DABS(SC)   )
55)          G2=((0.87-X(1) )/0.87 )*DLOG( DABS(SN))
56)          SCN = G1 + G2 - S
57)          G=8.314*T*(G1+G2-S)
58) C CALCULATION OF THE VOL. FRACTION OF NbCxNy
59)          LP = 4.4500 + 3.15*(10.**(-5.))*(T-273.)
60)          DECA = 40*(92.91 + X(1)*12 + (0.87-X(1))*14)/(6.023*LP**3)
61)          DEFE = 7.87
62)          PPTA = (TN3-X(2))*(92.91+12*X(1)+14*(0.87-X(1)))/92.91
63)          VF = (PPTA/DECA)/(PPTA/DECA+TFE/DEFE)
64)          TDC=T-273.
65)          WRITE (6,25) TDC,CA,CO,X(2),X(1),VF,G,RA1
66)       25 FORMAT(F6.1,1X,E9.4,1X,E8.3,1X,E8.3,1X,F5.3,1X,E10.4,1X,E10.4,
67)         *F7.4)
68)       80 CONTINUE
69)          STOP
70)          END
71) C CALCULATION OF RESIDUALS XC(1)=ATOM FRACTION C/NB,XC(2)=NB IN SOL
72)          SUBROUTINE RESID (N,XC,RC)
73)          IMPLICIT REAL*8 (A-H,O-Z),INTEGER*2 (I-N)
74)          INTEGER*2 N
75)          REAL*8 A,B,C,D,XC(N),RC(N),SC,SN
76)          COMMON T,TN,TC,TNB,SC,SN
77) C CHANGE HERE
78)          XC(2)=XC(2)/1000.0
79)          A=(TC-DABS(XC(1)*SC/(0.87*XC(2)))**1.1494)*(1/1.87-XC(2))**1.1494
80)          B=(TNB-XC(2))*(XC(1)/1.87-DABS(XC(1)*SC/(0.87*XC(2)))**1.1494)
81)          C=(TN-DABS((0.87-XC(1))*SN/(0.87*XC(2)))**1.1494)*(1/1.87-
82)         *XC(2))
83)          D=(TN3-XC(2))*((0.87-XC(1))/1.87-DABS((0.87-XC(1))*SN/(
84)         *0.87*XC(2)))**1.1494)
85)          RC(1) = A-B
86)          RC(2) = C-D
87) C CHANGE HERE
88)          XC(2)=XC(2)*1000.0
89)          RETURN
90)          END
91)          SUBROUTINE MONIT(N,XC,RC,FC,NCALL)
92)          IMPLICIT REAL*8 (A-H,O-Z),INTEGER*2 (I-N)
93)          INTEGER*2 N,NCALL,I
94)          REAL*8 FC,XC(N),RC(N)
95)          WRITE(6,90) NCALL,FC
96)       90 FORMAT('AFTER',I4,2X,'CALLS OF RESID'//'THE SUM OF SQUARES IS'
97)         *E12.5)
98)          WRITE(6,95) (XC(I),I=1,N)
99)       95 FORMAT('AT THE POINT',2F12.4)
100)         RETURN
101)         END
```

```
51)          S1=-(X(1)/.87)*DLOG( DABS( X(1)/.87) )
52)          S2=-((.87-X(1))/.87)*DLOG( DABS(.87-X(1))/.87)
53)          S=S1+S2
54)          G1=(X(1)/.87)*DLOG( DABS(SC)   )
55)          G2=((0.87-X(1) )/0.87 )*DLOG( DABS(SN))
56)          SCN = G1 + G2 - S
57)          G=8.314*T*(G1+G2-S)
58) C CALCULATION OF THE VOL. FRACTION OF NbCxNy
59)          LP = 4.4500 + 3.15*(10.**(-5.))*(T-273.)
60)          DECA = 40*(92.91 + X(1)*12 + (0.87-X(1))*14)/(6.023*LP**3)
61)          DEFE = 7.87
62)          PPTA = (TNB-X(2))*(92.91+12*X(1)+14*(0.87-X(1)))/92.91
63)          VF = (PPTA/DECA)/(PPTA/DECA+TFE/DEFE)
64)          TDC=T-273.
65)          WRITE (6,25) TDC,CA,CO,X(2),X(1),VF,G,RA1
66)       25 FORMAT(F6.1,1X,E9.4,1X,E8.3,1X,E8.3,1X,F5.3,1X,E10.4,1X,E10.4,
67)         *F7.4)
68)       80 CONTINUE
69)          STOP
70)          END
71) C CALCULATION OF RESIDUALS XC(1)=ATOM FRACTION C/NB,XC(2)=NB IN SOLU
72)          SUBROUTINE RESID (N,XC,RC)
73)          IMPLICIT REAL*8 (A-H,O-Z),INTEGER*2 (I-N)
74)          INTEGER*2 N
75)          REAL*8 A,B,C,D,XC(N),RC(N),SC,SN
76)          COMMON T,TN,TC,TNB,SC,SN
77) C CHANGE HERE
78)          XC(2)=XC(2)/1000.0
79)          A=(TC-DABS(XC(1)*SC/(0.87*XC(2)))**1.1494)*(1/1.87-XC(2))
80)          B=(TNB-XC(2))*(XC(1)/1.87-DABS(XC(1)*SC/(0.87*XC(2)))**1.1494)
81)          C=(TN-DABS((0.87-XC(1))*SN/(0.87*XC(2)))**1.1494)*(1/1.87-
82)         *XC(2))
83)          D=(TNB-XC(2))*((0.87-XC(1))/1.87-DABS((0.87-XC(1))*SN/(
84)         *0.87*XC(2)))**1.1494)
85)          RC(1) = A-B
86)          RC(2) = C-D
87) C CHANGE HERE
88)          XC(2)=XC(2)*1000.0
89)          RETURN
90)          END
91)          SUBROUTINE MONIT(N,XC,RC,FC,NCALL)
92)          IMPLICIT REAL*8 (A-H,O-Z),INTEGER*2 (I-N)
93)          INTEGER*2 N,NCALL,I
94)          REAL*8 FC,XC(N),RC(N)
95)          WRITE(6,90) NCALL,FC
96)       90 FORMAT('AFTER',I4,2X,'CALLS OF RESID'//'THE SUM OF SQUARES IS'
97)         *E12.5)
98)          WRITE(6,95) (XC(I),I=1,N)
99)       95 FORMAT('AT THE POINT',2F12.4)
100)         RETURN
101)         END
```

Instruction	Comments
46 - 57	Calculate the soluble C, N, N/(C + N) in the carbonitride the entropy of mixing S, the free energy of formation G.
58 - 63	Calculate the volume fraction of carbonitride at each temperature.
65 - 67	Print the results in Table Form.
71 - 90	Subroutine Resid calculates residuals of equations given.
91 - 101	Subroutine Monit monitors the progress of the iteration, controlled by the instruction 40 IPRINT. If different to zero, the progress of the iteration will be printed out.

Listing of the programme used to calculate the mean
flow stress of the material from the measured rolling load
after Leduc (1980).

```
10 DIM H[5],S[4],N[4],Q[4],S[4],R[4],A$[5]
20 R=69.85
30 DISP "IDENTIFICATION";
40 INPUT A$
50 PRINT A$
60 PRINT "PASS          H0        H1        HN     ALPHA      PHI      Q
70 DISP "NUMBER OF PASSES";
80 INPUT N9
90 FOR I=1 TO N9+1
100 DISP "H("I")";
110 INPUT H[I]
120 NEXT I
130 FOR I=1 TO N9
140 A[I]=1-(H[I]-H[I+1])/(2*R)
150 A[I]=ATN(SQR(1-(A[I]†2))/A[I])
160 C1=SQR(R/H[I+1])
170 R[I]=(H[I]-H[I+1])/H[I]
180 B[I]=(0.785*LOG(1-R[I])+C1*ATN(SQR(R[I]/(1-R[I]))))/(2*C1)
190 B[I]=SIN(B[I])/(C1*COS(B[I]))
200 N[I]=H[I+1]+2*R*(1-COS(B[I]))
210 C2=SQR((1-R[I])/R[I])
220 C3=1/C2
230 Q[I]=1.5708*C2*ATN(C3)-0.785-C2*C1*LOG(N[I]/H[I+1])
240 Q[I]=Q[I]+0.5*C2*C1*LOG(1/(1-R[I]))
250 DISP "P("I"),W("I")";
260 INPUT P[I],W[I]
270 S[I]=1000*P[I]/(W[I]*SQR(R*(H[I]-H[I+1]))*Q[I])
280 FIXED 3
290 PRINT I;H[I];H[I+1];N[I];A[I];B[I];Q[I];S[I]
300 NEXT I
310 DISP "HAVE YOU FINISHED";
320 INPUT P
330 IF P=0 THEN 30
340 REWIND
350 END
```

TABLE 1.1. *Data of typical structural steels* — After Baumgardt, H. et al (1981)

Steel	Chemical composition % (ladle analysis)						Mechanical properties [1]			ISO-V		Rules		
	C	Si	Mn	Ni	Nb		R_{eH} / R_m N/mm²		A_5 %	A_V-20 Joule	T_{27} °C	Germany	France	Great Britain
Structural Steels														
St 37-3	⩽0,17						225	340 – 470	24	27	-20	DIN 17100	NFA 35-501	BS 4360
St 52-3	⩽0,20	⩽0,55	⩽1,60				345	490 – 630	20	27	-20	DIN 17100	NFA 35-501	BS 4360, 968
High Strength Low Alloy Steels														
St E 355	0,20	0,10/ 0,50	0,90/ 1,60	–	⩽0,05		355	490 – 630	22	27	-20	SEW 089 (draft DIN 17102)	NFA 36-201-205- 208-506	BS 4360, 1501, 968,
St E 460	⩽0,5	0,10/ 0,50	1,10/ 1,50	0,60	⩽0,03	0,60Cu 0,12V	450	560 – 730	17	27	-20	SEW 089 (draft DIN 17102)	NFA 36-201	BS 4360
Shipbuilding Steels														
Grade A	⩽0,23	⩽0,35	⩾2,5×C	–	–		235	400 – 490	22	–	–		draft I A C S	
EH 36	⩽0,18	0,10/ 0,50	0,90/ 1,60	–	0,02/ 0,05		355	490 – 620	21	24 -40°C	–			
Cryogenic Steels														
11 Mn 5	⩽0,14	0,15/ 0,50	0,70/ 1,60	⩽0,30	⩽0,05		255	400 – 490	24	–	-55	——	NFA 36 -208	——
13 Mn 6	⩽0,15	0,15/ 0,50	0,70/ 1,60	⩽0,30	⩽0,05		325	490 – 570	21	–	-55	——	NFA 36 -208	——

1) at 30mm plate thickness

s block   p block

1st period (shown in d block area):
- 1 H: A3, A1
- 2 He: (A3), (A2)

d block

	IA	IIA	IIIA	IVA	VA	VIA	VIIA	VIII	VIII	VIII	IB	IIB	IIIB	IVB	VB	VIB	VIIB	0
2nd	3 Li: A2, A1, A3	4 Be: (A2), A3											5 B: H, T, R	6 C: R, H, A4	7 N: H, C	8 O: C, (R)	9 F	10 Ne: A1
3rd	11 Na: A2, A3	12 Mg: A3											13 Al: A1	14 Si: A1	15 P: C, O, C	16 S: O, M, R	17 Cl: A1, A3, A2	18 A: A1
4th	19 K: A2	20 Ca: A2, A1, A3	21 Sc: (A2), A3	22 Ti: A2, A3	23 V: A2	24 Cr: (A1), A2	25 Mn: A2, A1, C, C	26 Fe: A2, A1, A2	27 Co: A1, A2	28 Ni: A1	29 Cu: A1	30 Zn: A3	31 Ga: O	32 Ge: A4	33 As: A7	34 Se: A8, M	35 Br: O	36 Kr: A1
5th	37 Rb: A2	38 Sr: A2, A3, A1	39 Y: A2, A3	40 Zr: A2, A3	41 Nb: A2	42 Mo: A2	43 Tc: A3	44 Ru: A3	45 Rh: A1	46 Pd: A1	47 Ag: A1	48 Cd: A3	49 In: A6	50 Sn: A5, A4	51 Sb: A7	52 Te: A8	53 I: O	54 Xe: A1
6th	55 Cs: A2	56 Ba: A2, (T), (H)	57 La: A2, A1, H	72 Hf: A2, A3	73 Ta: A2	74 W: A2	75 Re: A3	76 Os: A3	77 Ir: A1	78 Pt: A1	79 Au: A1	80 Hg: R, T	81 Tl: A2, A3	82 Pb: A1	83 Bi: A7	84 Po: R, C	85 At	86 Rn
7th	87 Fr	88 Ra	89 Ac: A1															

f block

6th (continued)	58 Ce: A2, A1, H	59 Pr: A2, H	60 Nd: A2, H	61 Pm	62 Sm: (A2), R	63 Eu: A2	64 Gd: (A2), A3	65 Tb: (A2), A3	66 Dy: (T), A3	67 Ho: (T), A3	68 Er: A3	69 Tm: A3	70 Yb: A2, A1	72 Lu: (?), A3
7th (continued)	90 Th: A2, A1	91 Pa: T	92 U: A2, T, O	93 Np: A2, T, O	94 Pu: A2, T, A1, O, M, M	95 Am: H	96 Cm	97 Bk	98 Cf	99 Es	100 Fm	101 Md	102 No	103 Lw

TABLE 2.1. These Strukturbericht and other designations are used to denote the structures of the allotropic forms which are given in the order of their appearance.
A1 = f.c.c.; A2 = b.c.c.; A3 = c.p.h.; A4 = diamond cubic; A5 = b.c.t.; A6 = f.c.t.; A7 = rhombohedral; A8 = trigonal; H = hexagonal (usually ABAC···close-packed); R = rhombohedral; O = orthorhombic; C = complex cubic; T = tetragonal; M = monoclinic; ( ) = uncertain.

TABLE 2.2. *Data of Atomic Radii, Sizes of Intersticies, Melting Points and Density of the Most Common Elements in H.S.L.A. steels*

Element	Structure (1)	Atomic Radii (1) $\overset{\circ}{RA}$	Sizes of Intersticies in Å (2) r_6	r_4	Panling's (1) Electronegativity	Melting (1) Points $^\circ$C	Density (1) g/cc
Fe	b.c.c.	1.24	0.19	0.36	1.8	1536	7.87
	f.c.c.	1.27	0.53	0.29			
C	hex.	0.77	-	-	2.5	3930	2.30
N		0.71	-	-	3.0	- 209.7	1.165
Si	cubic	1.17			1.8	1407.	2.30
Mn	cubic	1.12			1.5	1517.	7.44
Al	f.c.c.	1.42	0.59	0.32	1.5	660.	2.70
Nb	b.c.c.	1.44	0.22	0.42	1.6	2468.	8.57
Ti	h.c.p.	1.45	0.60	0.33	1.5	1675.	4.54
	b.c.c.	1.42	0.22	0.41			
V	b.c.c.	1.33	0.21	0.39	1.6	1887.	6.10
S	f.c. ortho	1.06			2.5	113.	2.07
P	Cubic	1.10			2.1	44.	2.20
Cu	f.c.c.	1.28	0.53	0.29	1.9	1083.	8.93
Ni	f.c.c.	1.24	0.51	0.28	1.8	1453.	8.90

(1) Obtained from Science Data Book, edited by R. M. Tennent, 1971.

(2) Calculated through the assumption that the atoms are spherical of R radius then the radii of the inscribed spheres in the octahedral (r_6) and tetrahedral intersticies (r_4) are calculated for; f.c.c. and h.c.p: $r_6 = 0.414$ R and $r_4 = 0.225$ R
b.c.c: $r_6 = 0.155$ R and $r_4 = 0.291$R

TABLE 2.3. Solubility of Carbon and Nitrogen in γ and α-iron

	Temp. ^{O}C	wt. %	at %
C in γ	1150	2.04	8.3
N in γ	650	2.80	10.3
C in α	723	0.02	0.095
C in α	20	< 0.00005	< 0.00012
N in α	590	0.10	0.40
N in α	20	< 0.0001	< 0.0004

TABLE 2.4. Nb-C System Structures

Crystal		Lattice Parameter $\overset{o}{A}$			Description
Phase	Structure Type	a	b	c	
α (Nb)	bcc A2	3.294	-	-	Interstitial C in Nb max. solub. 3 at % at 2300°C
β (Nb$_2$C)	hcp	3.12	-	4.95	Limited solubility around the stoichiometric comp. (33.3 at % C) below 1500°C.
γ (NbC)	fcc B^1(NaCl)	4.47	-	-	Non stoichiometric carbide 'a' value depending on vacancy concentration

TABLE 2.5.   Nb-N System Structures

Phase	Crystal Structure	Type	Lattice Paremeter Å			Description
			a	b	c	
α-Nb(N)	b.c.c.	A2	3.3007	-	-	Basically Nb with N dissolved interstitially 2 at % at 1500°C and 18 at % at 2,300°.
β-Nb$_2$N	Hexagonal	L'3	3.058	-	4.961	Range of homogeneity 0.35 < N/Nb ≤ 0.5
γ-Nb N$_x$(Nb$_4$N$_3$)	Tetragonal	P 4/m	8.742	-	8.592	At N/Nb = 0.64 but exist as NbN$_{0.75}$ and NbN$_{0.71}$
δ-NbN$_x$	Cubic	B1	4.381	-	-	As NbN$_{0.88}$} at > 1250°C in the range of
			4.392	-	-	NbN$_{0.99}$) 0.7 < N/Nb < 0.95
δ'-NbN$_x$	Hexagonal	Anti-NiAs	2.968	-	5.5499	At 0.97 ≤ N/Nb ≤ 0.98
ϵ-NbN	Hexagonal	Ti P	2.959	-	11.271	At N/Nb = 1.00 and 1.018
Nb$_5$N$_6$	Hexagonal		5.193	-	10.380	At 1.18 < N/Nb < 1.20 at 700°C
Nb$_4$N$_5$	Tetragonal		6.873	-	4.298	Believed to be stabilized by impurities.

TABLE 2.6.   *Solubility Equations of Niobium Carbide in Austenite*

No	Author		Method (1)	Austenitization Temp. °C	Solubility Product $\log K'_C$	K'_C
1	Brown, J. R.	(1965)	D1	-	3.3 – 7900/T	%Nb. %C
2	De Kazinczy et al	(1963)	A	900 – 1200	-0.63 – 2500/T	%Nb. %C
		"	D2		2.90 – 7500/T	%Nb. %C
3	Imai and Shono	(1966)		1000 – 1200	7.58 – 14000/T	%Nb. %C
4	Johansen, T. et al	(1967)	C	950 – 1050	4.37 – 9290/T	%Nb. %C
5	Koyama, S. et al	(1971)	C	1050 – 1150	3.31 – 7970/T	%Nb. %C
6	Lakshmanan, V. K.	(1977)	C	950 – 1250	3.40 – 7920/T	%Nb. %C$^{0.87}$
		(1977)	B	950 – 1200	2.7 – 6900/T	%Nb. %C$^{0.87}$
7	Mandry and Dornelas	(1966)	B	950 – 1225	4.54 – 9600/T	%Nb. %C$^{0.87}$
8	Meyer, L.	(1966)	B	900 – 1300	3.04 – 7290/T	%Nb. %C
9	Mori et al	(1968)	B	1000 – 1300	3.18 – 7700/T	%Nb. %C$^{0.87}$
10	Narita, K. and Koyama, S.	(1966)	C	1100 – 1300	3.43 – 7900/T	%Nb. %C
11	Nilsson, R.	(1968)	A	1085 – 1115	-2.84 – 2.61	%Nb. %C
12	Nordberg and Aronsson	(1968)	D3	900 – 1200	2.96 – 7510/T	%Nb. %C
		"	D4	900 – 1200	3.11 – 7520/T	%Nb. %C$^{0.87}$
		"	D1	-	3.43 – 7200/T	%Nb. %C$^{0.87}$
13	Reistad and Sehlstedt	(1967)	B	880, 900, 1000	-3.38, -3.38, -2.93	%Nb. %C
14	Smith, R. P.	(1966)	C	1000 – 1300	3.7 – 9100/T	%Nb. %C
15	Wilson and Gieselman	(1962)	B	1204	-1.97, -2.14, -2.37	%Nb. %C

(1) Methods: A: Hardness measurements after quenching and tempering
      B: Isolation of precipitates and chemical analysis
      C: Equilibrium using H_2/CH_4 gas mixtures – Chemical Analysis
      D1: Theoretical equations obtained through thermodynamic analysis
      D2: Recalculated by Nordberg and Aronsson (1968) under the assumption that the hardness is proportional to the average distance between the coherent NbC particles.
   D3 & D4: Average of previous equations to 1968, assuming stoichimetric and non-stoichiometric precipitates

TABLE 2.7.   _Solubility Equations of Niobium Nitride in Austenite_

No	Author		Method	Austenitization Temp. $^{\circ}C$	Solubility Product $\log K'_N$	K'_N
1	Lakshmanan	(1977)	D1	-	4.41 - 10,341/T	$\%Nb\ \%N^{0.87}$
2	Mori et al	(1968)	B	1000 - 1300	3.79 - 10,150/T	$\%Nb\ \%N, \varepsilon\text{-}NbN_{0.9\text{-}1.0}$
3	Narita and Koyana	(1966)	C	1100 - 1300	2.89 - 8,500/T	$\%Nb\ \%N, \varepsilon\text{-}NbN_{0.9\text{-}1.0}$
4	Smith	(1962)	C	1191 - 1336	4.04 - 10,230/T	$\%Nb\ \%N, \varepsilon\text{-}NbN_{0.9\text{-}1.0}$

TABLE 2.8. Solubility Equations of Niobium Carbonitride in Austenite

No	Author		Method	Austenitization Temp. $^{\circ}C$	Solubility Product $\log K'_{C,N}$	$K'_{C,N}$
1	Irvine et al	(1967)	B	900 - 1200	2.26 - 6,770/T	%Nb (%C + 12/14%N)
2	Mandry and Dornelas	(1966)	B	950 - 1225	4.46 - 9,800/T	%Nb %C$^{0.83}$ %N$^{0.14}$
3	Meyer, L.	(1967)	B	900 - 1300	1.54 - 5,860/T	%Nb (%C + %N)
4	Mori et al	(1965)			4.09 - 10,400/T	%Nb %C$^{0.24}$ %N$^{0.63}$
5	Yamamoto et al	(1981)			1.93 - 6,570/T	%Nb (%C + 12/14%N)

TABLE 2.9.   Estimated Values of K'_N

	Estimated [1]
T°C	log [Nb] [%N]$^{0.87}$
1000	- 3.75 ± 0.15
1100	- 3.10 ± 0.20
1200	- 2.60 ± 0.20
1300	- 2.20 ± 0.20

[1] By Lakshmanan (1977), These values plotted as log K'_N vs 1/T gives the following equation.

$$\log [\%Nb] [\%N]^{0.87} = 4.41 - 10,341/T$$

TABLE 2.10   *Effects of Mn, Si, Cr and Ni on the Solution and Precipitation of Nb C and NbN in Iron Austenite*

Solubility Product	Experimental Equations	Temp-Range
log [%Nb] [%C]	$-7970/T + 3.31 + (1371/T-0.900)$ [% Mn] $- (75/T-0.0504)$ [% Mn]^2	
log [%Nb] [%C]	$-7970/T + 3.31 - (735/T-0.348)$ [% Si]	$1050 - 1150^{\circ}C$
log [%Nb] [%C]	$-7970/T + 3.31 + (1113/T-0.691)$ [% Cr] $- (38/T-0.0228)$ [% Cr]^2	
log [%Nb] [%C]	$-7970/T + 3.31 + (148/T -0.0904)$ [% Ni] $+ (8.5/T-0.0068)$ [% Ni]^2	
log [%Nb] [%N]	$-8500/T + 2.89 + (1085/T - 0.68)$ [% Mn] $- (48/T + 0.032)$ [% Mn]^2	
log [%Nb] [%N]	$-8500/T + 2.89 - (1900/T - 1.103)$ [% Si]	$1100 - 1250^{\circ}C$
log [%Nb] [%N]	$-8500/T + 2.89 + (1290/T - 0.77)$ [% Cr] $- (51/T + 0.034)$ [% Cr]^2	
log [%Nb] [%N]	$-8500/T + 2.89 + (694/T - 0.44)$ [% Ni] $- (29/T - 0.0178)$ [% Ni]^2	

(1)   Koyama et al (1971a) and (1971b)

TABLE 2.11. Wagner Thermodynamic Interaction Coefficients for Carbon and Nitrogen Alloys, ε_C^M and ε_N^M

Alloying Element		Reference	
	ε_C^M		
Mn	$- 5070/T$	Wada et al	(1971)
Si	$4.84 + 7370/7$	Wada et al	(1972a)
Cr	$7.02 - 21880/T$	Wada et al	(1972b)
Ni	$0.69 + 4600/T$	Grabke, et al	(1975)
Mo	$3.86 - 17870/T$	Srivastava	(1976)
	ε_N^M		
Mn	$17.2 - 31950/T$	Miroslava and Tuma	(1973)
Mn	$3.0 - 16140/T$	Mori et al	(1963)
Mn	$(8.2 - 21000/T)\pm0.5$	Grabke, et al	(1975)
Si	$-35. + 57700/T$	Mori et al	(1964b)
Cr	$9.6 - 26400/T$	Milinskaya and Tomlin	(1973)
Cr	$31.1 - 80000/T$	Mori et al	(1963)
Cr	$(43. - 92000/T)\pm 1$	Grabke et al	(1975)
Ni	4.5 ($1050^{o}C$)	Mori et al	(1963)
Ni	4.1 ($1250^{o}C$)		
Ni	$3000/T$	Milinskaya and Tomlin	(1973)
Mo	$- 9552/T$	Schenk and Steinmetz	(1966)

TABLE 2.12

Niobium-Alloy Interaction Coefficients Evaluated by Lakshmanan Using Koyama's Results and the Interaction Coefficients given in Table 2.11.

Alloying Element	ε^M_{Nb}
Mn	175 - 26260/T
Si	-100 + 160640/T
Cr	37 - 72625/T
Ni	$\sim$ 7000/T
Mo(*)	0

* ε^{Mo}_{Nb} = 0 assumed, considering a possible complete mutual solid solubility in the Mo-Nb binary system

Table 2.13 Diffusivities of elements in γ- and α-iron

Solvent	Solute	Activation energy. Q (kJ mol^{-1})	Frequency factor. D_o (cm^2 s^{-1})	Diffusion coefficient. $D_{910\,C}$ (cm^2 s^{-1})	Temperature range (°C)
γ-iron	C	135	0.15	1.5×10^{-7}	900-1050
	Fe	269	0.18	2.2×10^{-13}	1060-1390
	Co	364	3.0×10^2	24.0×10^{-12} (at 1050°C)	1050-1250
	Cr	405	1.8×10^4	58.0×10^{-12} (at 1050°C)	1050-1250
	Cu	253	3.0	15.0×10^{-11}	800-1200
	Ni	280	0.77	7.7×10^{-13}	930-1050
	P	293	28.3	3.6×10^{-12}	1280-1350
	S	202	1.35	1.5×10^{-9}	1200-1350
	W	376	1.0×10^3	12.0×10^{-12} (at 1050°C)	1050-1250
α-iron	C	80	6.2×10^{-3}	1.8×10^{-6}	
	N	76	3.0×10^{-3}	1.3×10^{-6}	
	Fe	240	0.5		700-750
	Co	226	0.2	2.1×10^{-11}	700-790
	Cr	343	3.0×10^4		
	Ni	258	9.7	3.7×10^{-11}	700-900
	P	230	2.9	2.0×10^{-10}	860-900
	W	293	3.8×10^2		

Data from Askill. J., *Tracer Diffusion Data for Metals. Alloys and Simple Oxides*, IFI/Plenum. 1970. Wohlbier. F. H., *Diffusion and Defect Data*. Materials Review Series, Vol 12. Nos 1-4, Trans Tech Publications. 1976, Krishtal, M. A., *Diffusion Processes in Iron Alloys*. translated from Russian by A Wald. ed. J. J. Becker, Israel Program for Scientific Translations. Jerusalem. 1970.

TABLE 2.14.   *Experimental Data of the Temperature-Time-Precipitation Diagrams. Figures 2.20 and 2.21.*

Reference	Deform. Method	Pptation. Analysis	Reheat Temp. °C	Reheat γ g.s. μm	Strain	Deformation Temp. °C	%C	%N	%Nb	%Si	% Mn	%Al
Hansen et al (1980)	Rolling	Extraction Replicas	1250	405	0.80	950	0.11	0.010	0.031	0.26	1.35	0.023
			1250	140	0.80	950	0.10	0.010	0.095	0.23	1.24	0.014
Hoogendoorn & Spanraft (1977)	Rolling	Electrolytic Extraction	1250	-	0.80	Ti	0.10	0.008	0.040	-	0.99	-
Jizaimarn et al (1974)	-	Hardness	1250	-	0.0	Not def.	0.06	-	0.090	0.06	1.26	-
			1250	-	0.0	Not def.	0.06	-	0.170	0.05	1.60	-
Le Bon et al (1975)	Torsion	Micro-hardness	1250	250	ε_i	Ti	0.17	0.011	0.040	0.31	1.35	0.017
Ouchi et al (1977)	Rolling	Hardness	1250	225	0.8	Ti	0.16	0.0054	0.031	0.36	1.41	0.020
Simoneau et al (1978)	-	Electrical Resistivity	1350	-	0.0	Not def.	0.07	0.0103	0.04	0.26	0.88	0.027
			1350	-	0.0	Not Def.	0.19	0.0072	0.058	0.01	0.65	0.008
Watanabe et al (1977)	Rolling	Chemical Extraction	1260	-(1)	0.41	980	0.063	0.0058	0.084	0.11	1.71	0.024
Weiss and Jonas (1979)	Compression	Strain to the peak	1100	-	-	- (2)	0.05	0.004	0.035	0.045	0.42	0.057
Yamamoto et al (1982)	Rolling	Extraction Replicas	-	140	0.69	T	0.19	0.0028	0.095	0.25	1.49	0.032

(1)   After reheating this steel was given a three roughing passes of 30% reduction in area and before rolling at 980°C the austenite grain size was ~ 25 μm

(2)   Dynamic precipitation.   Deformed at constant strain rate and pre-deformed 5%

TABLE 2.15   Lattice Mismatch for $Nb\ C_x\ N_y$ Precipitates in Austenite

Temperature °C	Orientation Relationship	Required Distortion of Matrix, % (*) $NbC_x\ N_{(0.87 - x)}$
	$[100]_{ppt} \parallel [100]_\gamma$	22.9%
1100 $a_\gamma = 3.6617\ \overset{o}{A}$	$[010]_{ppt} \parallel [010]_\gamma$	22.9%
$a_{NbC_x\ N_{0.87-x}} = 4.5027\ \overset{o}{A}$	$[001]_{ppt} \parallel [001]_\gamma$	22.9%
	$[100]_{ppt} \parallel [100]_\gamma$	23.4%
900	$[010]_{ppt} \parallel [010]_\gamma$	23.4%
$a_\gamma = 3.6437\ \overset{o}{A}$	$[001]_{ppt} \parallel [001]_\gamma$	23.4%
$a_{NbC_x\ N_{0.87-x}} = 4.4964\ \overset{o}{A}$		

(*) This is the % increase in the matrix (γ) lattice parameter
that would be required to bring the two lattices into
coincidence at the matrix - precipitate interface.

TABLE 3.1 Values for Avrami k, n relevant to microalloyed austenite after Roberts, W. (1980)

Composition of austenite									$T(°C)$	$\dot{\varepsilon}(s^{-1})$	ε	$k(s^{-1})$	n
C	Si	Mn	P	S	Al	Nb	V	N					
0.12	0.27	1.11	0.010	0.016	0.042	–	–	0.008	800	1	0.23±0.02	0.14	0.85±0.04
0.20	0.43	1.31	0.015	0.025	0.043	0.025	–	0.007	800	"	0.30±0.02	0.011	0.83±0.04
									900	"	"	0.019	0.87±0.05
									950	"	"	0.13	0.89±0.04
									800	"	0.17±0.01	0.0012	0.95±0.05
									900	"	"	0.0010	1.01±0.06
									1000	"	"	0.19	0.95±0.05
0.18	0.39	1.17	0.022	0.020	–	0.025	–	0.007	800	"	0.30±0.02	0.0062	0.83±0.06
									900	"	"	0.0053	0.90±0.03
0.09	0.35	1.35	0.035	0.020	–	–	0.09	0.008	850	"	"	0.0064	0.88±0.05
									900	"	"	0.057	0.87±0.05
									850	0.05	"	0.0064	0.87±0.06

TABLE 3.2   *Experimental Data Temperature-Time-Recrystallization Diagram*

Figures 3.11 and 3.12

Reference		Deformn. Method	Recrystallisation Analysis	Reheat. Temp. °C	Reheated γ g.s. μm	Deformn. ε (1)	Deformn. Temp. °C	Strain Rate $\dot{\varepsilon}$, sec⁻¹	% C	% N	% Nb	% Si	% Mn	% Al	% P
Cohen et al	(1979)	Rolling	Metallography	1250	140	0.80	950	2.6	0.10	0.010	0.095	0.23	1.3	0.014	0.010
Coladas et al	(1977)	"	"	1200	180	0.26	Ti	18.0	0.41	0.044	0.064	0.235	0.68	-	0.008
Davenport et al	(1977)	"	"	1300	-	0.26	Ti	-	0.08	0.020	0.090	-	1.25	0.018	-
Hansen et al	(1980)	"	"	1250	405	0.80	950	2.6	0.11	0.010	0.03	0.26	1.35	0.023	0.008
Hoogendoorn et al	(1977)	"	"	1250		0.80	Ti	-	0.10	0.008	0.04	-	0.99	-	-
Greday & Lamberigts	(1973)	Tension	"	1150	-	0.41	Ti	-	0.17	0.007	0.020	0.37	1.40	0.039	0.020
Lamberigts et al	(1977)	Tension	"	1200	-	0.41	Ti	-	0.165	0.0063	0.027	0.345	1.32	0.34	0.025
Le Bon et al	(1977)	Torsion	"	1250	250	$0.86\varepsilon_p$ (2)	Ti	16.0	0.17	0.011	0.04	0.31	1.35	0.017	0.014
Ohmori, Y.	(1966)	Rolling	"	1250	-	0.41	Ti	-							
Ouchi et al	(1977)	"	"	1250		0.80	1000	14.0	0.16	0.0054	0.031	0.36	1.41	0.027	0.018
Roberts, W.	(1980)	"	"	-	300	0.30	Ti	1.0	0.18	0.007	0.025	0.39	1.17	-	-
Yamamoto et al	(1981)		"		140	0.69	Ti		0.19	0.0028	0.095	0.25	1.49	0.032	-

(1) In all cases the strain given is the converted to equivalent tensile strain. For rolling: $\varepsilon = \dfrac{2}{\sqrt{3}} \ln 100/(100-\% \text{ Red})$

(2) ε_p is the strain to the peak

TABLE 4.1

CHEMICAL COMPOSITIONS OF EXPERIMENTAL STEELS

wt %

Code	C	N	Mn	Si	Al	Nb	V	Ti	S	P	Cu	Cr	Ni	Mo	Sn
97	0.084	0.0061	1.30	0.29	<0.005	0.03	<0.02	<0.02	0.007	.009	<0.02	<0.02	<0.02	<0.02	<0.02
99	0.080	0.0151	1.52	0.32	<0.005	0.03	<0.02	<0.02	0.006	0.006	<0.02	<0.02	<0.02	<0.02	<0.02
12	0.082	0.007	1.69	0.26	<0.005	0.03	<0.02	<0.02	0.006	<0.005	<0.02	<0.02	<0.02	<0.02	<0.02
22	0.084	0.0150	1.48	0.34	<0.005	0.06	<0.02	<0.02	0.006	0.006	<0.02	<0.02	<0.02	<0.02	<0.02
23	0.081	0.0141	1.42	0.32	<0.005	0.12	<0.02	<0.02	0.006	0.005	<0.02	<0.02	<0.02	<0.02	<0.02

TABLE 4.2

RELATIVE ERROR AND SIZE OF SAMPLE

$RE\ (\bar{L})$	Required Number of Grains for $\bar{L}$
0.010	4225
0.025	679
0.050	169
0.075	75
0.100	42

TABLE 5.1 SOLUBILITY OF NIOBIUM CARBONITRIDE ORIGINAL CONDITIONS

T C	CARBON S	NITROG S	NIOBIUM S	X	VOL.FRAC.	FREE ENERG	N/(N+C)

STEEL 97

STEEL 99

STEEL 22

STEEL 23

(Temperatures: 900.0, 950.0, 1000.0, 1050.0, 1100.0, 1150.0, 1200.0, 1250.0, 1300.0, 1350.0)

STEEL COMPOSITIONS INPUT IN MOL FRACTION

CONF	CARB. TOT.	NITROG TOT.	NIOBIUM TOT.
97	0.003880	0.000240	0.000190
99	0.003490	0.000590	0.000190
22	0.003883	0.000555	0.000358
23	0.003746	0.000575	0.000717

TABLE 5.2.   Solubility Temperatures
$^{\circ}$C

Author	Phase	Steel			
		97	99	22	23
Brown, J. R. (1965)	NbC	1066	1062	1138	1214
De Kazinczy et al -A (1963)	NbC	997	983	1226	1536
De Kazinczy et al -D2 (1963)	NbC	1127	1086	1170	1254
Imai and Shono (1966)	NbC	1102	1100	1144	1186
Johansen, T. et al (1967)	NbC	1060	1056	1120	1183
Koyama, S. et al (1971)	NbC	1076	1071	1148	1224
Lakshmanan, V.K. (1977)	$NbC^{0.87}$	1079	1075	1152	1230
Meyer, L. (1966)	NbC	1020	1015	1093	1170
Mori et al (1968a)	$NbC^{0.87}$	1093	1088	1170	1252
Narita and Koyama (1966)	NbC	1037	1033	1106	1179
Nordberg & Aronsson, D3, (1968)	NbC	1078	1073	1155	1237
" " D4, (1968)	$NbC^{0.87}$	1077	1073	1155	1237
" " D1, (1968)	$NbC^{0.87}$	950	946	1016	1085
Smith, R. P. (1966)	NbC	1172	1167	1244	1320
Mandry & Dornelas (1966)	$NbC^{0.87}$	1099	1095	1160	1225
Lakshmanan, V.K. (1977)	$NbC^{0.87}$	1065	1060	1147	1237
Lakshmanan, V. K. (1977)	$NbN^{0.87}$	1043	1103	1160	1217
Mori et al (1968a)	NbN	1075	1150	1212	1274
Narita and Koyana (1966)	NbN	1010	1091	1159	1228
Smith, (1962)	NbN	1042	1112	1171	1229
Irvine et al (1967)	Nb(C+12/14N)	1128	1133	1233	1334
Mandry and Dornelas (1966)	$NbC^{0.83}N^{0.14}$	1091	1098	1162	1224
Mori et al (1965)	$NbC^{0.24}N^{0.65}$	1150	1200	1266	1333
Meyer, L. (1967)	Nb(C+N)	1153	1162	1283	1410
Yamamoto et al (1981)	Nb(C+12/14N)	1186	1192	1304	1420
Model (1982)		1133	1160	1235	1315
Experimental (1982)	$NbC_x N_{(0.87-x)}$	< 1200	<1200	<1300	<1300

TABLE 5.3. Solubility Temperatures
^{o}C

Solubility Equation Author		Phase	Steel		
			HE 1	HE 4	HE 5
Irvine et al	(1967)	Nb(C + 12/14N)	1277	1136	1297
Mandry and Dornelas	(1966)	$NbC^{0.83} N^{0.14}$	1182	1099	1203
Mori et al	(1965)	$NbC^{0.24} N^{0.65}$	1335	1169	1361
Meyer, L.	(1967)	Nb(C + N)	1355	1195	1377
Yamamoto et al	(1981)	Nb(C + 12/14N)	1233	1275	1309
This model		$NbC_x N_{(0.87 - x)}$	1245	1218	1293
Experimental		-	1250	1150	1300

TABLE 5.4. Experimental Steels

Mori et al		Hoesch-Estel		This Work	
Steel	Nb/(C + N)	Steel	Nb/(C + N)	Steel	Nb/(C + N)
CN1	0.65	HE1	0.093	97	0.043
CN3	0.23	HE2	0.242	99	0.042
CN5	0.87	HE3	0.247	22	0.080
CN6	1.05	HE4	1.810	23	0.167
		HE5	0.584		

TABLE 5.5. Trial 3

Steel 99

T_s	x
1160°	0.446
1130°	0.429
1095°	0.403

TABLE 5.6. SOLUBILITY OF NIOBIUM CARBONITRIDE -EFFECT OF MANGANESE-
STEEL 97

T C	CARB. S	NITRO. S	NIOB. S	X	VOL.FRAC.	FREE ENER.	N/(N+C)
			0.002 Mn				
900.0	.3802E-02	.174E-03	.136E-04	0.475	0.1391E-03	-.1684E 06	0.4571
950.0	.3803E-02	.185E-03	.264E-04	0.510	0.1283E-03	-.1675E 06	0.4164
1000.0	.3810E-02	.197E-03	.435E-04	0.540	0.1099E-03	-.1668E 06	0.3824
1050.0	.3826E-02	.211E-03	.841E-04	0.565	0.8011E-04	-.1662E 06	0.3528
1100.0	.3856E-02	.228E-03	.139E-03	0.586	0.3437E-04	-.1658E 06	0.3293
1150.0	.3903E-02	.250E-03	.219E-03	0.602	-.3274E-04	-.1655E 06	0.3005
1200.0	.3972E-02	.279E-03	.331E-03	0.614	-.1266E-03	-.1653E 06	0.2994
1250.0	.4067E-02	.315E-03	.433E-03	0.624	-.2535E-03	-.1653E 06	0.2855
1300.0	.4192E-02	.360E-03	.630E-03	0.630	-.4183E-03	-.1654E 06	0.2779
1350.0	.4350E-02	.416E-03	.928E-03	0.634	-.6258E-03	-.1655E 06	0.2727
			0.010 Mn				
900.0	.3808E-02	.176E-03	.217E-04	0.465	0.1323E-03	-.1641E 06	0.4673
950.0	.3810E-02	.188E-03	.391E-04	0.500	0.1177E-03	-.1638E 06	0.4275
1000.0	.3821E-02	.201E-03	.666E-04	0.530	0.9474E-04	-.1636E 06	0.3937
1050.0	.3841E-02	.217E-03	.108E-03	0.555	0.6017E-04	-.1636E 06	0.3639
1100.0	.3873E-02	.236E-03	.167E-03	0.575	0.1046E-04	-.1638E 06	0.3326
1150.0	.3921E-02	.259E-03	.250E-03	0.593	-.5815E-04	-.1641E 06	0.3209
1200.0	.3987E-02	.287E-03	.359E-03	0.607	-.1495E-03	-.1645E 06	0.3045
1250.0	.4075E-02	.320E-03	.499E-03	0.618	-.2670E-03	-.1650E 06	0.2809
1300.0	.4137E-02	.360E-03	.675E-03	0.627	-.4139E-03	-.1656E 06	0.2718
1350.0	.4325E-02	.406E-03	.889E-03	0.635	-.5927E-03	-.1662E 06	0.2718
			0.020 Mn				
900.0	.3817E-02	.181E-03	.388E-04	0.451	0.1180E-03	-.1583E 06	0.4856
950.0	.3824E-02	.195E-03	.633E-04	0.485	0.9751E-04	-.1592E 06	0.4442
1000.0	.3839E-02	.211E-03	.984E-04	0.515	0.6818E-04	-.1598E 06	0.4130
1050.0	.3862E-02	.229E-03	.147E-03	0.540	0.2785E-04	-.1605E 06	0.3830
1100.0	.3897E-02	.249E-03	.211E-03	0.562	-.2564E-04	-.1614E 06	0.3562
1150.0	.3915E-02	.273E-03	.293E-03	0.581	-.9423E-04	-.1624E 06	0.3359
1200.0	.4007E-02	.299E-03	.395E-03	0.597	-.1800E-03	-.1635E 06	0.3174
1250.0	.4035E-02	.328E-03	.520E-03	0.611	-.2843E-03	-.1646E 06	0.2998
1300.0	.4131E-02	.360E-03	.668E-03	0.624	-.4033E-03	-.1658E 06	0.2846
1350.0	.4296E-02	.394E-03	.841E-03	0.636	-.5531E-03	-.1671E 06	0.2708
			0.040 Mn				
900.0	.3856E-02	.211E-03	.118E-03	0.403	0.5190E-04	-.1486E 06	0.5422
950.0	.3871E-02	.231E-03	.158E-03	0.437	0.1797E-04	-.1505E 06	0.5025
1000.0	.3892E-02	.251E-03	.207E-03	0.469	-.2237E-04	-.1525E 06	0.4647
1050.0	.3921E-02	.271E-03	.263E-03	0.498	-.6926E-04	-.1546E 06	0.4308
1100.0	.3956E-02	.291E-03	.327E-03	0.525	-.1227E-03	-.1568E 06	0.3999
1150.0	.3999E-02	.310E-03	.398E-03	0.551	-.1825E-03	-.1591E 06	0.3704
1200.0	.4049E-02	.328E-03	.477E-03	0.574	-.2484E-03	-.1615E 06	0.3431
1250.0	.4106E-02	.345E-03	.563E-03	0.597	-.3202E-03	-.1639E 06	0.3170
1300.0	.4170E-02	.360E-03	.655E-03	0.618	-.3974E-03	-.1663E 06	0.2920
1350.0	.4241E-02	.373E-03	.753E-03	0.638	-.4793E-03	-.1688E 06	0.2693
			0.050 Mn				
900.0	.3885E-02	.248E-03	.126E-03	0.364	-.1332E-04	-.1439E 06	0.5942
950.0	.3904E-02	.269E-03	.242E-03	0.401	-.5143E-04	-.1465E 06	0.5435
1000.0	.3928E-02	.288E-03	.271E-03	0.436	-.9310E-04	-.1492E 06	0.5033
1050.0	.3956E-02	.306E-03	.315E-03	0.470	-.1379E-03	-.1519E 06	0.4639
1100.0	.3990E-02	.322E-03	.402E-03	0.502	-.1854E-03	-.1547E 06	0.4278
1150.0	.4028E-02	.335E-03	.461E-03	0.533	-.2351E-03	-.1576E 06	0.3908
1200.0	.4070E-02	.346E-03	.523E-03	0.552	-.2865E-03	-.1605E 06	0.3570
1250.0	.4116E-02	.354E-03	.585E-03	0.589	-.3389E-03	-.1635E 06	0.3253
1300.0	.4165E-02	.360E-03	.619E-03	0.615	-.3919E-03	-.1665E 06	0.2957
1350.0	.4216E-02	.363E-03	.712E-03	0.638	-.4451E-03	-.1697E 06	0.2631

TABLE 5.7. SOLUBILITY OF NIOBIUM CARBONITRIDE -EFFECT OF SILICON-

T C	CARB. S	NITRO. S	NIOBI. S	STEEL 97 X	VOL.FRAC.	FREE ENER.	N/(N+C)
			0.0004 Si				
900.0	.3301E-02	.174E-03	0.119E-04	0.1405E-03	-.1597E 06	0.4568	
950.0	.3301E-02	.184E-03	0.237E-04	0.1306E-03	-.1586E 06	0.4160	
1000.0	.3305E-02	.195E-03	0.444E-04	0.1133E-03	-.1577E 06	0.3812	
1050.0	.3306E-02	.209E-03	0.784E-04	0.9490E-04	-.1570E 06	0.3517	
1100.0	.3323E-02	.225E-03	0.132E-03	0.4042E-04	-.1654E 06	0.3261	
1150.0	.3352E-02	.248E-03	0.211E-03	0.2584E-04	-.1659E 06	0.3000	
1200.0	.3399E-02	.275E-03	0.324E-03	0.1200E-03	-.1656E 06	0.2964	
1250.0	.3467E-02	.313E-03	0.478E-03	0.2487E-03	-.1655E 06	0.2851	
1300.0	.4191E-02	.360E-03	0.630E-03	0.4178E-03	-.1654E 06	0.2783	
1350.0	.4354E-02	.419E-03	0.933E-03	0.6325E-03	-.1554E 06	0.2740	
			0.0020 Si				
900.0	.3302E-02	.172E-03	0.113E-04	0.1409E-03	-.1705E 06	0.4655	
950.0	.3302E-02	.193E-03	0.223E-04	0.1314E-03	-.1693E 06	0.4231	
1000.0	.3308E-02	.194E-03	0.428E-04	0.1145E-03	-.1683E 06	0.3884	
1050.0	.3322E-02	.208E-03	0.760E-04	0.8636E-04	-.1675E 06	0.3568	
1100.0	.3348E-02	.225E-03	0.123E-03	0.4321E-04	-.1669E 06	0.3332	
1150.0	.3396E-02	.247E-03	0.205E-03	0.2204E-04	-.1664E 06	0.3130	
1200.0	.3463E-02	.276E-03	0.318E-03	0.1153E-03	-.1660E 06	0.3054	
1250.0	.3585E-02	.313E-03	0.471E-03	0.2429E-03	-.1658E 06	0.2955	
1300.0	.4184E-02	.360E-03	0.672E-03	0.4111E-03	-.1657E 06	0.2828	
1350.0	.4349E-02	.421E-03	0.923E-03	0.6165E-03	-.1657E 06	0.2785	
			0.0040 Si				
900.0	.3303E-02	.170E-03	0.107E-04	0.1415E-03	-.1714E 06	0.4766	
950.0	.3303E-02	.181E-03	0.215E-04	0.1323E-03	-.1701E 06	0.4341	
1000.0	.3308E-02	.194E-03	0.410E-04	0.1162E-03	-.1691E 06	0.3968	
1050.0	.3321E-02	.205E-03	0.678E-04	0.8921E-04	-.1682E 06	0.3663	
1100.0	.3348E-02	.224E-03	0.124E-03	0.4661E-04	-.1674E 06	0.3403	
1150.0	.3396E-02	.246E-03	0.201E-03	0.1744E-04	-.1669E 06	0.3187	
1200.0	.3459E-02	.275E-03	0.311E-03	0.1093E-03	-.1665E 06	0.3054	
1250.0	.3581E-02	.312E-03	0.452E-03	0.2358E-03	-.1662E 06	0.2955	
1300.0	.4105E-02	.360E-03	0.652E-03	0.4029E-03	-.1661E 06	0.2984	
1350.0	.4339E-02	.421E-03	0.917E-03	0.6165E-03	-.1660E 06	0.2841	
			0.0080 Si				
900.0	.3306E-02	.167E-03	0.946E-05	0.1425E-03	-.1732E 06	0.4985	
950.0	.3304E-02	.177E-03	0.195E-04	0.1341E-03	-.1718E 06	0.4543	
1000.0	.3308E-02	.174E-03	0.374E-04	0.1191E-03	-.1706E 06	0.4159	
1050.0	.3321E-02	.189E-03	0.678E-04	0.9374E-04	-.1695E 06	0.3838	
1100.0	.3345E-02	.203E-03	0.124E-03	0.5316E-04	-.1687E 06	0.3531	
1150.0	.3392E-02	.221E-03	0.115E-03	0.8598E-05	-.1680E 06	0.2948	
1200.0	.3449E-02	.243E-03	0.170E-03	0.9785E-04	-.1674E 06	0.3177	
1250.0	.3549E-02	.272E-03	0.297E-03	0.2217E-03	-.1671E 06	0.3067	
1300.0	.4039E-02	.310E-03	0.443E-03	0.3867E-03	-.1668E 06	0.2998	
1350.0	.4319E-02	.422E-03	0.896E-03	0.5987E-03	-.1666E 06	0.2954	
			0.0120 Si				
900.0	.3309E-02	.163E-03	0.836E-05	0.1434E-03	-.1751E 06	0.5207	
950.0	.3306E-02	.174E-03	0.195E-04	0.1358E-03	-.1735E 06	0.4729	
1000.0	.3309E-02	.185E-03	0.342E-04	0.1218E-03	-.1721E 06	0.4346	
1050.0	.3319E-02	.200E-03	0.628E-04	0.9797E-04	-.1709E 06	0.3978	
1100.0	.3341E-02	.218E-03	0.109E-03	0.5940E-04	-.1699E 06	0.3646	
1150.0	.3389E-02	.240E-03	0.180E-03	0.1326E-07	-.1690E 06	0.6910	
1200.0	.3489E-02	.249E-03	0.297E-03	0.8672E-04	-.1684E 06	0.3304	
1250.0	.3740E-02	.270E-03	0.234E-03	0.2079E-03	-.1679E 06	0.3184	
1300.0	.4027E-02	.309E-03	0.429E-03	0.3704E-03	-.1675E 06	0.3123	
1350.0	.4295E-02	.424E-03	0.875E-03	0.5810E-03	-.1673E 06	0.3069	

TABLE 6.1.   *One Pass Rolling Schedule - One End Water Quenching Technique*

STEEL 97

Slab Code	(1) Initial Dimen. mm	Reheating Temp. T°C	Time of Reheat. at T°C mm.	γ g.s. on Reheat. μm	Holding Time secs	Rolling Temp.1 °C	Def.1 %	Load KN	Time before Quench. secs	Quench Temp. °C	Final Dimens. mm	γ g.s. after Quench mm	Fraction Rex. %	α g.s. (μm) at °C/sec — % Polyg. α 2.4	2.0	1.3	1.2
9	17.22 x 58 x 138	1195	45	157 x 159 (158)	39	1048	25.64	139	38	875	12.81 x 58 x 184	66 x 69 (68)	100	12 / 61	14 / 70	18 / 75	18 / 80
10	17.22 x 58.5 x 143	1195	45	157 x 159 (158)	48	998	25.3	160	25	875	12.87 x 59 x 187	68 x 80 (74)	60				
11	17.16 x 58.6 x 143	1195	45	(165)	61	952	24.9	170	19	875	12.88 x 59 x 186	75 x 137 (101)	21				
12	17.15 x 58.5 x 142	1196	48	(165)	78	900	25.1	200	5	870	12.89 x 59 x 185	126 x 227 (169)	0	12 / 45	13 / 52	16 / 68	18 / 83
17	17.13 x 57 x 144	1215	45	(165)	82	910	25.2	189	50	776	12.81 x 59 x 188	118 x 237 (167)	0			18 / 65	20 / 75

(1)   Pre-rolled from 25.8 x 57.5 x 100 mm

(2)   The grain size between parentheses is the square root of the product of the transverse and longitudinal measurements.

TABLE 6.2.   One Pass Rolling Schedules - One End Water Quenching Technique

STEEL 99

Slab Code	(1) Initial Dimen. mm	Reheating Temp. °C	Time of Reheat. at °C mm	γ g.s. on Reheat. μm	Holding Time secs	Rolling Temp 1 °C	Def.1 %	Load KN	Time before Quench.secs.	Quench. Temp. °C	Final Dimens. mm	γ g.s. after Quench mm	Fraction Rex. %	α g.s. (μm) at °C/sec / % Polyg. α			
														2.4	2.0	1.3	1.2
13	17.22 x 55 145	1198	45	157 x 157 (157)	36	1050	25.7	138	39	875	12.80 x 56 x 190	61 x 70 (65)	95	9 / 35	11 / 43	13 / 61	16 / 61
14	17.28 x 55.6 142	1198	45	(157)	49	1000	25.7	154	30	875	12.84 x 56 x 5 183	51 x 114 (76)	33				
15	17.21 x 55 x 144	1204	45	(157)	60	956	24.5	168	20	875	13.0 x 56 x 186	69 x 137 (97)	15				
16	17.29 x 56 x 142	1200	45	(157)	75	900	24.80	203	6	870	13 x 57.5 x 184	107 x 213 (151)	0		12 / 50	15 / 58	16 / 64
18	17.04 x 55 144	1198	45	(157)	75	906	26.31	186	44	778	12.55 x 57 x 187	98 x 270 (163)	0			17 / 48	18 / 62

(1)   Pre-rolled from 25.8 x 54.5 x 100 mm

(2)   The grain size between parentheses is the square root of the product of the transverse and longitudinal measurements.

TABLE 6.3. DETAILS OF THE TWO PASS ROLLING SCHEDULE – STEELS 97, 99, 22 AND 23

Steel	22	23	22	23	22	23
Slab Code	105	106	107	108	109	110
Reheat time at T, mm	75	95	75	90	80	90
Y g.s. on Reheat. μm	375	190	375	190	375	190
Holding Time 1 (sec)	35	54	54	36	34	32
Rolling Temp.1 (°C)	1100	1090	1090	1100	1100	1100
Def. 1 % / Load KN	33 / 121	33 / 158	33 / 140	33 / 135	33 / 148	33 / 138
100% Recryst. Y g.s.	75	52	75	52	75	54
Holding Time 2 (sec)	26	24	27	22	28	29
Rolling Temp 2 (°C)	1000	1000	990	1000	1000	988
Def. 2 % / Load KN	25 / 125	25 / 159	25 / 135	25 / 130	25 / 162	25 / 133
Time Before WQ or Anneal (Sec)	4	4	1020	1020	66600	63000
WQ Temp. (°C)	980	985	1000	1000	1000	1000
Fraction Recryst.(%)	5	0	55	20	90	60
Recryst. Y g.s. μm	-	-	38	29	40	30
Non-Recryst. Y dimens. μm	50 × 96 (69)	45 × 74 (58)	51 × 92 (68)	40 × 80 (57)	40 × 85 (58)	-
Comments					some α on gbs	

TABLE 6.3 (continued)

Steel	97	99	97	99	97		23	22
Slab Code	55	54	53	64	63		114	113
Reheat time at T, mm	45	45	45	45	45		90	60
γ g.s. on Reheat. μm	180	160	180	160	180		190	375
Holding Time 1 (sec)	25	30	27	31	43		35	39
Rolling Temp.1 (°C)	1110	1110	1104	1102	1090		1100	1105
Def. 1 % / Load KN	33 / 131	33 / 149	33 / 140	33	33		33 / 117	33 / 126
100% Recryst. g.s.	65	56	65	56	65		54	72
Holding Time 2 (sec)	44	42	44	48	43		40	43
Rolling Temp 2 (°C)	925	926	925	924	925		950	955
Def. 2 % / Load KN	25 / 167	25 / 192	25 / 175	25 / 195	25 / 180		25 / 192	25
Time Before WQ or Anneal(Sec)	637	30	30	10	10		61,200	61,200
WQ Temp. (°C)	925	925	925	925	925		950	950
Fraction Recryst.(%)	25	2	5	0	2		40	70
Recryst. γ g.s. μm	-	-	-	-	-		32	41
Non-Recryst. γ dimens. μm	-	-	-	-	-		-	-

TABLE 6.3. (continued)

Steel	97	99		97	99	22	23
Slab Code	31	32		49	50	123	124
Reheat time at T, mm	45	45		120	120	80	90
γ g.s. on Reheat. μm	180	160		250	220	375	190
Holding Time 1 (sec)	37	35		28	31	42	25
Rolling Temp.1 (°C)	1100	1100		1110	1102	1100	1080
Def. 1 %	33	33		33	33	33	33
Def. 1 Load KN	189	170		179	185	145	115
100% Recryst. γ g.s.	65	56		72	70	70	54
Holding Time 2 (sec)	32	34		40	41	35	35
Rolling Temp 2 (°C)	950	945		945	940	950	950
Def. 2 %	25	25		25	25	25	25
Def. 2 Load KN	144	148		--	--	156	136
Time Before WQ or Anneal(Sec)	3	2		180	192	127	125
WQ Temp. (°C)	942	940		950	950	950	950
Fraction Recryst.(%)	5	0		19	10	5	2
Recryst. γ g.s. μm	-	-		42	--	--	--
Non-Recryst. γ dimens. μm	52 × 91 (68)	48 × 90 (67)		52 × 99 (72)	53 × 110 (76)	45 × 96 (66)	44 × 92 (63)

TABLE 6.3 (continued)

Steel	97	99	97	99	99	22	23
Slab Code	33	34	61	62	99	111	112
Reheat time at T, mm	45	45	45	45	65	60	90
γ g.s. on Reheat. μm	180	160	180	160	170	375	190
Holding Time 1 (sec)	36	36	33	35	32	48	35
Rolling Temp.1 (°C)	1100	1104	1100	1105	1100	1100	1100
Def. 1 %	33	33	33	33	33	33	33
Def. 1 Load KN	180	198	185	188	--		
100% Recryst. γ g.s.	65	56	65	56	56	70	54
Holding Time 2 (sec)	35	37	30	31	30	37	38
Rolling Temp 2 (°C)	946	946	952	950	950	950	950
Def. 2 %	25	25	25	25	25	25	25
Def. 2 Load KN	142	156	140	158	--	--	148
Time Before WQ or Anneal (Sec)	430	430	3000	3800	18000	5000	5000
WQ Temp. (°C)	950	950	950	950	950	950	950
Fraction Recryst. (%)	28	15	85	50	90	34	15
Recryst. γ g.s. μm	--	--	40	35	38	--	--
Non-Recryst. γ dimens. μm	53 x 104 (74)	52 x 102 (73)	55 x 95 (72)	51 x 85 (66)	-	-	-

TABLE 6.3 (continued)

Measurement								
Steel	99	97	99	97		99	97	99
Slab Code	48	47	36	35		66	65	56
Reheat time at T, mm	120	120	40	40		45	45	45
γ g.s. on Reheat. μm	230	240	160	180		160	180	160
Holding Time 1 (sec)	40	35	39	38		30	28	32
Rolling Temp.1 (°C)	1100	1112	1100	1102		1100	1090	1104
Def. 1 % / Load KN	33 / –	33 / –	33 / 158	33 / 177		33 / –	33 / –	33 / 153
100% Recryst. γ g.s.	67	73	56	65		56	65	56
Holding Time 2 (sec)	61	61	59	56		43	42	44
Rolling Temp 2 (°C)	906	902	888	898		925	925	928
Def. 2 % / Load KN	25 / –	25 / –	25 / 192	25 / 199		25 / 180	25 / 165	25 / 182
Time Before WQ or Anneal (Sec)	3	4	4	2		3000	3260	1530
WQ Temp. (°C)	884	900	866	878		925	925	925
Fraction Recryst.(%)	0	0	0	0		35	60	20
Recryst. γ g.s. μm	–	–	–	–		–	42	–
Non-Recryst. γ dimens. μm	48 × 91 (66)	56 × 102 (76)	48 × 93 (67)	49 × 92 (67)		–	–	–

TABLE 6.3. (continued)

Steel	97	99	22	23	97	99	97
Slab Code	21	22	119	120	23	24	51
Reheat time at T, mm	40	40	60	90	40	40	120
γ g.s. on Reheat. μm			375	190	180	160	250
Holding Time 1 (sec)	42	34	32	25	42	31	30
Rolling Temp.1 (°C)	1088	1095	1105	1100	1089	1100	1110
Def. 1 % / Load KN	33 / 184	33 / -	33 / 169	33 / -	33 / 191	33 / 170	33 / -
100% Recryst. γ g.s.			75	54			75
Holding Time 2 (sec)	34	39	62	44	30	48	55
Rolling Temp 2 (°C)	896	888	900	900	900	904	904
Def. 2 % / Load KN	25 / 220	25 / 218	25 / 184	25 / -	25 / 224	25 / 196	25 / -
Time Before WQ or Anneal(Sec)	103	107	138	140	370	405	1800
WQ Temp. (°C)	900	900	900	900	900	900	900
Fraction Recryst.(%)	5	2	0	0	9	5	22
Recryst. γ g.s. μm	-	-	-	-	-	-	-
Non-Recryst. γ dimens. μm	40 × 82 (57)	38 × 78 (54)	51 × 92 (68)	45 × 70 (56)	35 × 90 (56)	36 × 120 (66)	59 × 109 (80)

TABLE 6.3. (continued)

Property								
Steel	23	22	97	23	22	99	97	99
Slab Code	118	117	71	116	115	26	25	52
Reheat time at T, mm	100	100	65	90	75	40	40	120
γ g.s. on Reheat. μm	195	380		190	375			225
Holding Time 1 (sec)	37	35	28	49	50	35	38	35
Rolling Temp.1 (°C)	1100	1100	1100	1100	1100	1100	1098	1088
Def. 1 %	33	33	33	33	33	33	33	33
Def. 1 Load KN	-	-	-	164	156	167	150	-
100% Recryst. γ g.s.	54	75		54	75			70
Holding Time 2 (sec)	60	55	55	53	55	50.	54	43
Rolling Temp 2 (°C)	904	900	902	900	900	894	888	902
Def. 2 %	25	25	25	25	25	25	25	25
Def. 2 Load KN	-	-	-	195	-	206	175	-
Time Before WQ or Anneal(Sec)	172 61,400	61,200	40,000	5250	5100	3096	3056	1800
WQ Temp. (°C)	900	900	900	900	900	900	900	900
Fraction Recryst.(%)	15	25	90	10	15	15	39	10
Recryst. γ g.s. μm	-	-	35	-	-	-	-	-
Non-Recryst. γ dimens. μm	-	-	-	-	-	40 × 116 (68)	47 × 120 (75)	40 × 140 (75)

TABLE 6.3. (continued)

Steel	Slab Code	Reheat time at T, mm	γ g.s. on Reheat. μm	Holding Time 1 (sec)	Rolling Temp.1 (°C)	Def. 1 %	Load KN	100% Recryst. γ g.s.	Holding Time 2 (sec)	Rolling Temp 2 (C)	Def. 2 %	Load KN	Time Before WQ or Anneal (Sec)	WQ Temp. (°C)	Fraction Recryst.(%)	Recryst. γ g.s. μm	Non-Recryst. γ dimens. μm
97	27	50		34	1100	33	177		64	845	25	189	3	830	0	-	48 x 100 (69)
99	28	55	375	32	1100	33	174		65	848	25	182	3	832	0	-	46 x 101 (68)
22	125	80		47	1100	33	160	75	62	850	25	190	2	835	0	-	-
23	126	95	190	49	1100	33	170	54	64	850	25	210	3	838	0	-	-
99	74	65		35	1100	33	165		70	850	25	195	10	850	0	-	-
97	57	65		28	1108	33	171		65	860	25	204	158	850	5	-	-
23	128	90	190	50	1100	33	168		70	850	25	200	10	850	0	-	-

Steel	99	23	97	99	97	99	22
Slab Code	58	130	29	30	59	60	121
Reheat time at T, mm	65	90	40	40	40	40	90
γ g.s. on Reheat. μm		190					380
Holding Time 1 (sec)	28	50	37	36	31	27	35
Rolling Temp.1 (°C)	1104	1100	1100	1098	1100	1100	1100
Def. 1 % / Load KN	33 / 173	33 / 170	33 / 171	33 / 173	33 / -	33 / -	33 / 160
100% Recryst. γ g.s.							
Holding Time 2 (sec)	78	70	65	64	60	72	74
Rolling Temp 2 (°C)	854	850	849	848	850	844	855
Def. 2 % / Load KN	25 / 217	25 / 214	25 / 167	25 / 168	25 / -	25 / -	25 / 183
Time Before WQ or Anneal(Sec)	156	100	422	420	3600	2400	5000
WQ Temp. (°C)	850	850	850	850	850	850	850
Fraction Recryst.(%)	2	0	10	5	25	15	0
Recryst. γ g.s. μm	-	-	-	-	-	-	-
Non-Recryst. γ dimens. μm	-	-	-	-	-	-	-
Comments							~ 10% α on g.b.s.

TABLE 6.3 (continued)

TABLE 6.3. (continued)

Steel	Slab Code	Reheat time at T, mm	γ g.s. on Reheat. μm	Holding Time 1 (sec)	Rolling Temp 1 (°C)	Def. 1 % / Load KN	100% Recryst. γ g.s.	Holding Time 2 (sec)	Rolling Temp 2 (°C)	Def. 2 % / Load KN	Time Before WQ or Anneal (Sec)	WQ Temp. (°C)	Fraction Recryst. (%)	Recryst. γ g.s. μm	Non-Recryst. γ dimens. μm	Comments
23	122	100	195	45	1090	33 / 168		66	854	25 / 214	5400	850	0	-	- - -	∿ 20% α on g.b.s.
97	37	40		35	1100	33 / 169		92	800	25 / 215	135	800	0	-	47 x 92 (66)	∿ 15% α
99	38	40		33	1100	33 / 164		89	800	25 / 223	110	800	0	-	44 x 90 (63)	Fully recovered str
97	39	40		36	1100	33 / -		90	800	25 / -	400	800	5	-	54 x 104 (75)	∿ 20% α
99	40	40		38	1100	33 / 135		86	800	25 / 205	405	800	0	-	54 x 98 (73)	Fully recovered str

TABLE 6.4
Data Used to Obtain The Mean Flow Stress Plotted in Figure 6.9

(in mm)

Slab Code	h_f	W_{fr}	W_{fb}	W_f	h_o(mm)	$\bar{W}_o$	L_1(KN)	L_2(KN)
21 WQ	12.90	62.62	58.0	61.08	25.55	56.09	184	220
21 AC	12.81	61.82	57.97	60.37	25.55	56.09	169	196
22 WQ	12.75	59.52	56.10	58.38	26.10	53.91	-	218
22 AC	12.90	59.25	55.02	57.84	26.10	53.91	166	200
23 WQ	12.81	61.10	56.23	59.48	25.55	56.09	191	224
23 AC	12.75	61.77	56.49	60.0	25.55	56.09	179	198
24 WQ	12.80	59.18	54.70	57.68	26.10	53.91	170	196
24 AC	12.81	59.36	54.69	57.80	26.10	53.91	163	184
25 WQ	12.78	61.43	56.80	59.89	25.55	56.09	150	175
25 AC	12.80	60.40	55.37	59.41	25.55	56.09	166	194
26 WQ	12.80	59.61	55.35	58.19	26.10	53.91	167	206
26 AQ	12.75	59.07	54.84	57.66	26.10	53.91	158	199

h_o, h_f = Initial and final thickness

W_{ob}, W_{fb} = width initial and final at the surface

W_{or}, W_{fr} = width initial and final at mid thickness

$\bar{W}_o$, $\bar{W}_f$ = average initial and final width

L_1 = total load in the first pass

L_2 = total load in the second pass

WQ = water quenched

AQ = air cooled

TABLE 6.5.

Nitrogen Analysis in Steel Millings

Slab Code	Treatment		Free Nitrogen (ppm)		Total N (ppm) (Leco)
	Hold. Temp. ^{o}C	Hold. Time (s)	Polaron	Leco(*)	
97	- As cast & rolled to billets		30	-	65
99	- As cast & rolled to billets		50	-	156
97-1	- Reheated at 1200°C		54	-	65
99-1	- Reheated at 1200°C		145	-	156
97-B	- Reheated Roll.1100 WQ$_{1080}$		42	-	65
99-B	- Reheated Roll.1100 WQ$_{1080}$		37	56	156
97-A	- Reheated Roll.1100→WQ$_{900}$		31	48	65
99-A	- Reheated Roll.1100→WQ$_{900}$		61	113	156
31-WQ	950	3	34	57	65
32-WQ	945	2	74	131	156
35-WQ	900	2	32	52	65
36-WQ	898	4	66	125	156
27-WQ	845	3	34	58	65
28-WQ	848	3	75	135	156
39-WQ	800	400	29	43	65
40-WQ	800	400	53	103	156

* These values correspond to the differences in N contents
between the: (total N values (Leco)) -
(the N content remaining in the millings after extracting the
free nitrogen (Leco)).

TABLE 6.6.   Yields and Chemical Analysis of Residues

Steel 97

Slab Code	Treatment		Wt. of Steel dissolved gr	Wt. of Residues gr	Wt. %						
	Hold. Temp. °C	Hold. Time (s)			C*	N	Nb	Si / SiO$_2$	Mn	Fe	S
97-0	Reheat. 1200°C		14.2589	0.092	25.02	-	-	31.5 / 68	0.080	1.2	0.35
97-A	Reheat. + Roll. 1100→WQ$_{900}$		27.6473	0.123	20.35	0.97	1.00	29.75 / 63.8	-	-	0.99
97-B	Reheat. + Roll. 1100WQ$_{1080}$		20.7242	0.134	12.09	0.25	-	34.9 / 74.8	0.10	5.5	0.28
31	950	3	21.0079	0.112	32.17	0.45	0.90	30.9 / 64.7	-	-	1.44
33	950	430	20.5327	0.133	31.75	1.12	4.17	26.1 / 55.93			1.06
53	925	30	19.5259	0.126	19.91	1.80	2.10	21.2 / 45.4			0.74
35	900	2	19.2885	0.115	33.24	1.91	1.10	31.7 / 67.9			1.26
23	900	370	14.7599	0.095	18.73	0.56	4.43	23.9 / 72.6			0.64
25	900	3056	11.6979	0.076	17.22	1.06	4.62	31.9 / 68.4	0.05	0.65	0.22
27	850	3	25.6355	0.142	30.67	0.80	0.90	28.0 / 66.4	0.1	4.20	0.73

*   Contaminated with C of the cement in acetone, used to bind
    the powder to be X-rayed.

Table 6.6 (continued) - Steel 99

Slab Code	Treatment Hold Temp °C	Hold Time (s)	Wt. of Steel dissolved gr	Wt. of Residues gr	C*	N	Nb	Si / SiO2	Mn	Fe	S
99-0	Reheat 1200°C		15.2019	0.108	21.14	-	-	28.5 / 61.1	-	-	0.55
99-A	Reheat + Roll. 1100→WO 900		20.4596	0.115	22.90	1.58	1.17	26.2 / 56.1	0.10	2.0	0.93
99-B	Reheat + Roll. 1100,WQ	1080	19.1685	0.105	21.58	1.09	1.10	29.5 / 63.2	-	-	0.98
32	950	2	23.8899	0.155	15.31	1.10	2.31	32.5 / 69.6	0.02	0.25	0.65
34	950	430	20.4276	0.123	-	-	4.98	31.0 / 66.4			-
54	925	30	17.9198	0.125	11.56	0.55	2.58	32.8 / 70.3	0.06	1.50	0.28
36	900	4	25.2017	0.176	18.74	1.14	2.36	38.1 / 81.6			0.58
24	900	405	9.5188	0.067	16.69	0.76	4.05	25.1 / 53.8	0.095	0.13	0.44
26	900	3096	11.5180	0.081	15.32	0.67	4.27	26.2 / 56.1	0.04	1.22	0.69
28	850	3	20.1275	0.141	20.63	0.93	1.28	29.9 / 64.1			0.64
74	850	10	19.7055	0.135	17.69	0.96	1.75	28.7 / 61.5			
58	850	156	21.5457	0.162	18.95	1.10	2.87	31.0 / 66.4			
60	850	2400	17.7045	0.124	20.93	1.67	4.11	28.7 / 61.5			0.76

*Contaminated with C of the cement in acetone, used to bind the powder to be X-rayed

TABLE 6.7 Yields and Chemical Analysis of Residues - Steel 22

Slab Code	Treatment		Wt. of Steel dissolved gr	Wt. of Residues gr	wt %						
	Hold Temp. ^{0}C	Hold Time ^{0}C			C*	N	Nb	Si / SiO$_2$	Mn	Fe	S
22-0	Reheat. 1300^{0}C		12.4558	0.0962	-	-	-	18.99 / 40.69	-	-	0.41
101	Reheat. + Roll. 1100, WQ$_{1080}$		22.9055	0.1990	7.21	0.53	1.50	20.39 / 43.70	0.30	0.80	0.28
105	1000	4	10.9777	0.0836	21.38	1.40	2.76	17.99 / 38.55	0.15	0.11	0.46
109	1000	66,600	9.0724	0.0548	12.01	0.92	9.93	-	-	-	0.46
119	900	138	12.8079	0.0924	18.64	0.90	7.49	34.99 / 74.98	0.90	0.0	0.64
115	900	5,100	11.5211	0.0973	9.84	1.66	7.40	16.0 / 34.29	-	-	0.32
117	900	61,200	15.2158	0.1186	15.11	1.64	7.70	16.11 / 34.52	0.78	-	0.73
121	850	5,000	11.5225	0.0917	16.02	0.70	7.16	-	-	-	0.49

* Contaminated

TABLE 6.7 *Yields and Chemical Analysis of Residues - Steel 23*

Slab Code	Treatment		Wt. of Steel dissolved gr	Wt. of Residues gr	wt %						
	Hold Temp. ^{o}C	Hold Time ^{o}C			C*	N	Nb	Si / SiO_2	Mn	Fe	S
23-0	Reheat. 1300°C		21.0294	0.1081	12.00	0.55	1.17	19.99 / 42.83	-	-	0.89
102	Reheat. + Roll. 1100;WQ$_{1080}$		24.8402	0.1607	15.99	1.16	6.0	26.89 / 57.62	0.80	0.5	0.42
106	1000	4	10.0178	0.0655	17.12	1.38	8.72	18.88 / 40.46	-	-	0.73
110	988	63,000	10.0533	0.0741	20.03	1.92	15.50	18.99 / 40.69	-	-	0.49
120	900	140	12.2581	0.0514	19.84	2.88	22.08	22.15 / 47.46	0.95	-	0.84
116	900	5,250	13.6532	0.0821	13.48	1.68	18.25	-	-	-	0.39
118	900	61,400	14.8208	0.1285	10.69	1.80	13.18	19.95 / 42.75	0.80	-	0.19
128	850	10	29.2827	0.2284	7.51	0.48	8.06	25.24 / 54.10	-	-	0.40
130	850	100	26.2011	0.2015	6.80	0.52	11.29	29.50 / 63.2	0.87	0.0	0.16
122	850	5,400	15.5636	0.0992	12.17	0.91	16.50	-	-	-	0.37

* Contaminated

TABLE 6.8.   X-Ray Diffractometry Analysis – Steels 97 and 99

Slab Code	Holding Temp. °C	Holding Time s	Mole Ratios		Lattice Parameter a, Å	Estimated Composition	Particle Size Å (3)
			(N+C)/Nb (1)	N/(C+N) (2)			
STEEL 97							
97-B	1100°C	3	-	-	-	-	-
97-A	1100°C	7 (4)	0.87	0.30	4.4442	$NbC_{0.61}N_{0.26}$	-
31	950°C	3	"	0.285	4.4450	$NbC_{0.62}N_{0.25}$	70
53	925°C	30	"	0.270	4.4475	$NbC_{0.64}N_{0.23}$	-
35	898°C	2	"	0.260	4.4478	$NbC_{0.64}N_{0.23}$	80
25	900	3056	"	0.250	4.4495	$NbC_{0.65}N_{0.22}$	250
27	845	3	"	0.220	4.4520	$NbC_{0.68}N_{0.19}$	
STEEL 99							
99-B	1100	3	0.87	0.36	4.4350	$NbC_{0.56}N_{0.31}$	-
99-A	1100	7 (4)	"	0.33	4.4396	$NbC_{0.58}N_{0.29}$	-
32	945	2	"	0.30	4.4420	$NbC_{0.61}N_{0.26}$	55
54	925	30	"	0.30	4.4421	$NbC_{0.61}N_{0.26}$	-
36	988	4	"	0.285	4.4455	$NbC_{0.62}N_{0.25}$	50
26	900	3096	"	0.260	4.4470	$NbC_{0.64}N_{0.23}$	170
28	848	3	"	0.280	4.4465	$NbC_{0.63}N_{0.24}$	-

(1) From thermodynamic analysis, Chapter 2.
(2) Obtained from Fig. 2.11 plotting the lattice parameter values on line P - Q
(3) Average particle size
(4) After rolling at 1100°C, air cooled down to 900°C (~ 45 secs) and quenched.   This time ~ 7 secs.
     has been calculted through the temperature compensated time W.

TABLE 6.9.   *X-ray Diffractometry Analysis - Steels 22 & 23*

Slab Code	Holding Temp. °C	Holding Time s	Mole Ratios		Lattice Parameter	Estimated Composition	Particle Size Å (3)
			(N+C)/Nb(1)	N/(C+N)(2)			
STEEL 22							
101	1100	2	0.87	0.33	4.4385	$NbC_{0.58} N_{0.29}$	-
105	1000	4	0.87	0.32	4.4400	$NbC_{0.59} N_{0.28}$	-
109	1000	66,600	0.87	0.27	4.4467	$NbC_{0.64} N_{0.23}$	-
119	900	138	0.87	0.29	4.4433	$NbC_{0.62} N_{0.25}$	-
115	900	5,100	0.87	0.27	4.4458	$NbC_{0.64} N_{0.23}$	510
117	900	61,200	0.87	0.29	4.4444	$NbC_{0.62} N_{0.25}$	
STEEL 23							
102	1100	3	0.87	0.340	4.4380	$NbC_{0.57} N_{0.30}$	120
106	1000	4	0.87	0.325	4.4395	$NbC_{0.59} N_{0.28}$	250
110	1000	63,000	0.87	0.30	4.4416	$NbC_{0.61} N_{0.26}$	780
120	900	140	0.87	0.31	4.4406	$NbC_{0.60} N_{0.27}$	350
116	900	5,250	0.87	0.29	4.4430	$NbC_{0.62} N_{0.25}$	-
118	900	61,400	0.87	0.295	4.4425	$NbC_{0.61} N_{0.26}$	560
128	850	10	0.87	0.290	4.4430	$NbC_{0.62} N_{0.25}$	180
122	850	5,400	0.87	0.285	4.4432	$NbC_{0.62} N_{0.25}$	220

(1)   From thermodynamic analysis Chapter 2.
(2)   From Fig 2.11 plotting lattice parameter values on line P - Q
(3)   Average particle size.

```
LIST / THIN / CALC
LABEL =
15-OCT-82    15:00:06
  100.030  LIVE SECONDS
 DENSITY =  7.80 GM/CC
THICKNESS =  0.01 UM
KV= 100.    TILT=  0.    TKOFF= 20.
                        WTZ
ELEM        CPS         ELEM
SI K        21.299      13.915
S  K         1.576       0.961
CA K        17.725       9.377
TI K         0.519       0.302
MN K         2.458       1.548
FE K       115.792      73.897
```

```
LIST / THIN / CALC
LABEL =
15-OCT-82    16:19:05
  100.010  LIVE SECONDS
 DENSITY =  8.00 GM/CC
THICKNESS =  0.10 UM
KV= 100.    TILT=  0.    TKOFF= 20.
                        WTZ
ELEM        CPS         ELEM
SI K        31.807       5.172
CA K         2.651       0.343
TI K         1.640       0.220
FE K         4.080       0.570
NB K       254.347      93.696
```

```
LIST / THIN / CALC
LABEL =
15-OCT-82    13:35:17
  100.010  LIVE SECONDS
 DENSITY =  5.00 GM/CC
THICKNESS =  0.10 UM
KV= 100.    TILT=  0.    TKOFF= 20.
                        WTZ
ELEM        CPS         ELEM
SI K        25.770       2.006
S  K       586.124      40.521
MN K       835.433      57.265
NB K         1.104       0.207
```
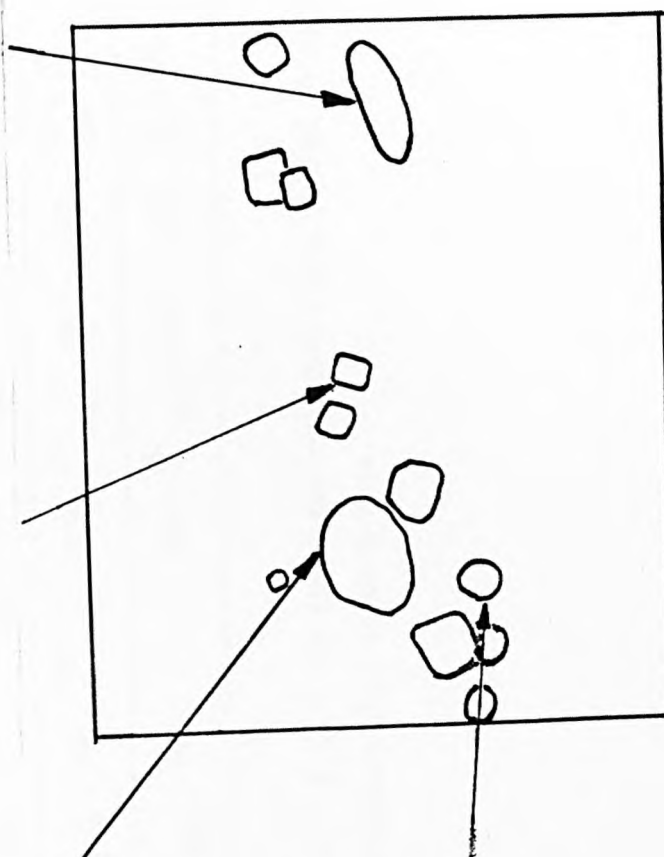
```
LIST / THIN / CALC
LABEL =
15-OCT-82    16:15:11
  100.019  LIVE SECONDS
 DENSITY =  8.00 GM/CC
THICKNESS =  0.08 UM
KV= 100.    TILT=  0.    TKOFF= 20.
                        WTZ
ELEM        CPS         ELEM
SI K        37.279       4.726
CA K         3.020       0.307
TI K         1.789       0.190
MN K         1.788       0.199
FE K         3.991       0.448
NB K       315.993      94.129
```

Table 6.10   Microanalisis of particles (STEM 400), obtained after roughing at
1100°C . Micrograph shown in Fig. 6.32.a.

TABLE 6.11. Two Pass Rolling Schedule - Air Cooled Slabs

STEEL 97

Slab Code	Initial Dimens. mm	Soaking Temp. Min.	Time of Soaking min.	γ g.s. on Reheat μm	Holding Time 1 secs.	Roll. Temp 1. °C	Def. 1. %	Load KN	Holding Time 2 secs	γ g.s. μm	Frac. Rex.%	Roll. Temp 2 °C	Def.2 %	Load KN	Time of anneal or time before AC s.	AC Temp °C	γ g.s.(1) μm	Frac Rex.%	Final Dimen. mm	α g.s. μm	% Polyg.	Acicular Island size μm	Trans. Temp °C (2)
47	25.6 x 57.5 100	1200	120	240	30	1108	33	170	45	73	100	906	25	185	2	886	56 x 102 76	0	12.8 x 58.5 190	16	95	45	756
21	25.6 x 57.5 100	1200	50	180	33	1104	33	168	44	60	100	906	25	196	110	910	40 x 82 57	5	12.8 x 58.5 190	17	96	42	756
23	25.6 x 57.5 100	1204	50	180	36	1108	33	179	46	60	100	915	25	198	404	910	38 x 90 58	9	12.8 x 58.5 190	17	96	40	756
25	25.6 x 57.5 100	1196	50	180	31	1098	33	166	52			900	25	194	3000	900	35 x 85 54	39	12.8 x 58.5 190	19	98	45	756

(1) Obtained from Table 6.3.   in the water quenched slabs rolled in parallel.

(2) Measured by two thermocouples in each case.

TABLE 6.12. Two Pass Rolling Schedule - Air Cooled Slabs

STEEL 99

Slab Code	Initial Dimens. mm	Soaking Temp. Min.	Time of Soaking min.	γ g.s. on Reheat μm	Holding Time 1. °C	Roll. Temp. 1 °C	Def. 1. %	Load KN	Holding Time 2 secs	γ g.s. μm	Frac. Rex.%	Roll. Temp. 2 °C	Def.2 %	Load KN	Time of anneal or time before AC s.	AC Temp. °C	γ g.s. (1) μm	Frac. Rex.%	Final Dimen. mm.	α g.s. μm	% Polyg.	Acicular island size μm	Trans.(2) Temp.°C
48	25.6 x 56 / 100	1200	120	230	33	1088	33	175	53	67	100	904	25	210	2	892	48 x 91 / 66	0	12.8 x 58.5 / 190	16	70	35	726
22	25.6 x 56 / 100	1200	50	160	32	1102	33	166	48	67	100	894	25	200	110	900	45 x 95 / 65	2	12.8 x 58.5 / 190	14	85	36	726
24	25.6 x 56 / 100	1200	50	160	31	1100	33	163	52	58	100	904	25	184	432	904	40 x 85 / 58	5	12.8 x 58.5 / 190	15	92	38	726
26	25.6 x 56 / 100	1206	50	160	38	1100	33	158	52	58	100	894	25	199	3060	902	40 x 85 / 58	15	12.8 x 58.5 / 190	16	94	35	726

(1) Obtained from Tables 6.3. in the water quenched slabs rolled in parallel

(2) Measured by two thermocouples in each case

TABLE 6.13   Details of Two Pass Rolling Schedules for Steel 12

Slab Code	Soak Temp °C	Time of Reheat. at T, min.	γ g.s. on Reheat. μm	Holding Time 1 secs.	Roll. Temp. 1 °C	Def. 1 %	Def. 1 Load KN	Holding Time 2 secs	γ g.s. μm	Frac.Rex. %	Roll. Temp. 2 °C	Def. 2 %	Def. 2 Load KN	Time before W.Q./A.C. or Anneal. Sec.	W.Q./A.C. Temp. °C	γ g.s. μm	Frac.Rex. %	α g.s. μm	% Polyg.	Acicular islands size μ	Comments
41	1200	~100	180	40	1098	33	–	–	–	–	–	–	–	51	900	75	100	15	55	35	1°C/sec One End W.Q.
42	1200	50	160	40	1098	33	160	59	68	100	894	25	–	3	880	46 × 84	62 / 0	12	63	29	1°C/sec One End W.Q.
43AC	1200	45	160	50	1088	33	169	58	68	100	884	25	180	120	900	–	–	12	80	25	A.C. on nails 715°C = Ar3
44WQ	1200	45	160	33	1102	33	168	54	68	100	904	25	190	1170	900	49 × 117	40	–	–	–	W.Q.
44AC	1200	45	160	45	1085	33	158	54	68	100	892	25	196	1150	~900	–	–	14	94	18	A.C. on nails 715°C = Ar3
46WQ	1200	45	160	32	1106	33	181	49	68	100	894	25	188	380	~900	56 × 98	74 / 32	–	–	–	W.Q.

AC = Air cooled

WQ = Water quenched

TABLE 6.14   Strength Properties (1)

Steel Code	Proof Strength (0.2%) MN/m^2	U.T.S. MN/m^2	Elongation %	Red.Area %	α g.s. μm	Vol.Fraction Acic.Struct. % (2)	
97	414	543	29.4	76.3	15	5	(50)
99	421	598	23.8	72.2	16	16	(37)
22	483	643	22.0	72.1	16	30	(50)
23	486	654	23.9	73.6	15	13	(45)

(1) Specimens for these tests were obtained from air-cooled slabs after a 2 pass rolling at 1100°C and 900°C, with reductions of 33 and 25% respectively. Steels 97 and 99 reheated at 1200°C for 4 hours and steels 22 and 23 at 1300°C for 1½ hours. The distribution of these specimens in the slabs is given in Figure   These values are the average of three tests for each steel.

(2) The figures between parentheses are the size in μm of the acicular island

TABLE 6.15

Impact Properties Charpy V-notch

Slab Code	α g.s. μm	Acicular Structure %	ITT ^{o}C at 27 Joules	Upper Shelf Energy Joules
97	15	5	- 20	182
99	16	16	+ 7	150
22	16	30	+ 46	138
23	15	13	+ 52	138
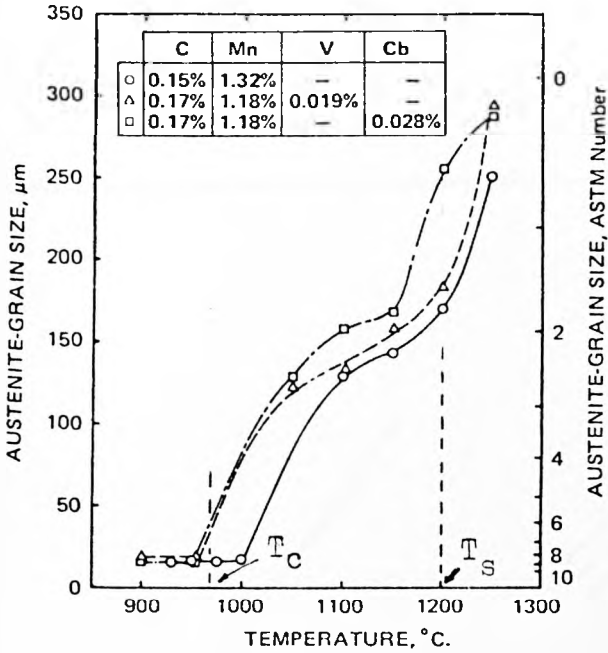
FIG 11.a — How reheating temperature affects austen-
ite grain size in three steels.

After Tanaka et al (1977b).
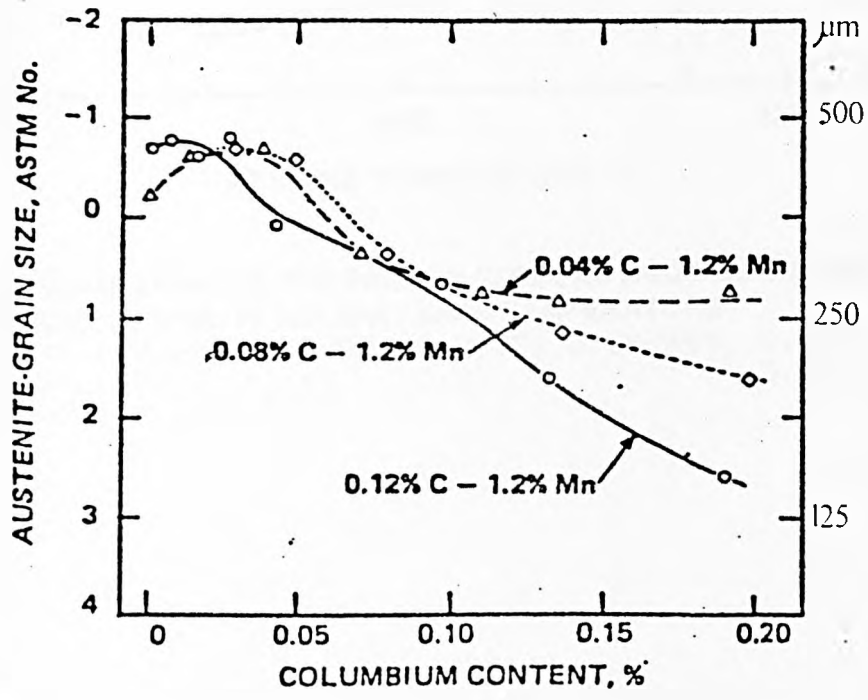
Fig 1.1.b Effect of columbium on austenite-grain
size of three base compositions reheated to 1250°C.
for 1 hour. After Kozasu et al (1977).
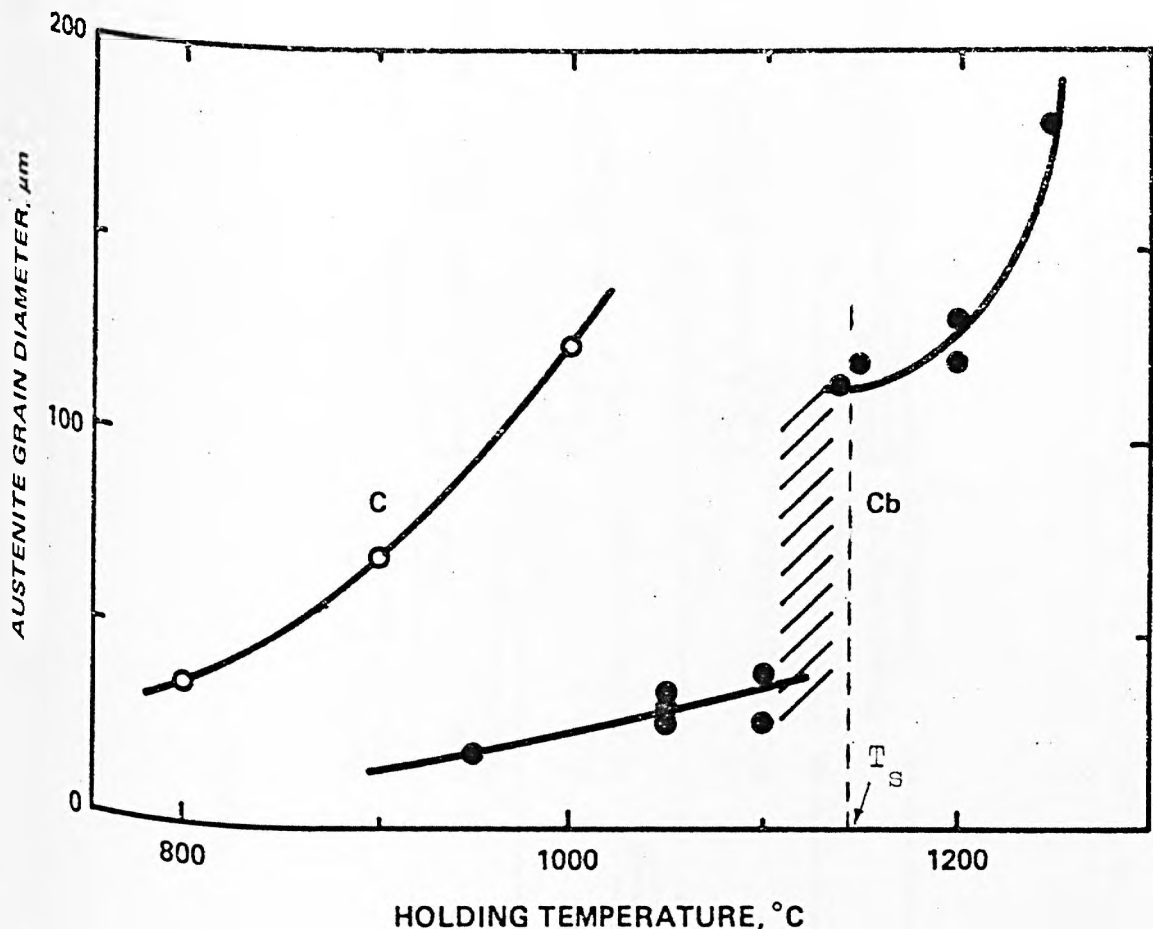
Fig.11.c GRAIN COARSENING IN THE CARBON STEEL (C) AND THE COLUMBIUM STEEL (Cb). 30-MINUTE HOLD AT EACH TEMPERATURE

Nb steel: 0.06%C,1.40%Mn,0.29%Si,0.043%Nb, 0.017%N
C   " : 0.09   1.45   0.30   0.001
After Cuddy (1981)
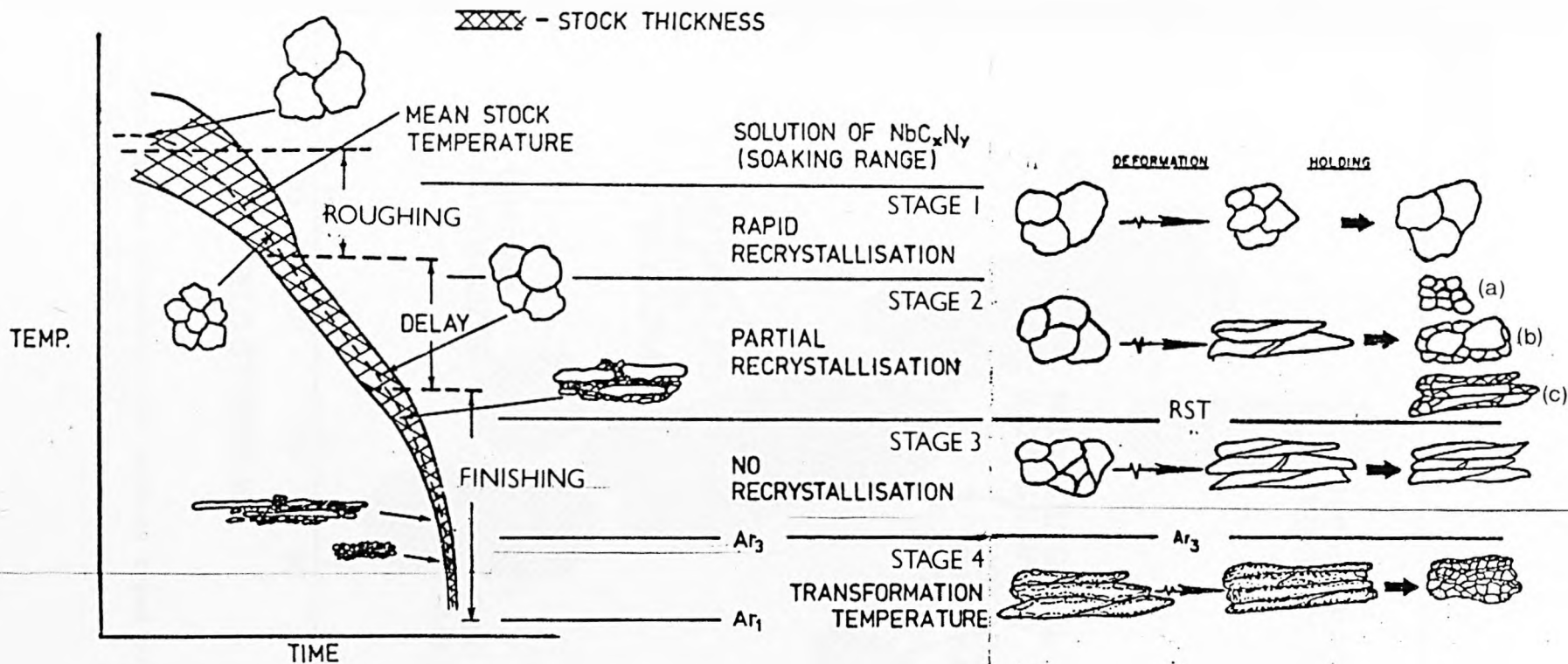
Fig. 1.2 Four stages of Controlled Rolling Nb microalloyed steels.
RST, Recrystallization Stop Temperature, is the rolling temperature below which recrystallization
does not take place. Modified from Figs.given by Baird&Preston(1973) and Cohen & Hansen(1979).
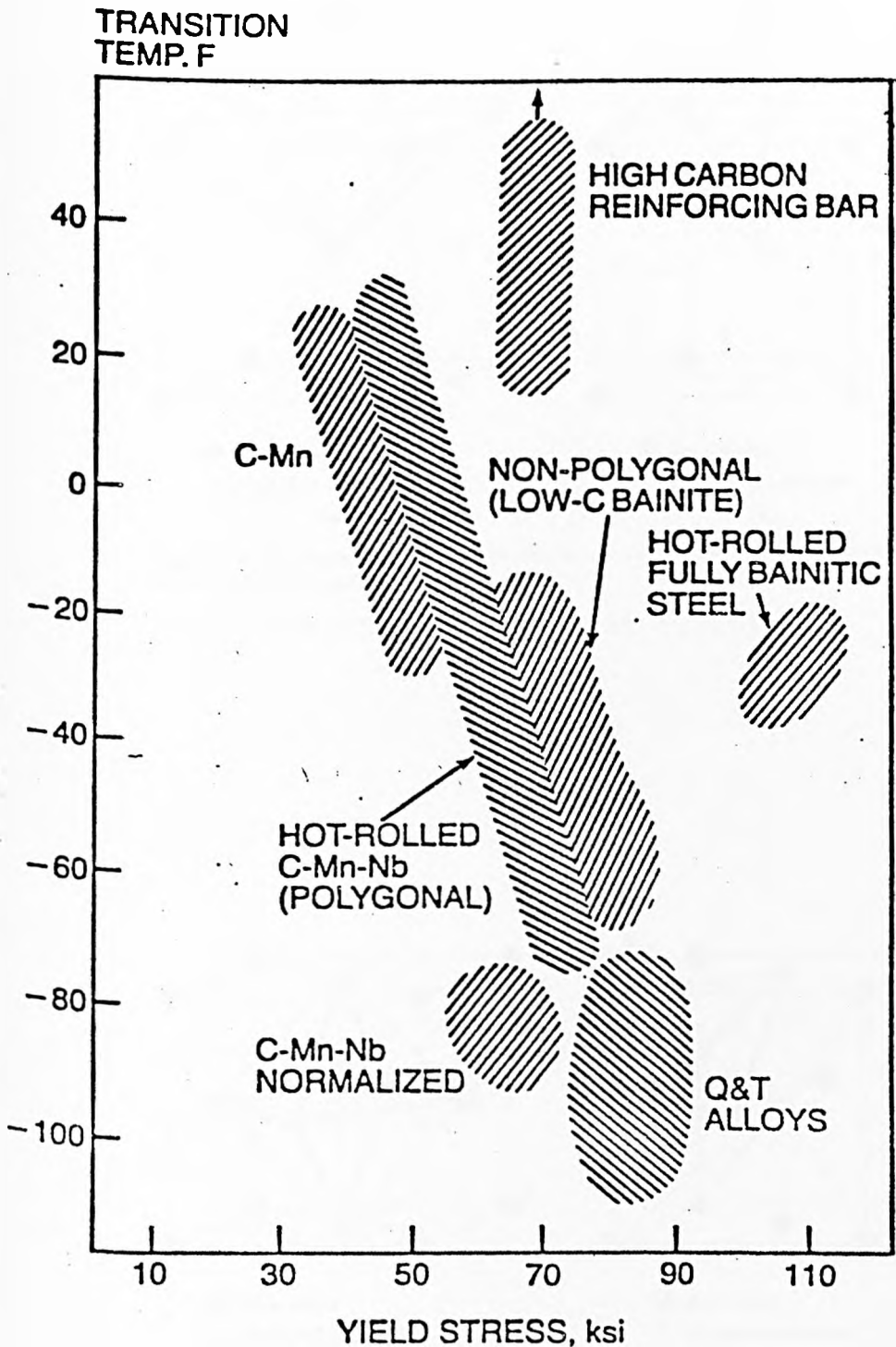
Fig 1.3 . Properties attainable in various types of steel. After DeArdo et al (1981).

- ● Metal atoms
- ○ Octahedral interstices

(a)

- ● Metal atoms
- ○ Tetrahedral interstices

(b)
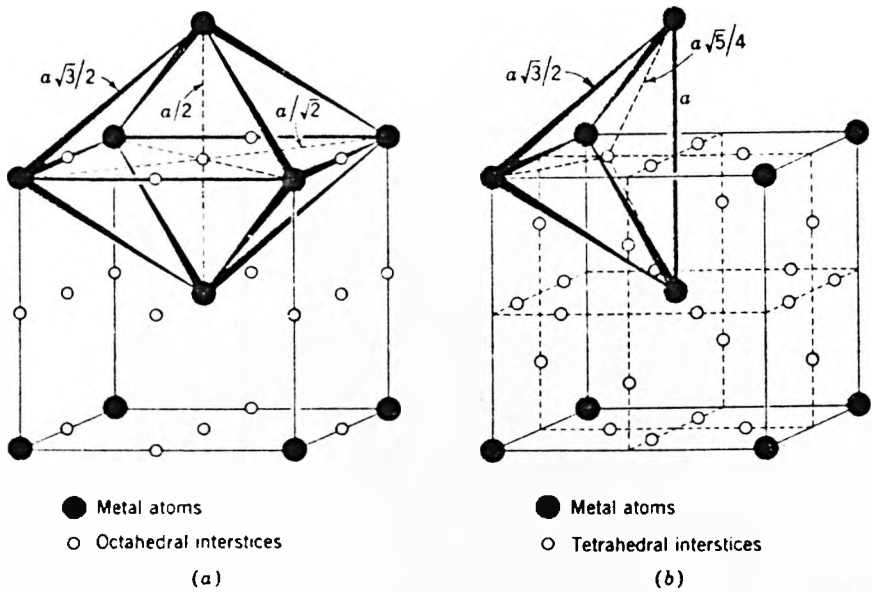
Fig. 2.1 The interstitial voids in the b.c.c. structure. (a) Octahedral voids; (b) tetrahedral voids.

After Barrett and Massalski (1980).

- ● Metal atoms
- ○ Octahedral interstices

(a)

- ● Metal atoms
- ○ Tetrahedral interstices

(b)
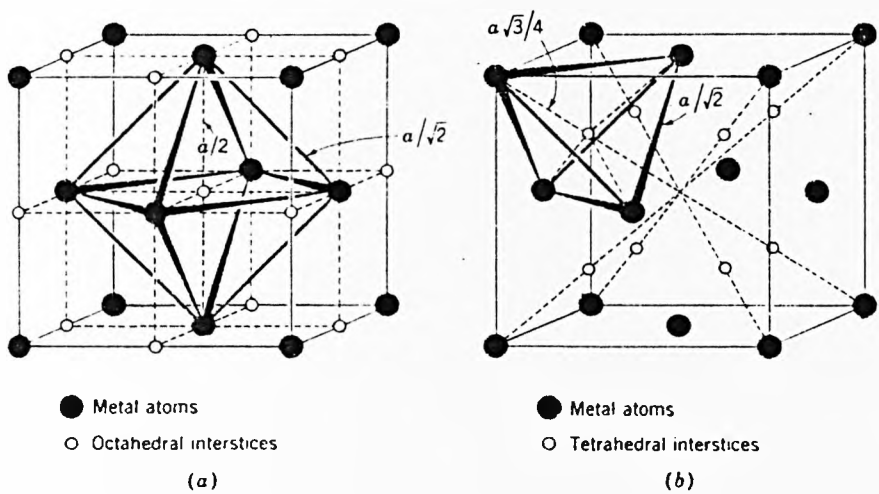
Fig. 2.2 The interstitial voids in the f.c.c. structure. (a) Octahedral voids (as in austenite); (b) tetrahedral voids.

After Barrett and Massalski (1980).
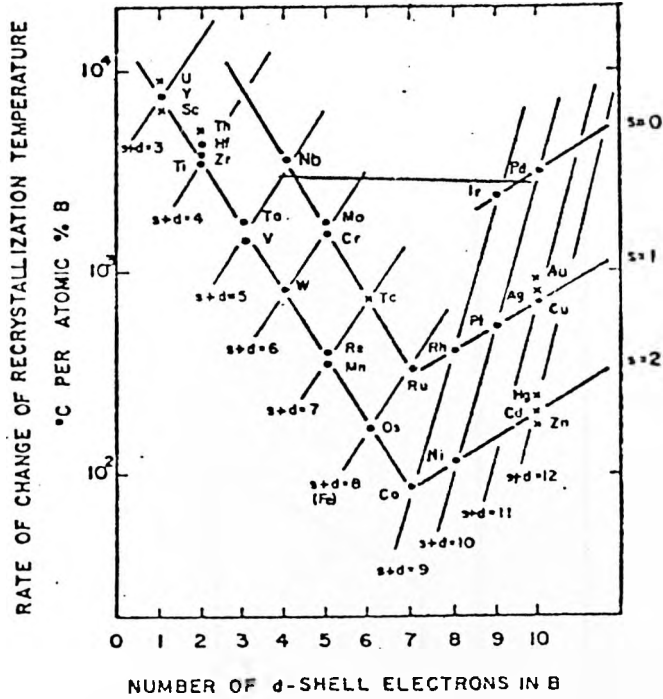
Fig. 2.3 Effect of the addition of transition elements on the recrystallization temperature of deformed alpha iron   The elements identified by crosses were not investigated by Abrahamson. and are located here in the positions indicated by the periodic table. According to the diagram, the effectiveness of a given element in retarding recrystallization depends on the difference between the quantity $(2s + d)$ for Fe and for the element, where $s = 2$ and $d = 6$ for Fe.

After Abrahamson and Blakeney (1960).
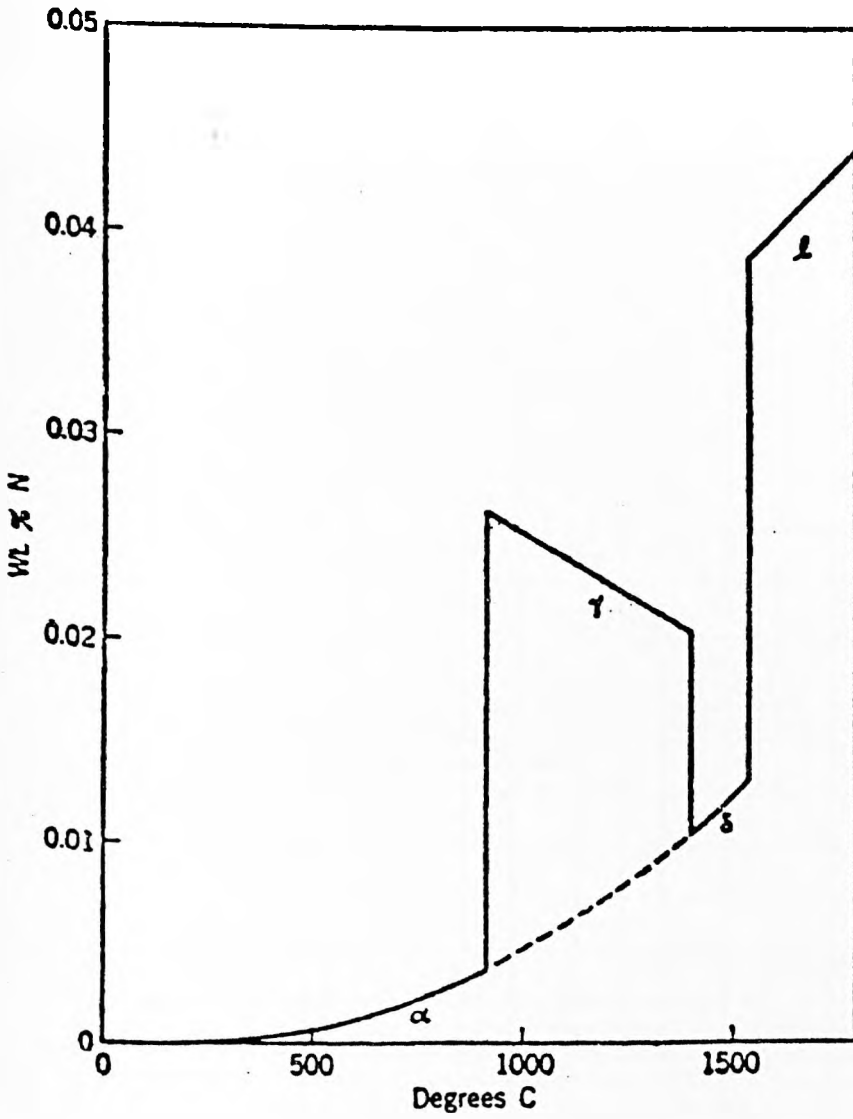
Fig. 2.4 The solubility of nitrogen gas at 1 atmosphere
in pure iron under equilibrium conditions
Darken and Gurry (1953).
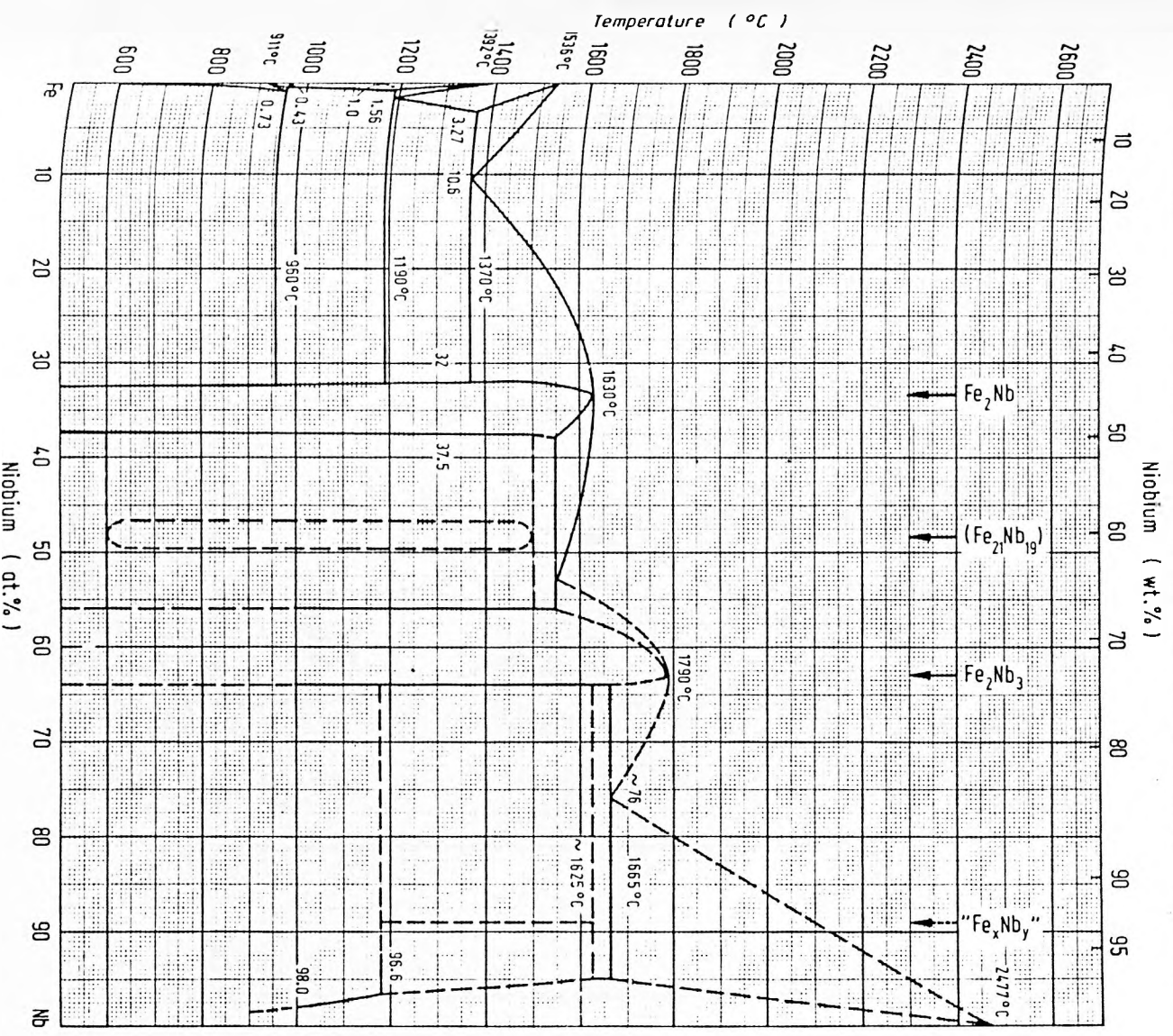
Fig. 2.5 Iron-Niobium phase diagram.
After Kubaschewski, O. (1982).
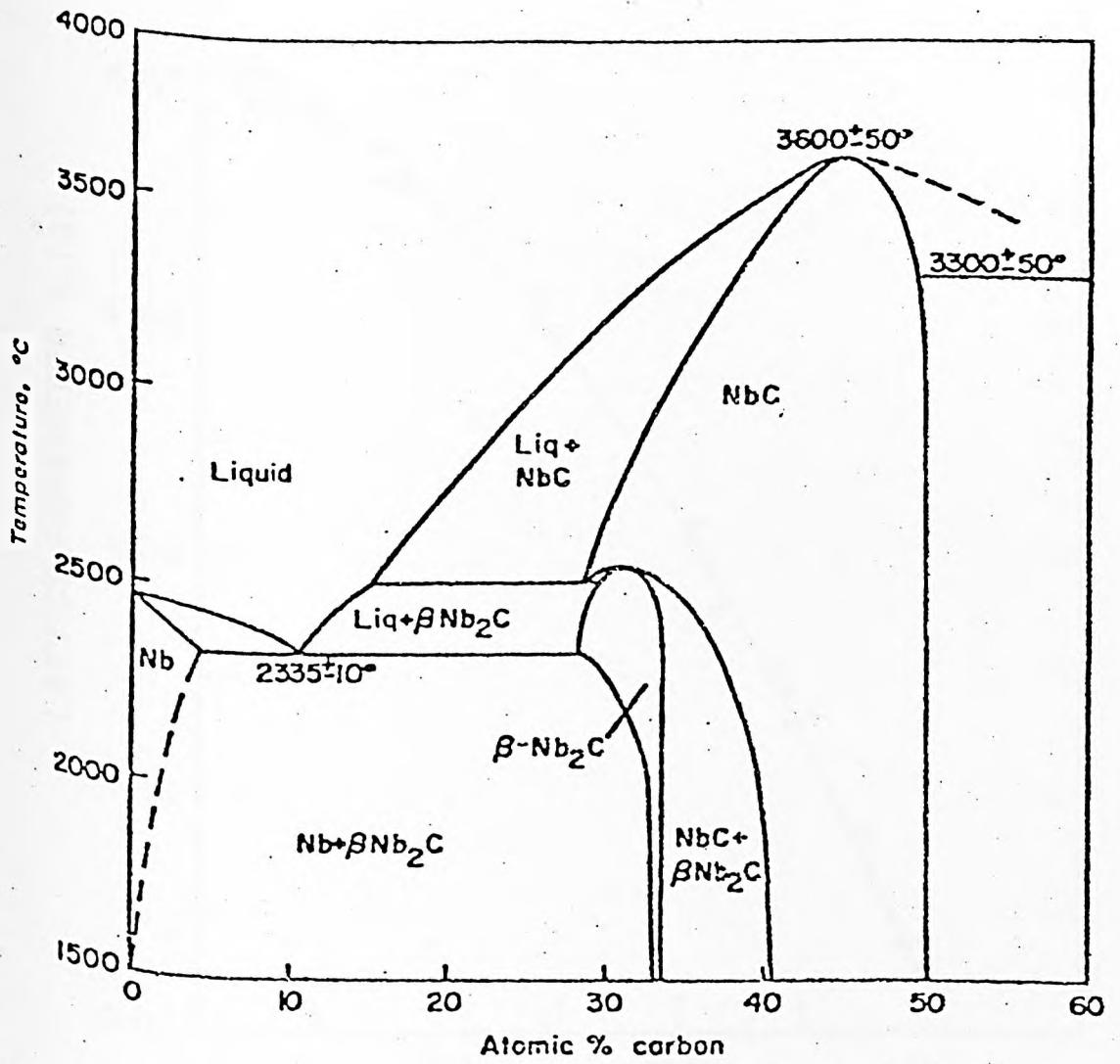
Figure 2.6 The niobium-carbon phase diagram (after Storms et al. (1969)).

$$a_0 = 4.09847 + 0.71820(C/Nb) - 0.34570(C/Nb)^2$$
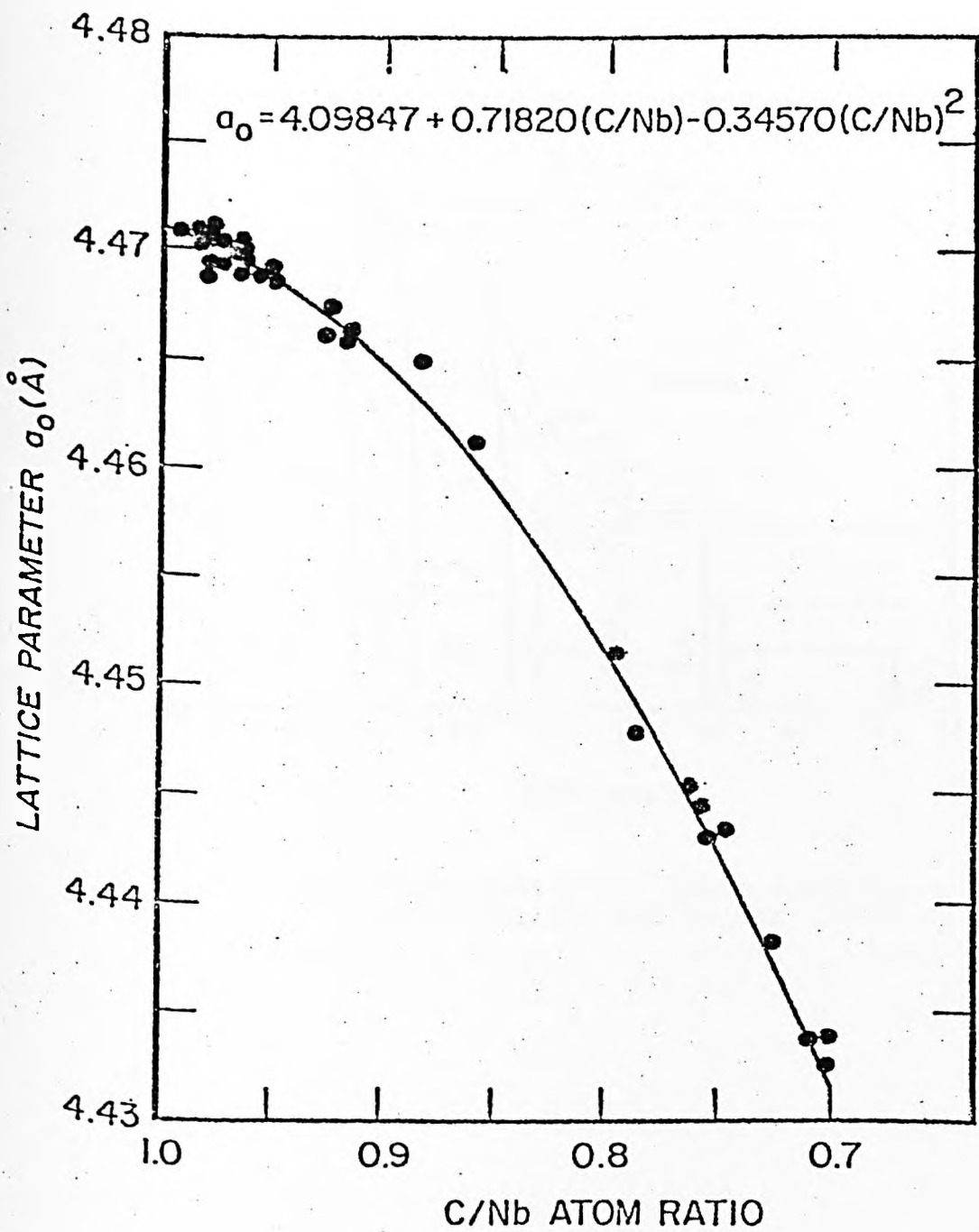
Figure 2.7 Relation between lattice parameter and nonstoichiometry

for the cubic niobium carbide

After Storms and Krikorian (1960)
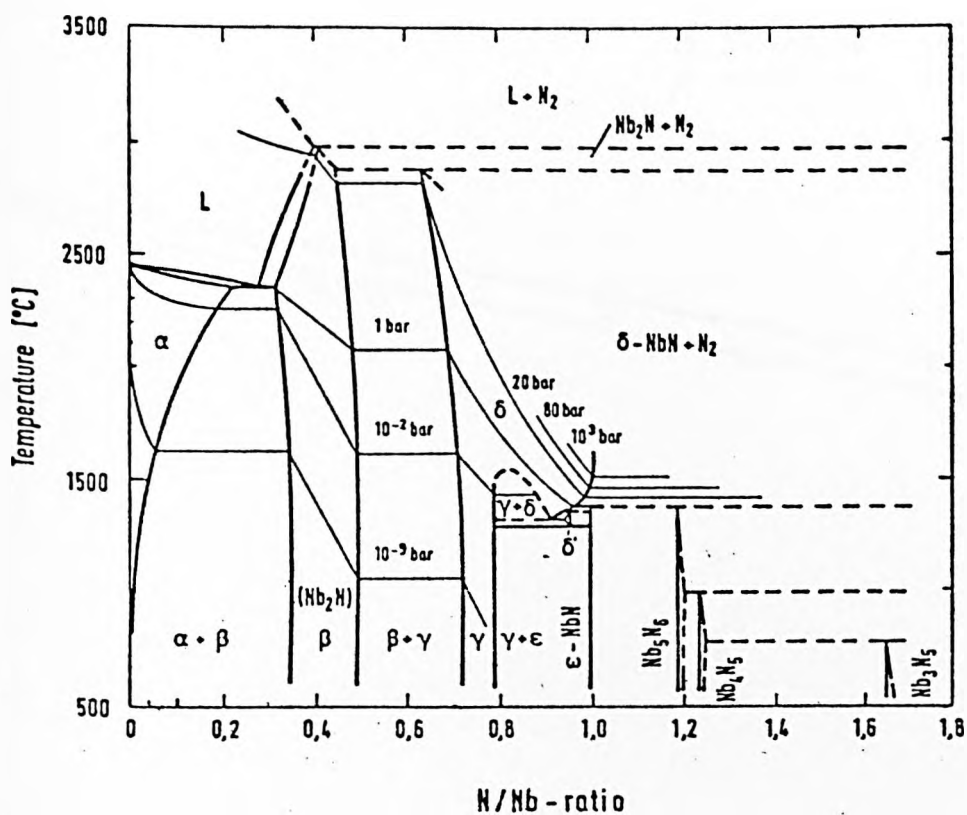
Fig. 2.8 Niobium-Nitrogen phase diagram.
          After Politis and Rejman (1978).
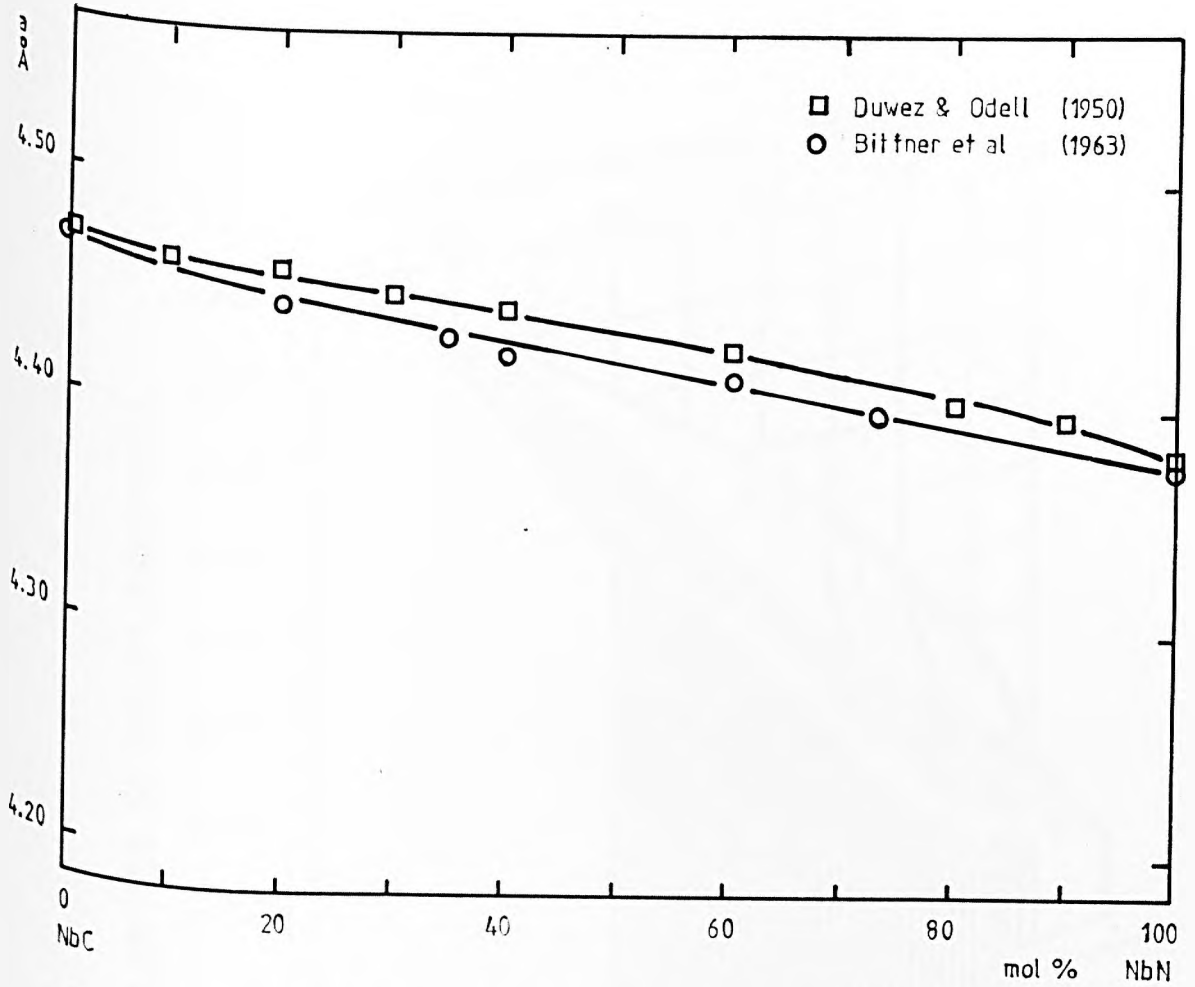
FIG. 2.9   LATTICE PARAMETER   AS A FUNCTION OF INTERSOLUBILITY OF NbC–NbN
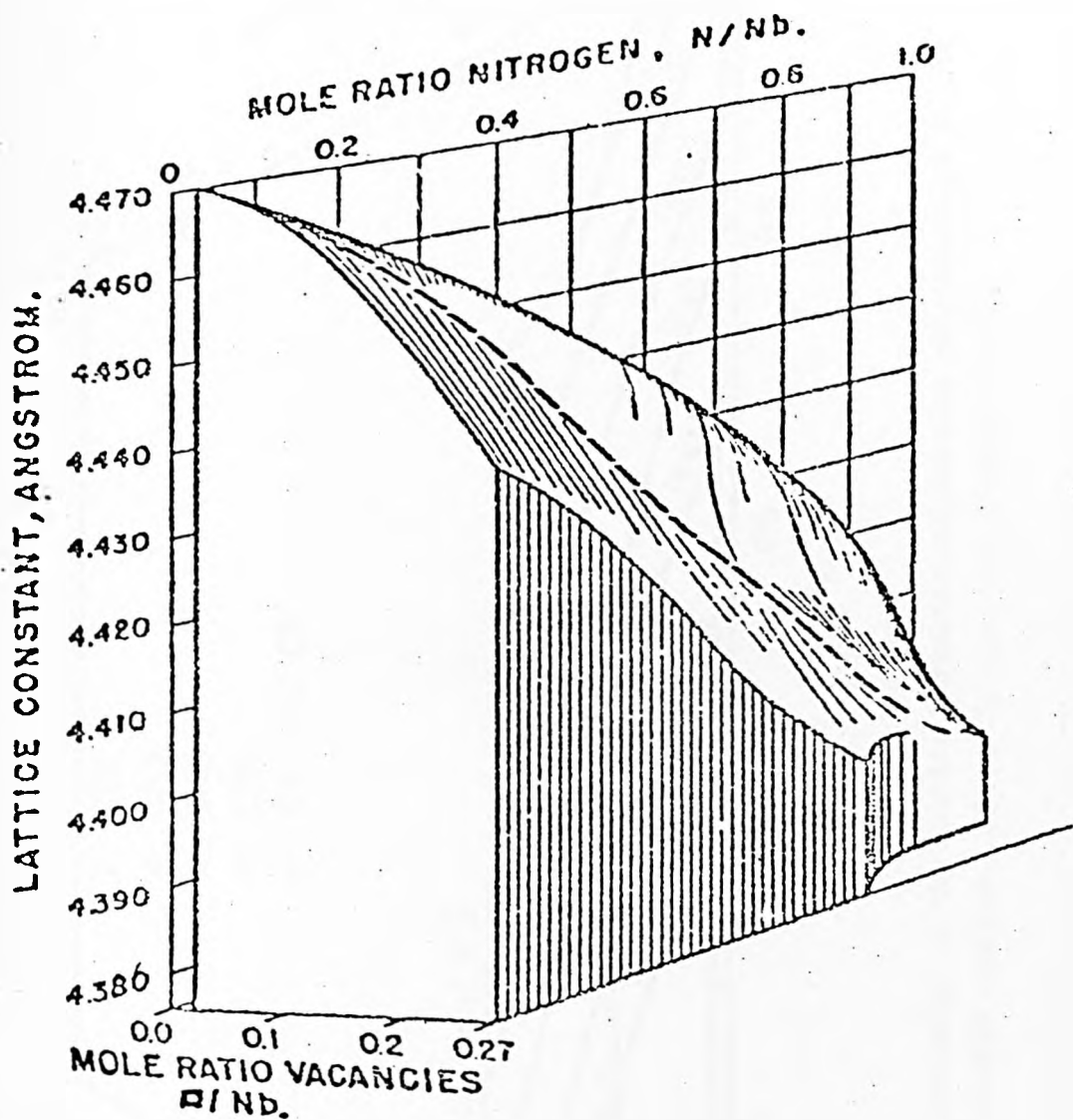
Fig. 2.10   Lattice parameter vs composition in the system Nb-NbC-NbN
After Storms and Krikorian (1969).
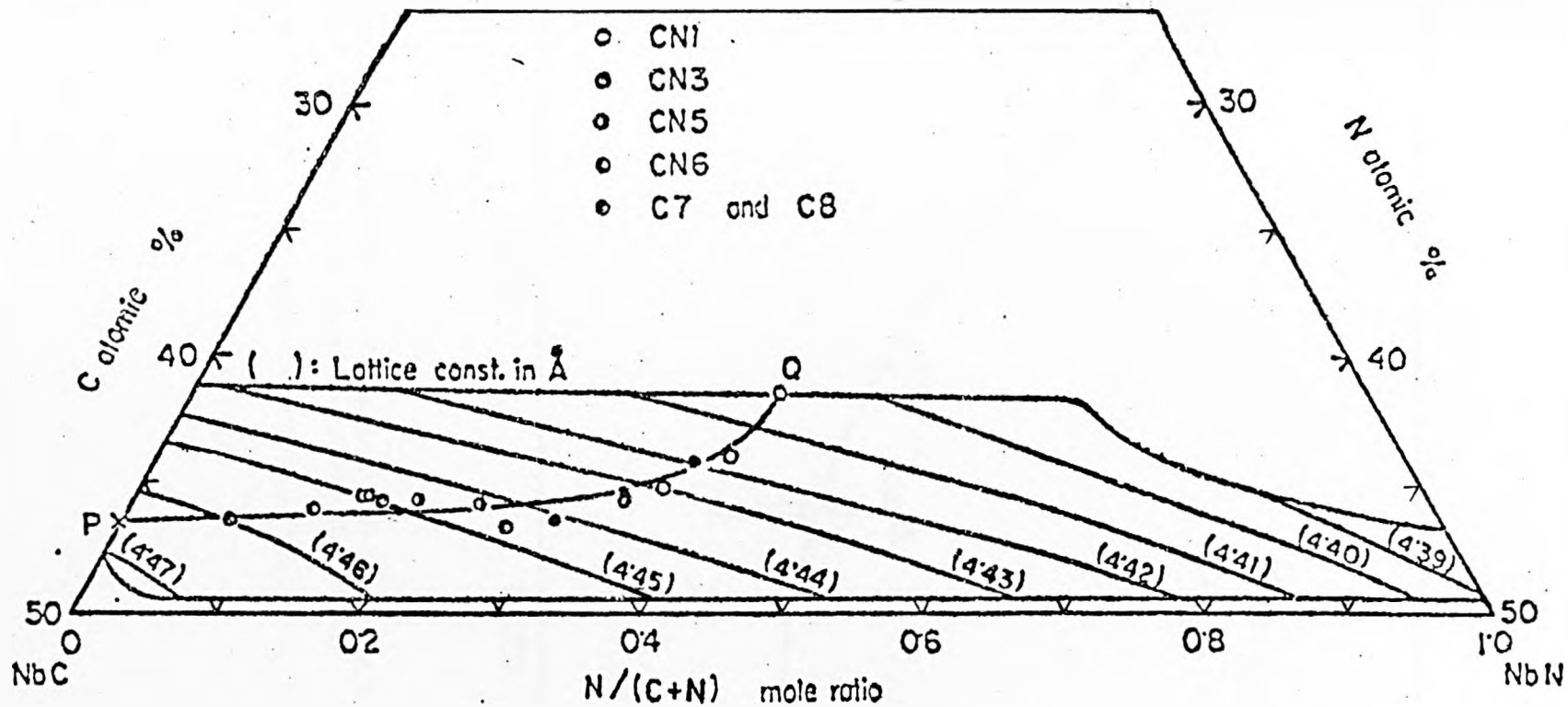
Fig. 2.11   Representation of the lattice parameter-composition relationships in the Nb–NbC–NbN system. After Brauer and Lesser (1959)
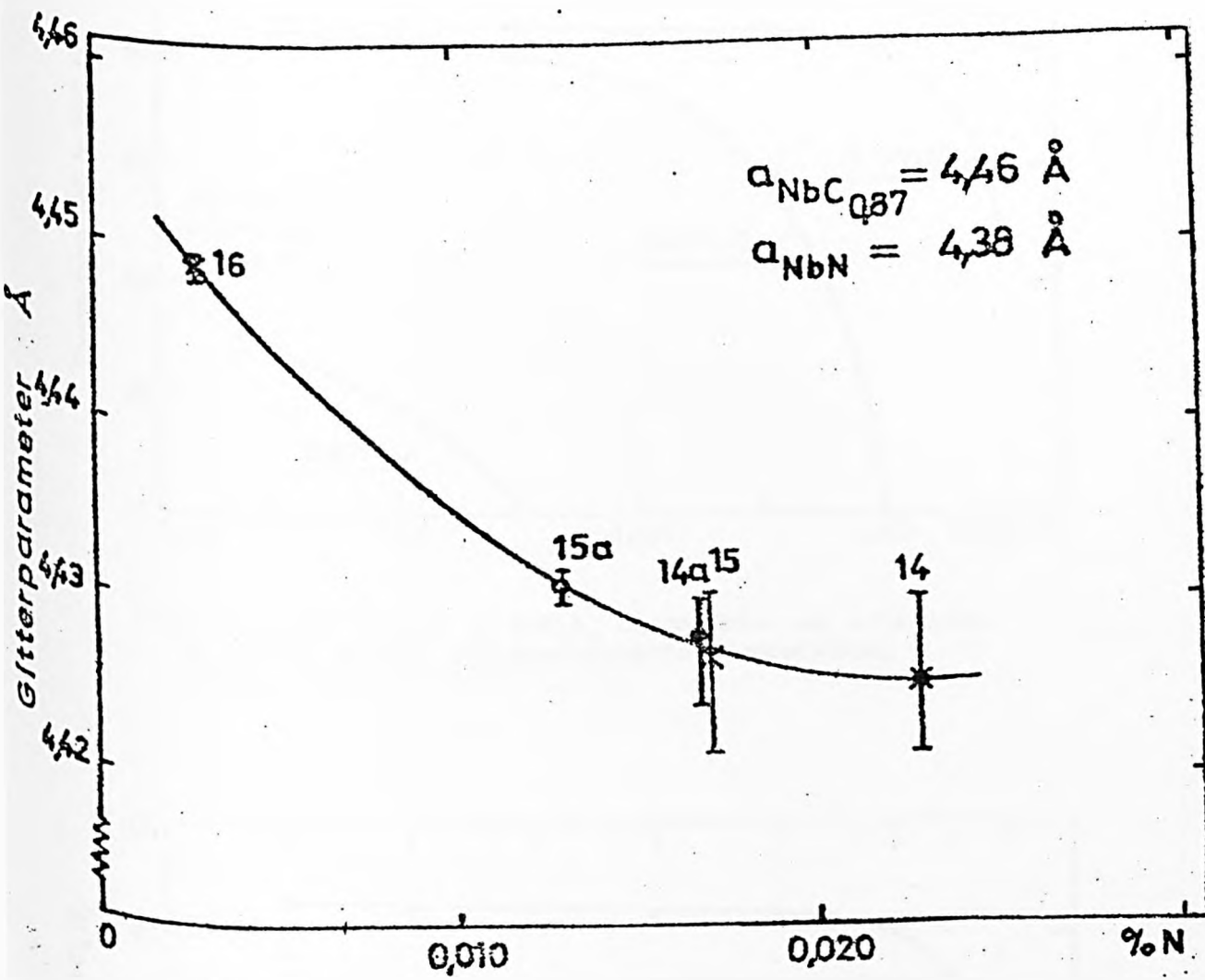
Fig..2.12 Lattice parameter of extraoted NbX-phase as a function of % N of steel. All steels contain 0.03 % C.

After Aronsson and Jonsson-Holmquist (1970).
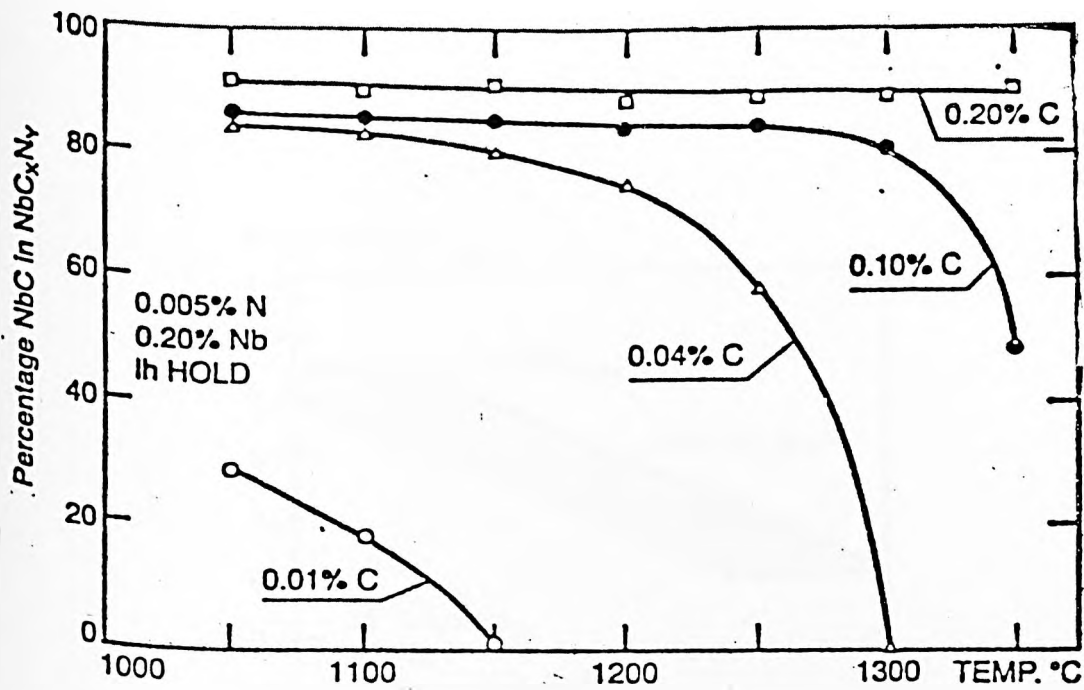
Fig. 2.13.a   Change in NbC$_x$N$_y$ composition as a function
of carbon content and precipitation temperature.
After Hoesch-Estel (1981)
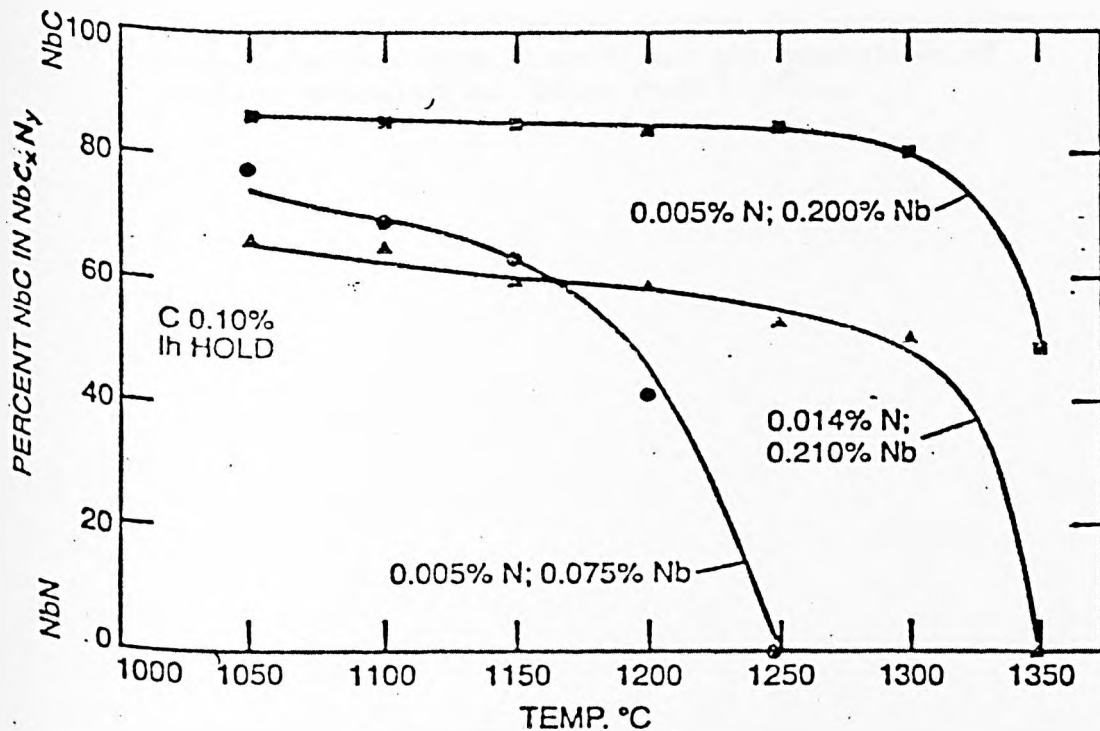
Fig. 2.13.b Change in NbC$_x$N$_y$ composition with tempera-
ture and niobium content. After Hoesch-Estel(1981).
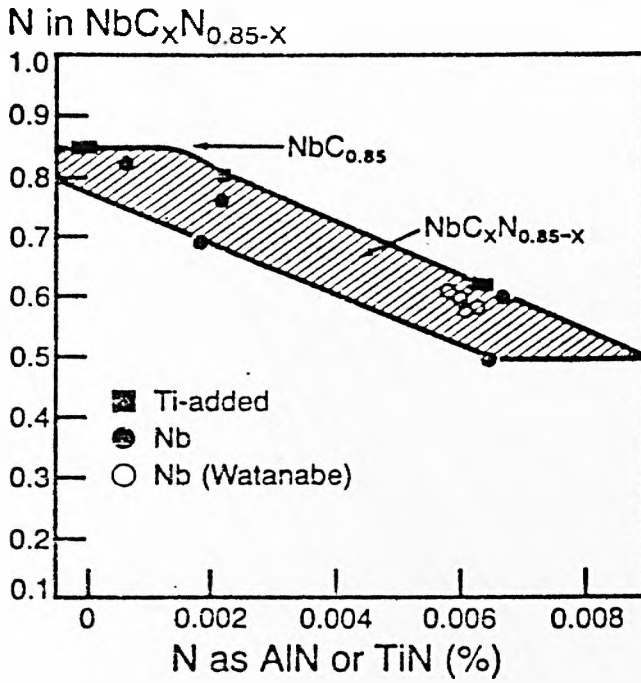
Fig 2.14 . The relationship between the nitrogen content uncombined with Al or Ti and the composition of niobium carbonitride. After Ouchi (1981).
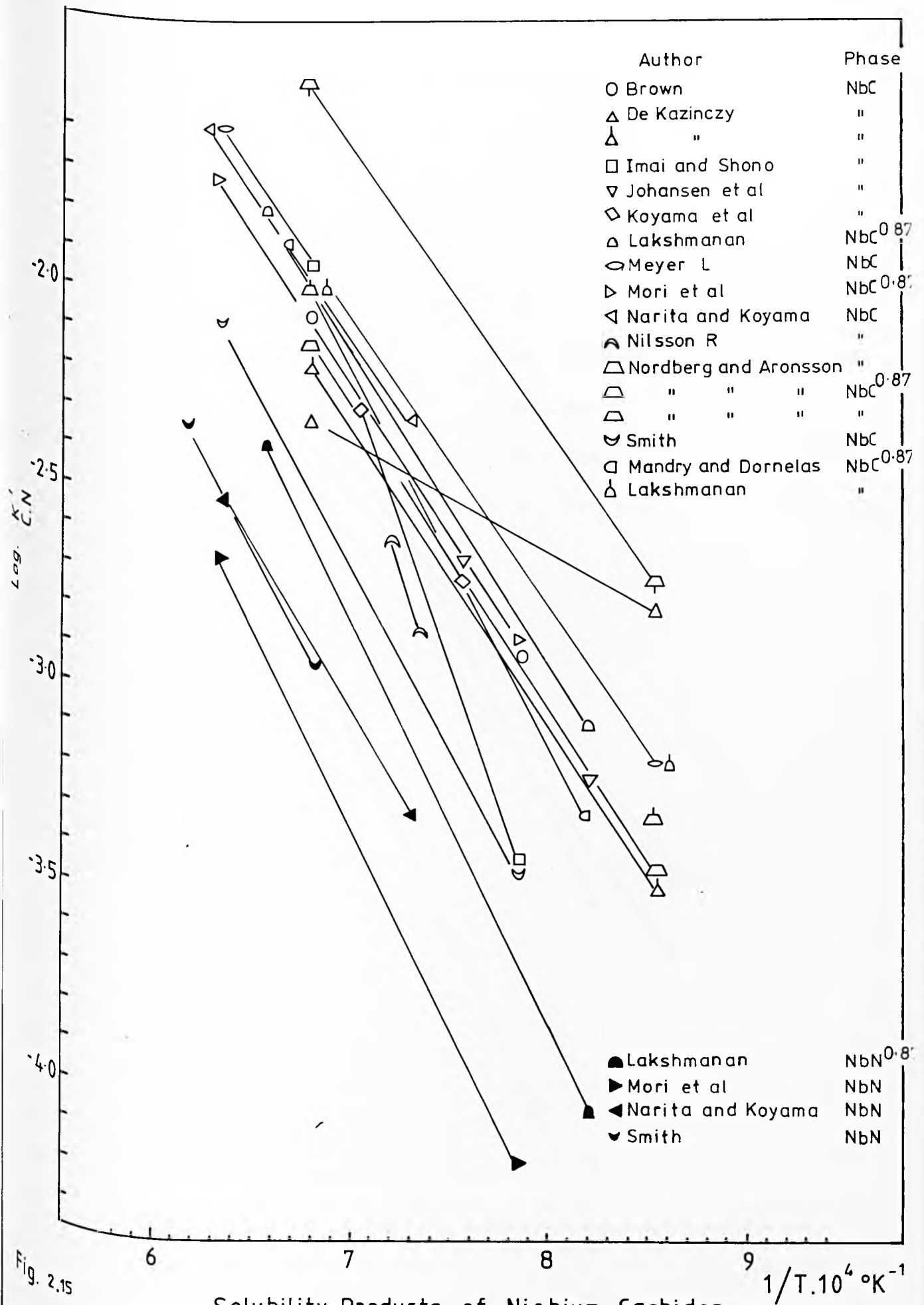
Fig. 2.15

Solubility Products of Niobium Carbides and Niobium Nitrides.

Fig. 2.16   Solubility Products of Niobium Carbonitrides

Fig.2.17 Schematic Representation of the Carbonitride – Austenite Equilibrium in the Fe –Nb –C –N System.

The figure shows a tetrahedron with vertices labeled Nb (top), Fe (left), C (bottom), and N (right). Labels include:

- $\delta\, NbC_x N_y$
- $\delta\, NbC_x N_{0\cdot 87-X}$
- $\delta\, NbN_{0\cdot 87}$
- $\epsilon\, NbN$
- T_3
- X_{Fe}
- $\gamma + NbC_x N_y$
- δNbC_x
- T_2
- X_{Nb}
- γ
- T_1
- X_C
- X_{Nb}
- X_N
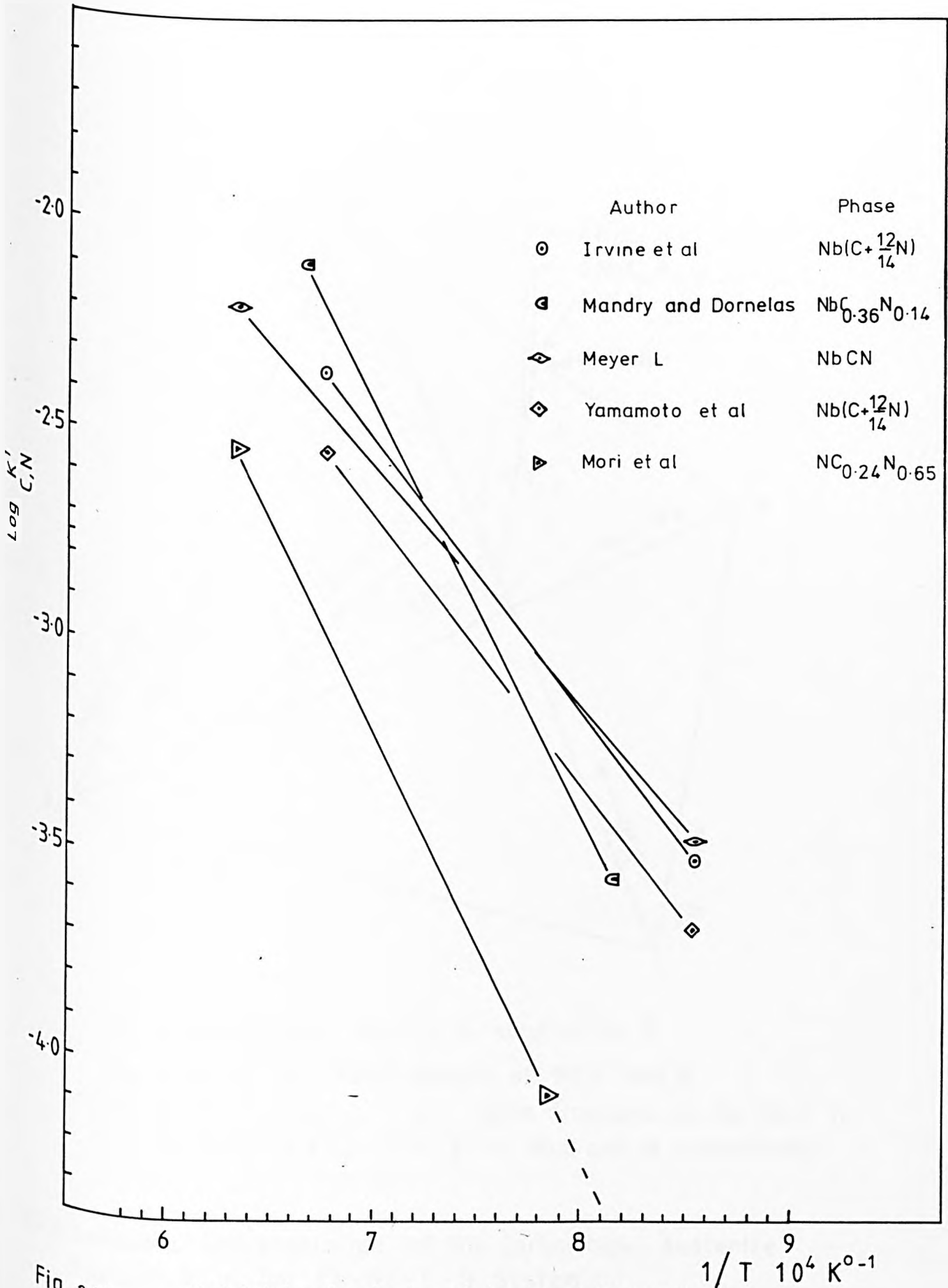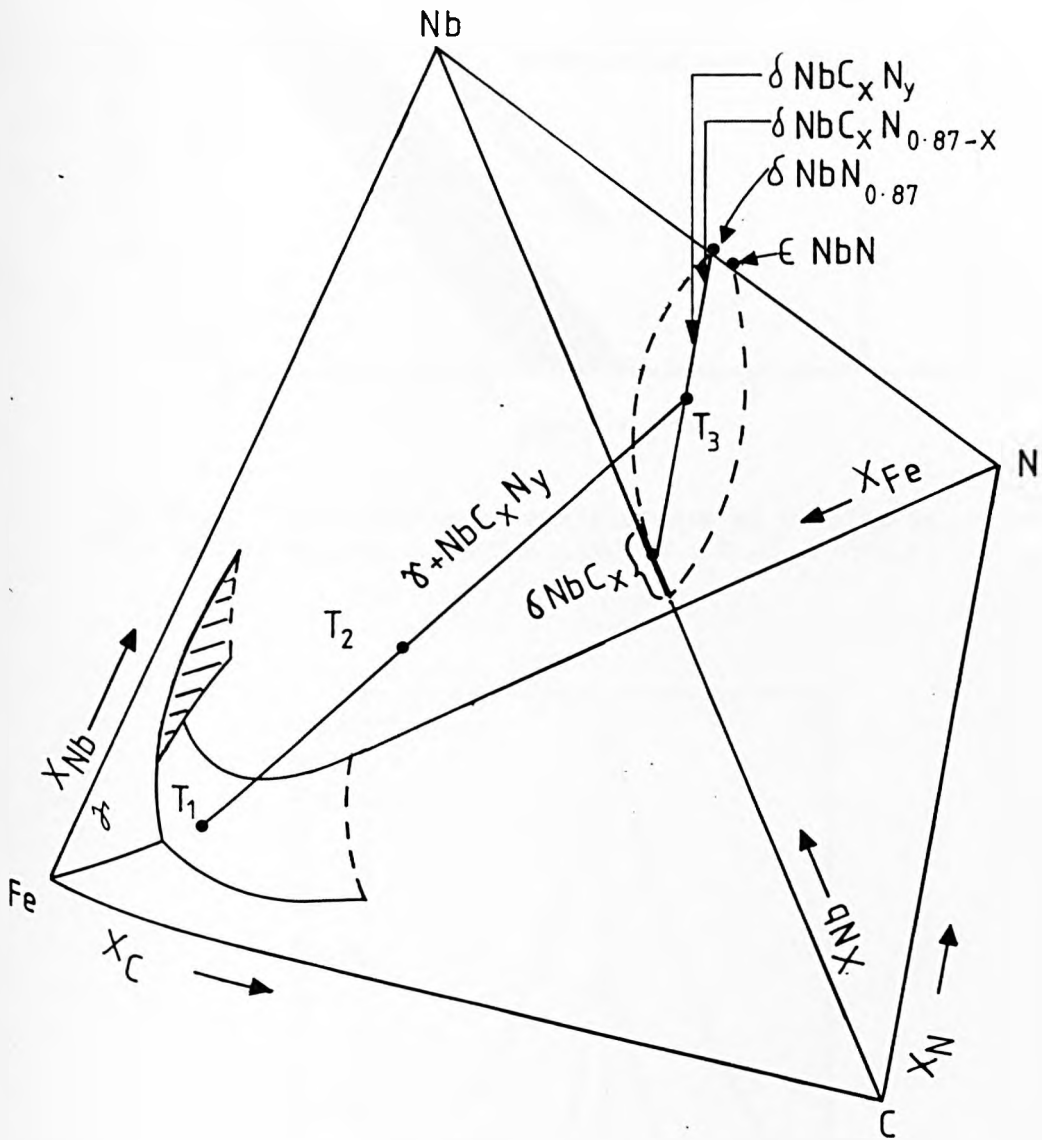
$T_1 = [Nb], [C], [N],$ Nb,C,N in solution in γ.

$T_2 = Nb, C, N$ Total amount of Nb,C and N.

$T_3 = \dfrac{1}{1+X+y} \quad \dfrac{x}{1+X+y} \quad \dfrac{y}{1+X+y}$ atom fractions in the Nb C N for Nb,C and N respectively.
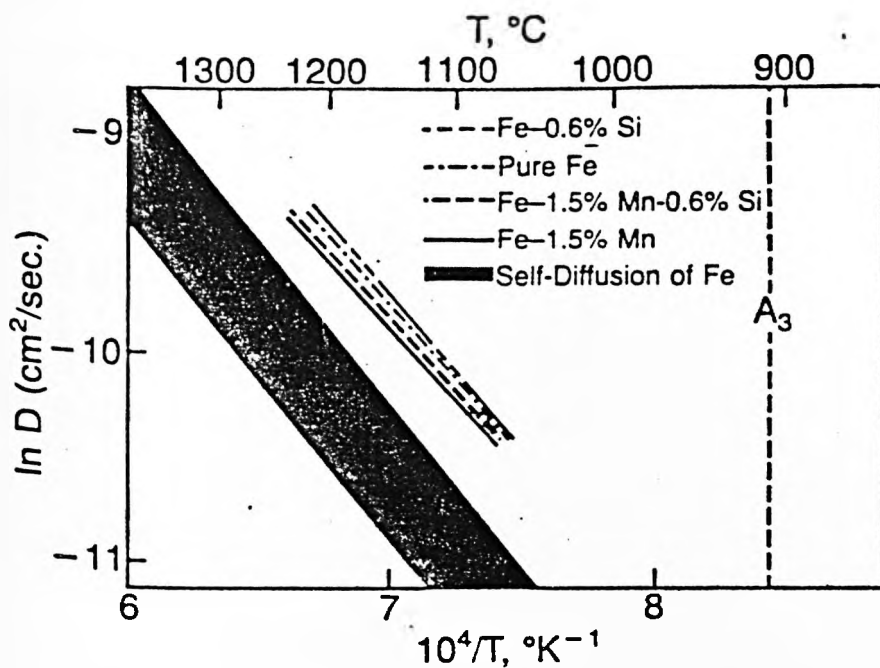
Fig. 2.18   Interdiffusion coefficients of niobium in
Pure binary alloys. After Kurokawa et al (1981).
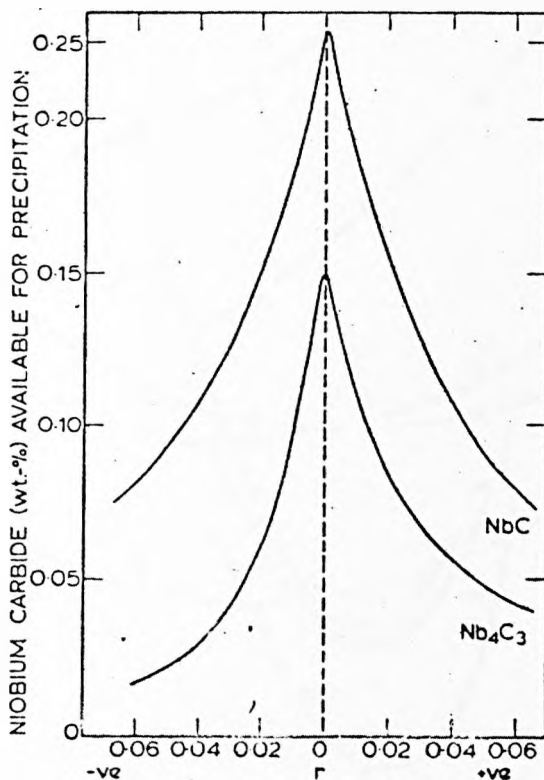
Fig. 2.19 Amount of niobium carbide available for precipitation at
923 K (after solution-treatment at 1373 K) as function of
degree of deviation from stoichiometry, r. Positive values
of r indicate C-rich compositions, negative values Nb-
rich.
After Wadsworth et al (1976).
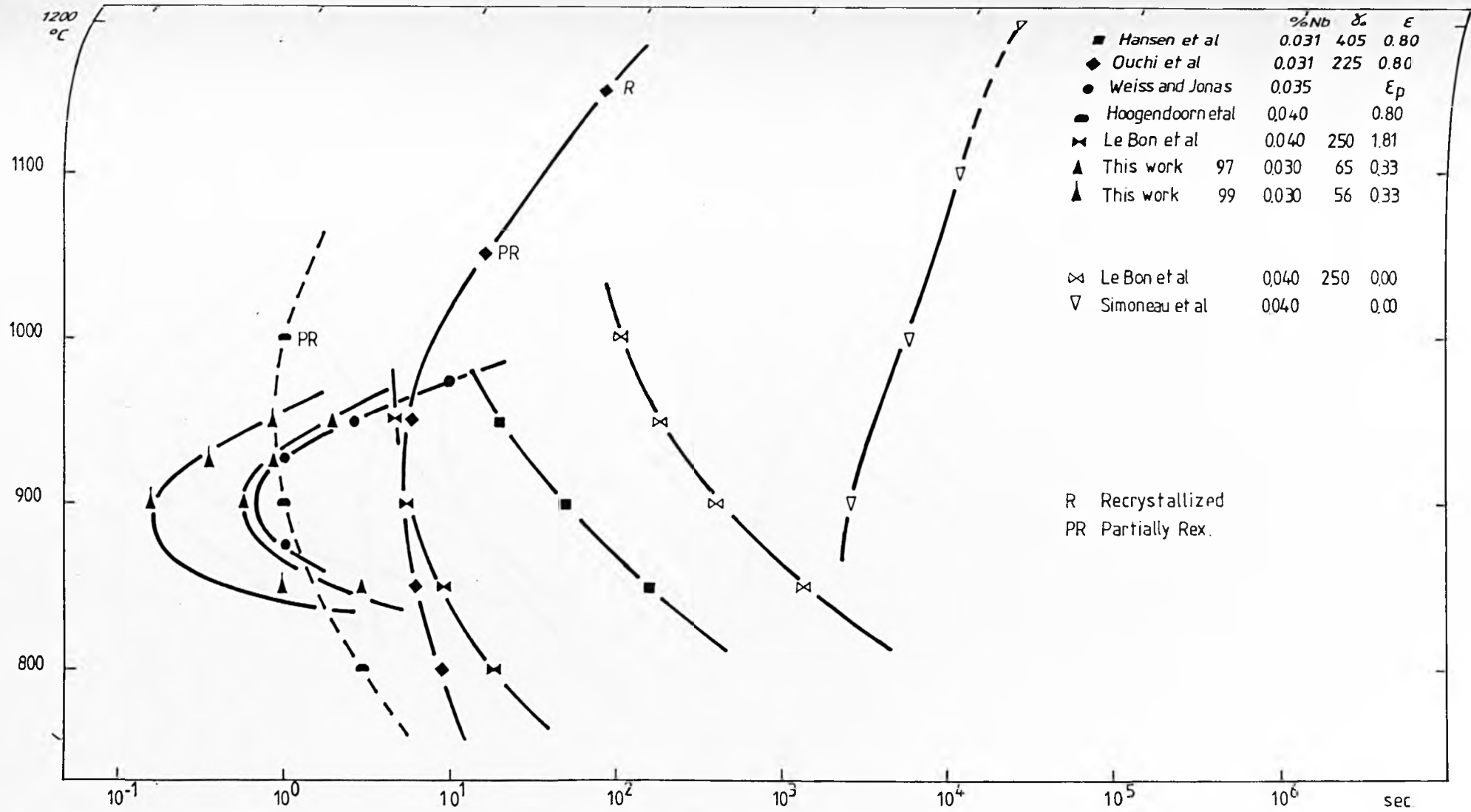
FIG. 2.20 PRECIPITATION START (5%) FOR STEELS ≤ 0.04%Nb – FULL COMPOSITION AND TREATMENT GIVEN IN TABLE 2.14
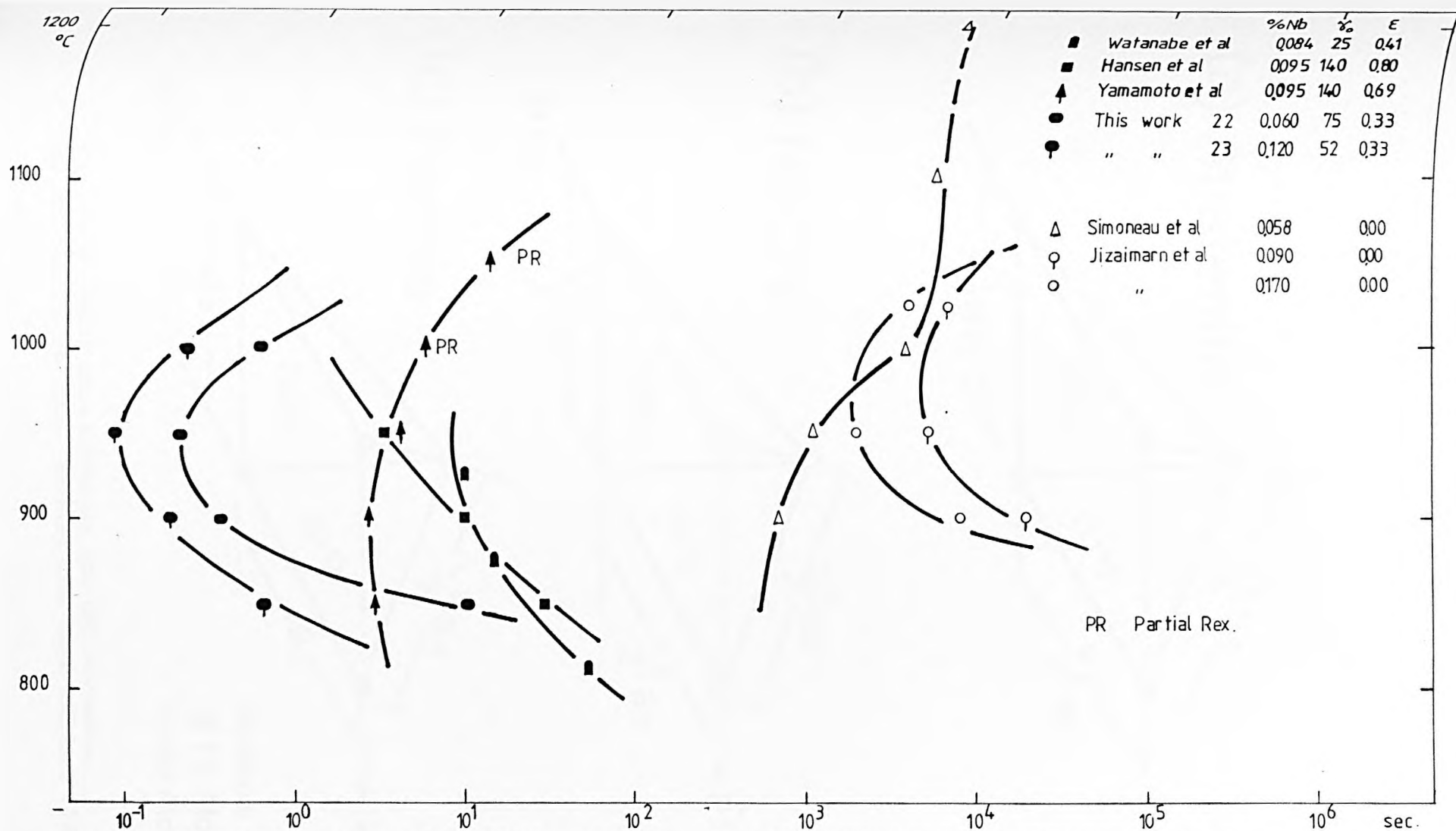
FIG. 2.21 PRECIPITATION START (5%) FOR STEELS ≥ 0.04%Nb — FULL COMPOSITION AND TREATMENT GIVEN IN TABLE 2.14

		%Nb	γ_o	ϵ
◖	Watanabe et al	0.084	25	0.41
◼	Hansen et al	0.095	140	0.80
▲	Yamamoto et al	0.095	140	0.69
◓	This work	22	0.060	75	0.33
♀	" "	23	0.120	52	0.33

△	Simoneau et al	0.058	0.00
♀	Jizaimarn et al	0.090	0.00
○	"	0.170	0.00

PR Partial Rex.

(a) Austenite

$\frac{\sqrt{2}}{2} a_0$

[$\bar{1}$10]

(001) (111)

$\frac{\sqrt{2}}{2} a_0$

[110] $\frac{\sqrt{2}}{2} a_0$

(b) NbCN

$\frac{\sqrt{2}}{2} a_0$

[$\bar{1}$10]

(001) (111)

$\frac{\sqrt{2}}{2} a_0$

[110] $\frac{\sqrt{2}}{2} a_0$

(c) Ferrite

$\frac{\sqrt{3}}{2} a_0$

[010]

(001) (011)

a_0

[100] a_0

Symbols
● Fe Atoms
O Nb Atoms
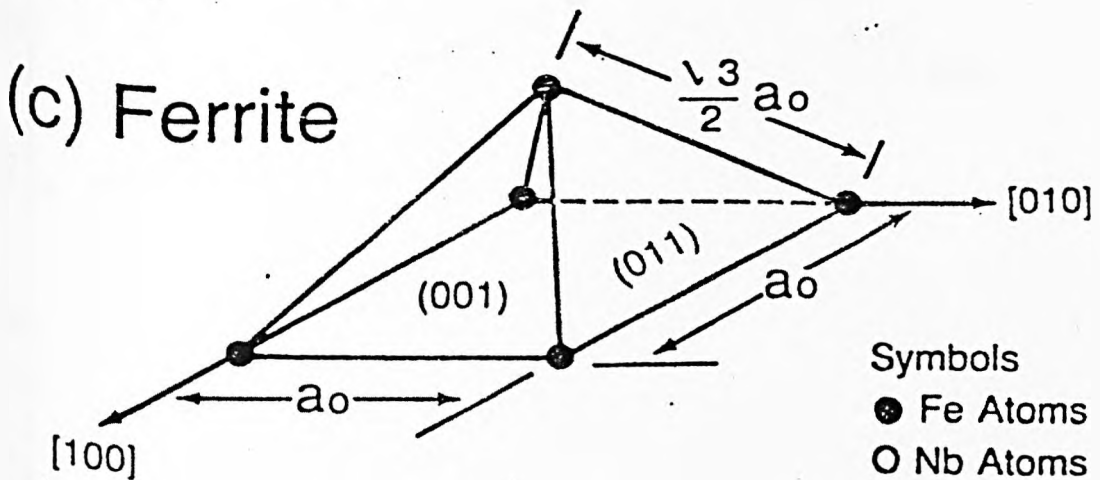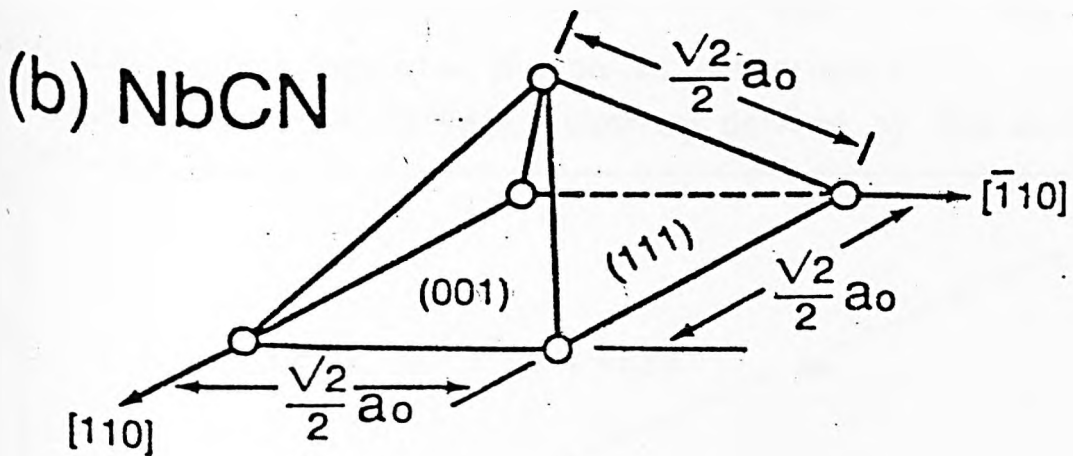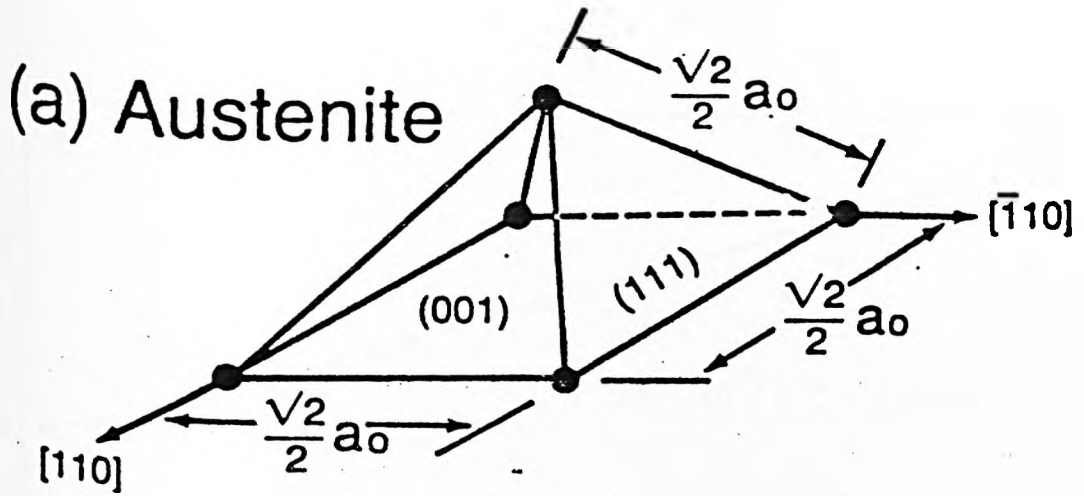
Fig. 2.22 Metal-atom octahedra for (a) austenite, (b) NbC and (c) ferrite. Adapted from Jack and Jack (1973).

$$a_\gamma = 9 \times 10^{-5}, T\,{}^\circ C + 3.5627$$

γ

$$a_\alpha = 7.95 \cdot 10^{-5}\,T\,{}^\circ C + 2.8539$$

$\propto$
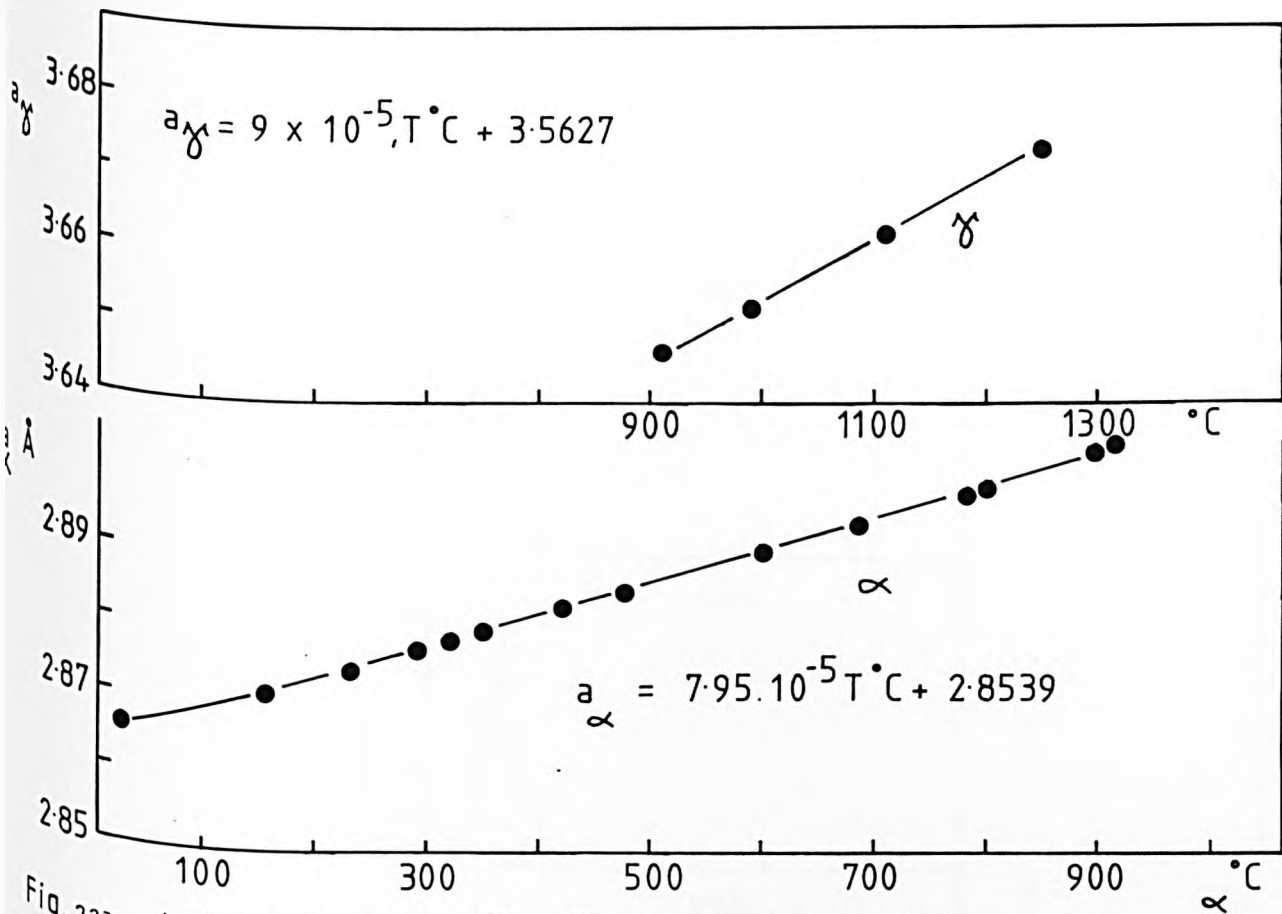
Fig. 2.23 Lattice Spacings of $\propto$, γ, iron vs Temperature.
After Goldschmidt(1962). Equations derived by the author.

$$a = 3.15 \times 10^{-5}\,T\,{}^\circ C + 4.4680$$

NbC
0.884
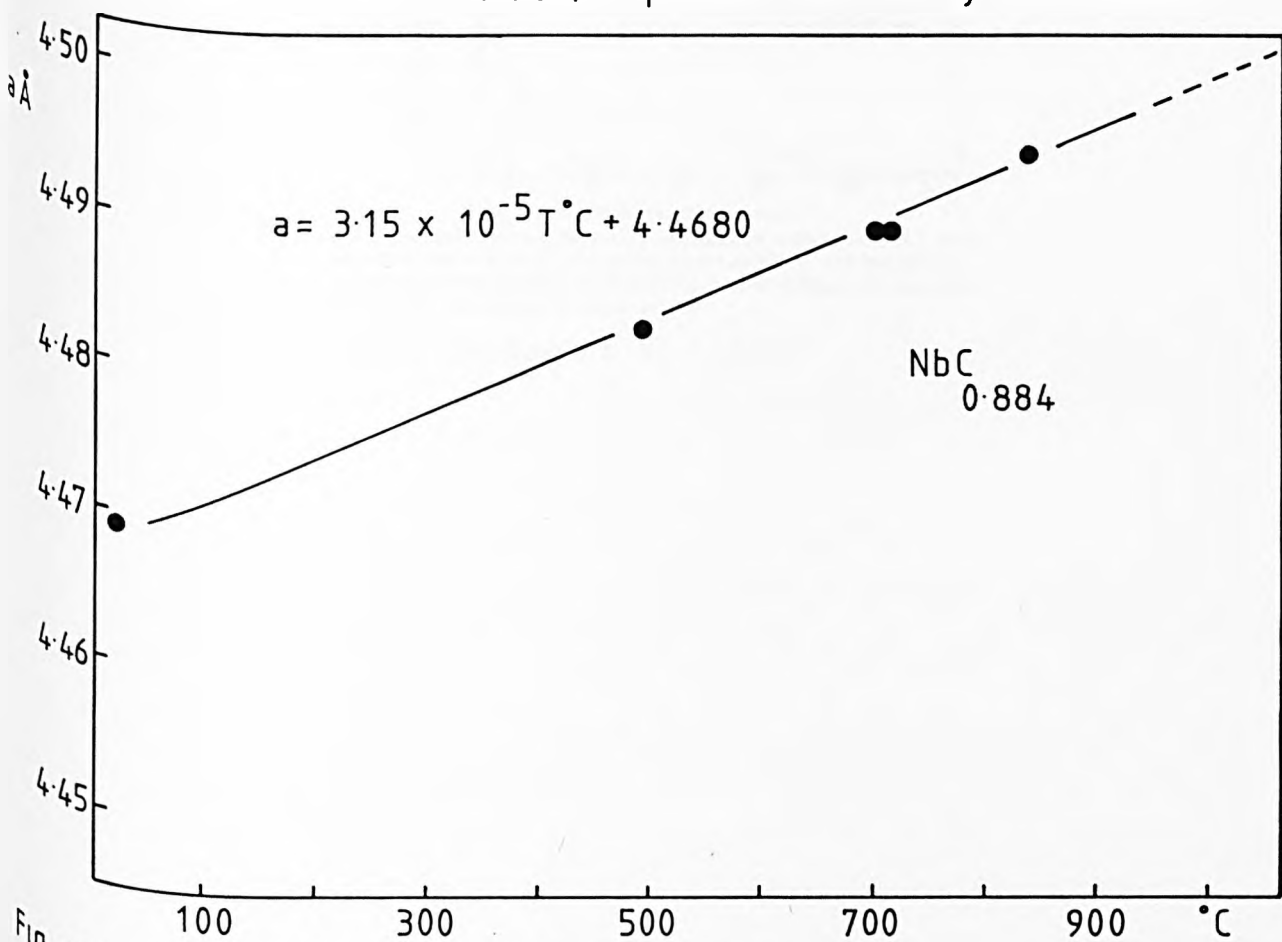
Fig. 2.24 Lattice Spacing of $NbC_{0.88}$ vs Temperature.
After Elliott & Kempter(1958). Equation derived by the author.
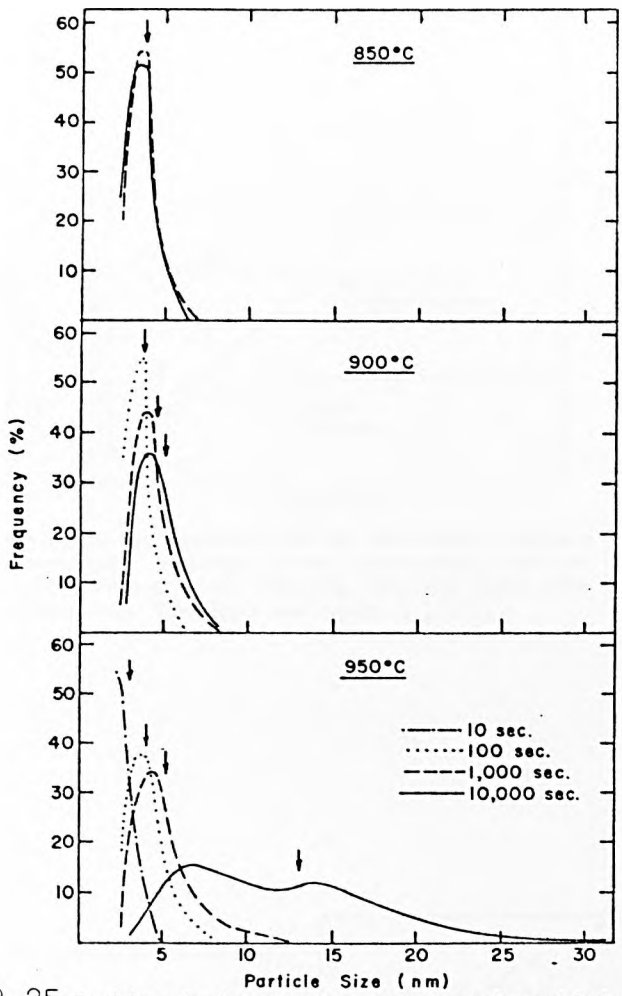
Fig.2.25-Precipitate-size frequency distribution curves for steel 3 after solutionizing at 1250°C, hot rolling 50 pct at 950°C, and holding for various time-temperature combinations. Arrows indicate average particle sizes for the respective distributions.

After Hansen et al (1980).
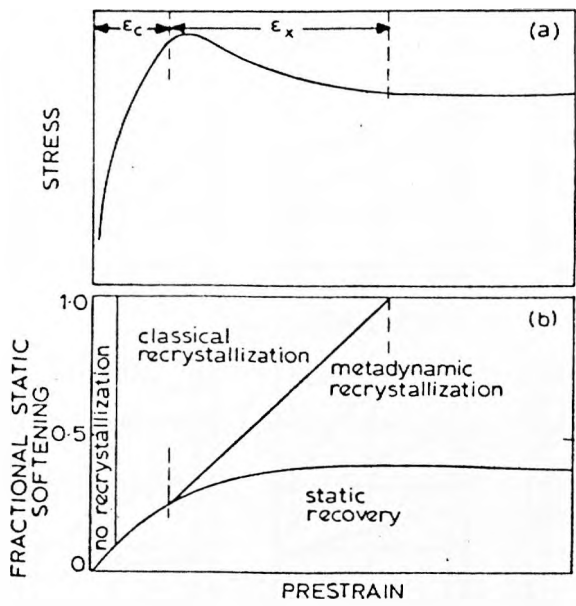
Fig. 3.1 Schematic representation of (a) relationship between stress/strain behaviour during deformation, and (b) mechanisms of static softening that take place after deformation. After Djaic and Jonas. (1973)
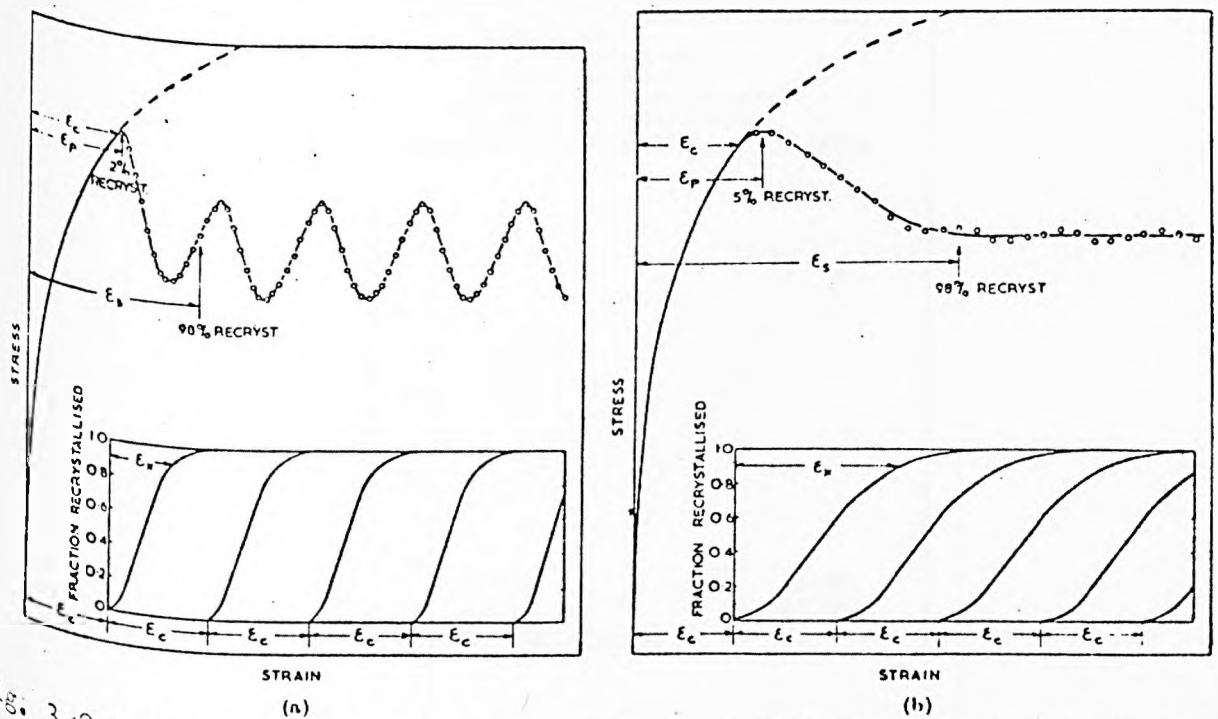
Fig. 3.2 Predicted stress-strain curves for dynamic recrystallization (a) critical strain to initiate recrystallization, $\epsilon_c > \epsilon_r$, the strain occurring in the time for a large fraction of recrystallization. (b) $\epsilon_c < \epsilon_r$.

After Luton and Sellars (1969).
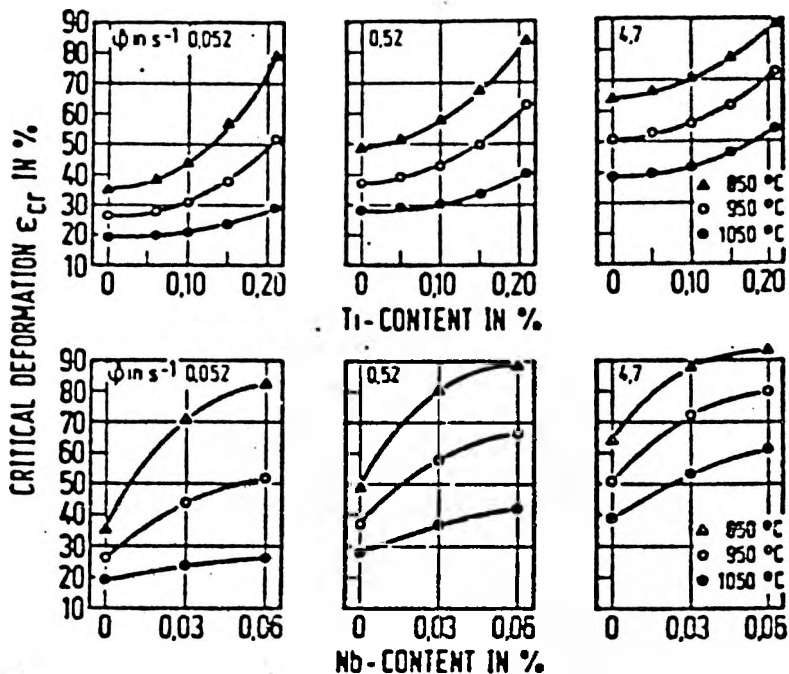
Fig. 3.3 . Influence of Ti and Nb on the deformation required for dynamic softening in connection with different deformation conditions. After Meyer and Robiller (1980).
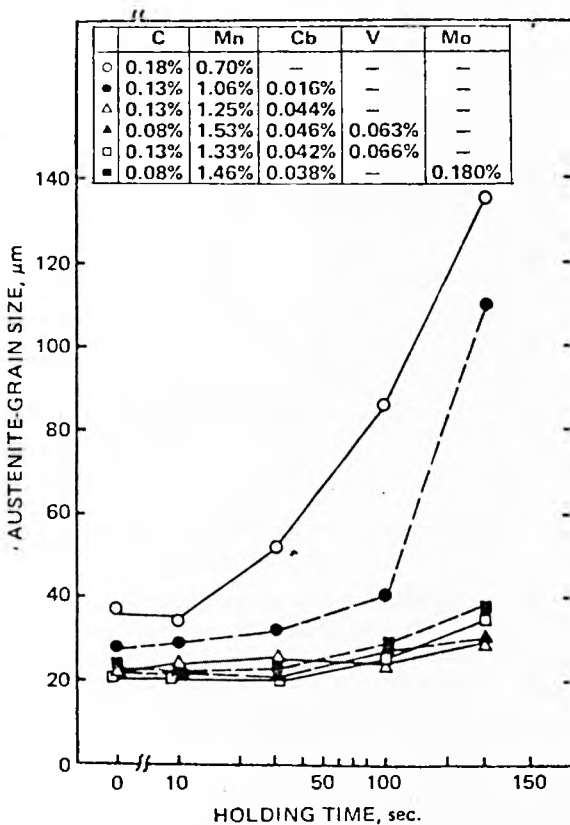
FIG. 3.4— Variation of austenite grain size with holding time. The steels were 68% hot-rolled and held at 1050°C. (1922°F.). After Tanaka et al (1977b).
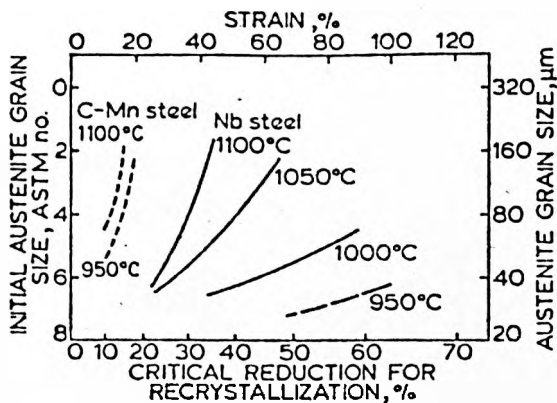
Fig. 3.5 Effects of deformation temperature and initial grain size on critical amount of deformation required for completion of recrystallization in plain C and Nb steels; after Tanaka *et al.* (1977b).
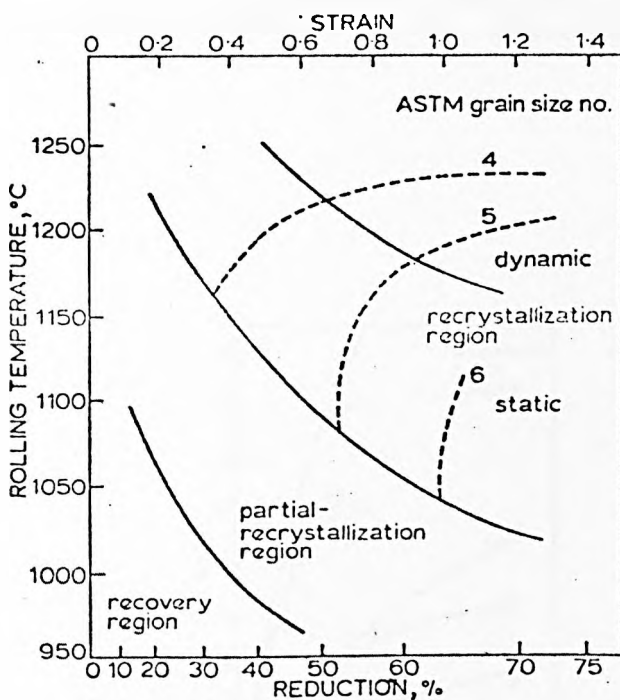
Fig.3.6 Austenite recrystallization and resulting grain size as function of rolling temperature and reduction for 0.03%Nb steel; steel was reheated to 1250°C for 20 min, rolled with one pass, and quenched; initial grain-size number was 1.0; after Ouchi *et al.* (1977).
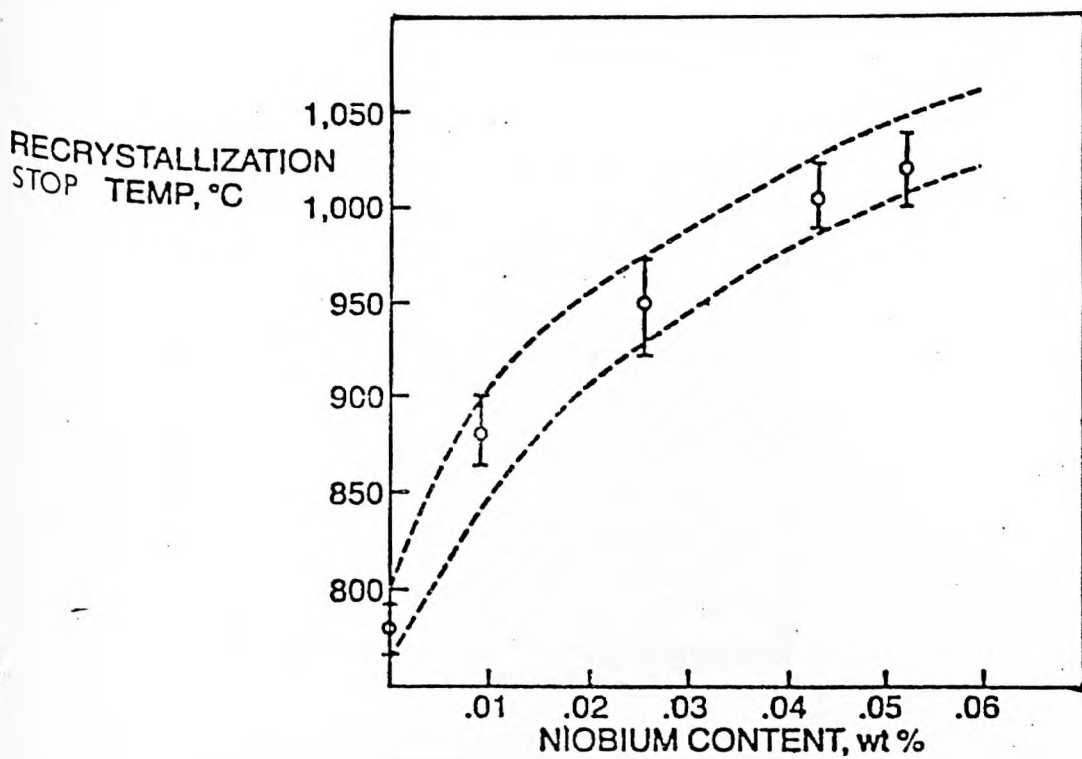
Fig. 3.7   The influence of niobium content on the recrystallization temperature of austenite as determined in hot compression testing. After Cuddy (1981).
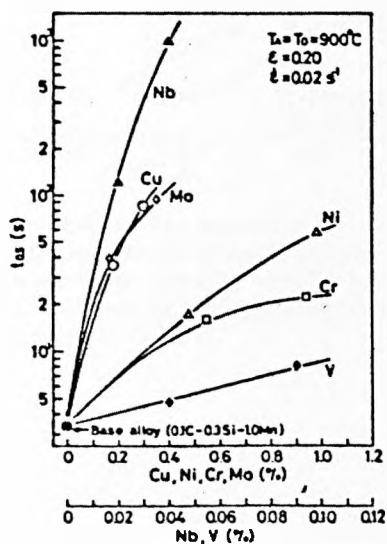
Fig. 3.8   Retardation effect of various alloying elements on the recrystallization of austenite.

After Maehara et al (1980).
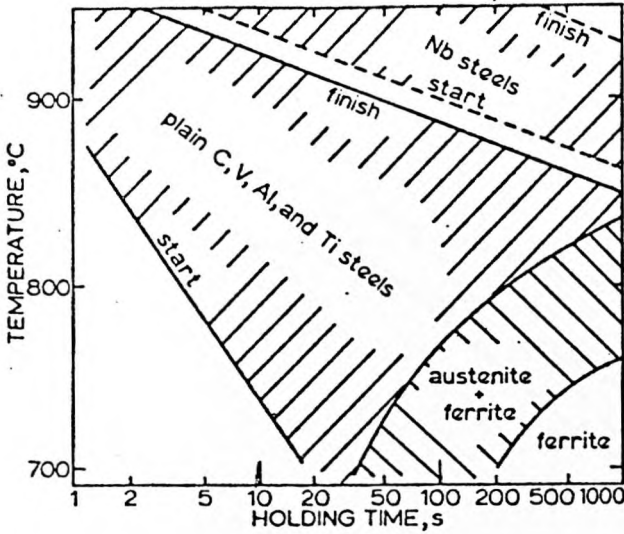
Fig.3.9 Recrystallization of austenite following
single deformation of 50% in various steels;
after Irvine *et al.* (1970).
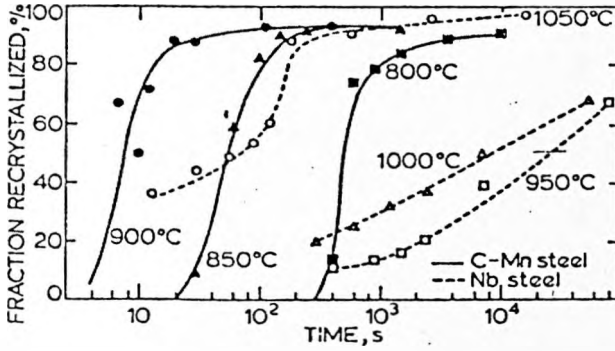
Fig.3.10 Fraction recrystallized in austenite as
function of holding time in plain C and Nb
steels; steels were reheated to 1250°C, hot
rolled to 30%, and held at rolling tempera-
ture; after Ohmori (1966).

A. DEFORMED AT DIFFERENT T OF ANNEALING

	%Nb	γₒ	ε
◆ Ouchi et al	0.031	250	0.80
■ Hansen et al	0.031	405	0.80
● Sellars eq.	0.040	200	0.33
◖ "	"	65	"
○ "	0.00	65	0.33

B. DEFORMED AND ANNEALED AT T

		%Nb	γₒ	ε
▼ Lamberigts et al		0.027	200	0.41
▮ Roberts, W.		0.025	300	0.30
▲ Greday et al		0.020	120	0.41
△ This work	97	0.030	65	0.33
△ " "	99	"	56	"
○ Sellars eq.		0.000	65	0.33
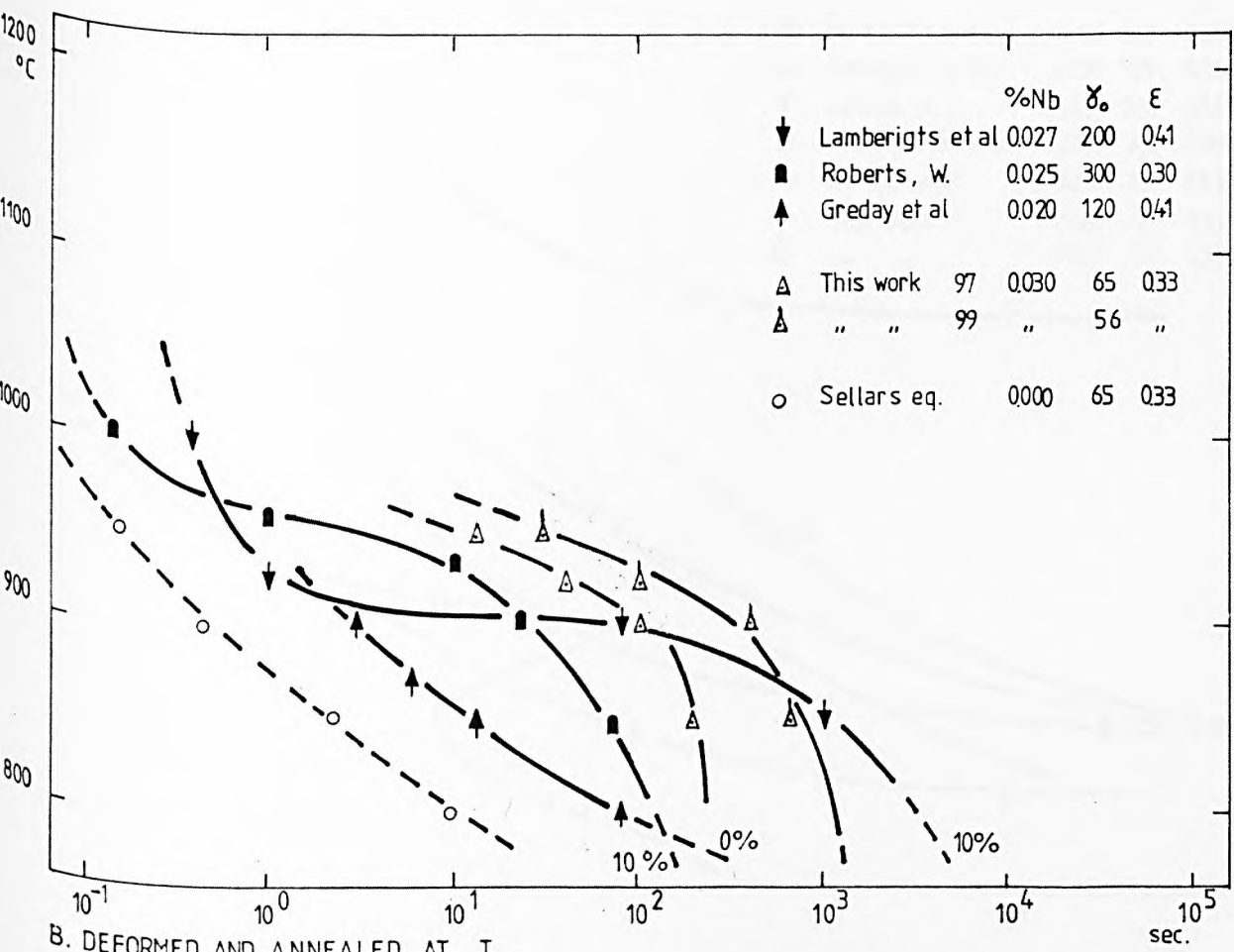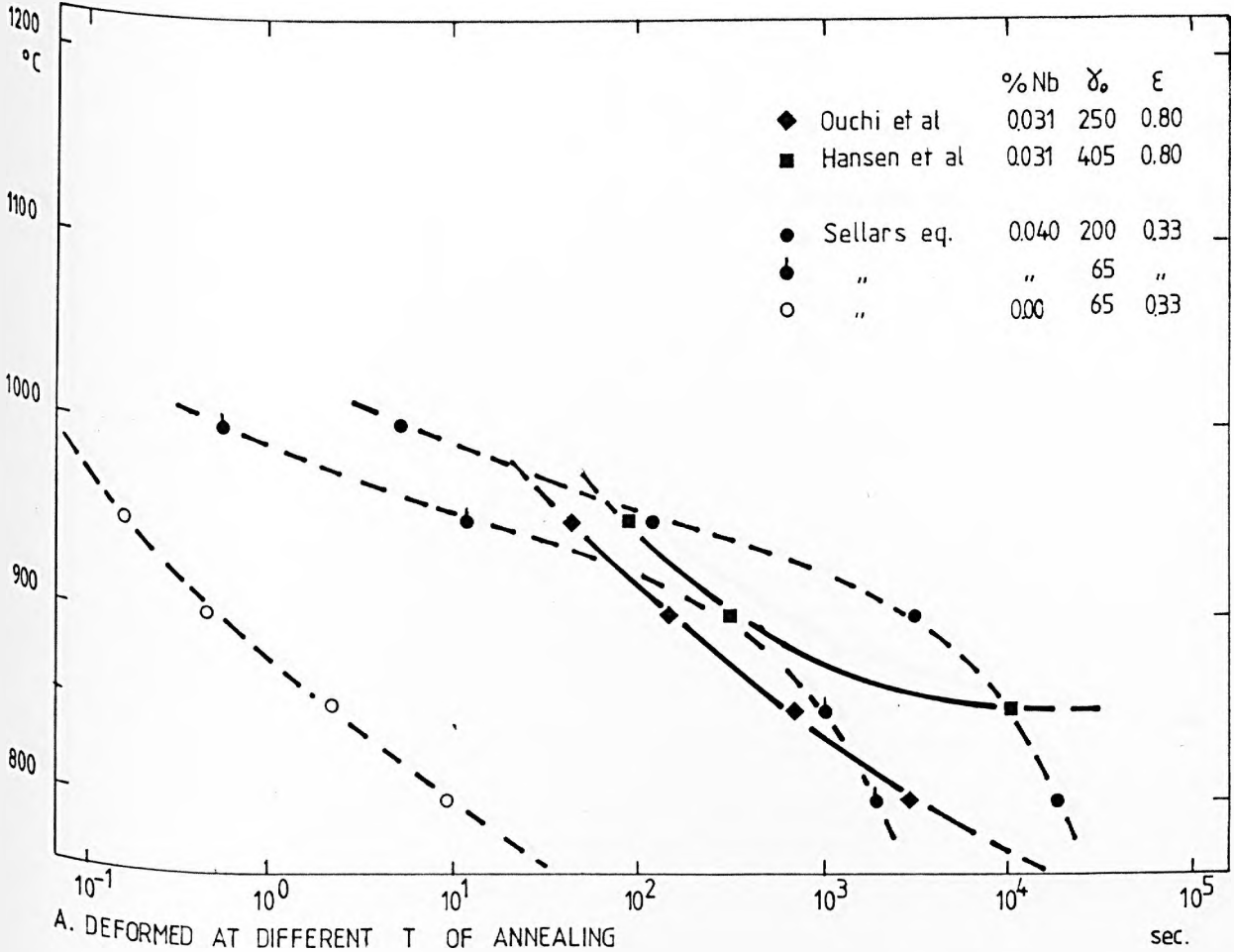
FIG. 3.11   RECRYSTALLIZATION START (5%) FOR STEELS WITH ≤ 0.04%Nb - FULL ANAL. & TREATMENT IN TABLE 3.2

FIG. 3.12   RECRYSTALLIZATION START (5%) FOR STEELS WITH ≥ 0.04% Nb - FULL ANAL. & TREATMENT IN TABLE 3.2

TEMPERATURE, °C

	Nb,%	ε	d_0, μm
▲ Irvine et al.	0·04	0·69	250*
▼ Le Bon et al.	0·04	0·86ε_p	250
■ Kozasu et al.	0·04	range	220
▲ Kozasu et al.			110
▼ Kozasu et al.			55

Nb-free steel

	Nb,%	ε	d_0, μm
○ Phillips and Crane	0·027	0·5	450*
□ Wilber et al.	0·02	0·36	60*
◇ Weiss et al.	0·015	0·30	110
	+0·025%Ti		
● Cordea and Hook	0·011	0·43	270

$(t_{0·5}\dot{\varepsilon}^4)/d_0^2$, s·μm⁻²

$1/T$, K⁻¹ × 10⁴
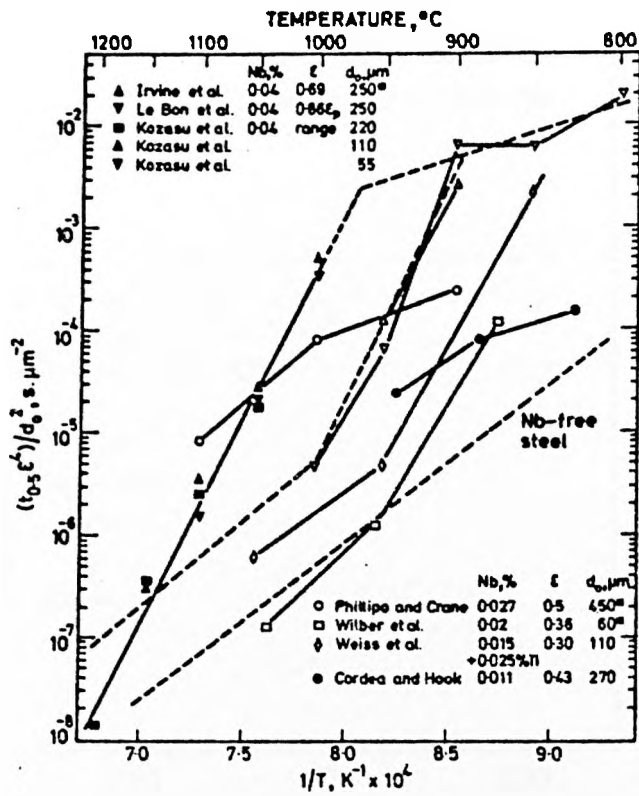
Fig.3.13 Temperature dependence of strain and grain size compensated time to 50% recrystallization or restoration in niobium-treated HSLA steels (grain sizes marked* are estimated values). After Sellars (1979)

	T,°C	d_0,μm	
+ Barraclough	1150	110	(5140)
×	1050	110	(5140)
✴	950	110	(5140)
□ Priestner et al.	1000	56	
○	900	44	
▽ Le Bon et al.	range	250	
◆		250	0·04% Nb
◆ Kozasu et al.	range	220	0·04% Nb
▲		110	0·04% Nb
▼		55	0·04% Nb
■ Weiss et al.	850°C	110	0·015% Nb
●		12	+0·025% Ti

RECRYSTALLIZED GRAIN SIZE, μm
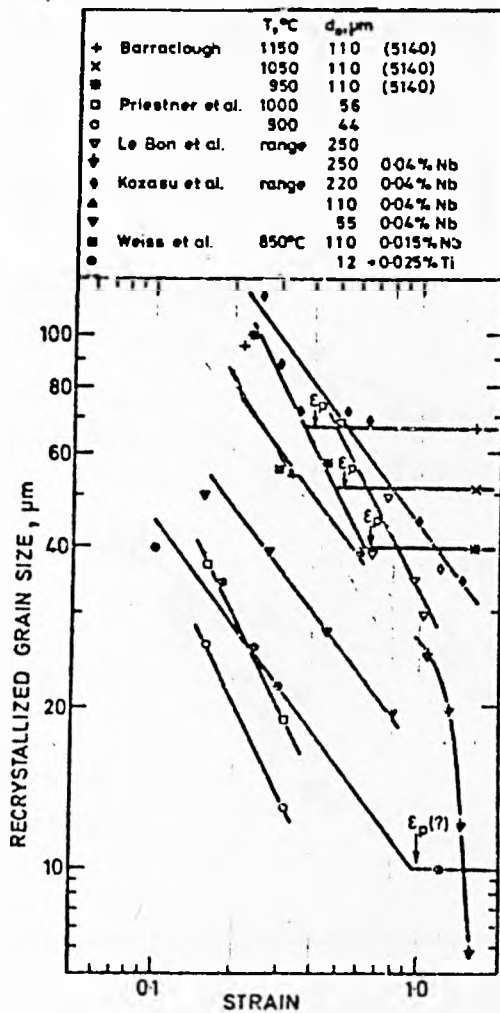
STRAIN

Fig.3.14 Dependence of statically recrystallized grain size on strain. After Sellars (1979)
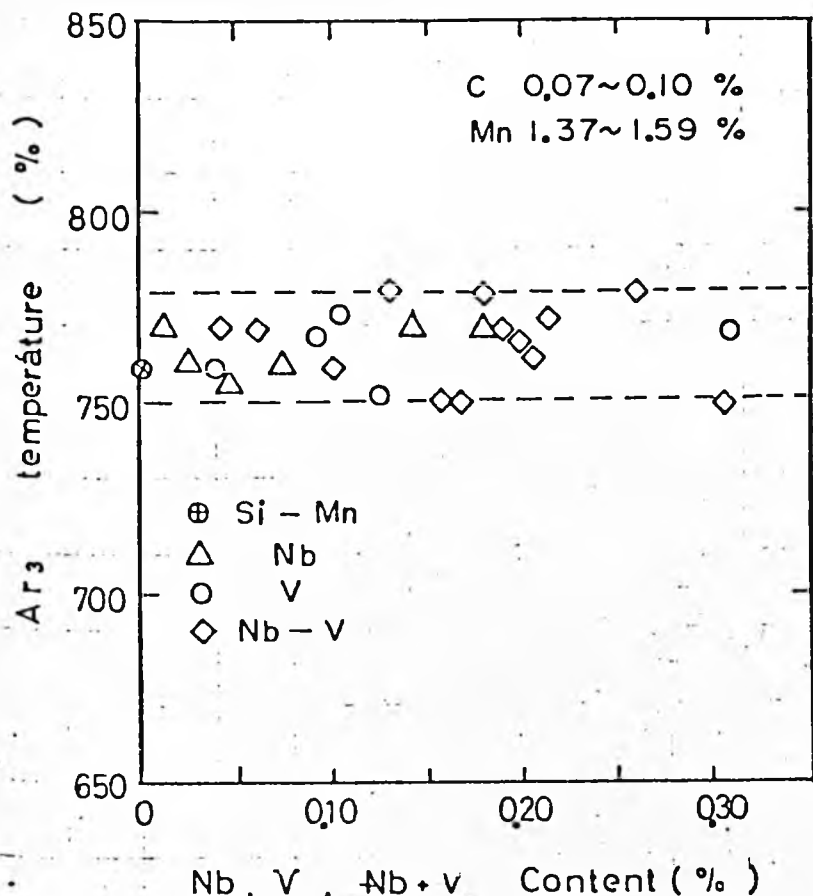
Fig. 3.15 Effect of Niobium and Vanadium on
the Transformation Temperature, Ar₃.
After Ouchi et al (1981).
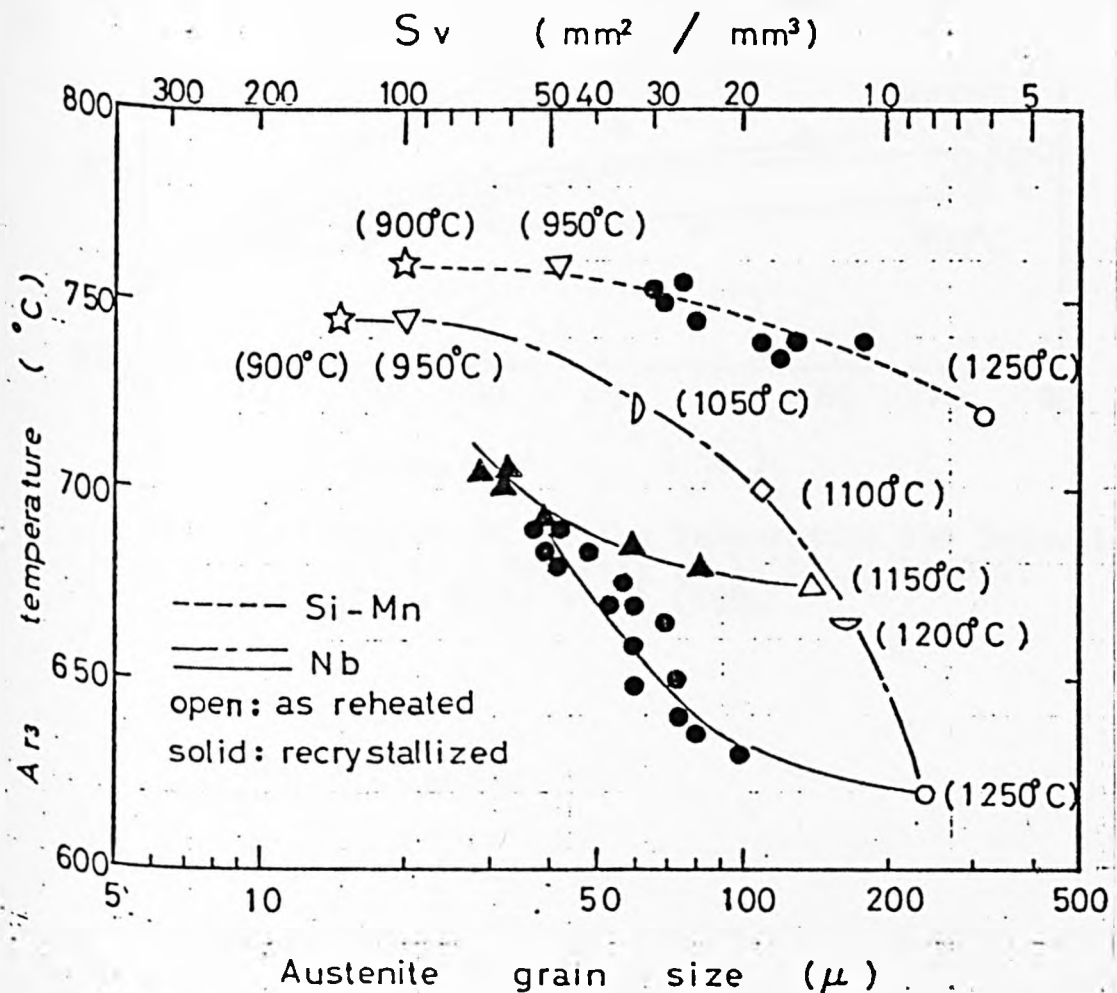
Fig. 3.16 Effect of Yg.s. on Ar₃. After Ouchi et al (1981).
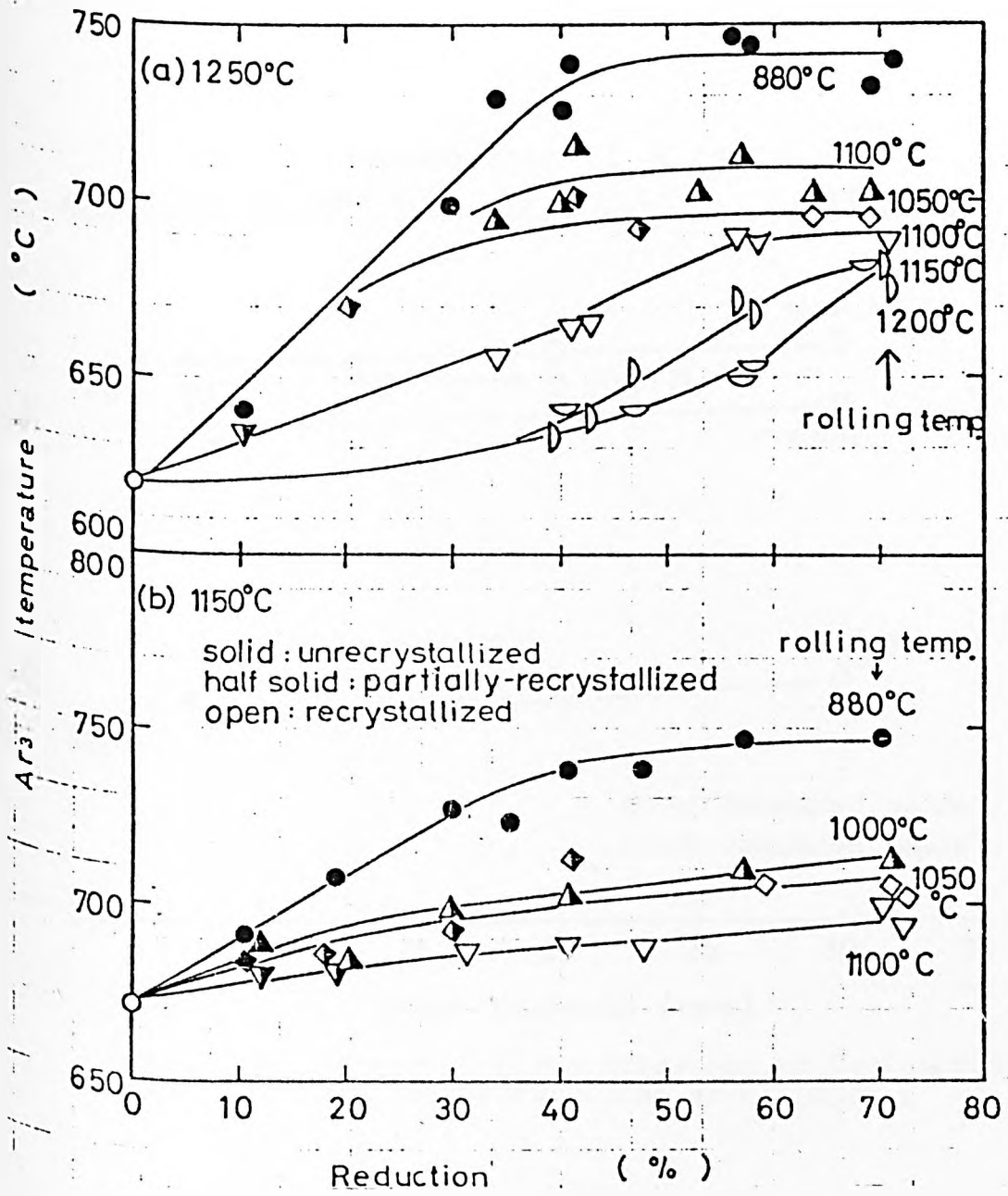
Fig. 3.17 Effect of Rolling Temperature and Reduction on the Ar₃. Reheatig at 1250 and 1150°C. After Ouchi et al (1981).
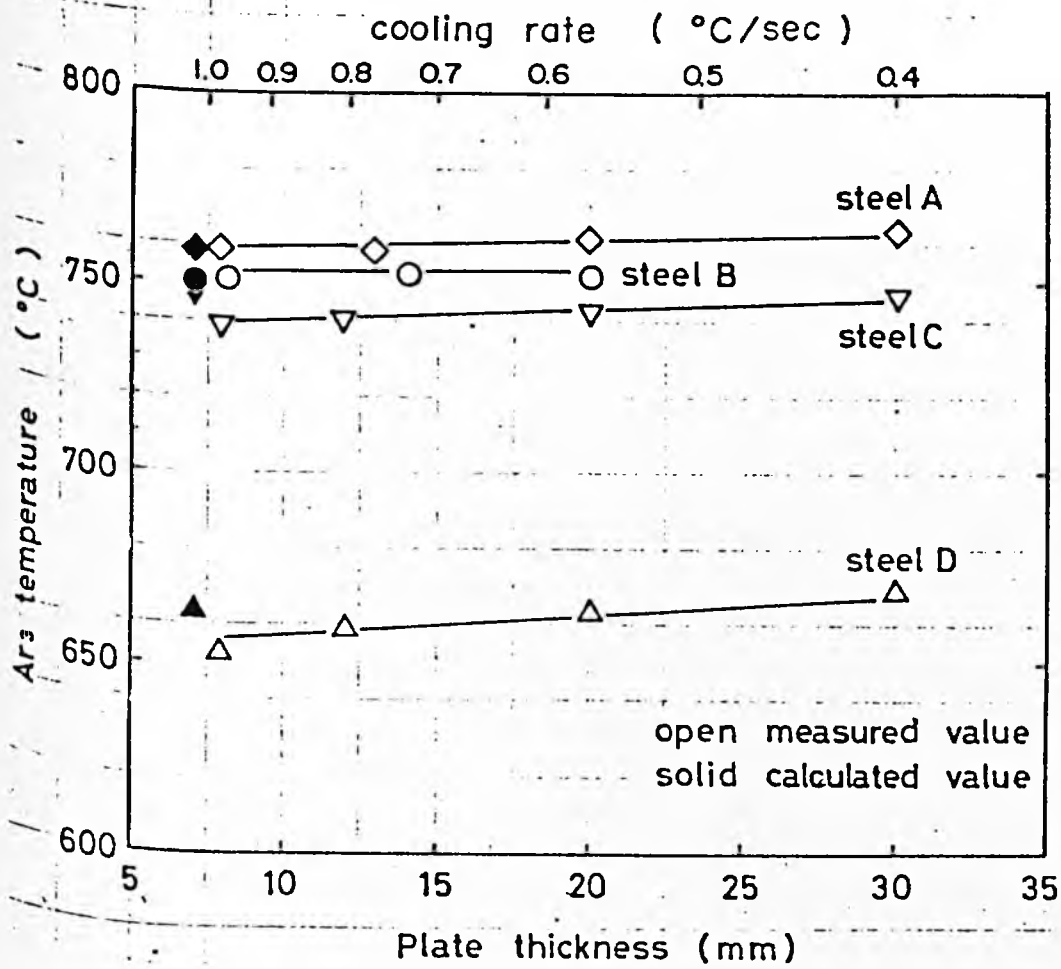
Fig. 3.18   Effect of Plate thickness or Cooling rate on the Ar₃. After Ouchi et al (1981).
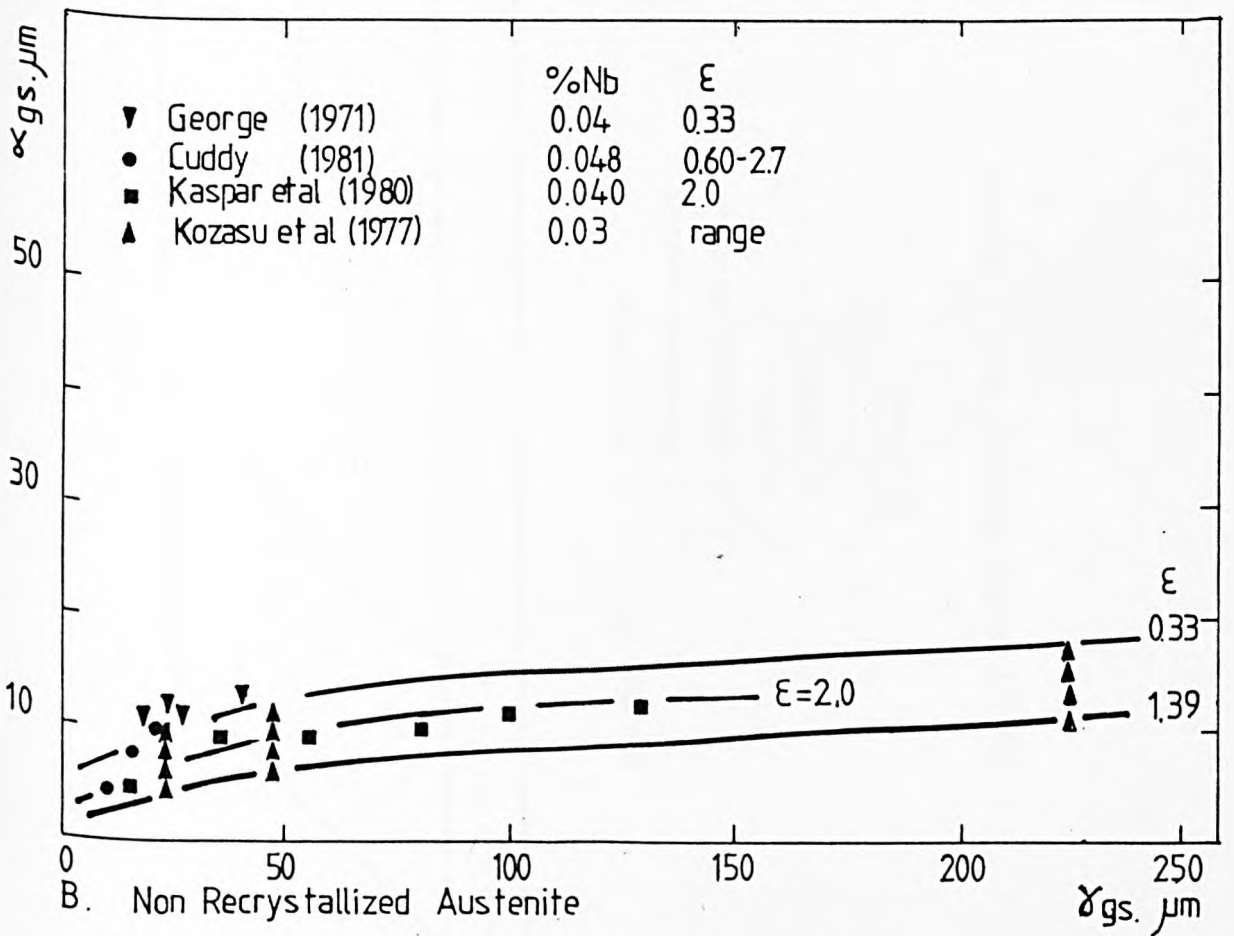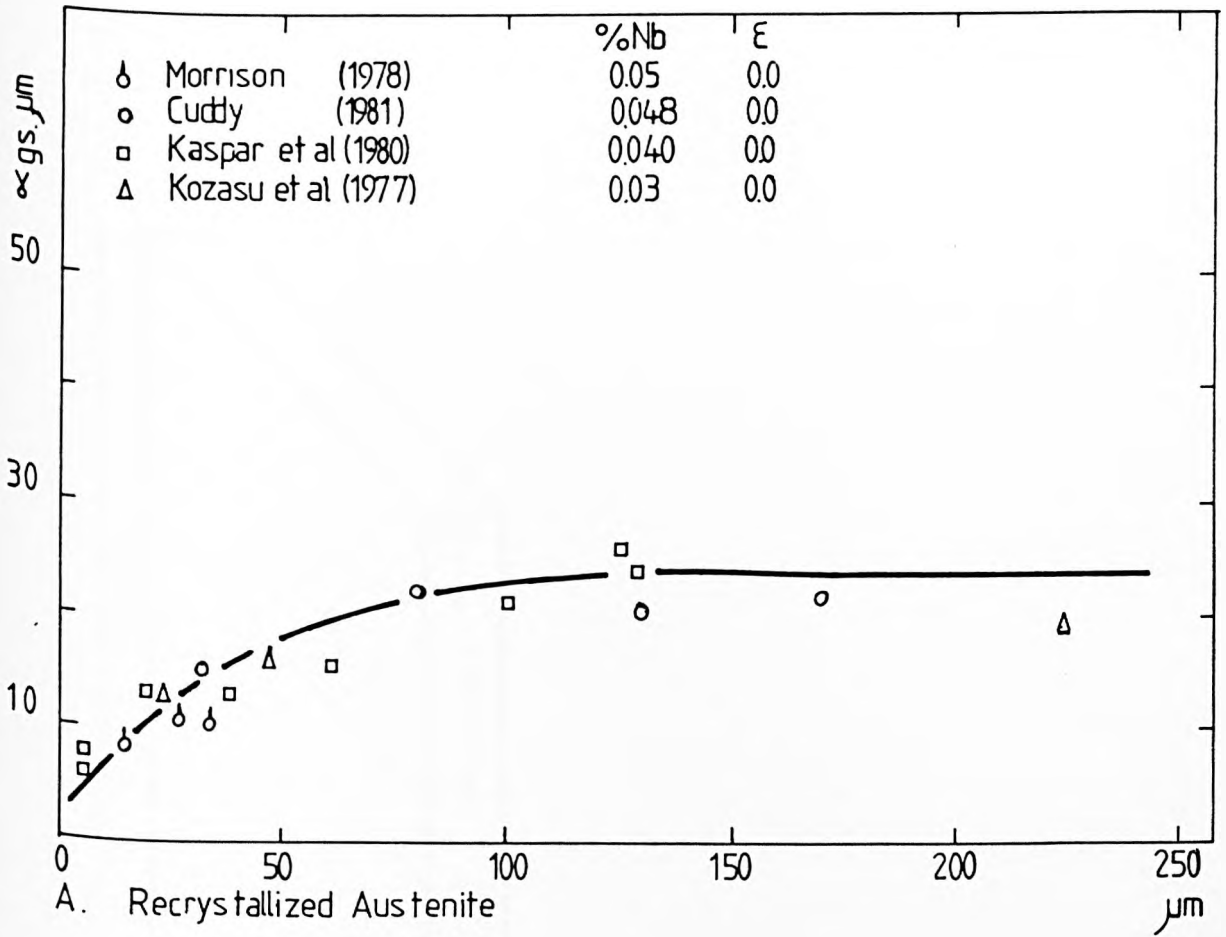
Fig. 3.19 Austenite/Ferrite grain sizes dependance
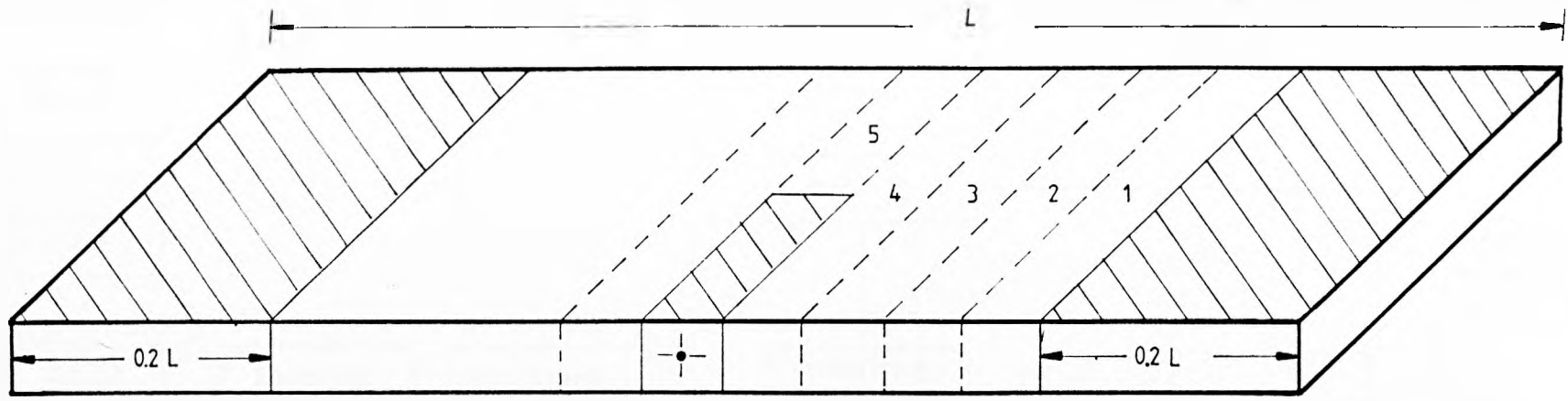
Specimens for :   1 Metallography
                  2 Free Nitrogen Analysis
                  3 Electrolytic Dissolution
                  4 Foils
                  5 Replicas

� Scrap

Fig. 4.1   SLABS SECTIONING PLAN   schematic
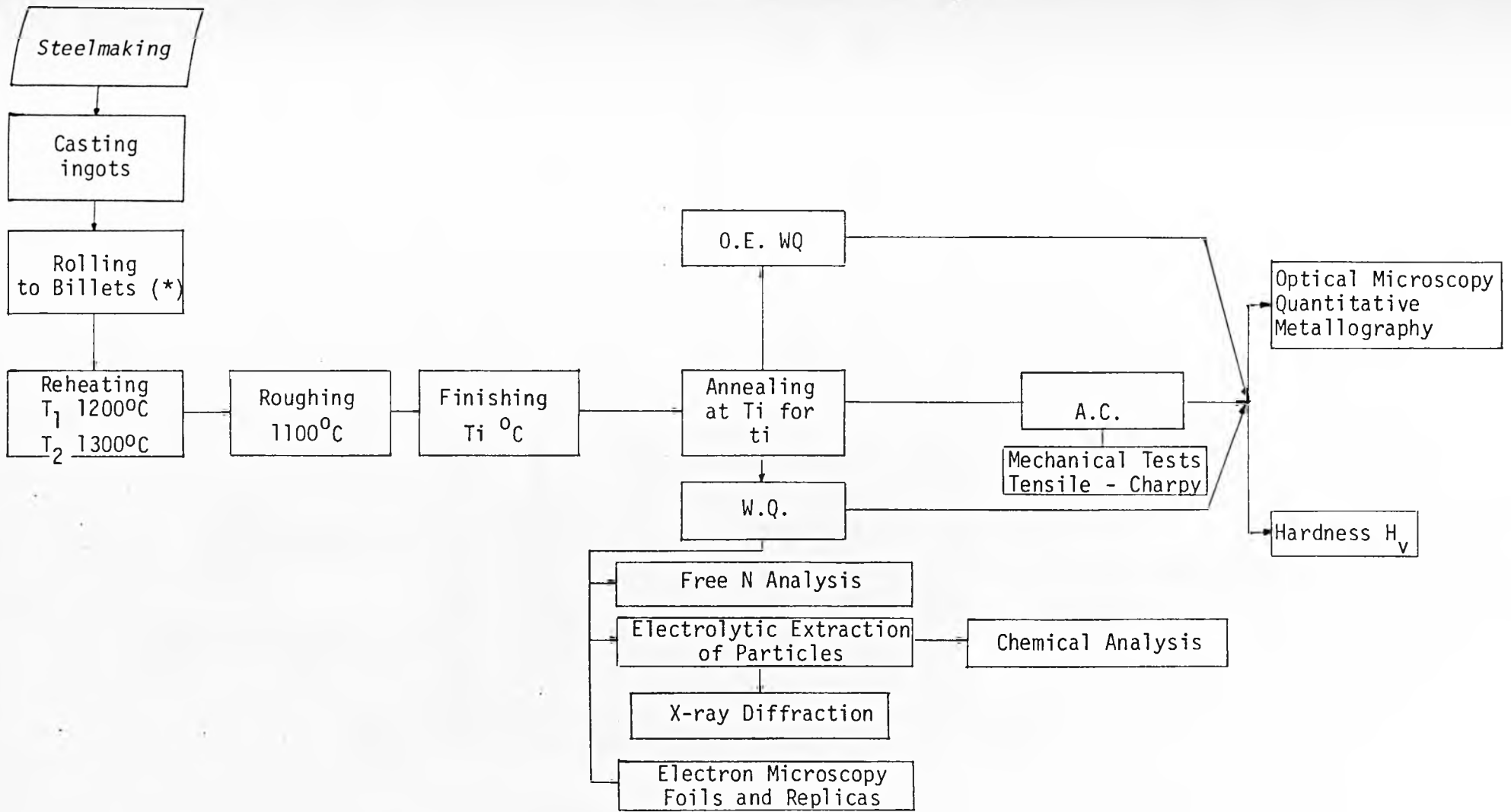
Figure 4.2   Experimental Techniques

*Carried out at B. S.C. Laboratories, Hoyle Street
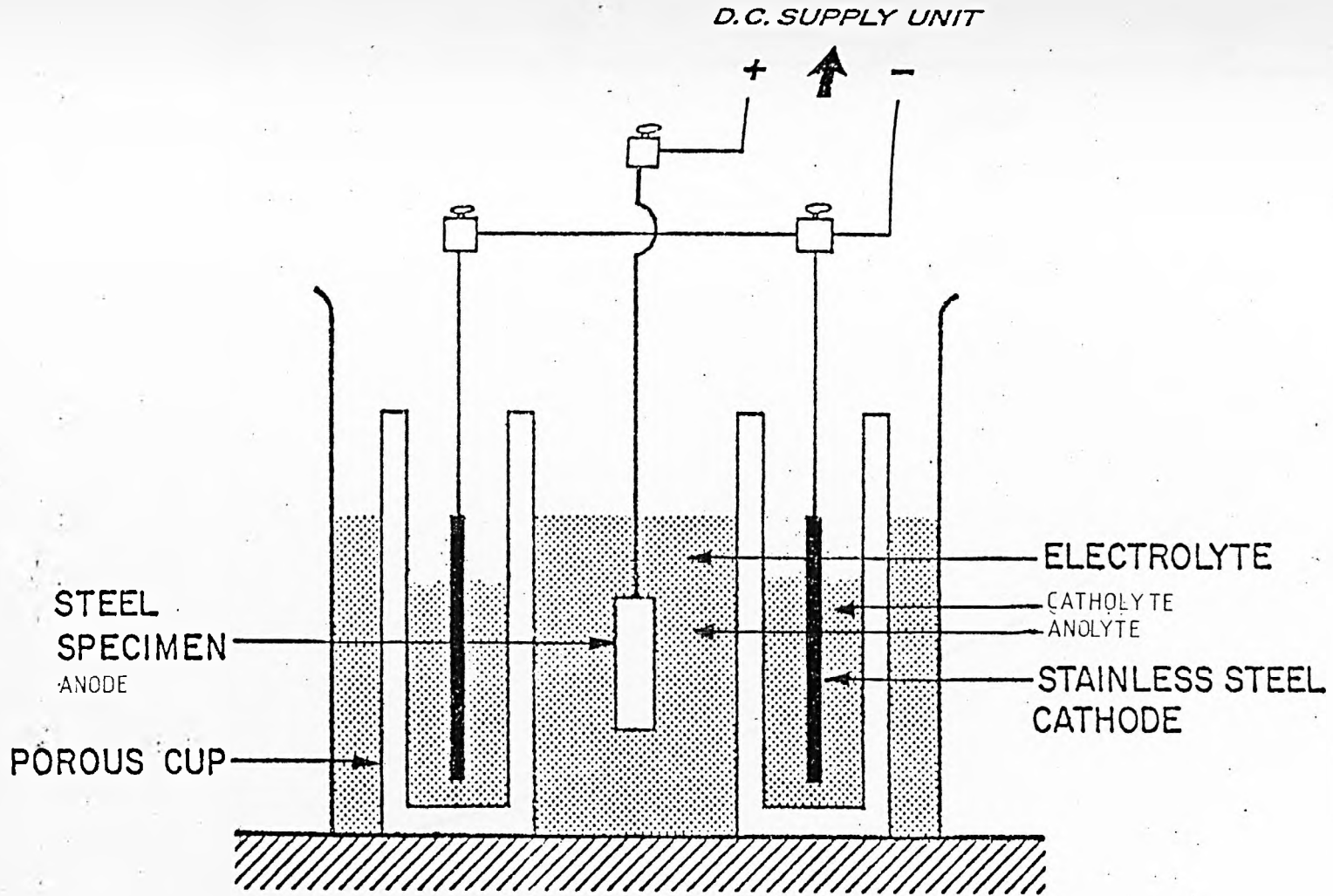
Figure 4.3   The cell assembly
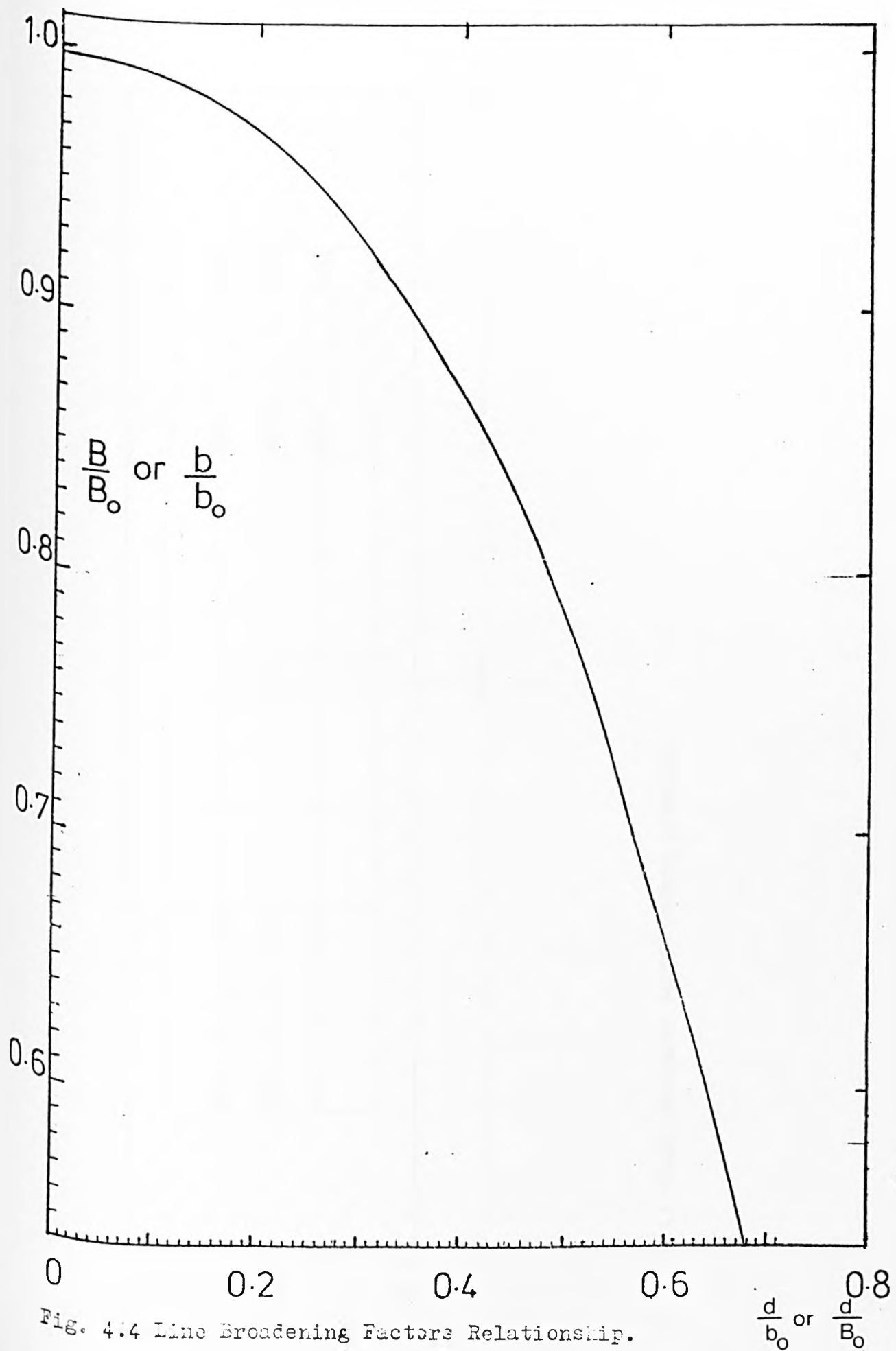
Fig. 4.4 Line Broadening Factors Relationship.
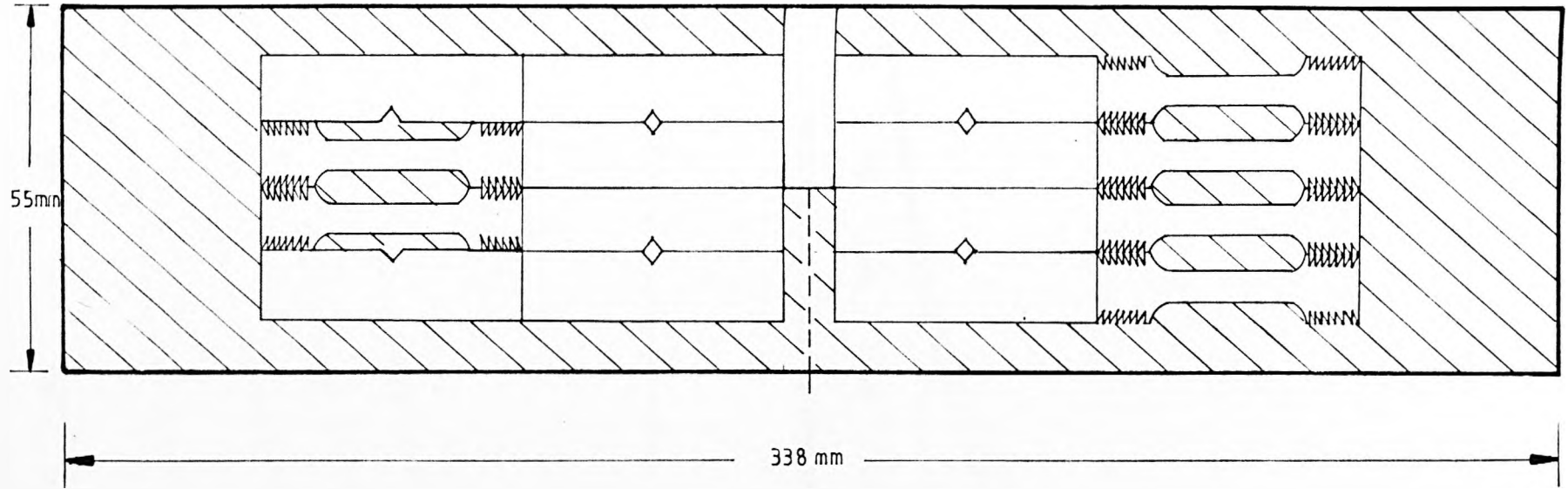
Fig. 4.5 TENSILE AND CHARPY V-NOTCH SPECIMENS DISTRIBUTION

FIG. 5.1.a   NIOBIUM IN SOLUTION VS TEMPERATURE

FIG. 5.1.b NITROGEN IN SOLUTION VS TEMPERATURE

X10⁻⁴ $X10^{-4}$

C in sol. mol Fraction

FIG. 5.1.c CARBON IN SOLUTION VS TEMPERATURE

$X10^1$

oC

N /(N + C) in NbCxNy

$X10^{-2}$

FIG. 5.2 NITROGEN RATIO IN CARBONITRIDE VS TEMPERATURE

$X10^1$

oC
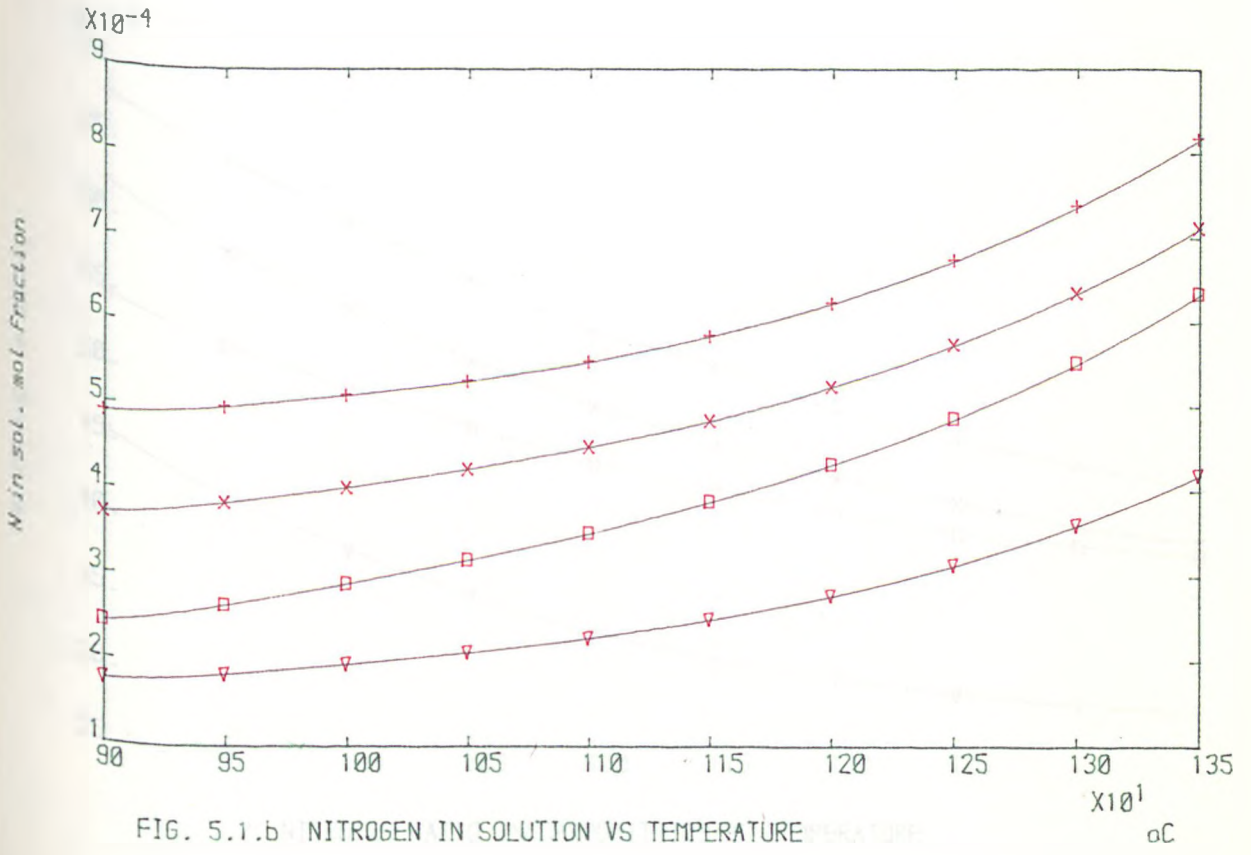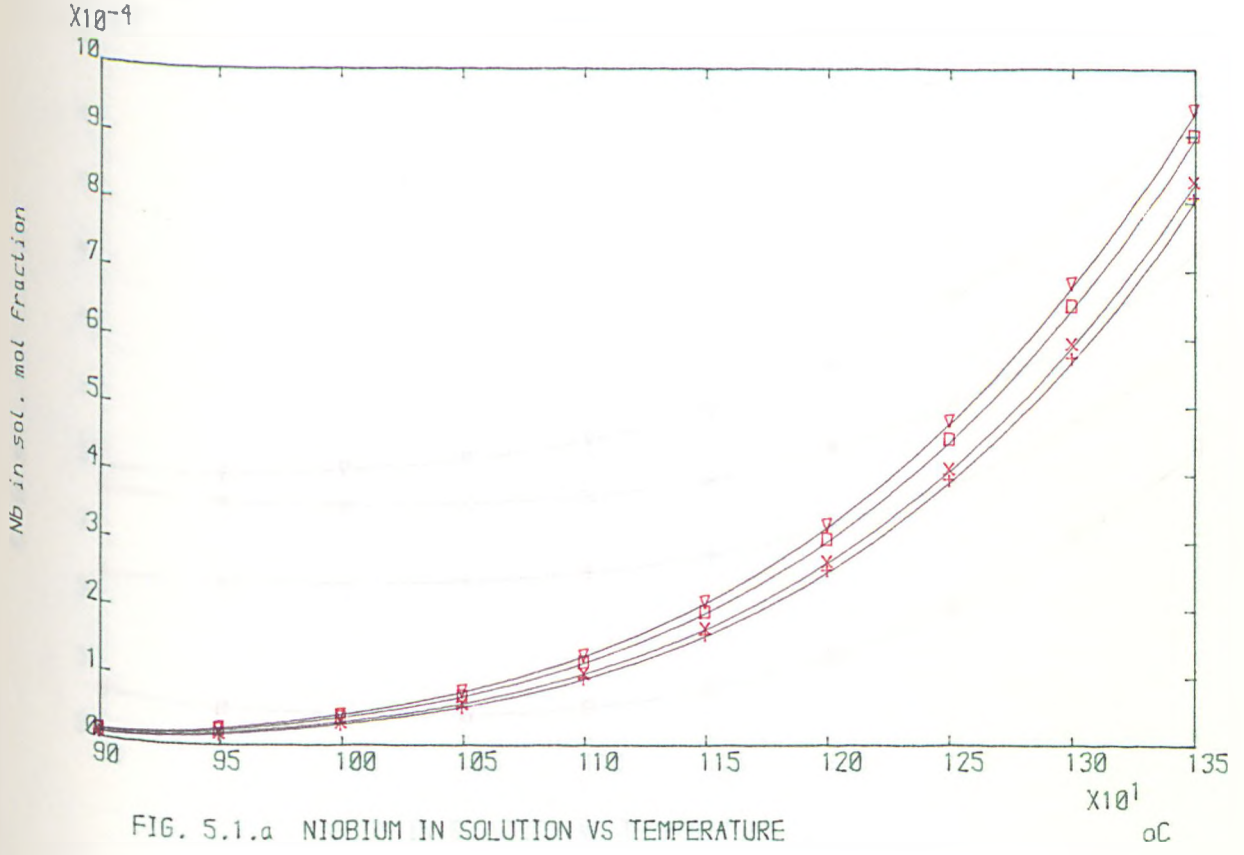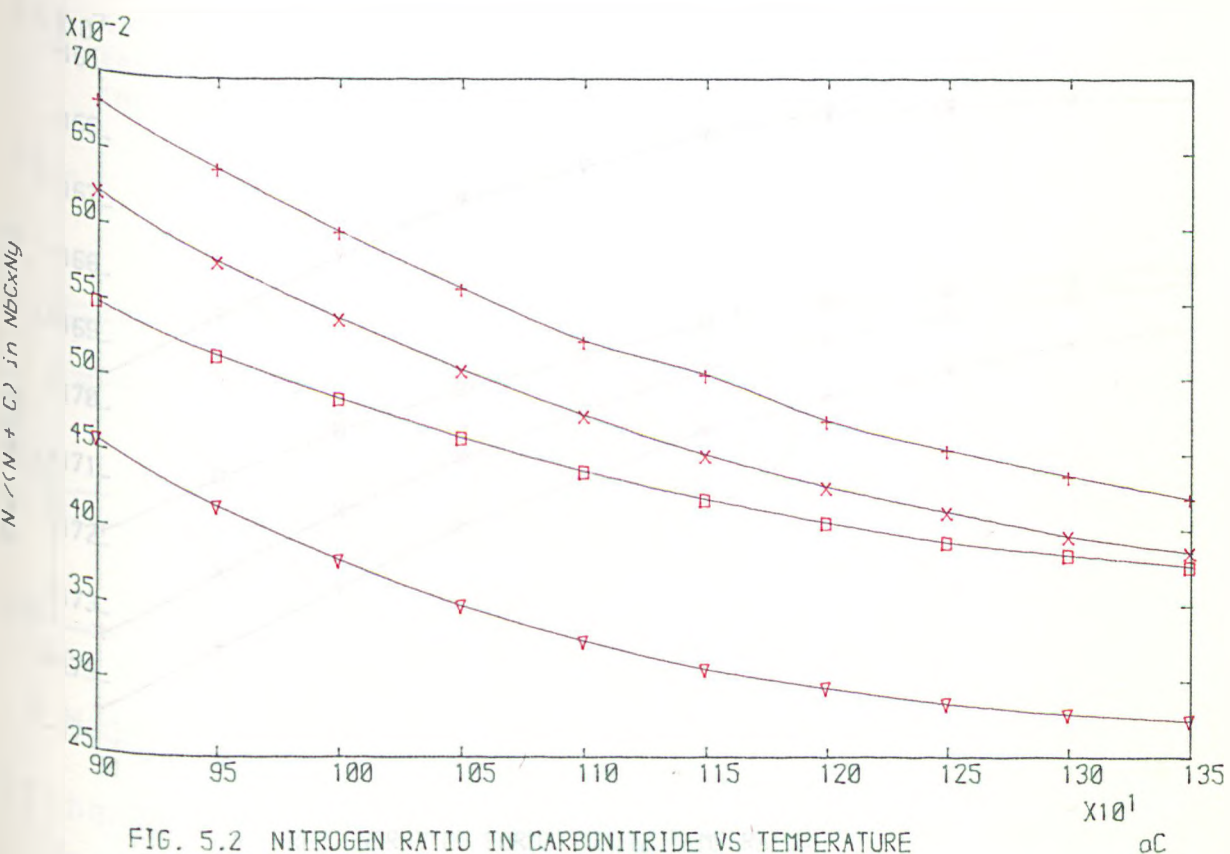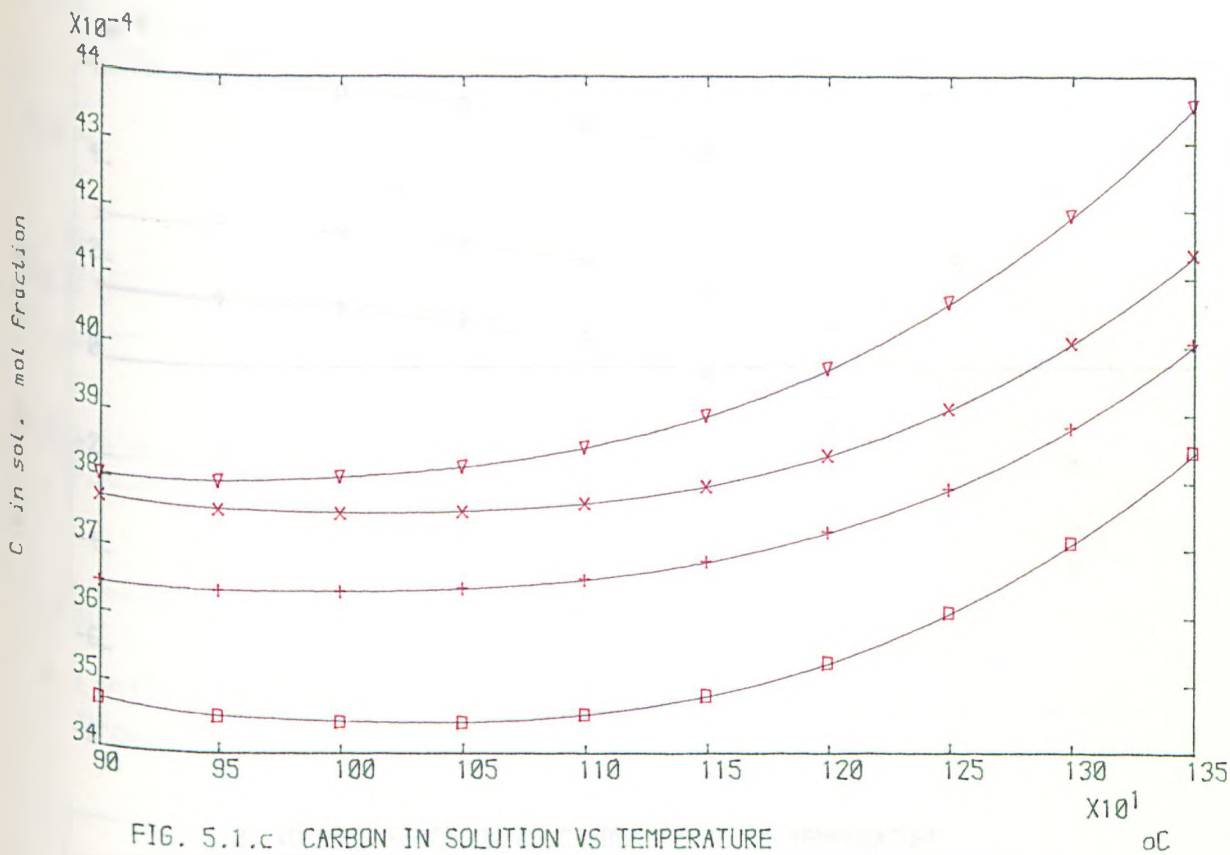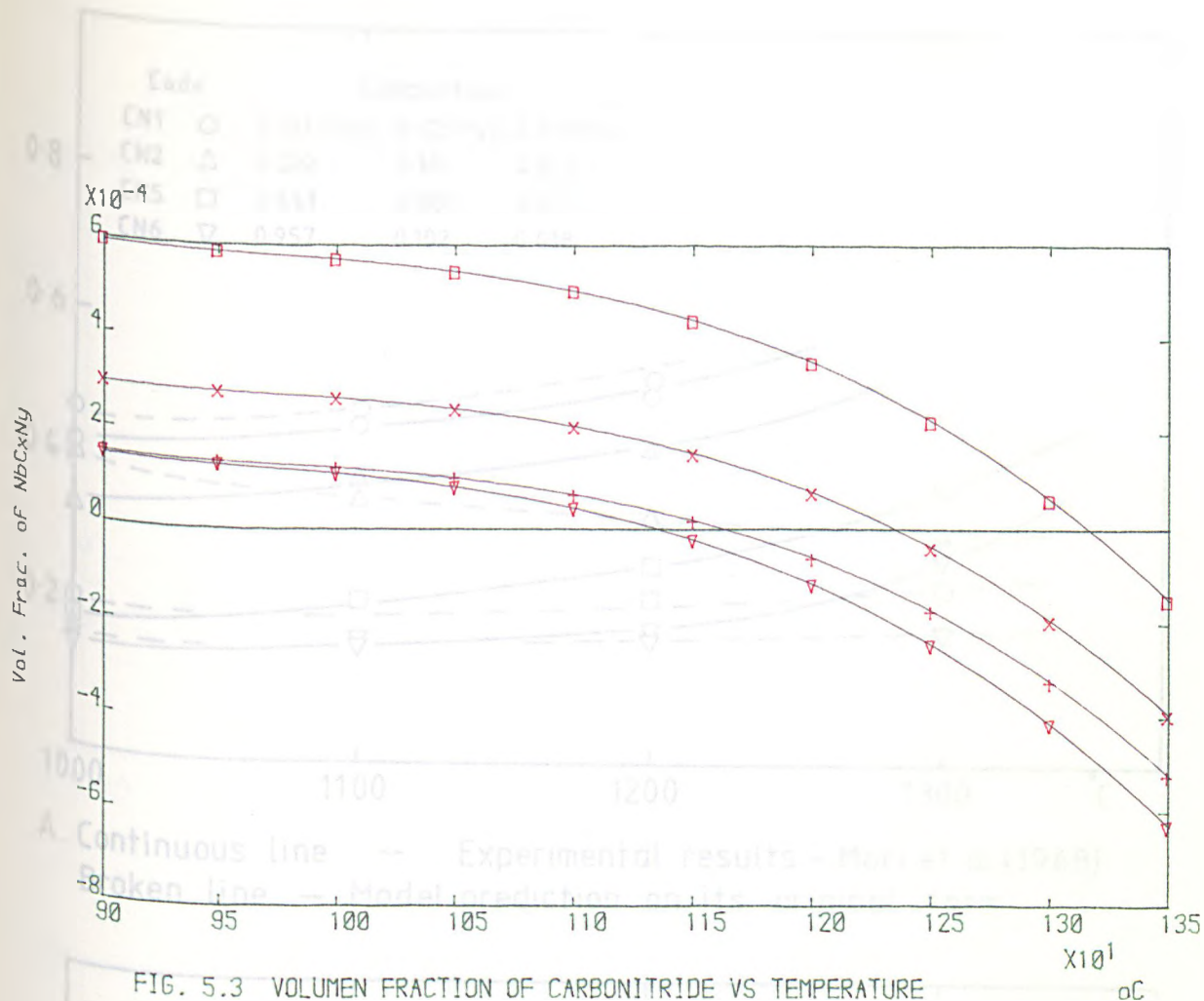
FIG. 5.3 VOLUMEN FRACTION OF CARBONITRIDE VS TEMPERATURE

FIG. 5.4 FREE ENERGY OF FORMATION VS TEMPERATURE

Code   Composition
CN1   ○   0·197%Nb, 0·029%C, 0·012%N
CN2   △   0·207   0·101   0·016
CN5   □   0·641   0·081   0·017
CN6   ▽   0·957   0·102   0·018
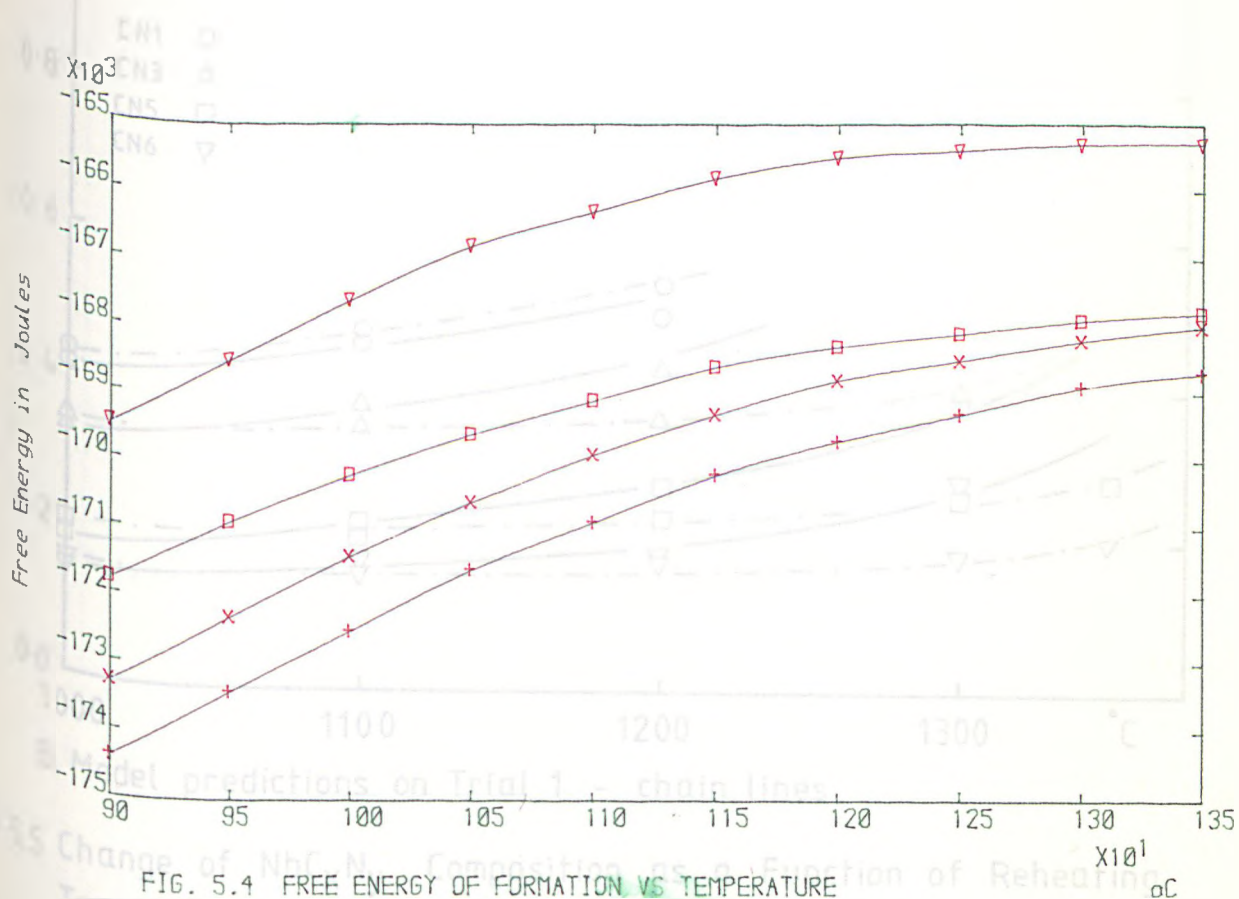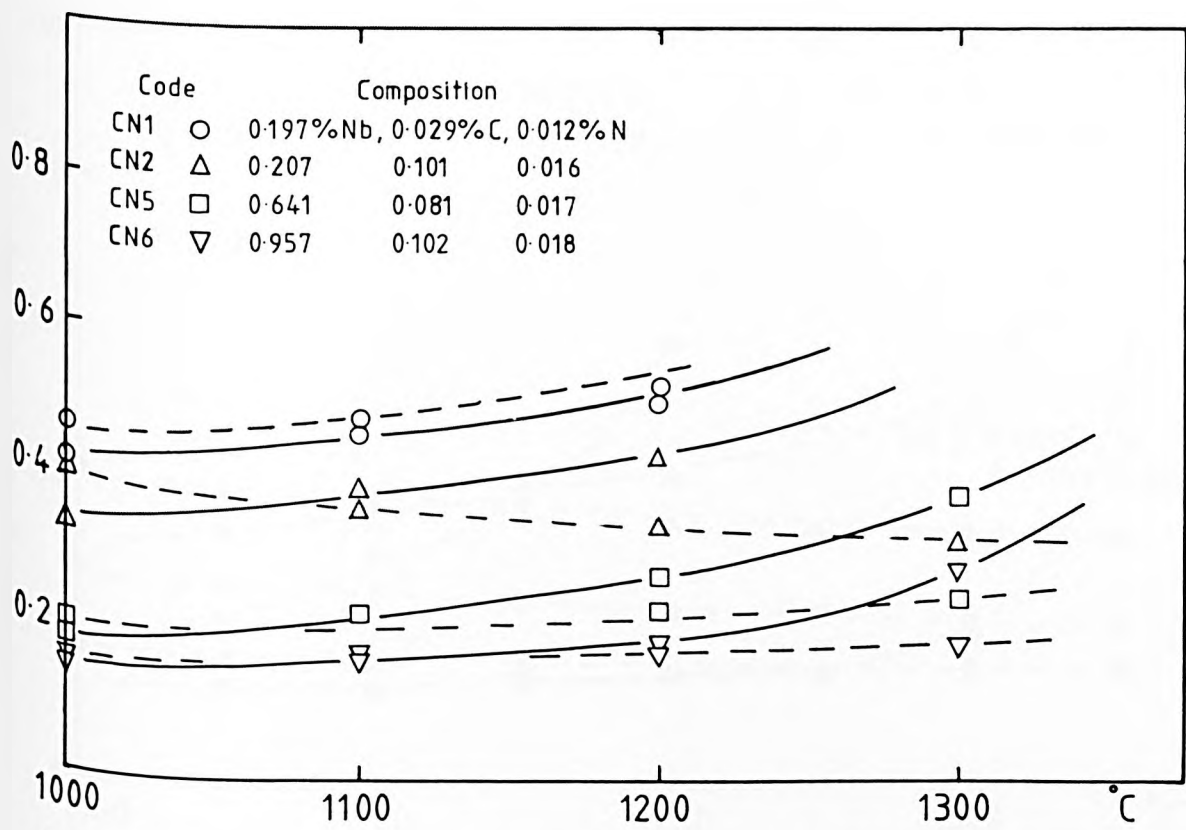
A. Continuous line   —   Experimental results – Mori et al (1968)
    Broken line — Model prediction on its original form.

CN1   ○
CN3   △
CN5   □
CN6   ▽
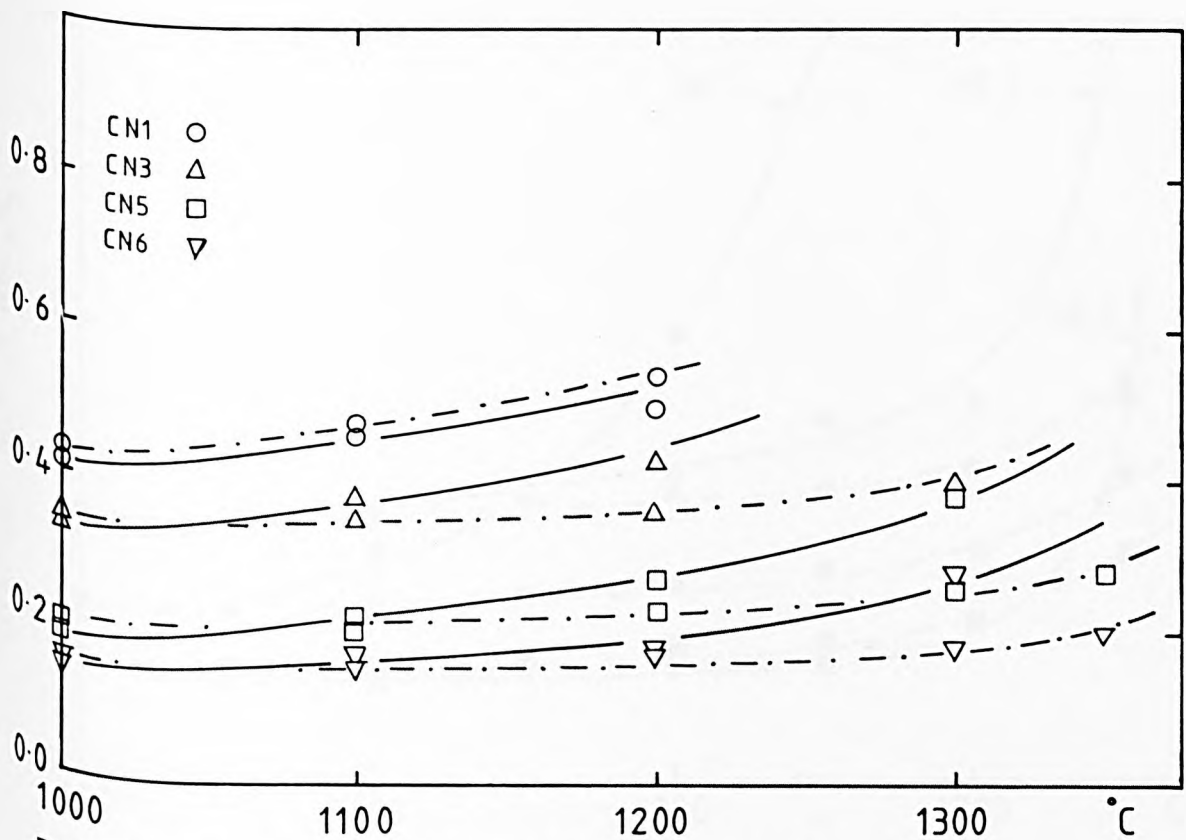
B. Model predictions on Trial 1 – chain lines

Fig.5.5 Change of NbC_xN_y Composition as a Function of Reheating
    Temperature.   Data of Mori et al (1968)
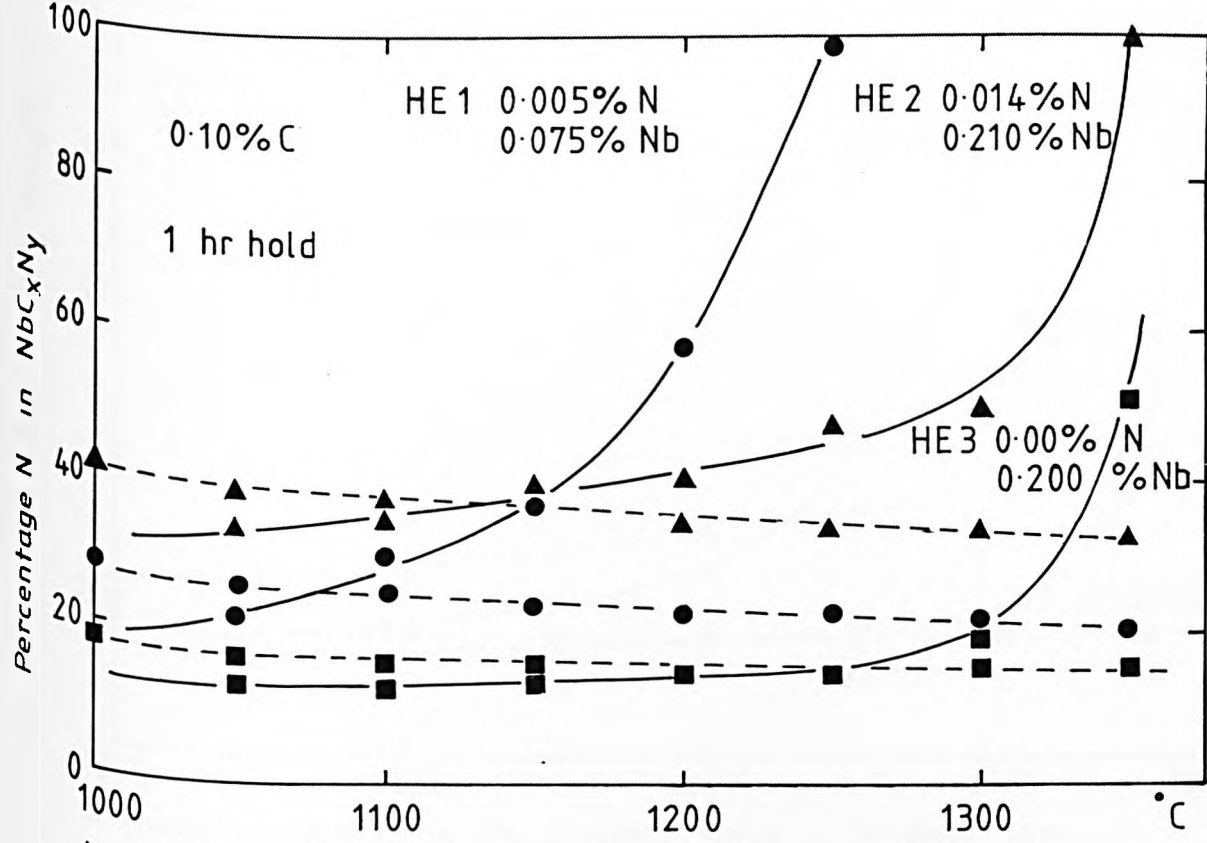
A. Model prediction on its original form – broken lines.
   Experimental data – continuous lines.
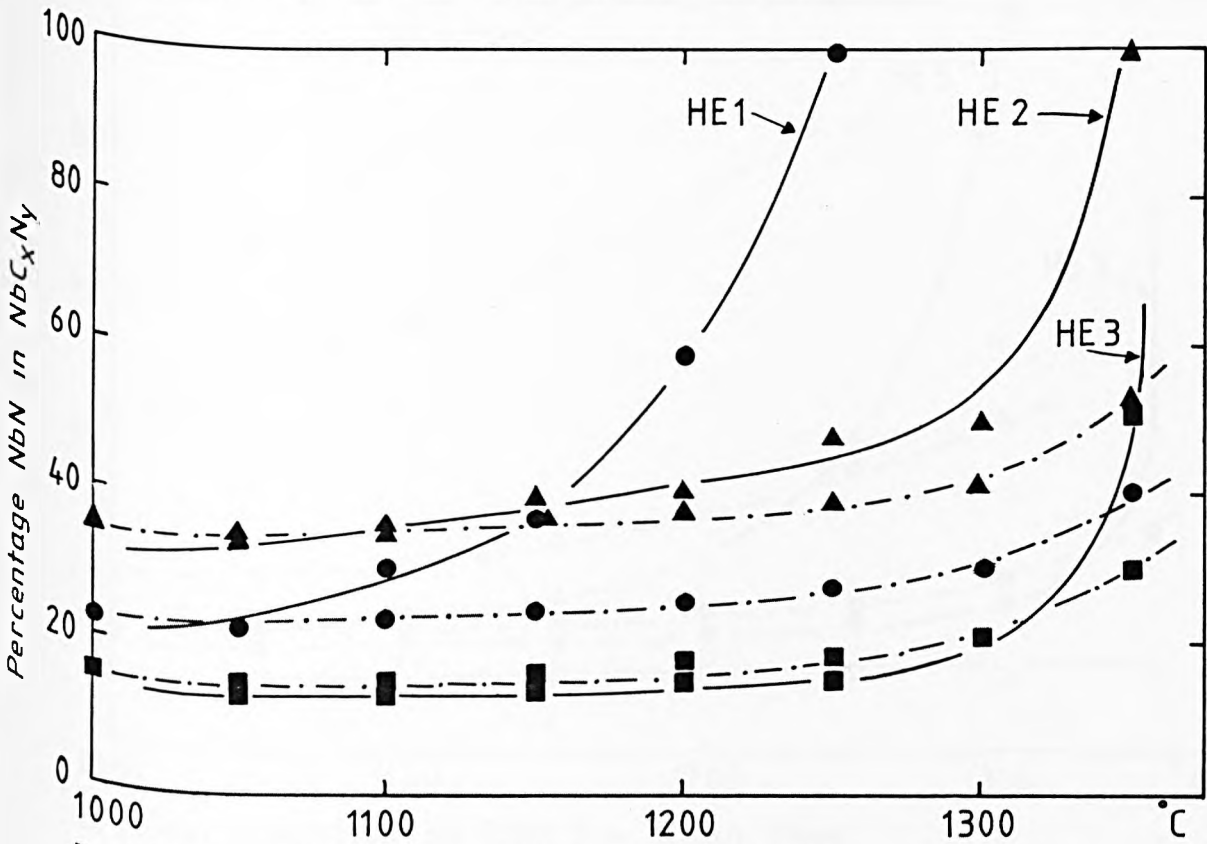
B. Model prediction on Trial 1 – chain lines.
   Experimental data – continuous lines.

Fig. 5.6 Effect of Nb and N on the NbC_xN_y Composition as a Function of Temperature.

Data replotted from Fig. 2.13.b . Given by Hoesch-Estel (1981)
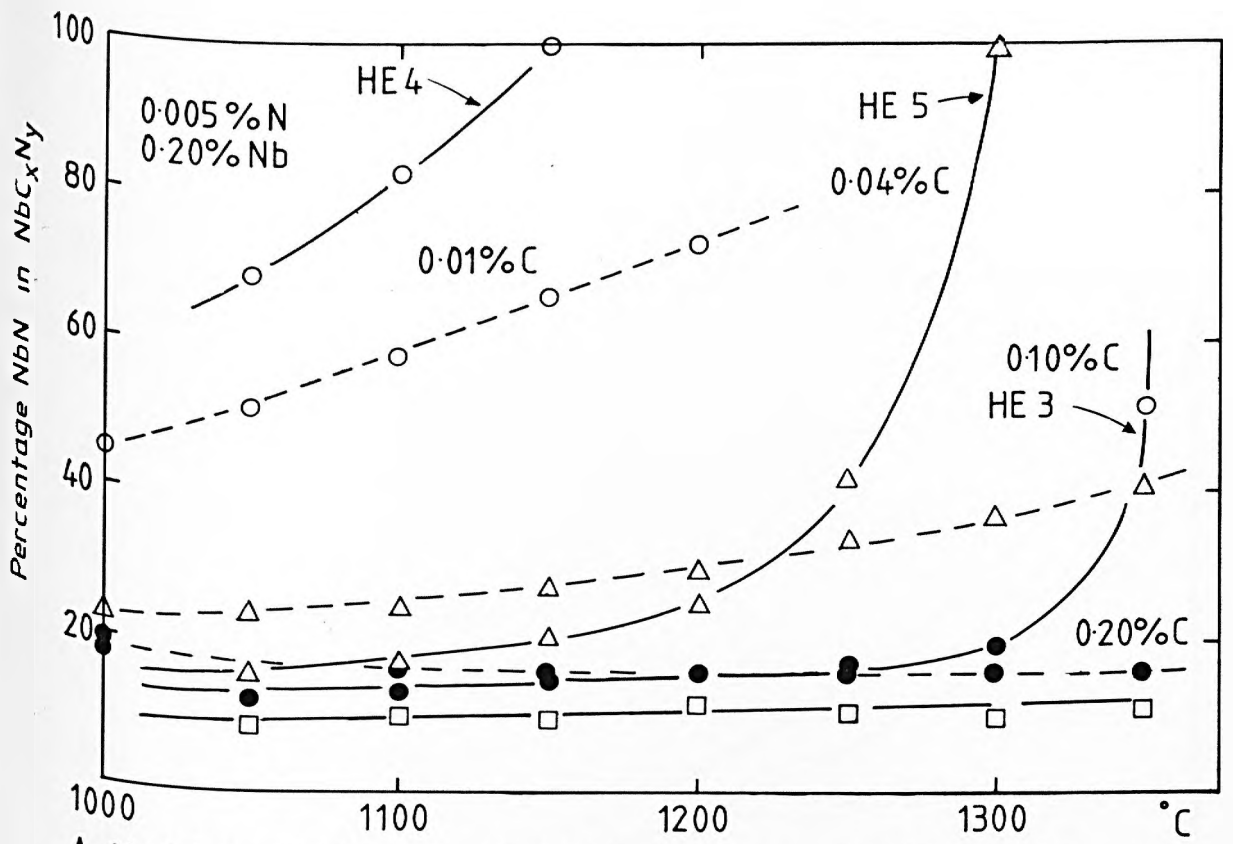
A. Model prediction on its original form – broken lines.
   Experimental data – continuous lines.
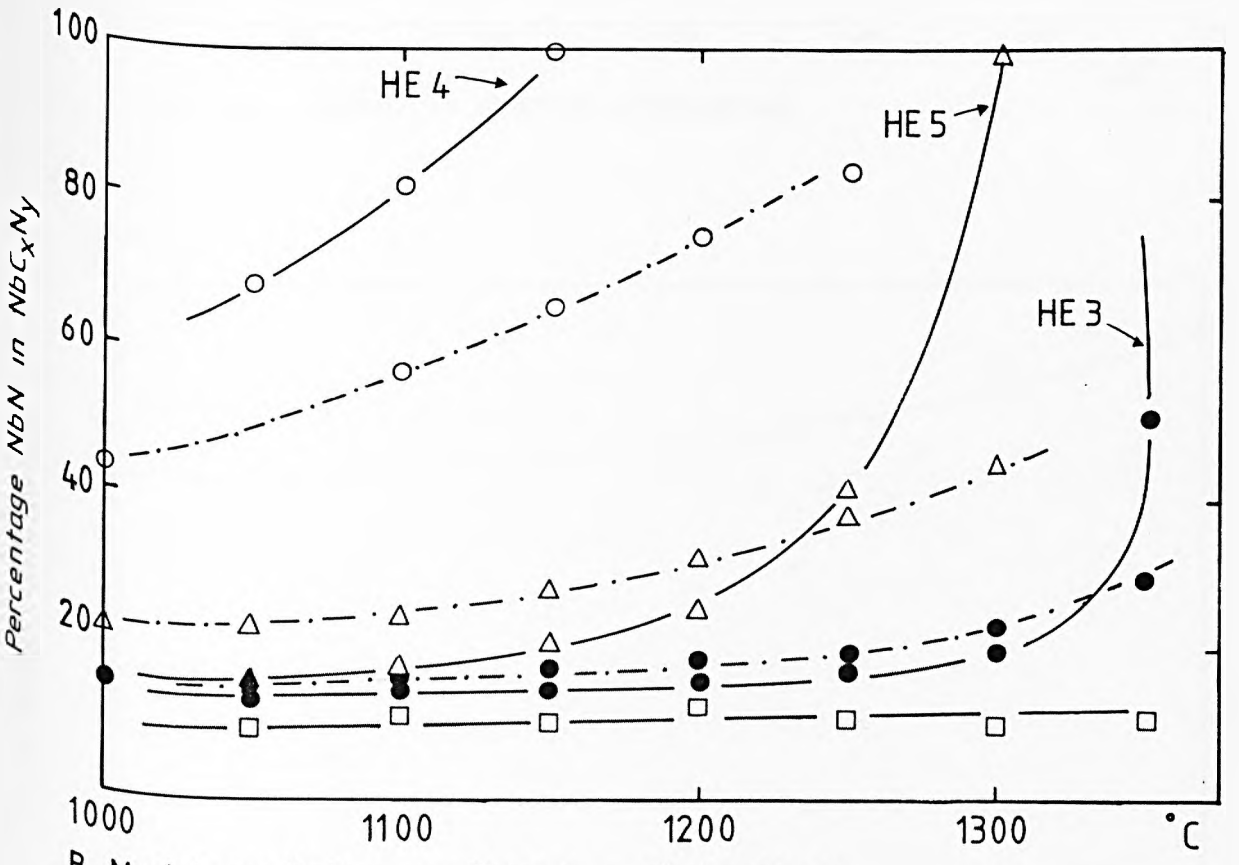
B. Model prediction on Trial 1 – chain lines.
   Experimental data – continuous lines.

Fig.5.7 Effect of C on the NbC_xN_y Composition vs Temperature.

Data replotted from Fig. 2.13.a Given by Hoesch-Estel (1981)
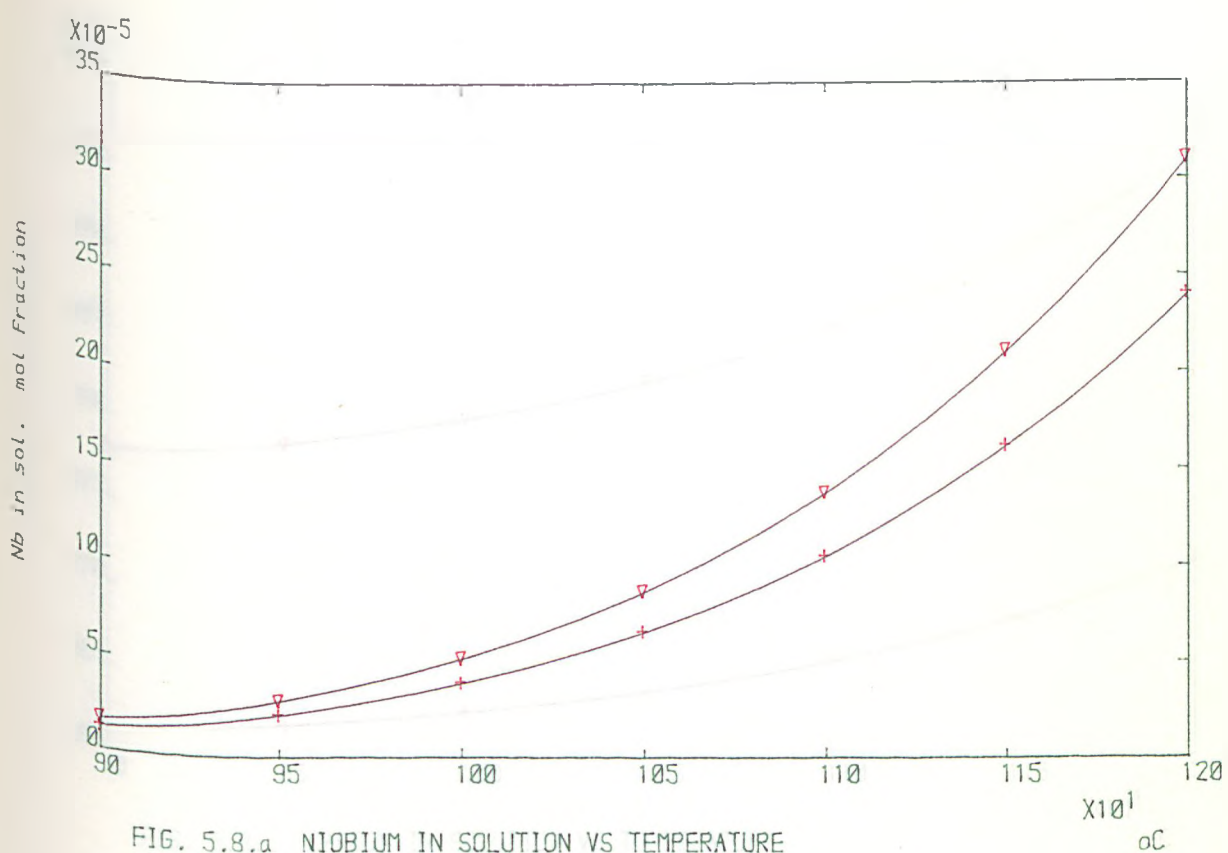
FIG. 5.8.a NIOBIUM IN SOLUTION VS TEMPERATURE
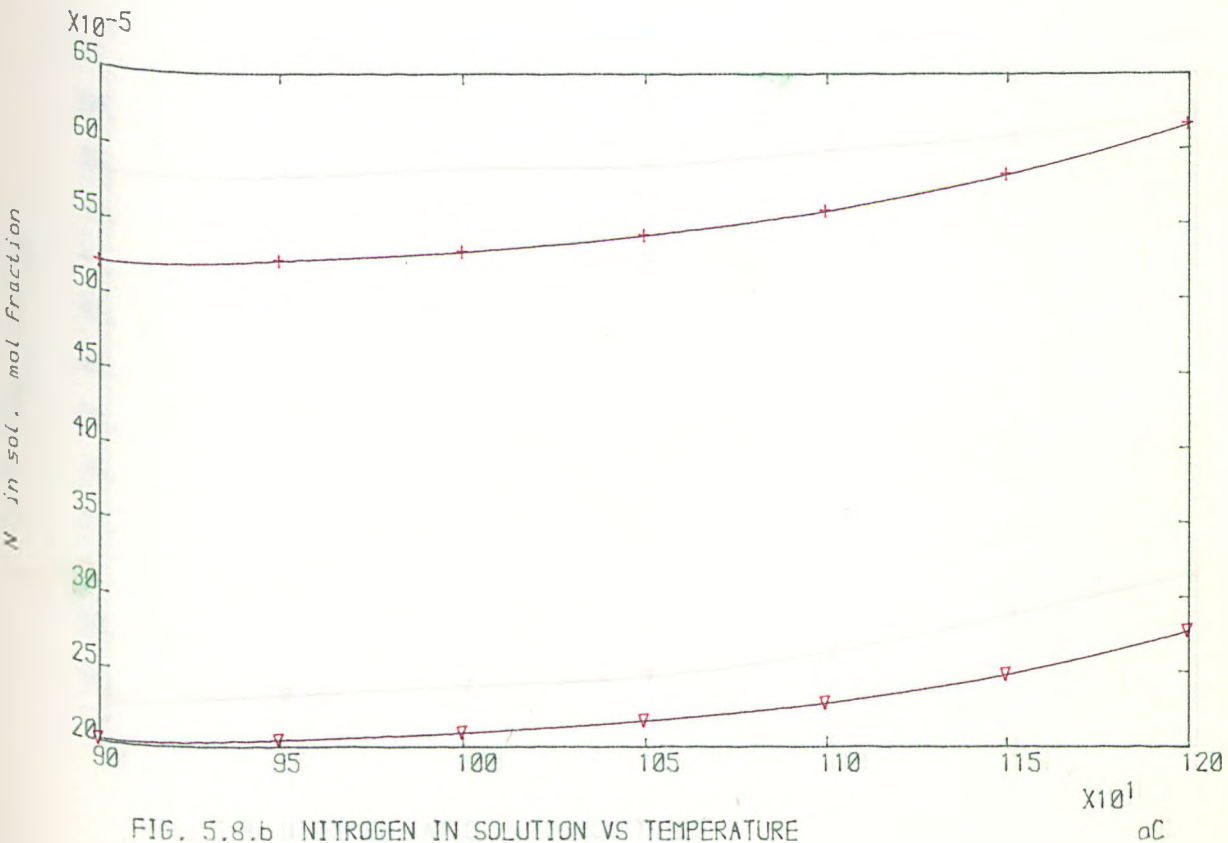
FIG. 5.8.b NITROGEN IN SOLUTION VS TEMPERATURE
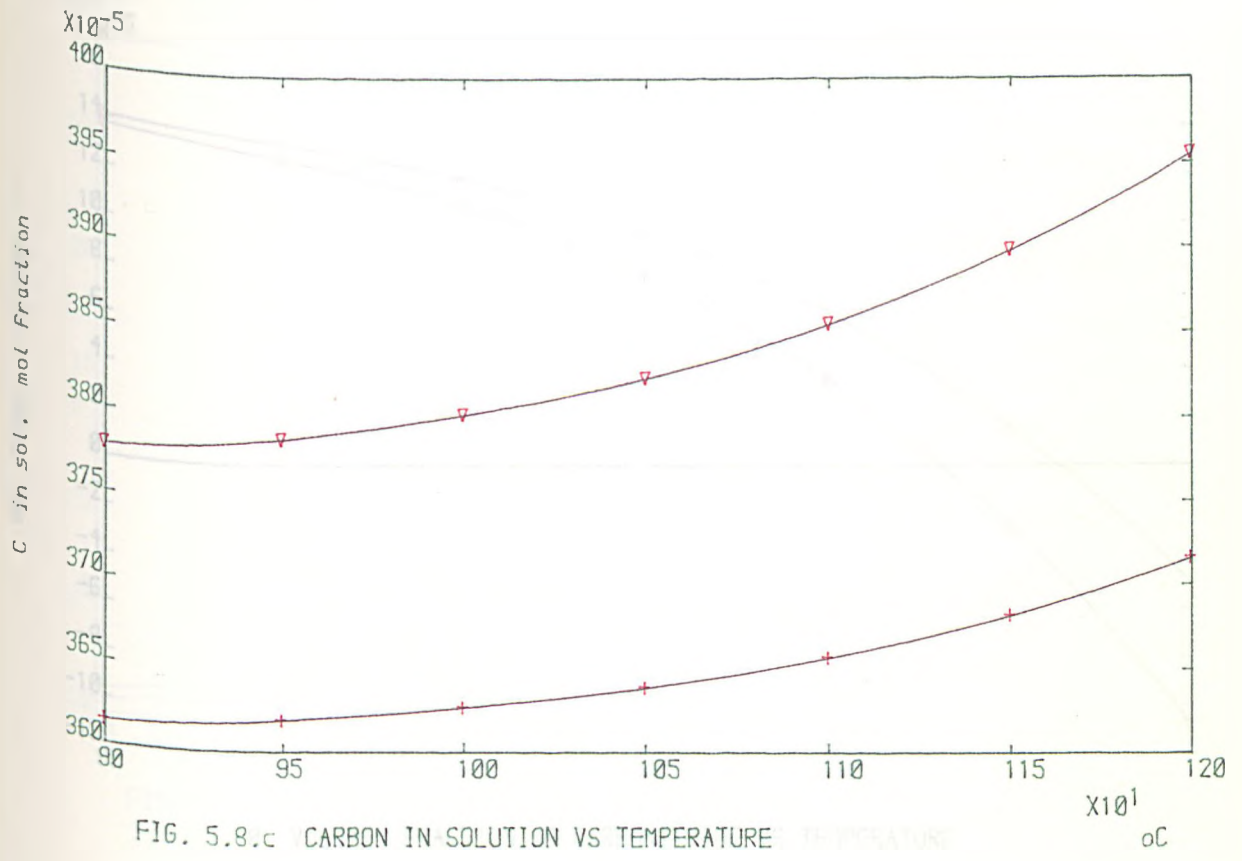
FIG. 5.8.c CARBON IN SOLUTION VS TEMPERATURE   oC

FIG. 5.9 NITROGEN RATIO IN CARBONITRIDE   oC

FIG. 5.10   VOLUMEN FRACTION OF CARBONITRIDE VS TEMPERATURE   oC

FIG. 5.11   FREE ENERGY OF FORMATION VS TEMPERATURE   oC
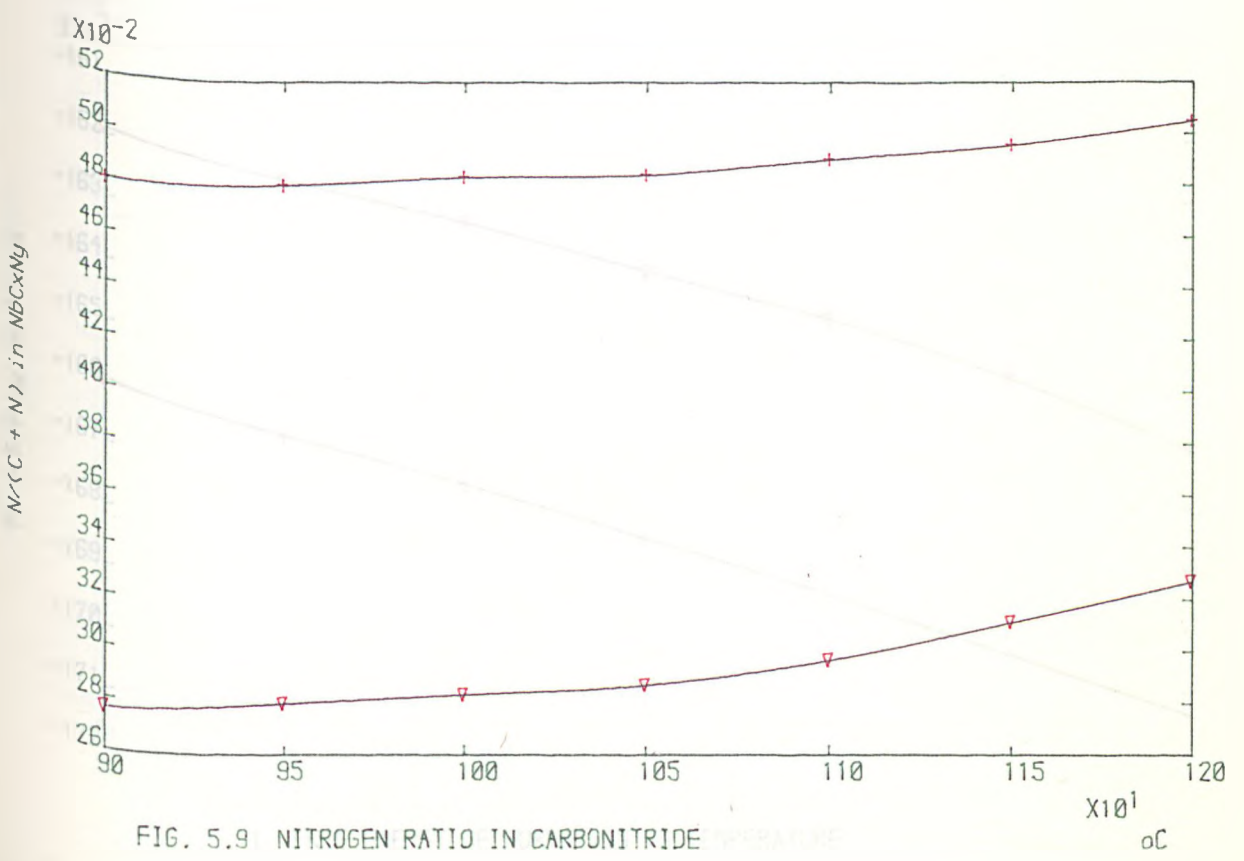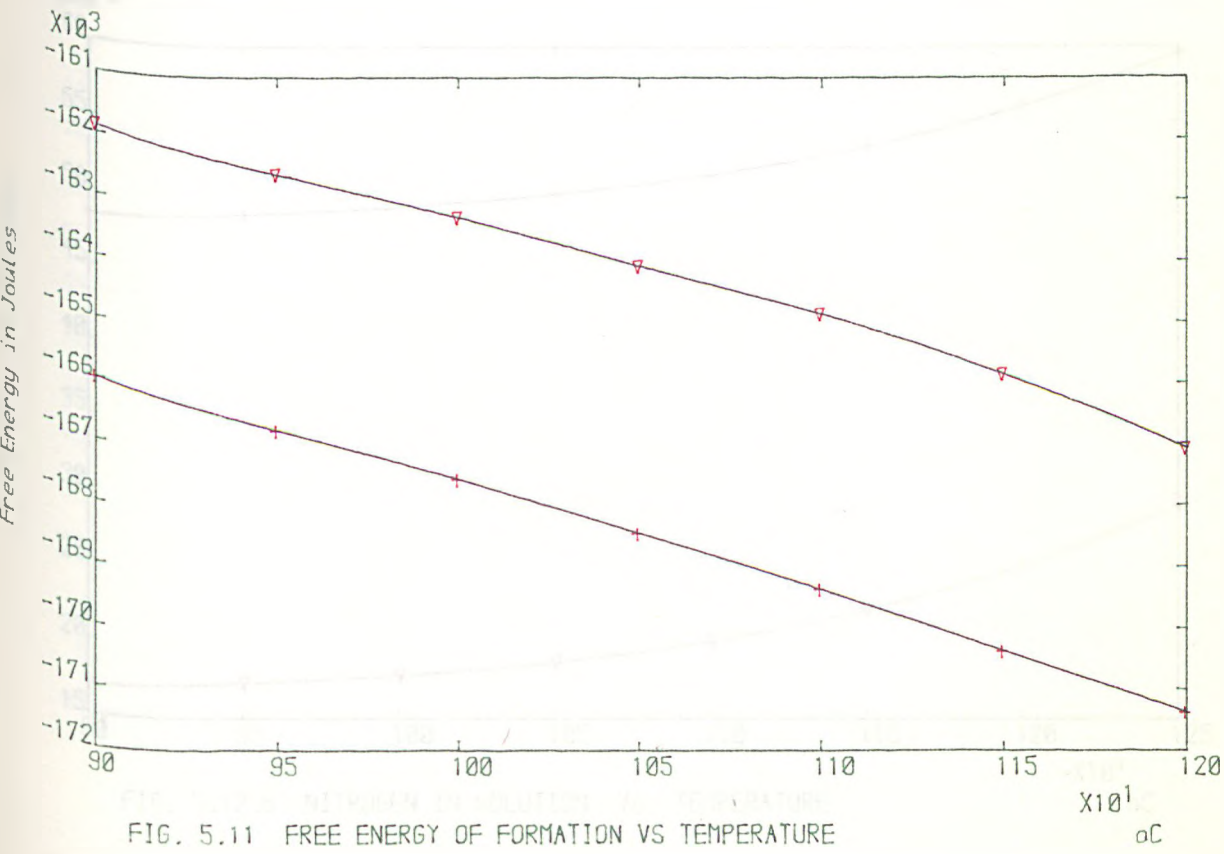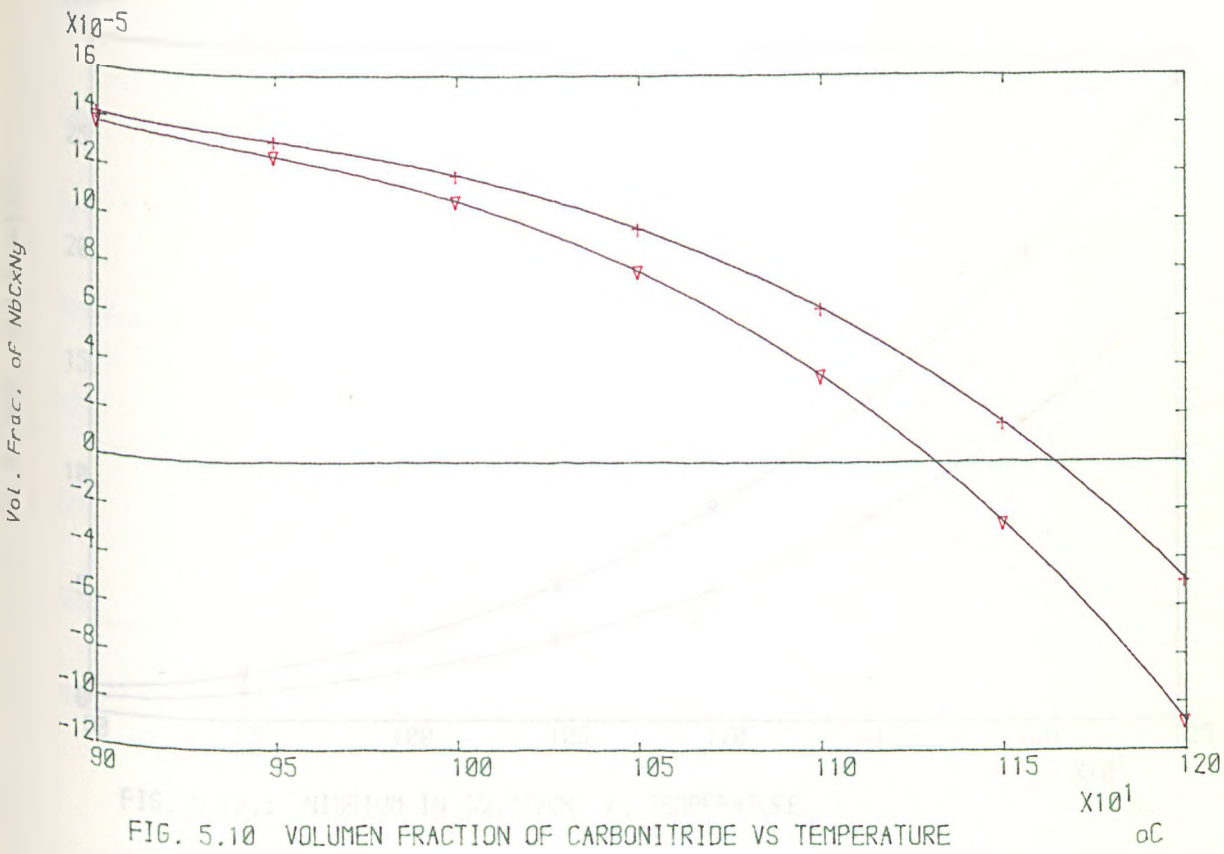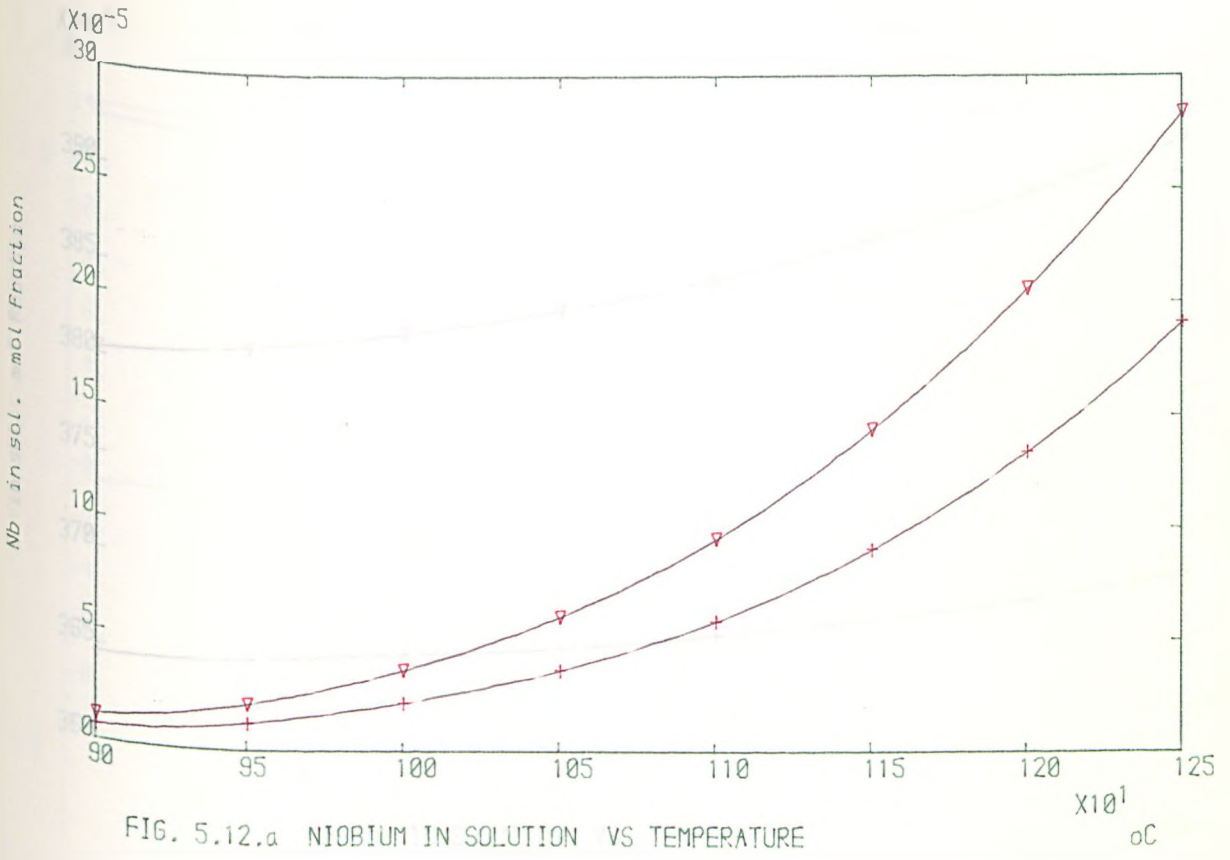
FIG. 5.12.a NIOBIUM IN SOLUTION VS TEMPERATURE
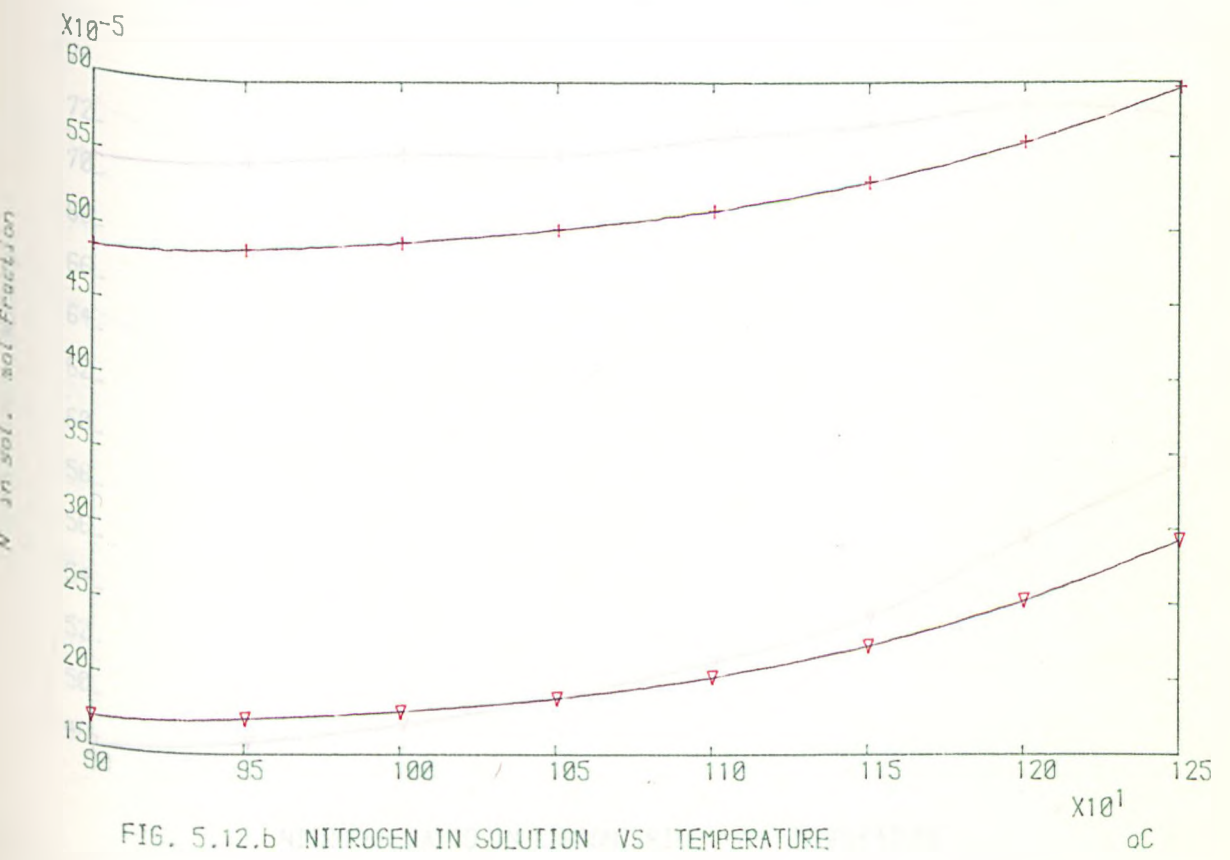
FIG. 5.12.b NITROGEN IN SOLUTION VS TEMPERATURE
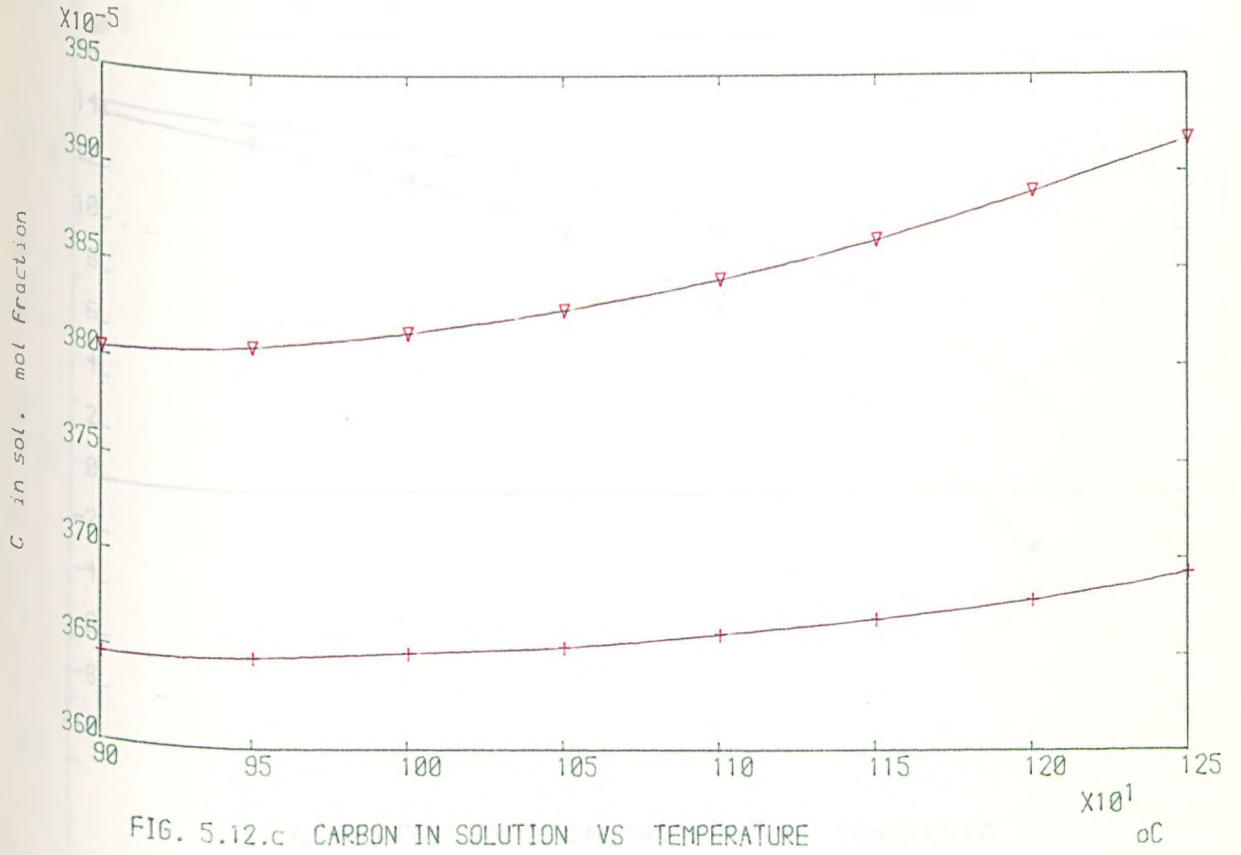
FIG. 5.12.c CARBON IN SOLUTION VS TEMPERATURE
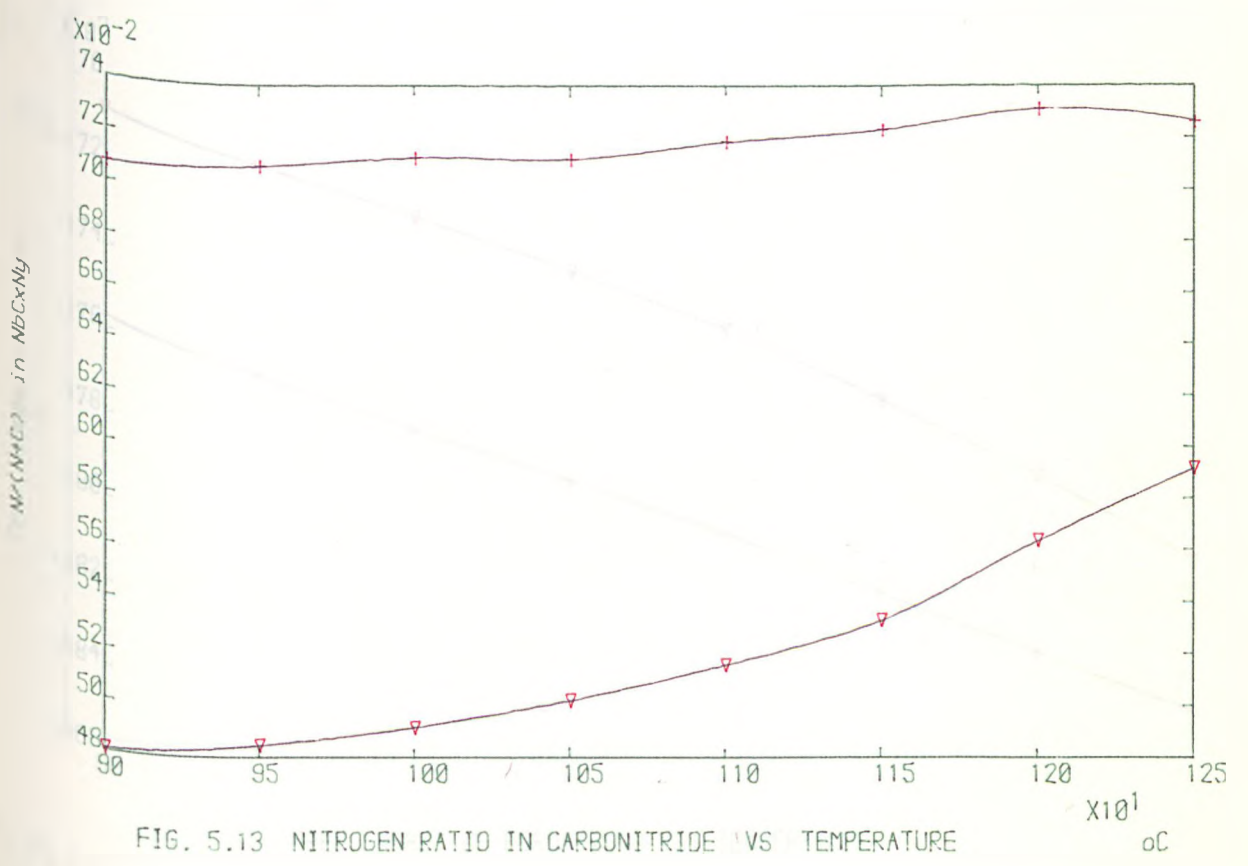
FIG. 5.13 NITROGEN RATIO IN CARBONITRIDE VS TEMPERATURE
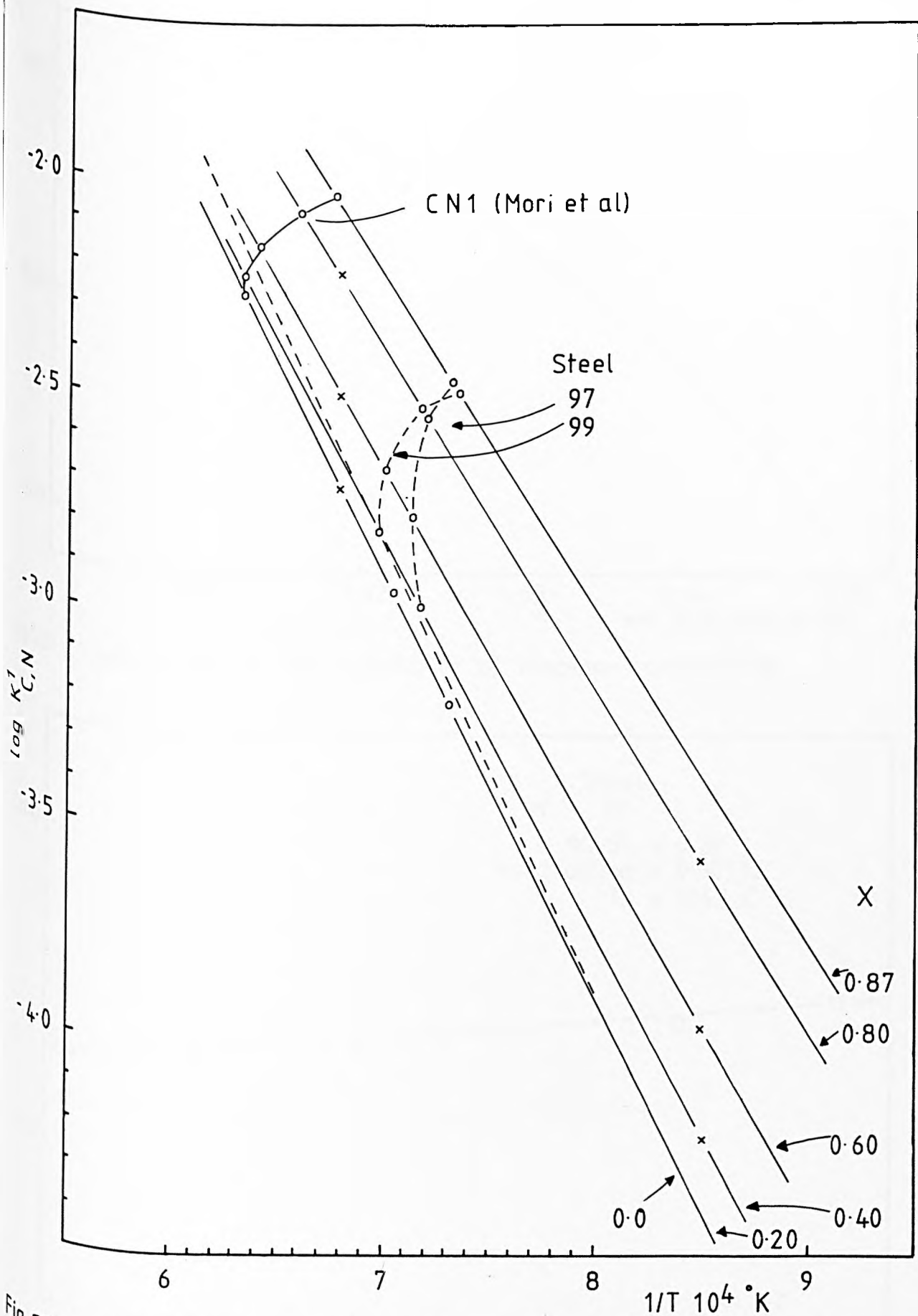
Fig. 5.16 Solubility Product of Nb C_x $N_{(0.87-x)}$ in Austenite as a Function of Temperature.
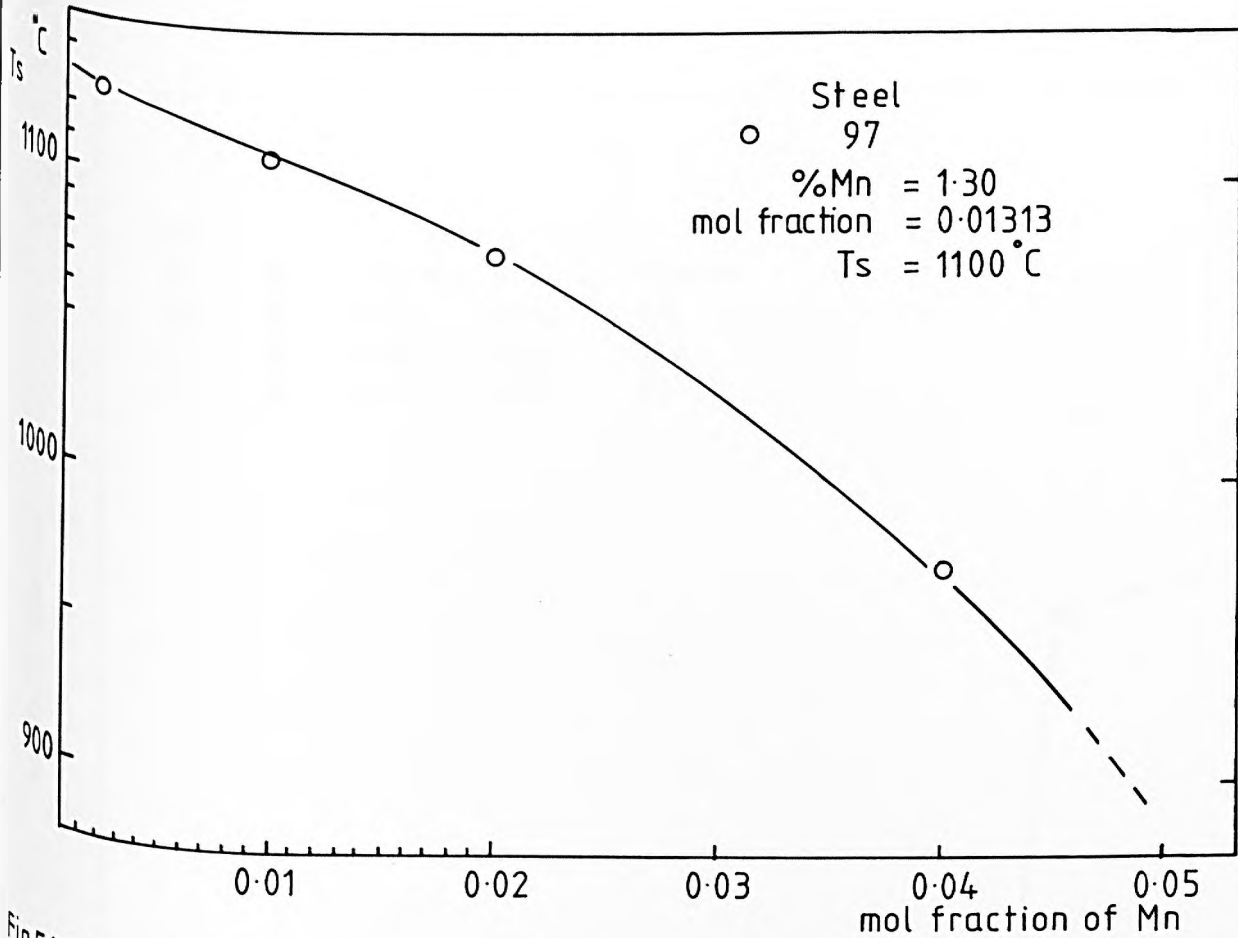
Fig 5.17 Effect of Mn on the Solubility of Niobium Carbonitride.
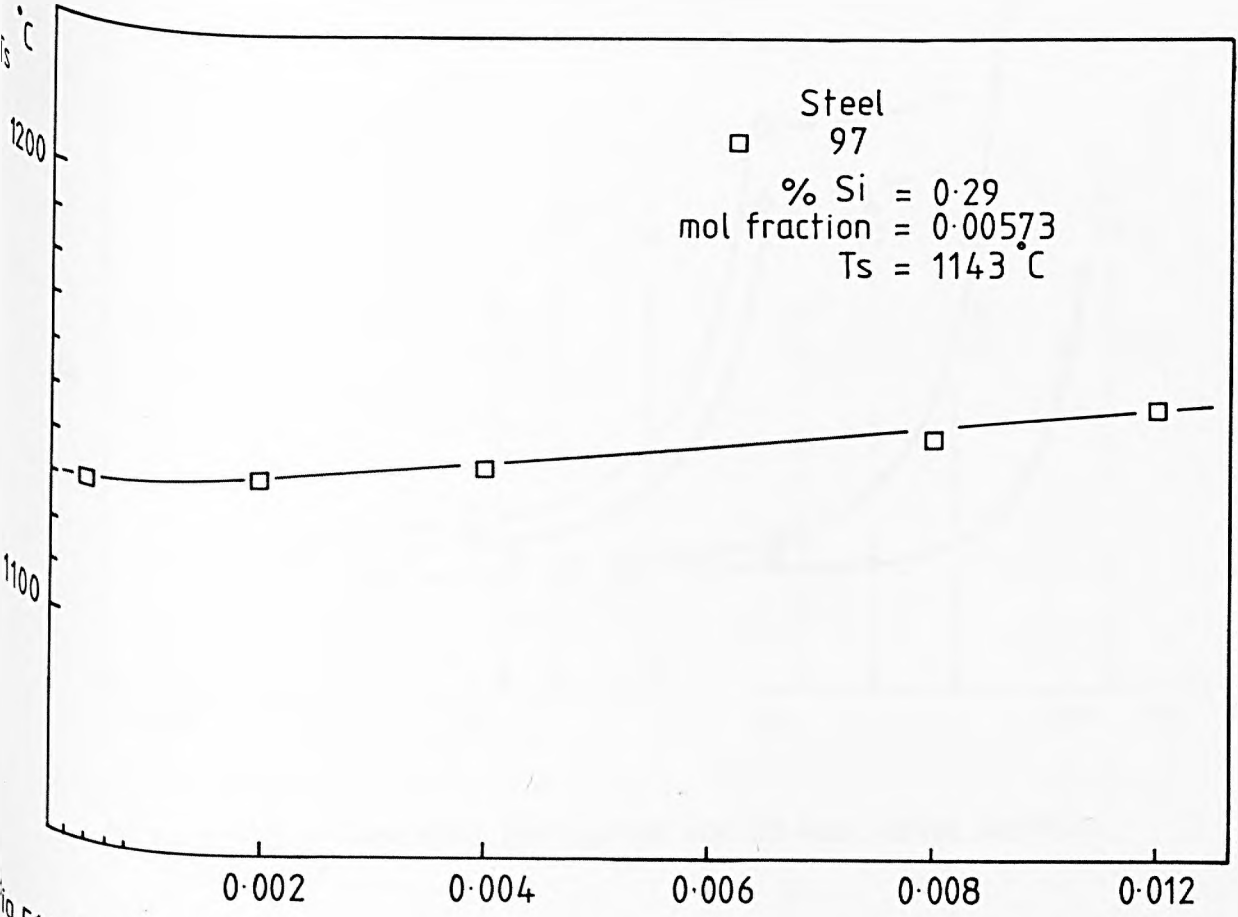
Fig 5.18 Effect of Silicon on the Solubility of Niobium Carbonitride.
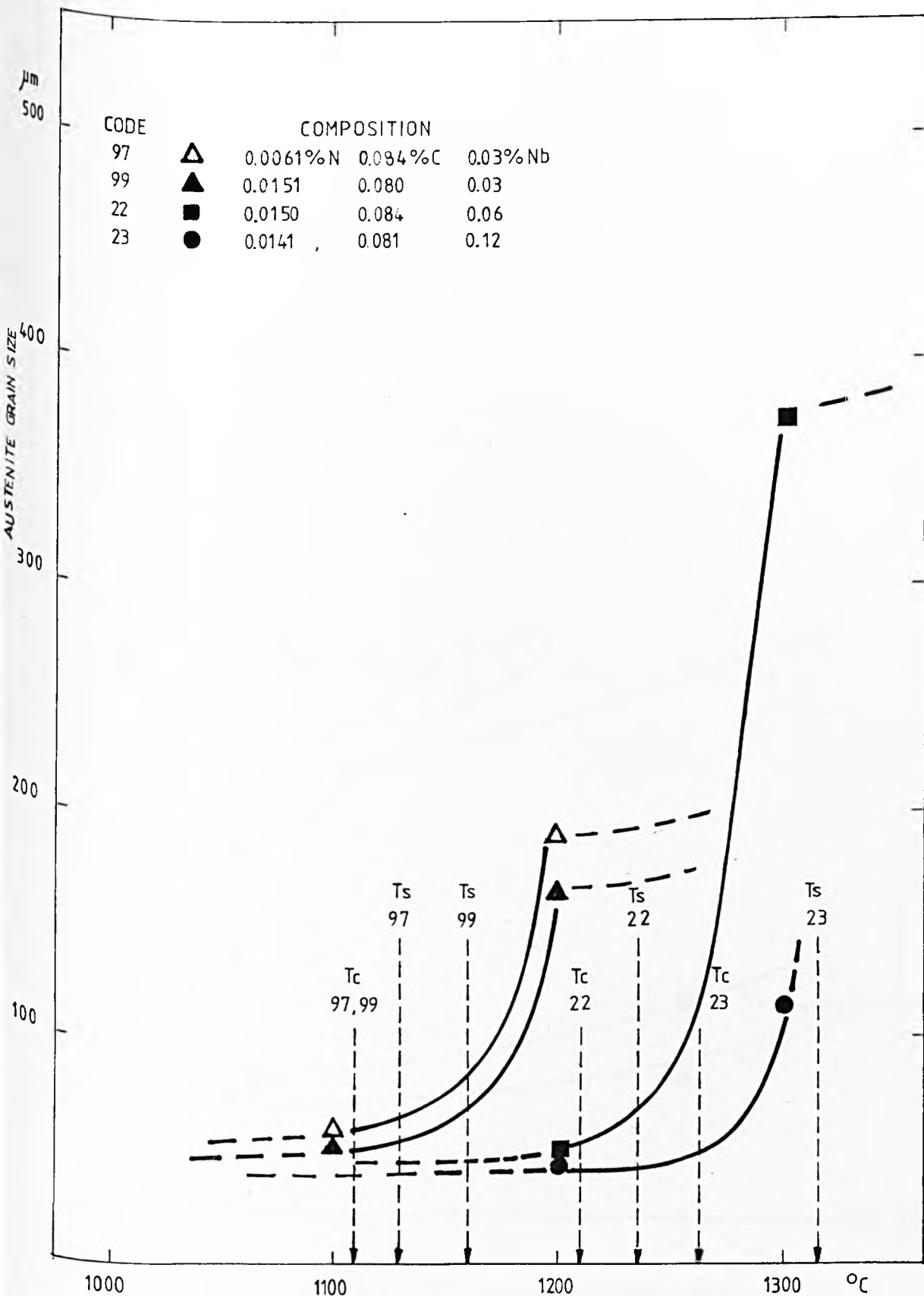
FIG. 6.1a EFFECTS OF REHEATING TEMPERATURE FOR ONE HOUR, ON THE AUSTENITE
GRAIN SIZE
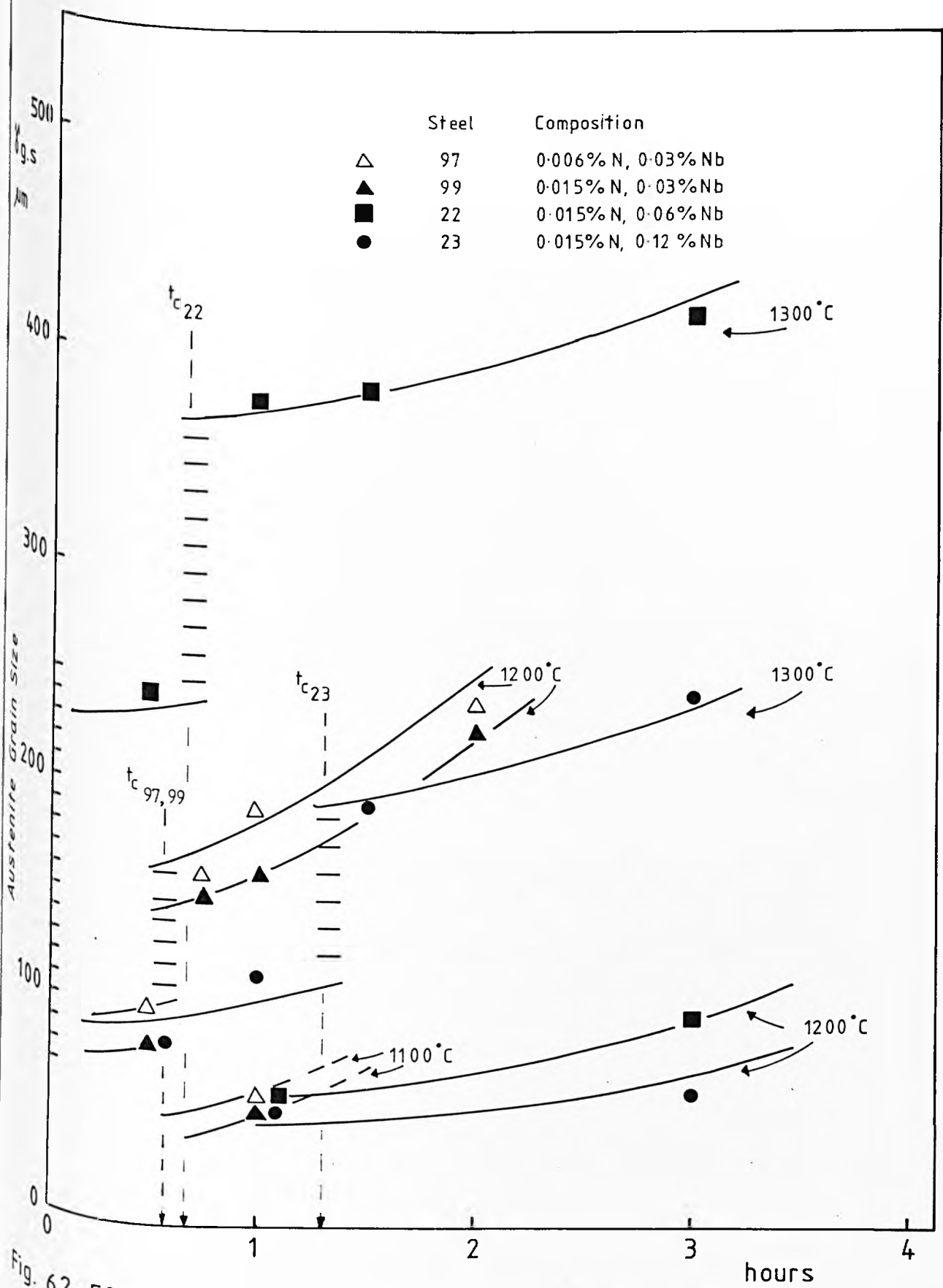
Fig. 6.2.a Effect of Reheating Time on Austenite Grain Size
at Different Temperatures.

Fig. 6.1.b. As reheated prior austenite grains where
            grain coarsening has become generalized.
            Reheated at 1200°C for 45 minutes
            x 200

Fig. 6.2.b. As reheated mixed prior austenite grain
            sizes. Note the areas where grain
            coarsening has taken place preferentially.
            Reheated for 45 minutes at 1200°C.
            x 200
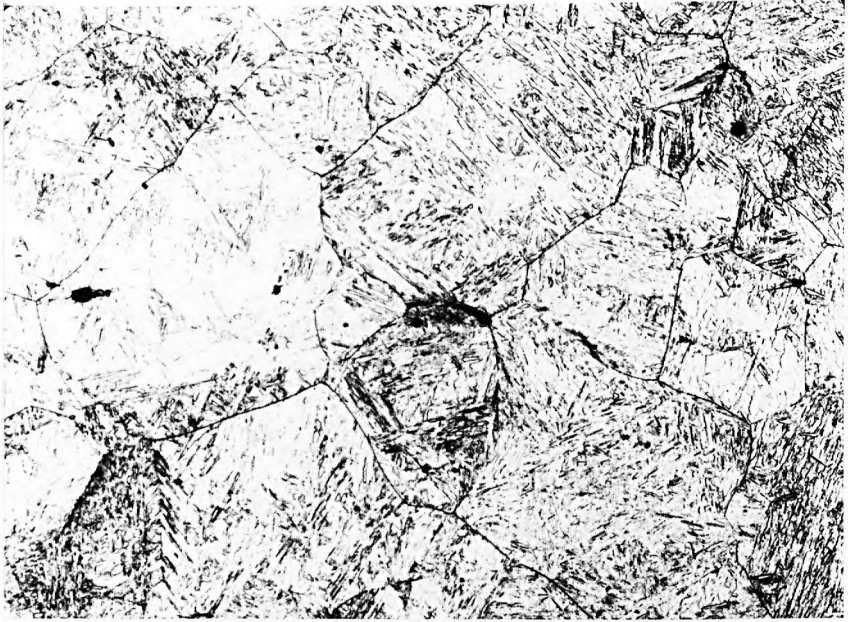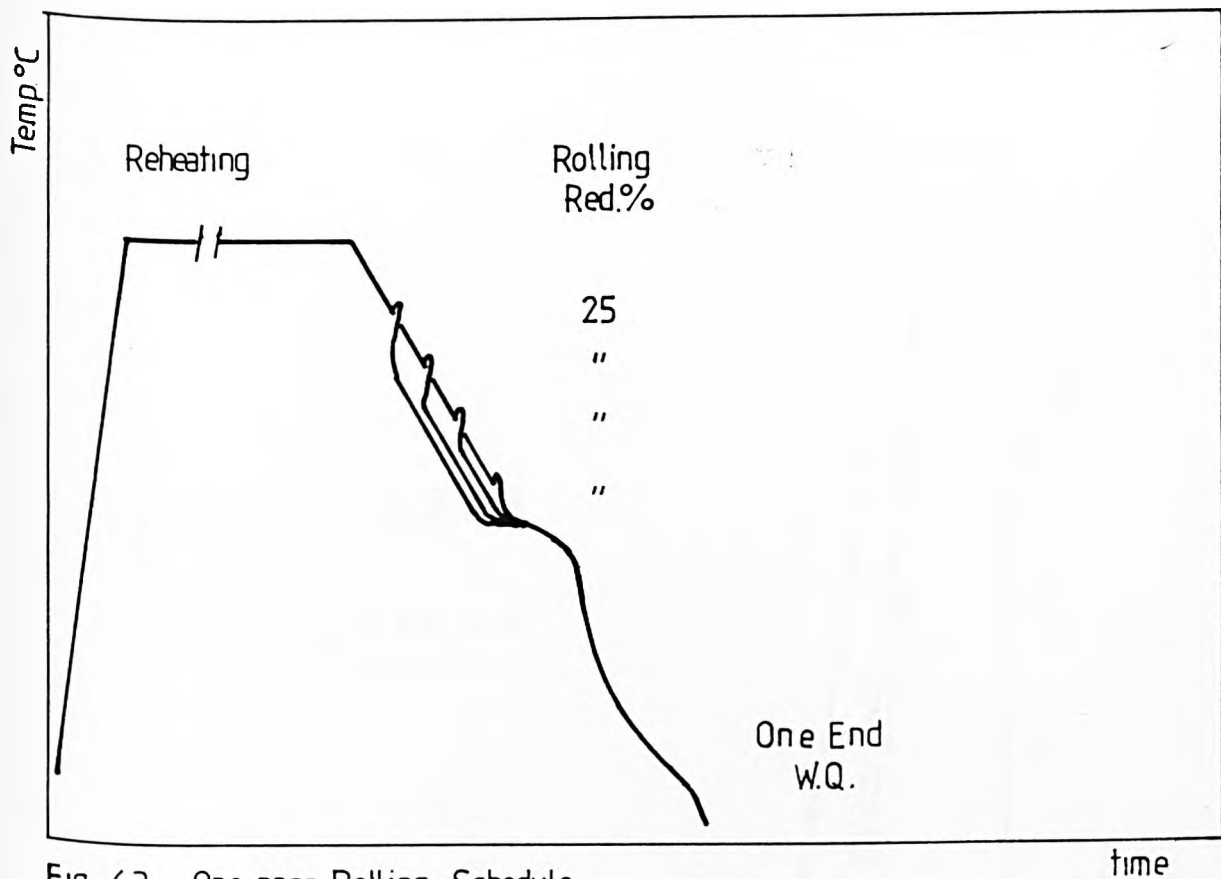
Fig. 6.3   One pass Rolling Schedule
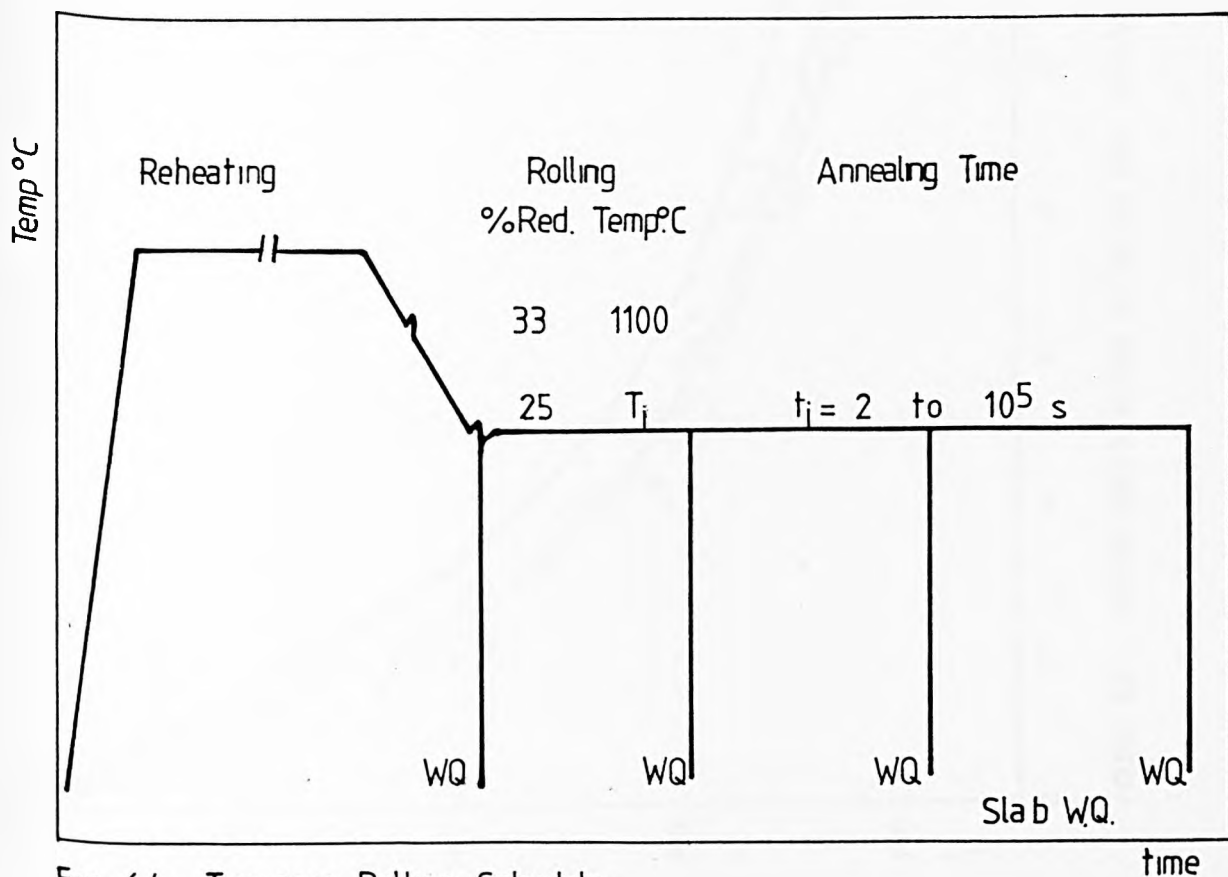
Fig. 6.4   Two pass Rolling Schedule
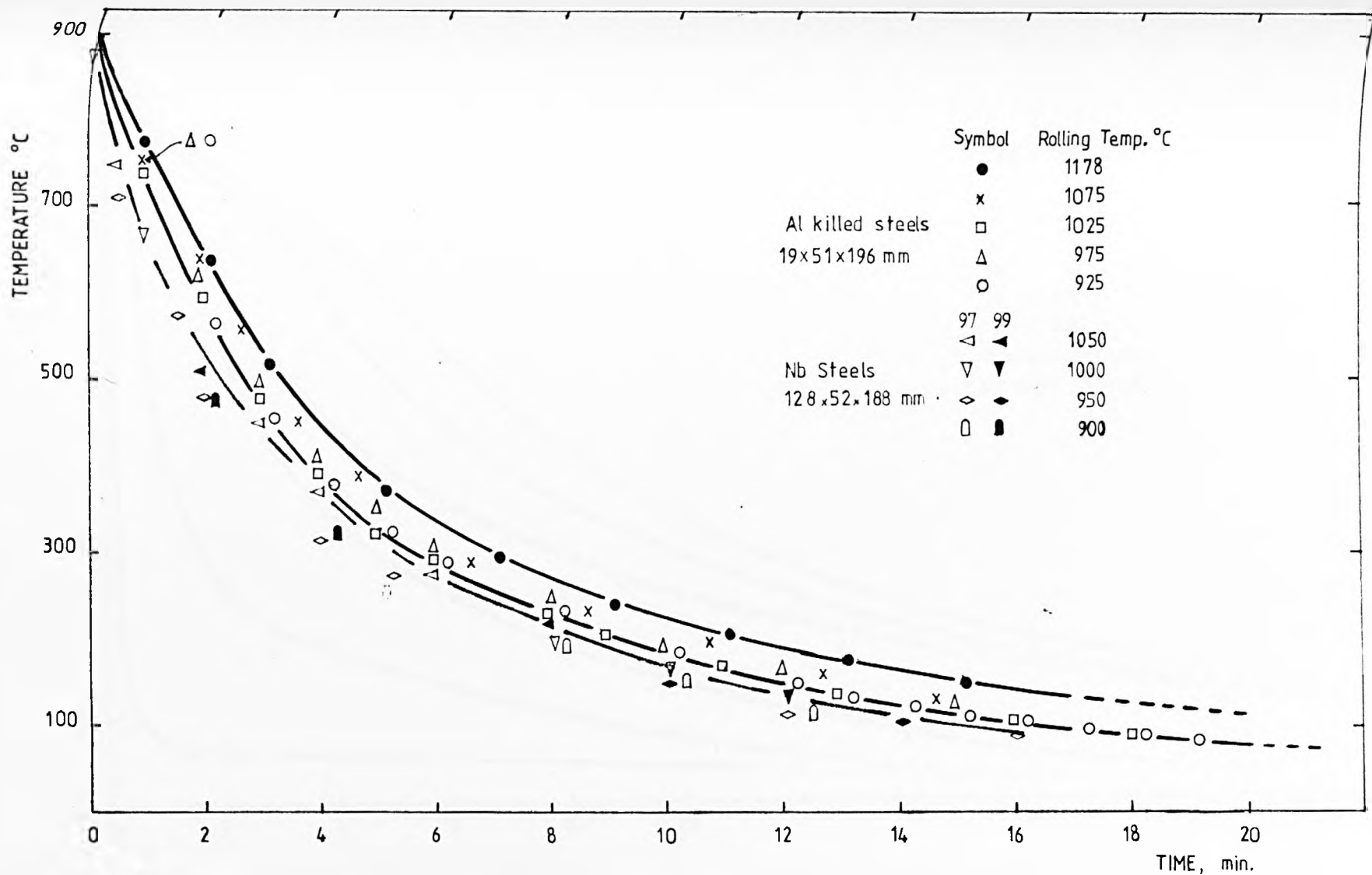
FIGURE 6.5 COOLING CURVES - MIDDLE OF ROLLED BAR - SERIES I
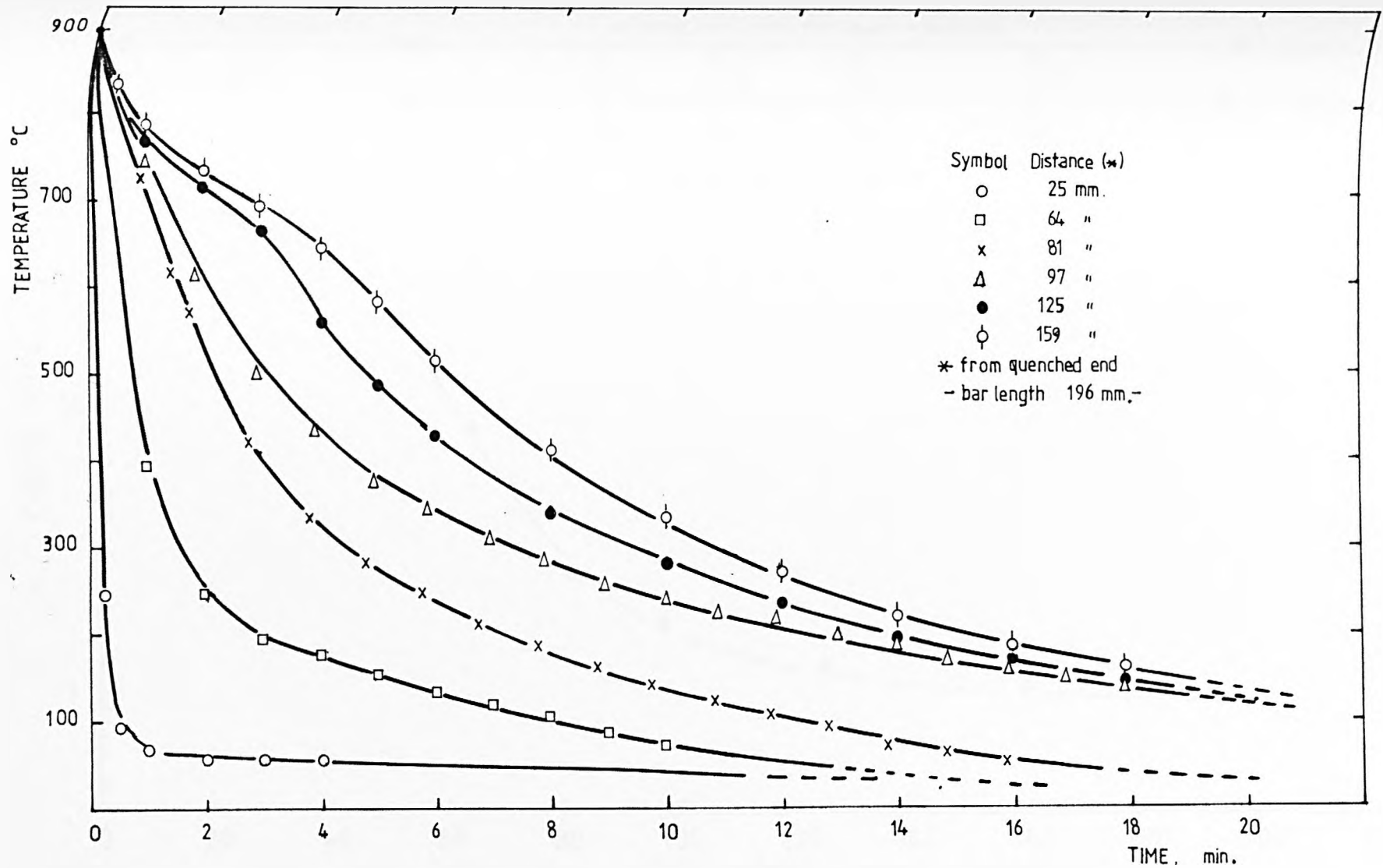
FIGURE 6.6   COOLING CURVES-SERIES I
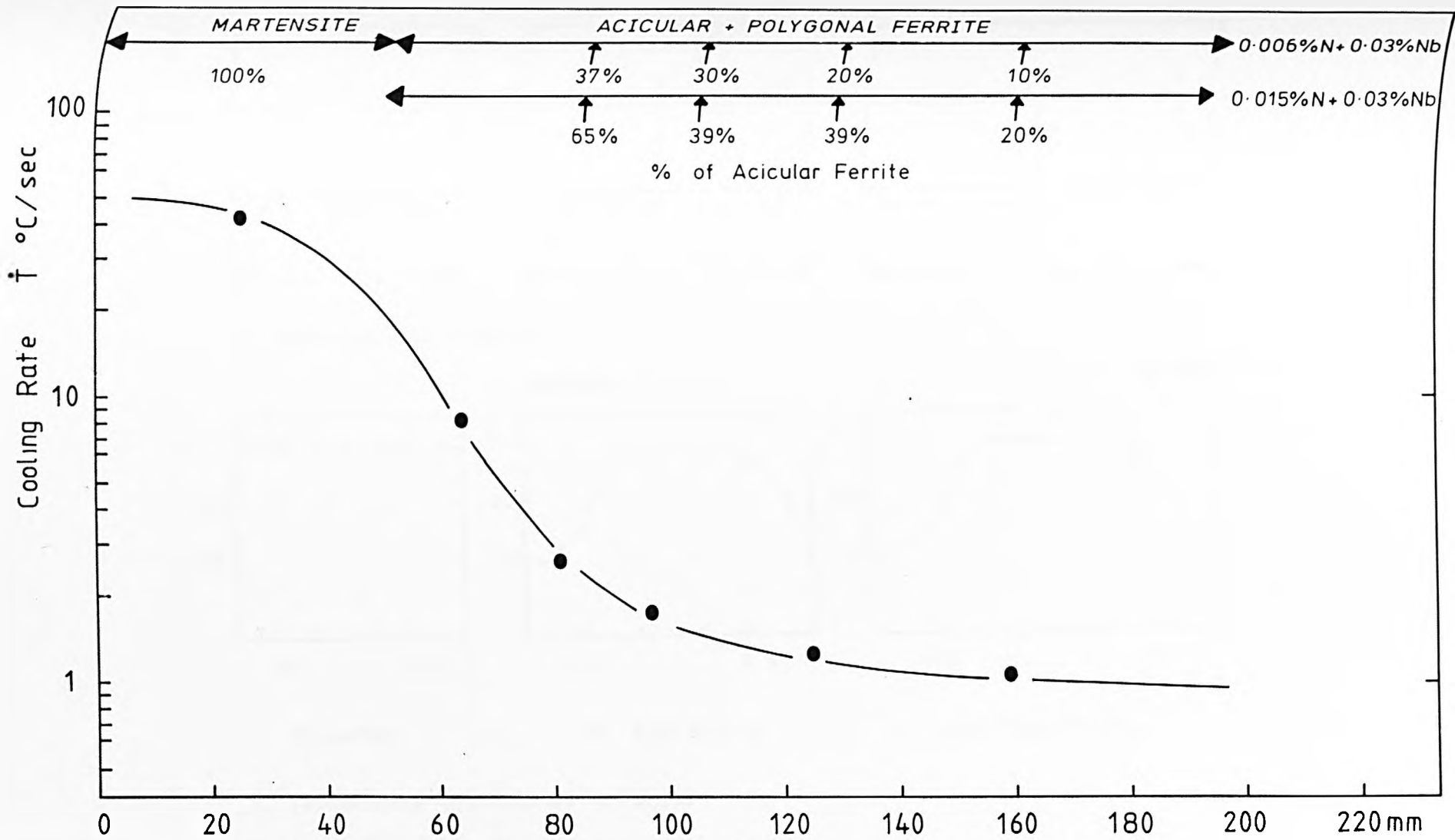
Fig. 6.7   Cooling Rate–Microstructure   vs   Distance from Quenched End.
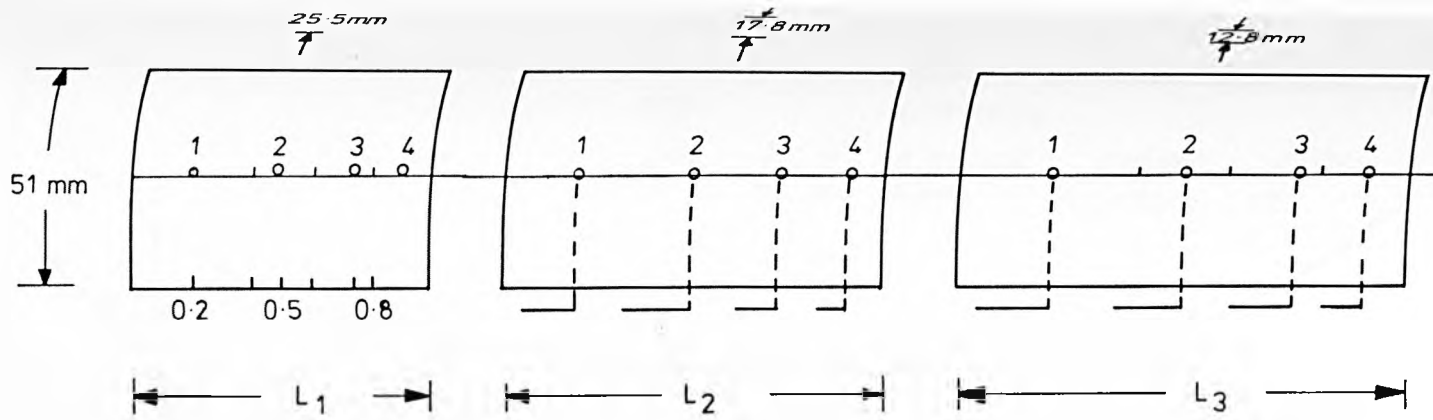
a. Thermocouples position.
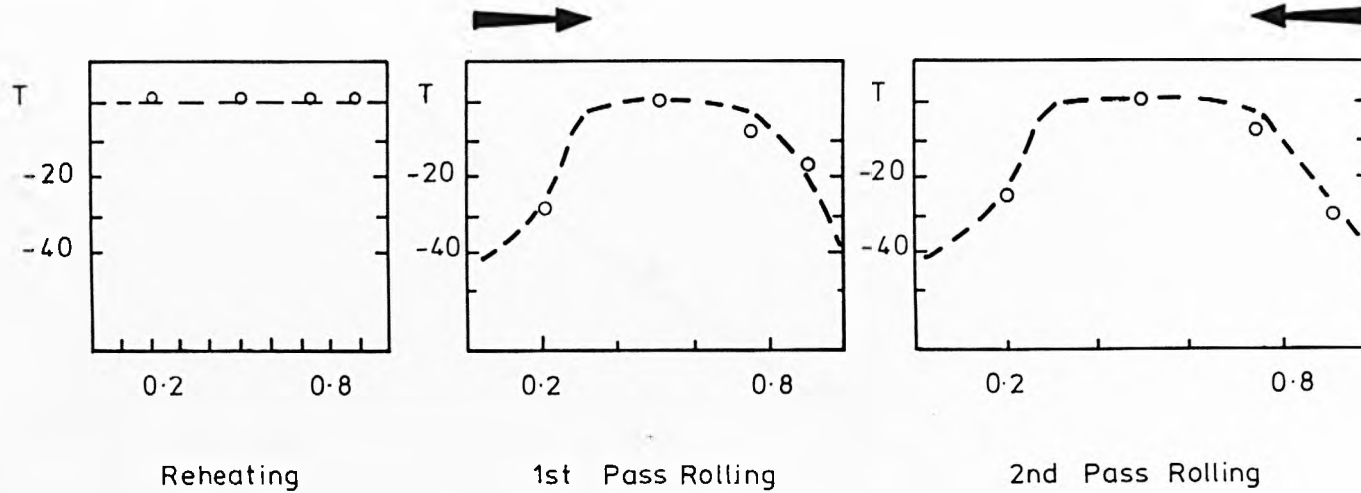
b. Temperature Distribution in Slabs.

Fig. 68 Measurement of temperatures during rolling.
Two pass rolling schedule, 2nd pass at 900°C.
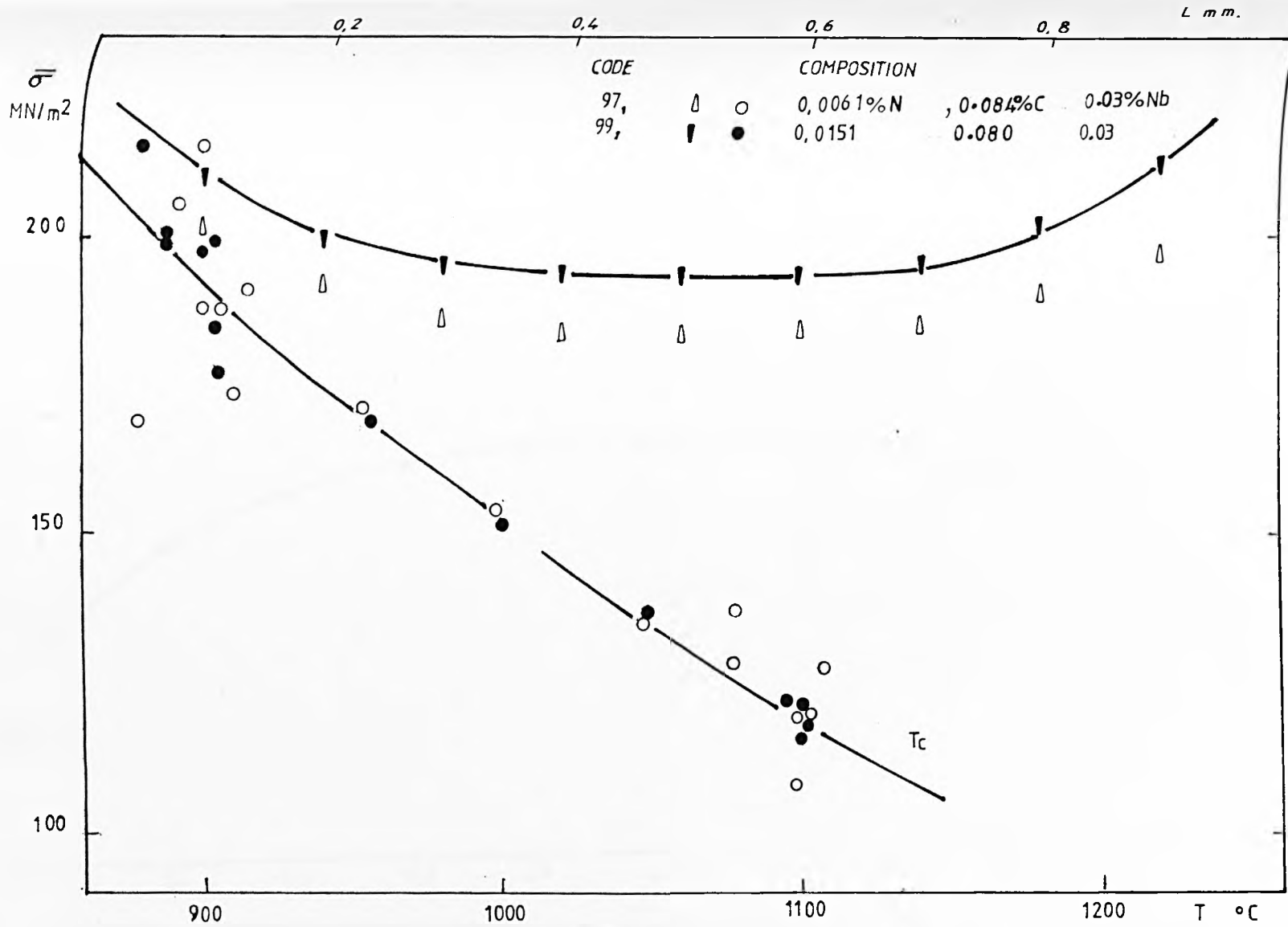
FIG. 6.9. CALCULATED MEAN FLOW STRESS, $\overline{\sigma}$ VS TEMPERATURE OF ROLLING, T, AND SLAB LENGTH, L.
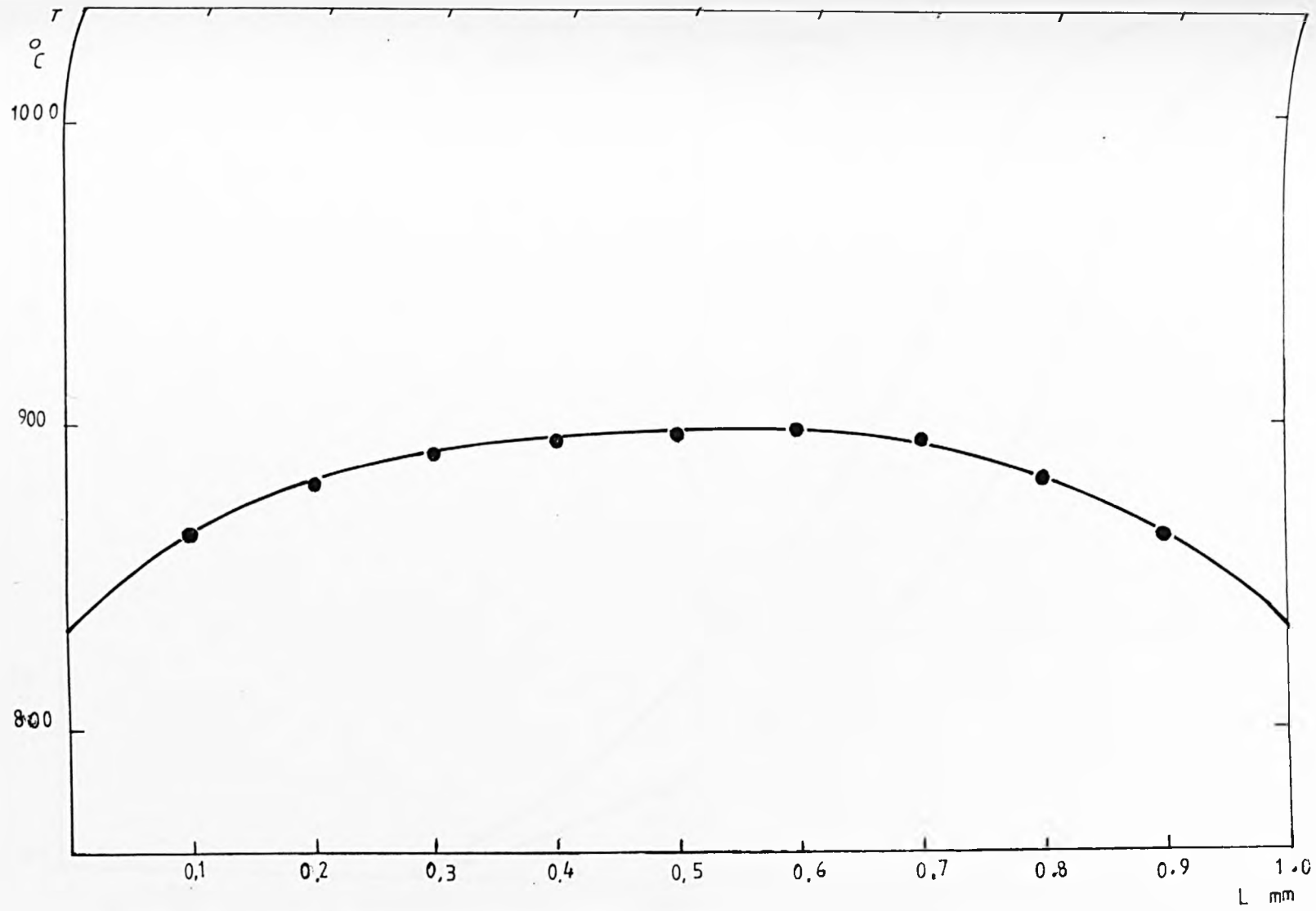
FIG. 6.10   TEMPERATURE DISTRIBUTION THROUGH SLAB LENGTH.
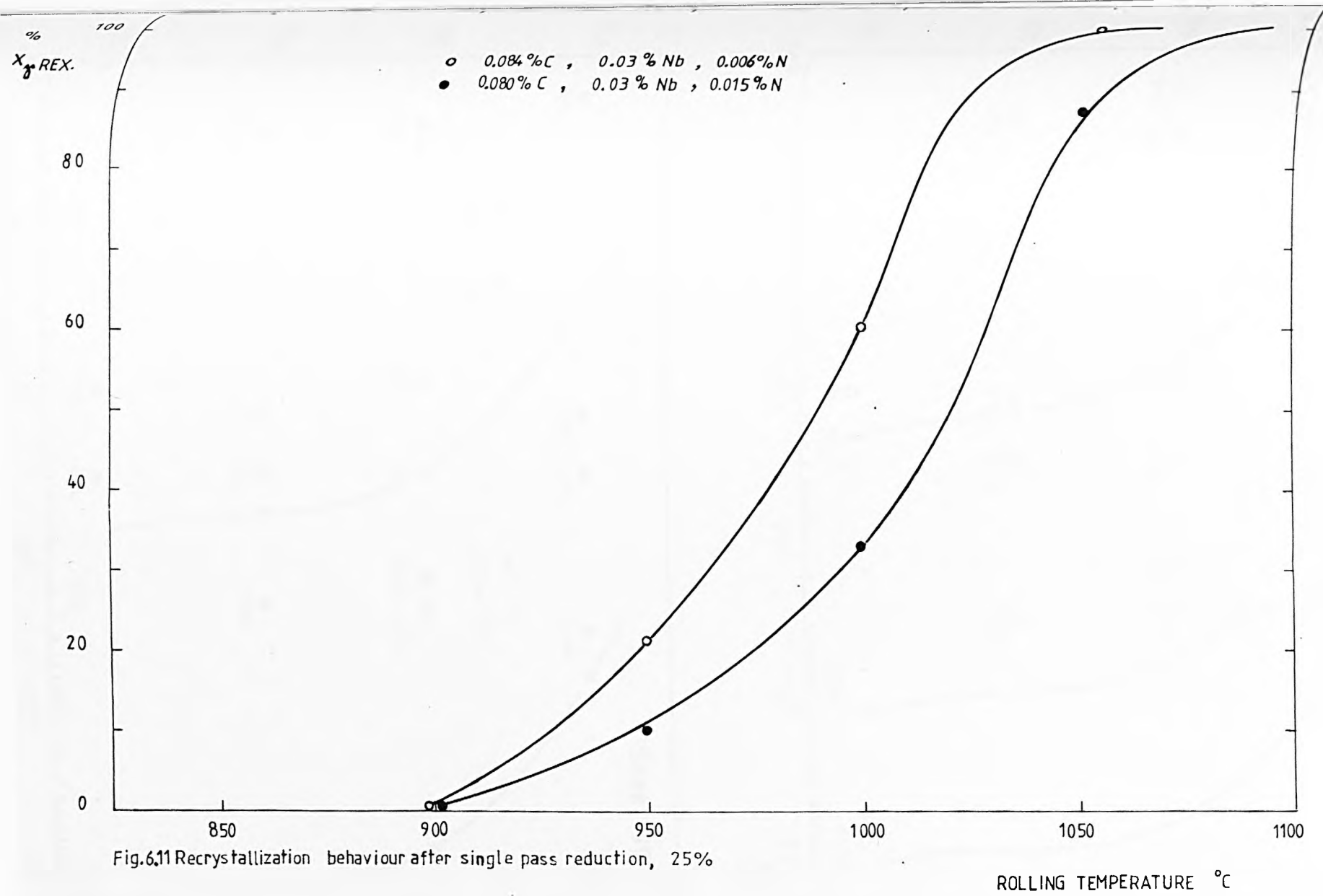
Fig. 6.11 Recrystallization behaviour after single pass reduction, 25%

o	0.084 %C ,	0.03 % Nb ,	0.006%N
●	0.080% C ,	0.03 % Nb ,	0.015% N

% $X_{\%}$ REX.

ROLLING TEMPERATURE °C
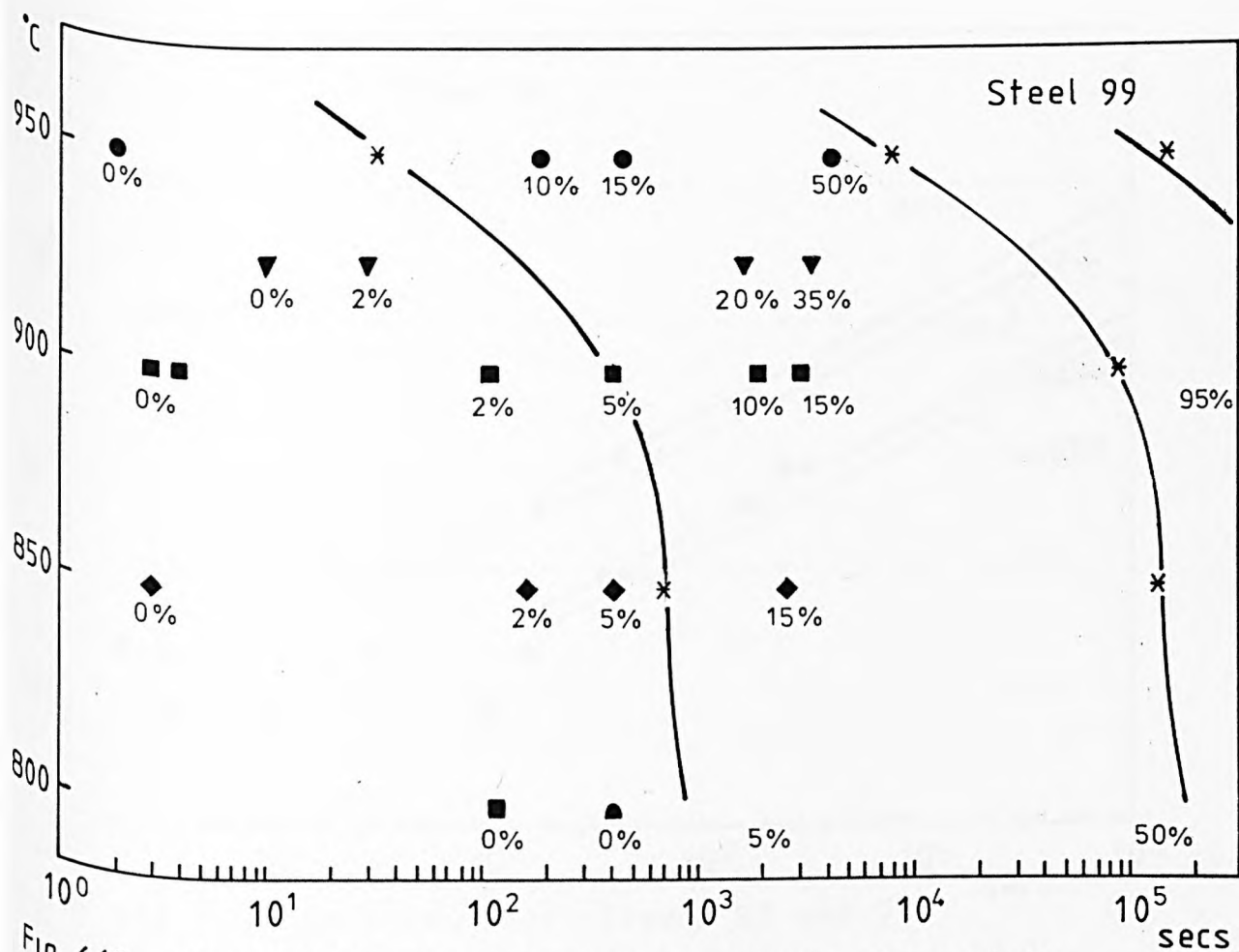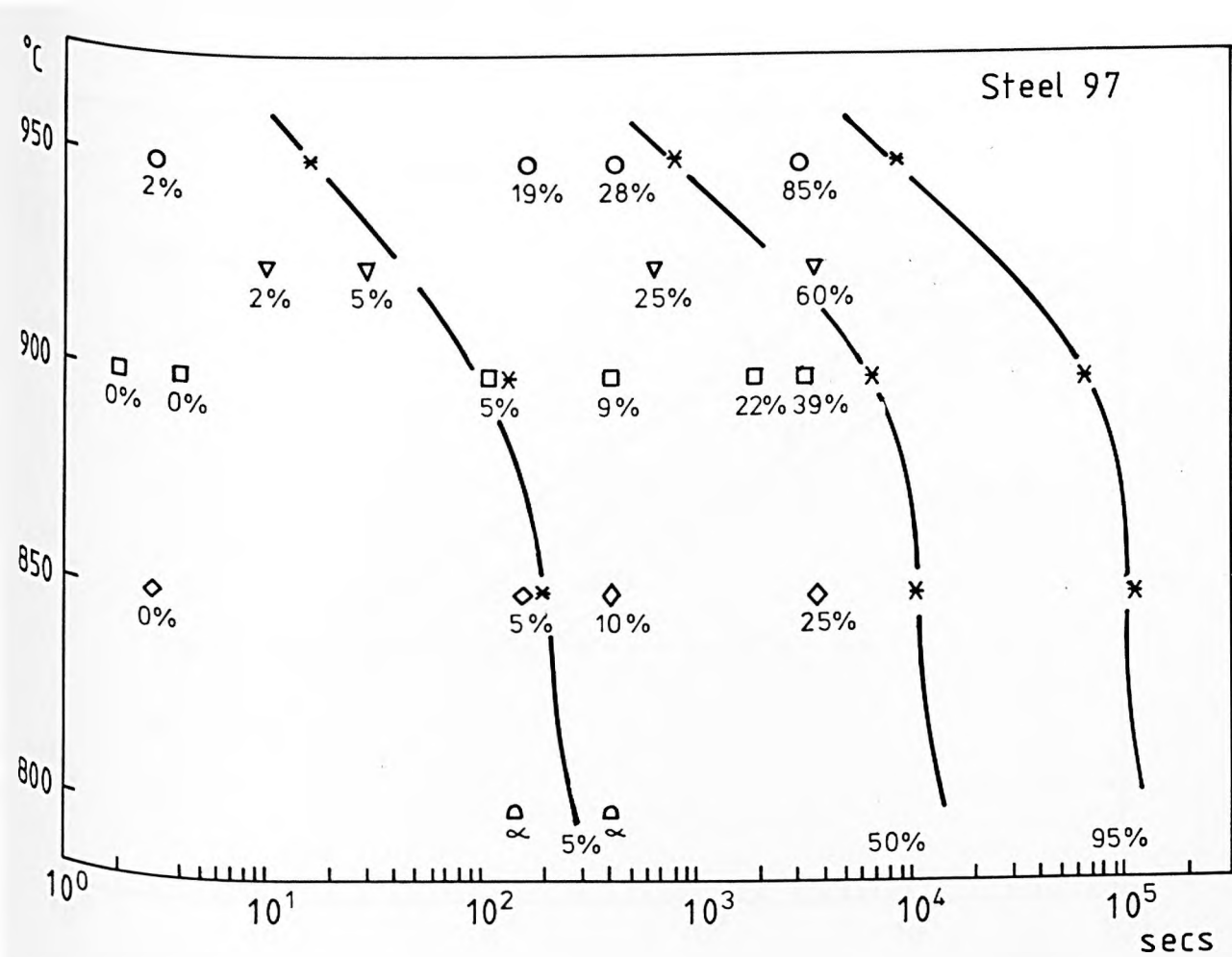
Fig. 6.12 Recrystallization Kinetics for Steels 97 and 99
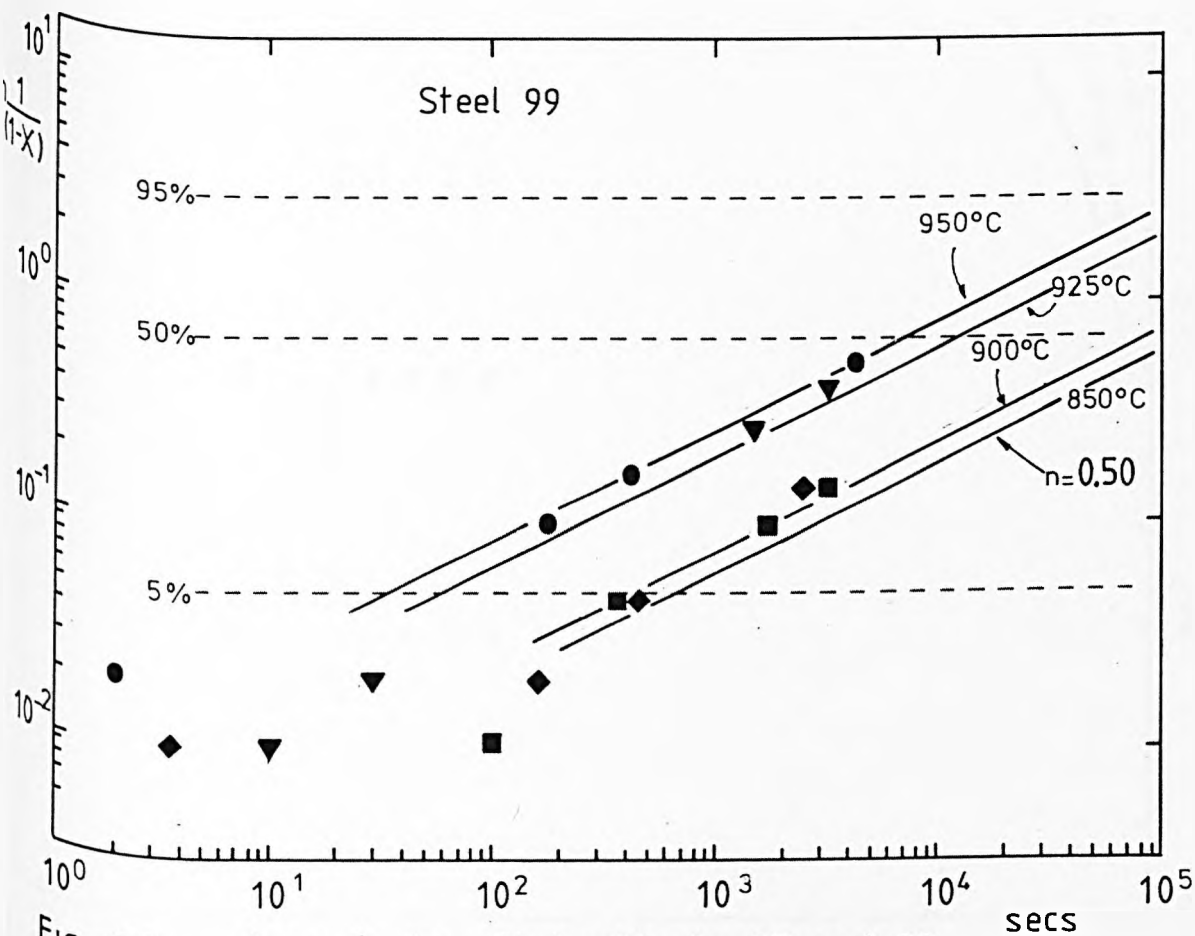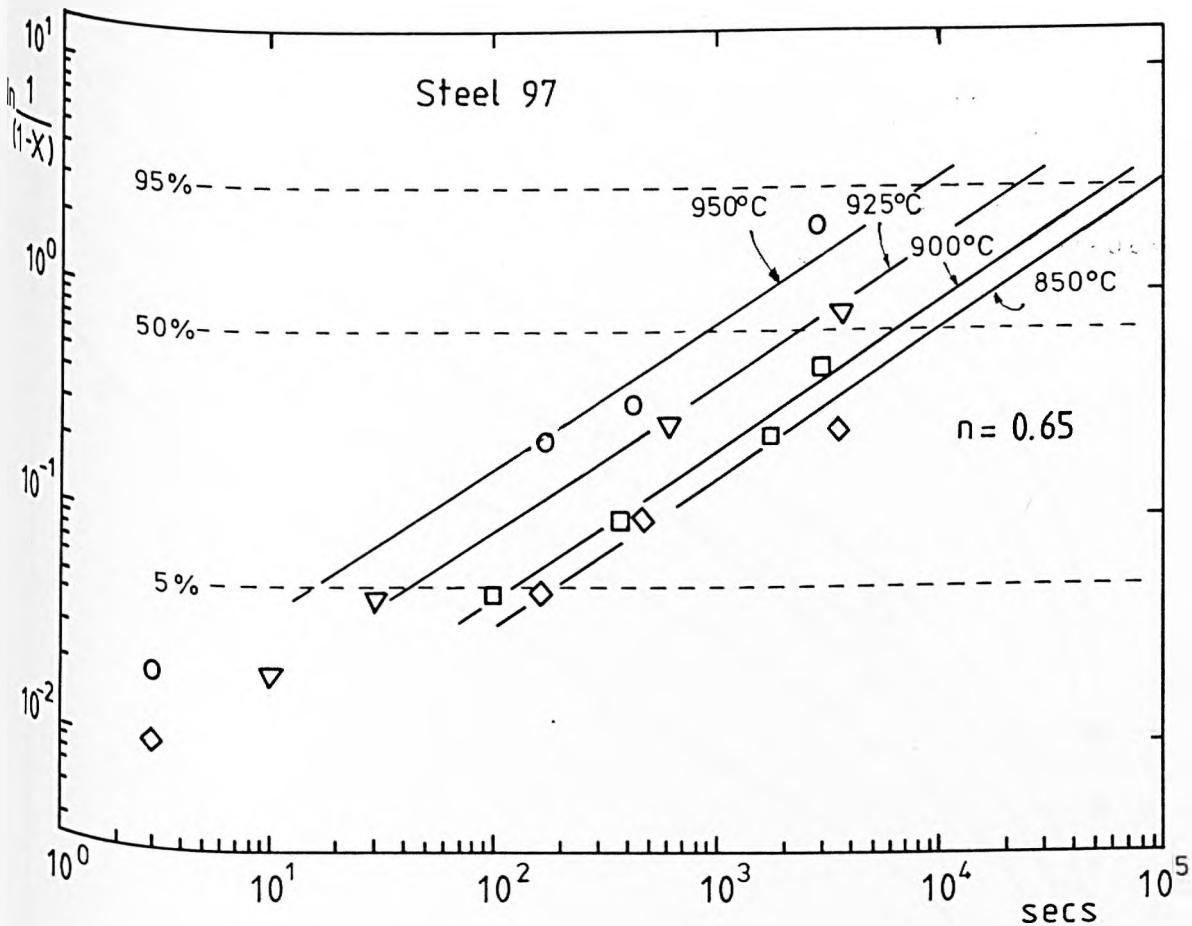
Fig. 6.13   Avrami's Law Plot – Steels 97 and 99
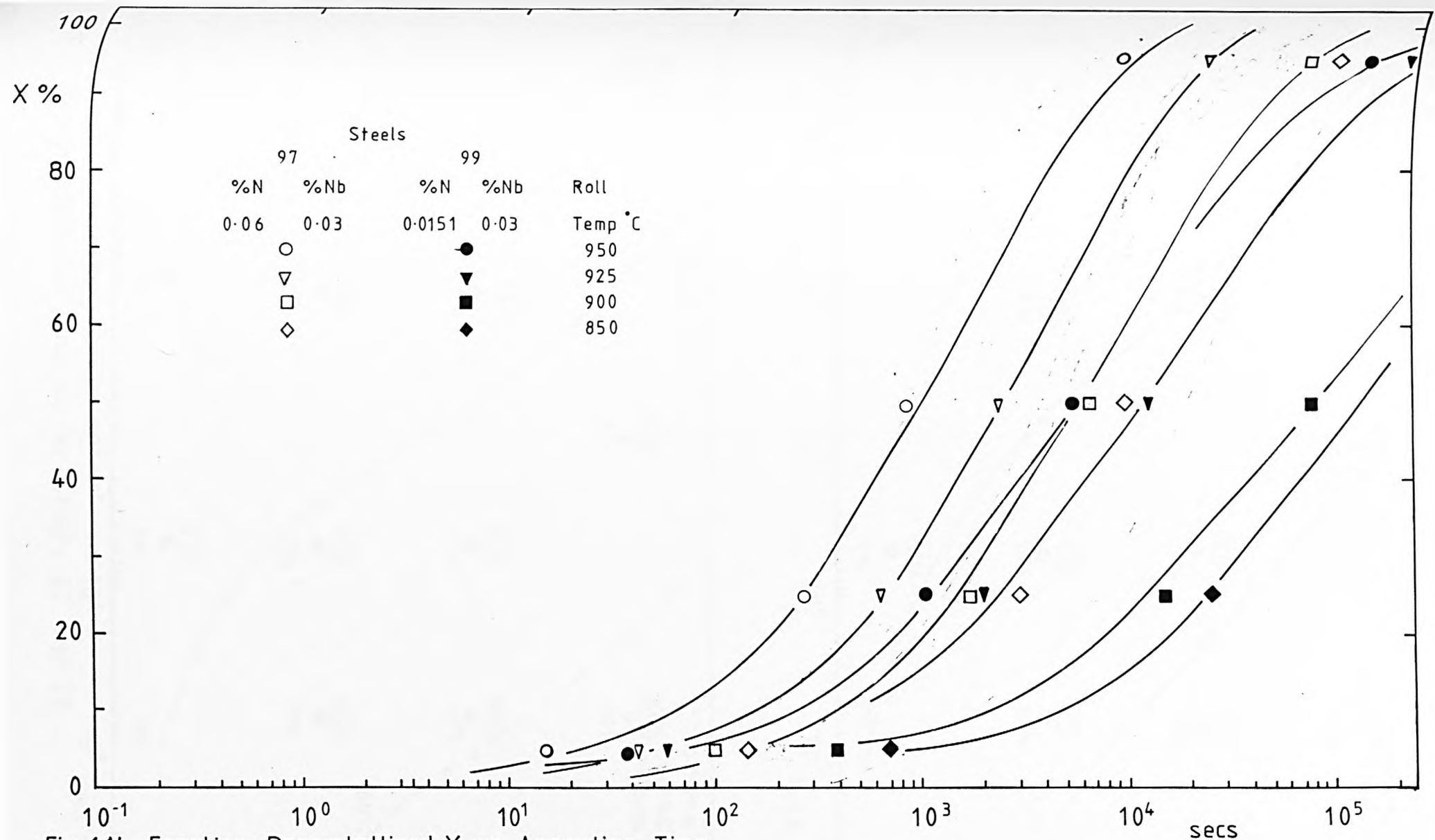
Fig.6.14 Fraction Recrystallised, X, vs Annealing Time

Fig. 6.15 Recrystallisation Kinetics for Steels 22 and 23
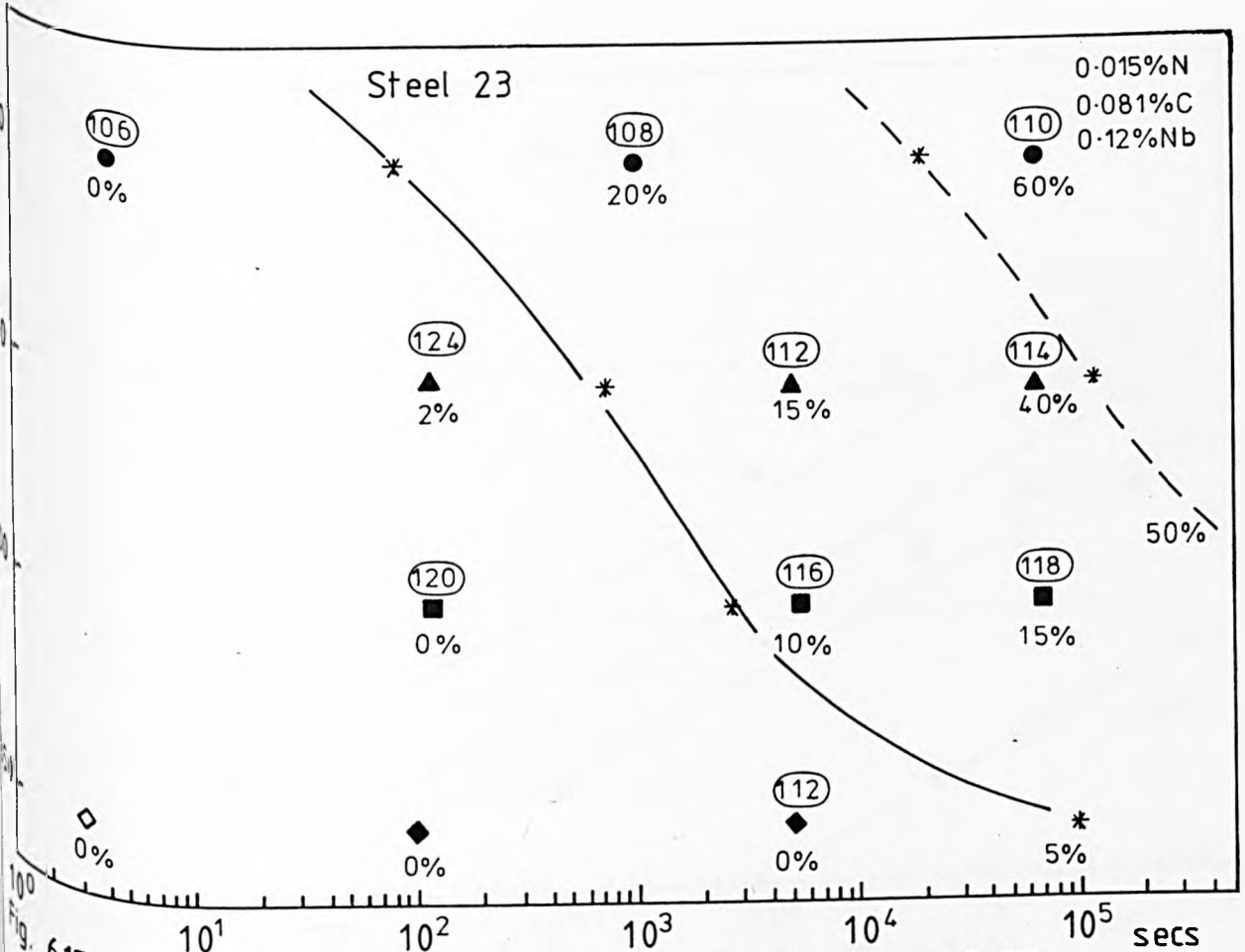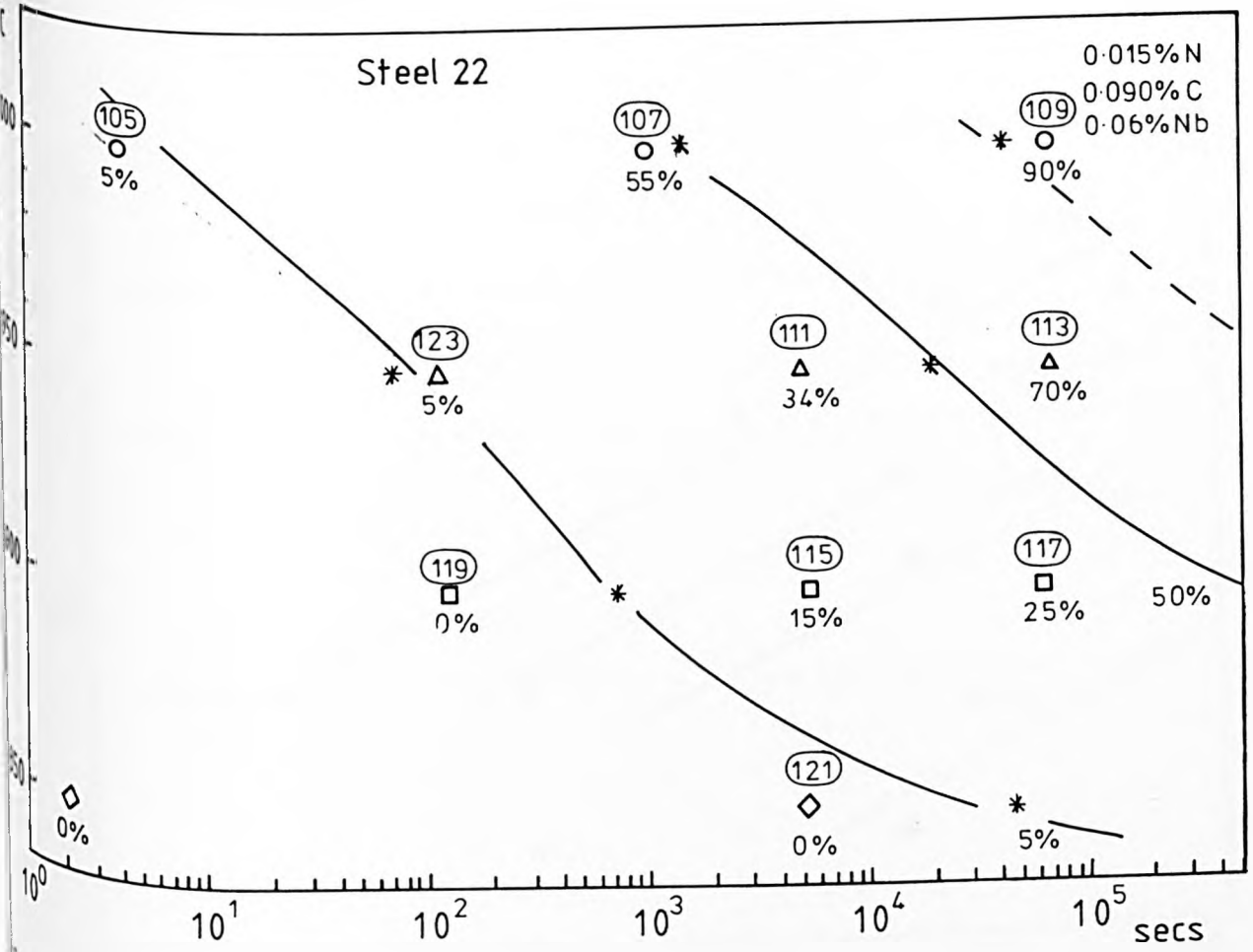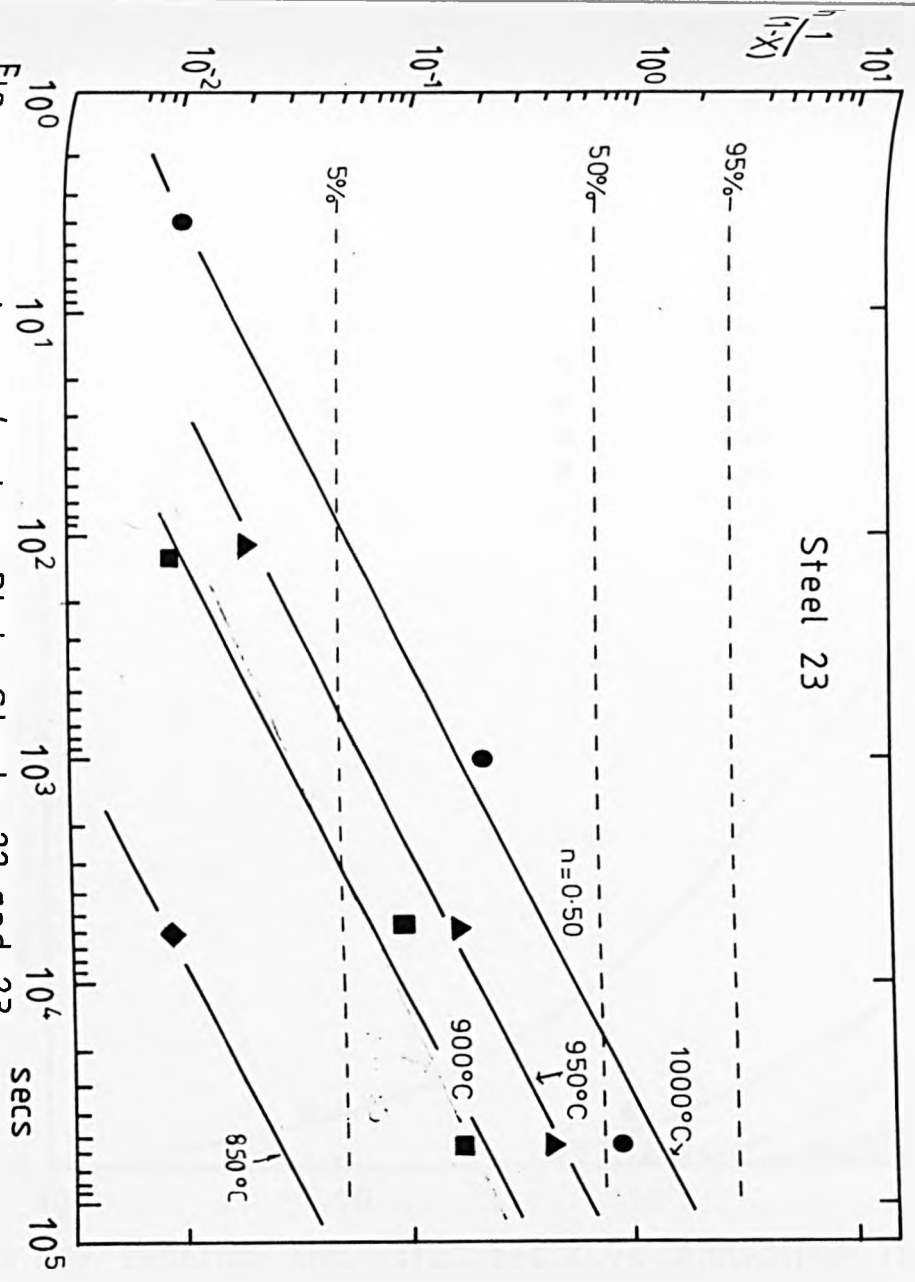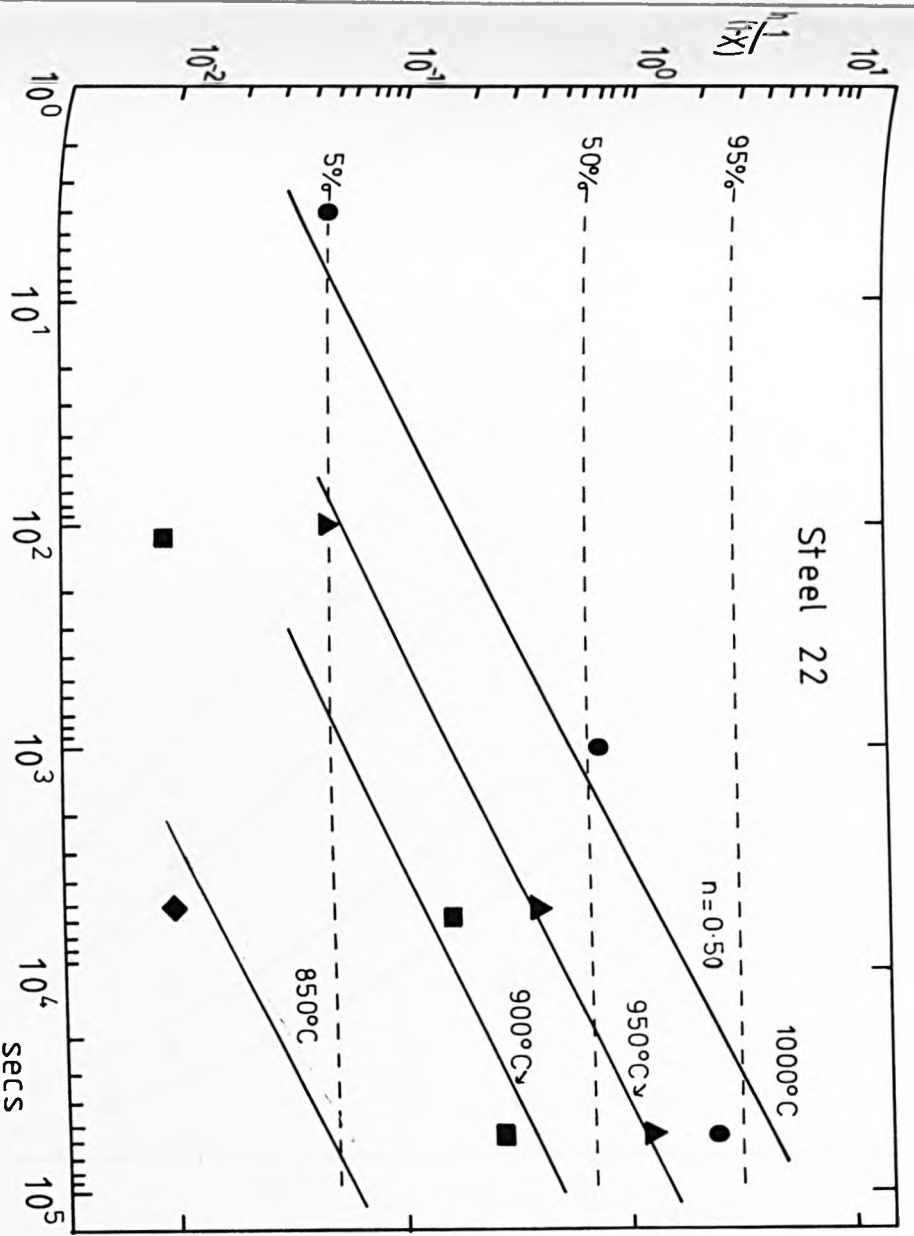
Fig. 6.16 Avrami's Law Plot – Steels 22 and 23
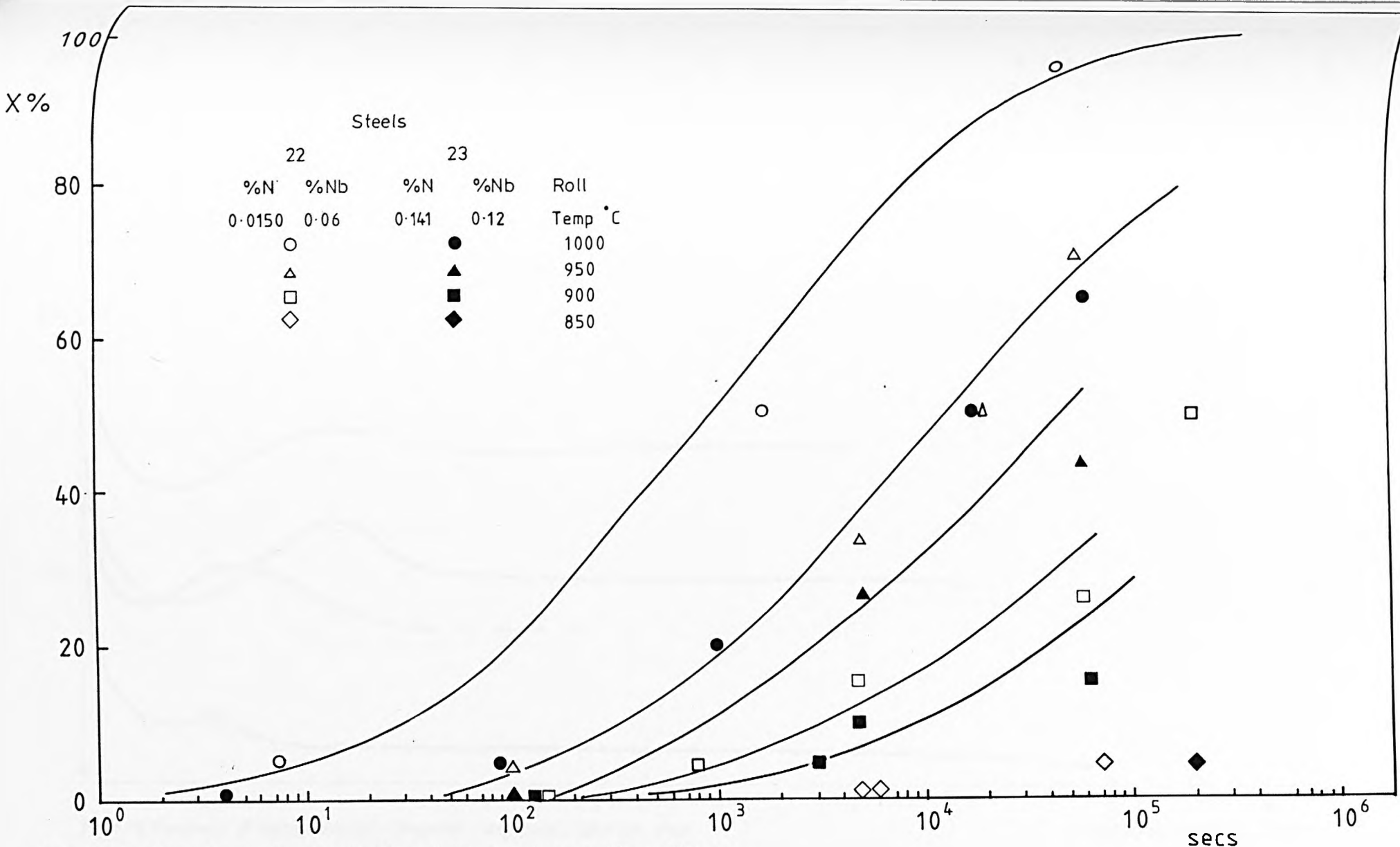
Fig. 6.17 Fraction Recrystallised, X, vs Annealing Time
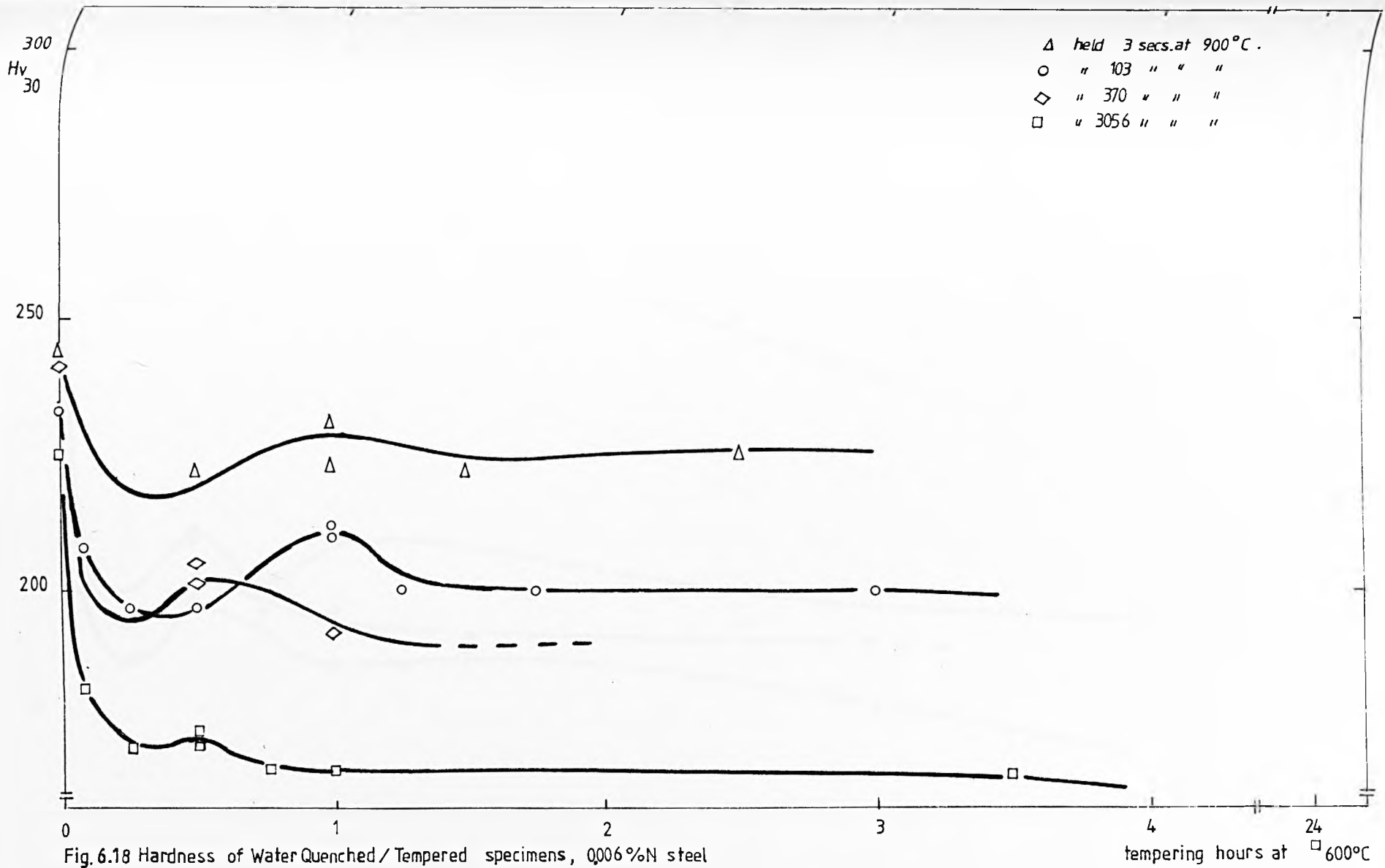
Fig. 6.18 Hardness of Water Quenched / Tempered specimens, 0.006 % N steel

Fig. 6.19 Hardness of Water Quenched/Tempered specimens, 0,015% N steel

tempering hours at 600 °C

held 2 s at 900°C.
" 107 " " "
" 405 " " "
" 3096 " " "
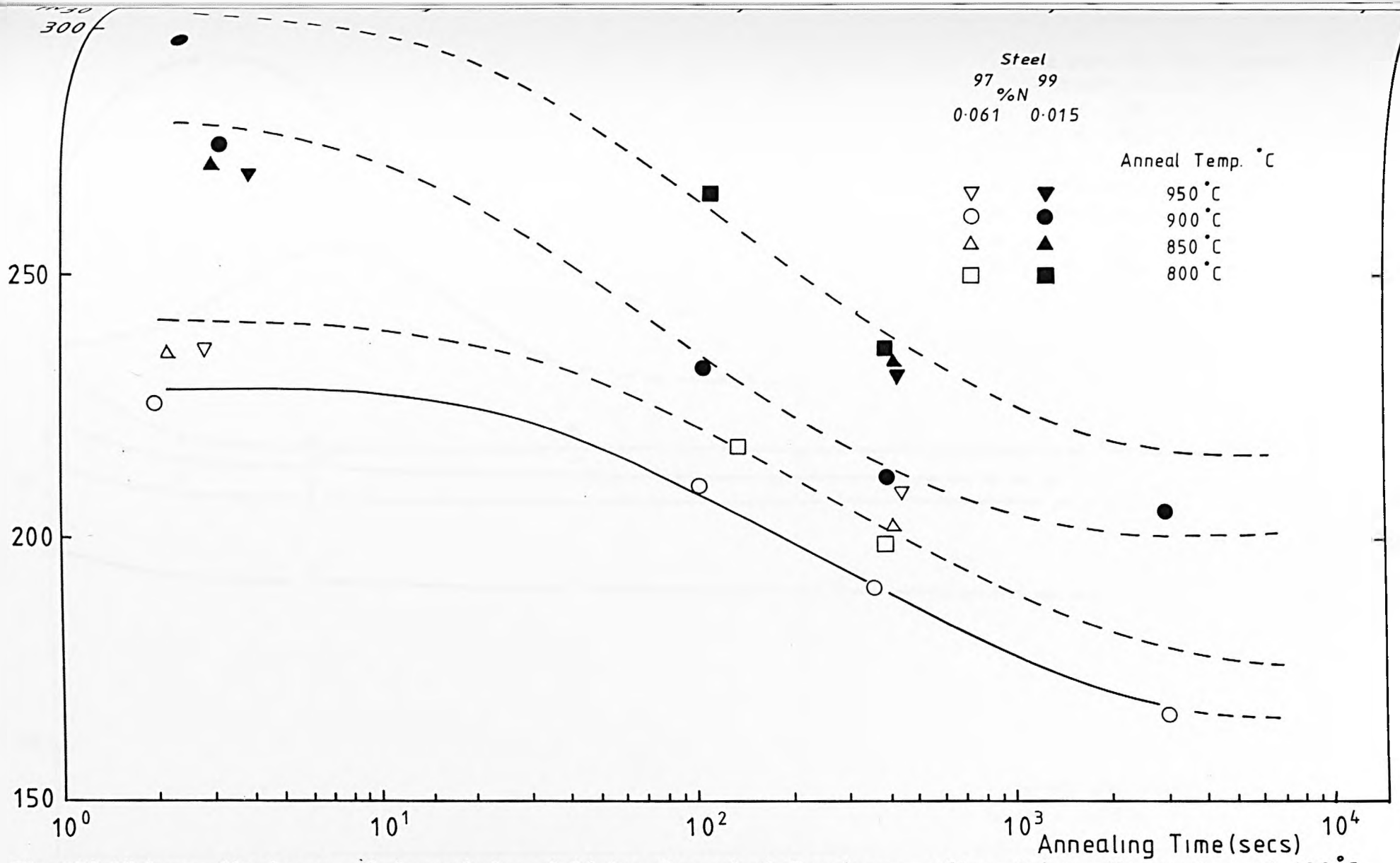
Fig. 6.20 Vickers Hardness of Annealed and Water Quenched Specimens after 1 hour Tempering at 600°C.
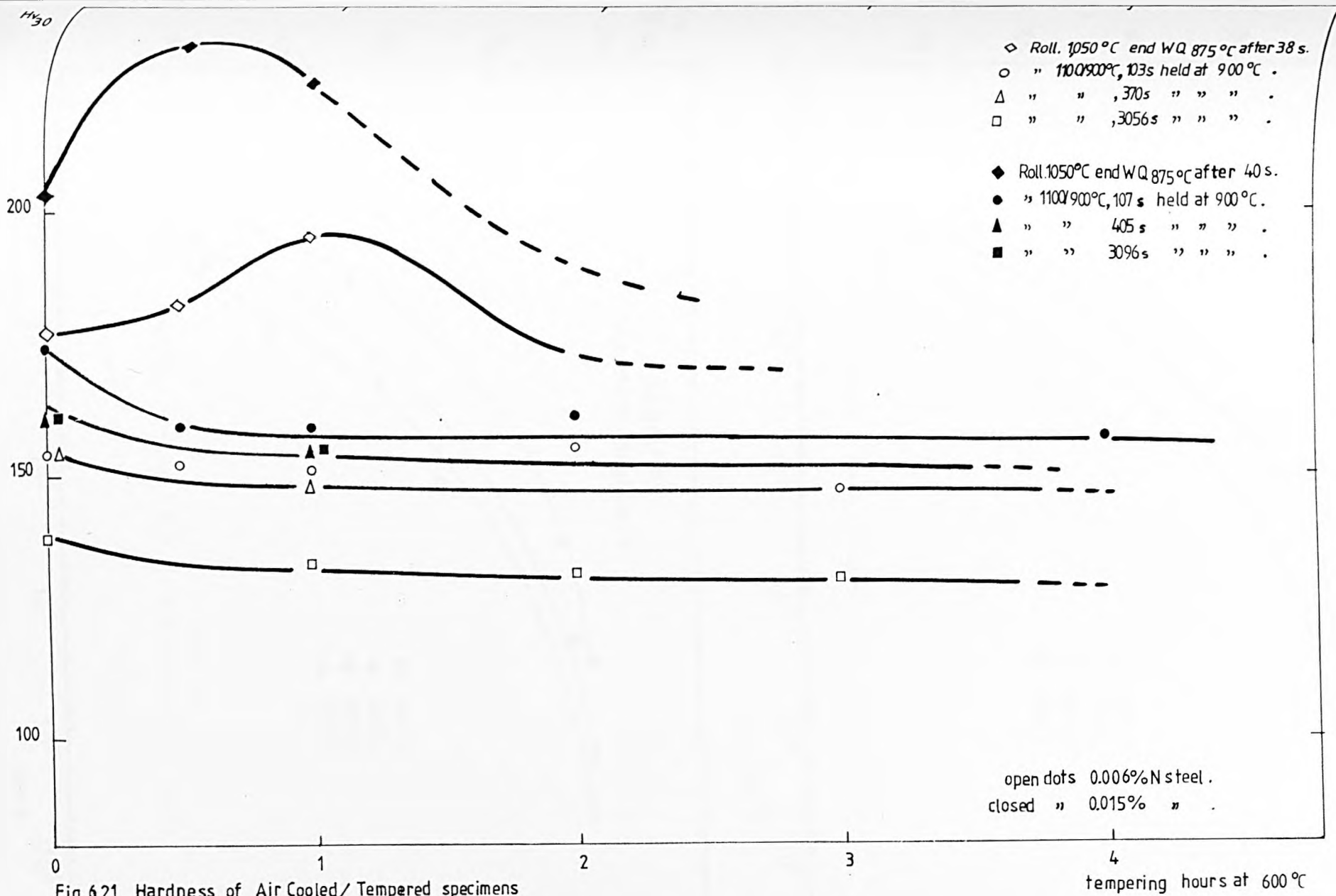
Fig. 6.21 Hardness of Air Cooled / Tempered specimens

◇ Roll. 1050 °C end WQ 875 °C after 38 s.
○ „ 1100/900°C, 103s held at 900 °C.
△ „ „ , 370s „ „ „ .
□ „ „ , 3056s „ „ „ .

◆ Roll. 1050°C end WQ 875 °C after 40 s.
● „ 1100/900°C, 107 s held at 900 °C.
▲ „ „ 405 s „ „ „ .
■ „ „ 3096 s „ „ „ .

open dots 0.006% N steel .
closed „ 0.015% „ .

tempering hours at 600 °C
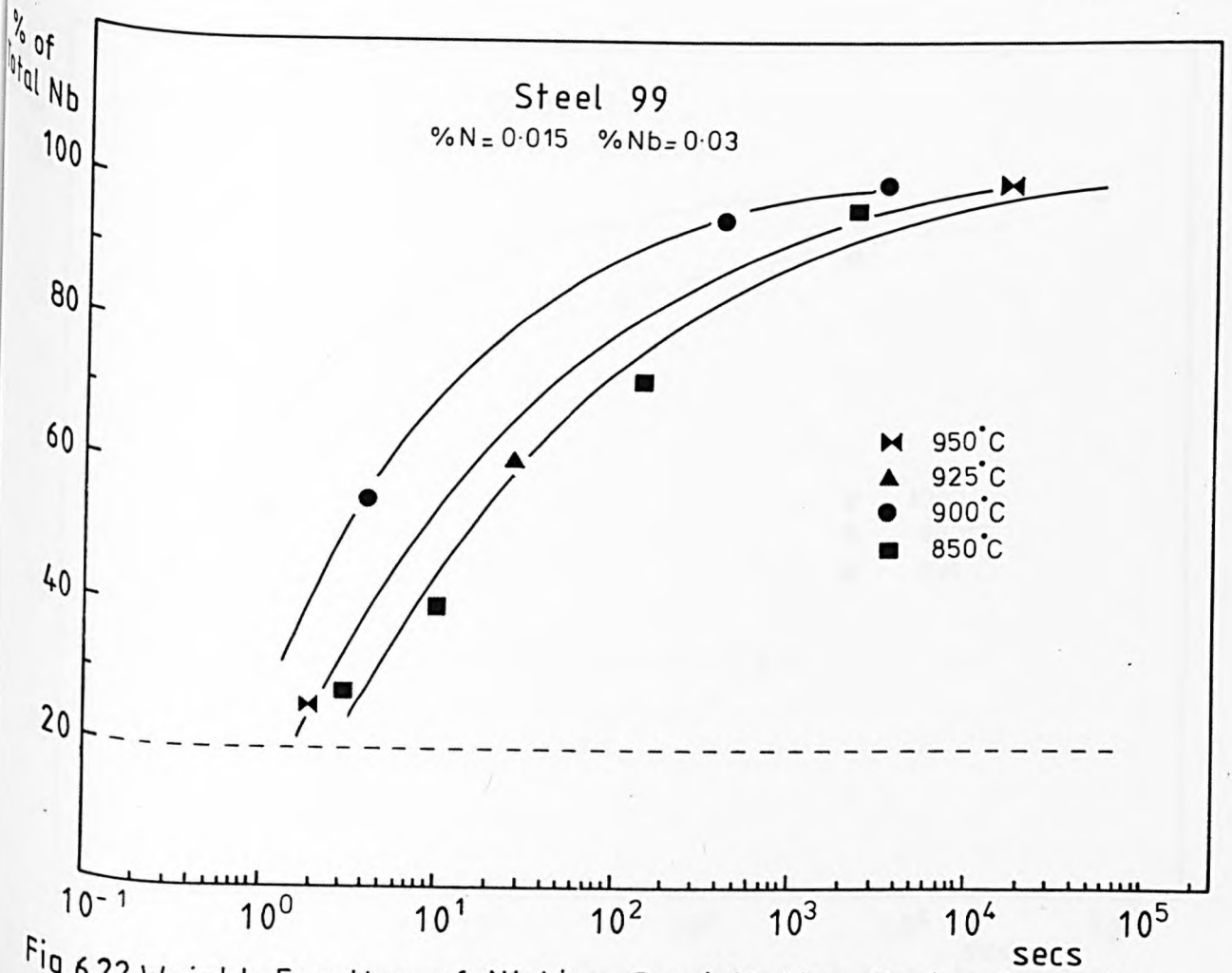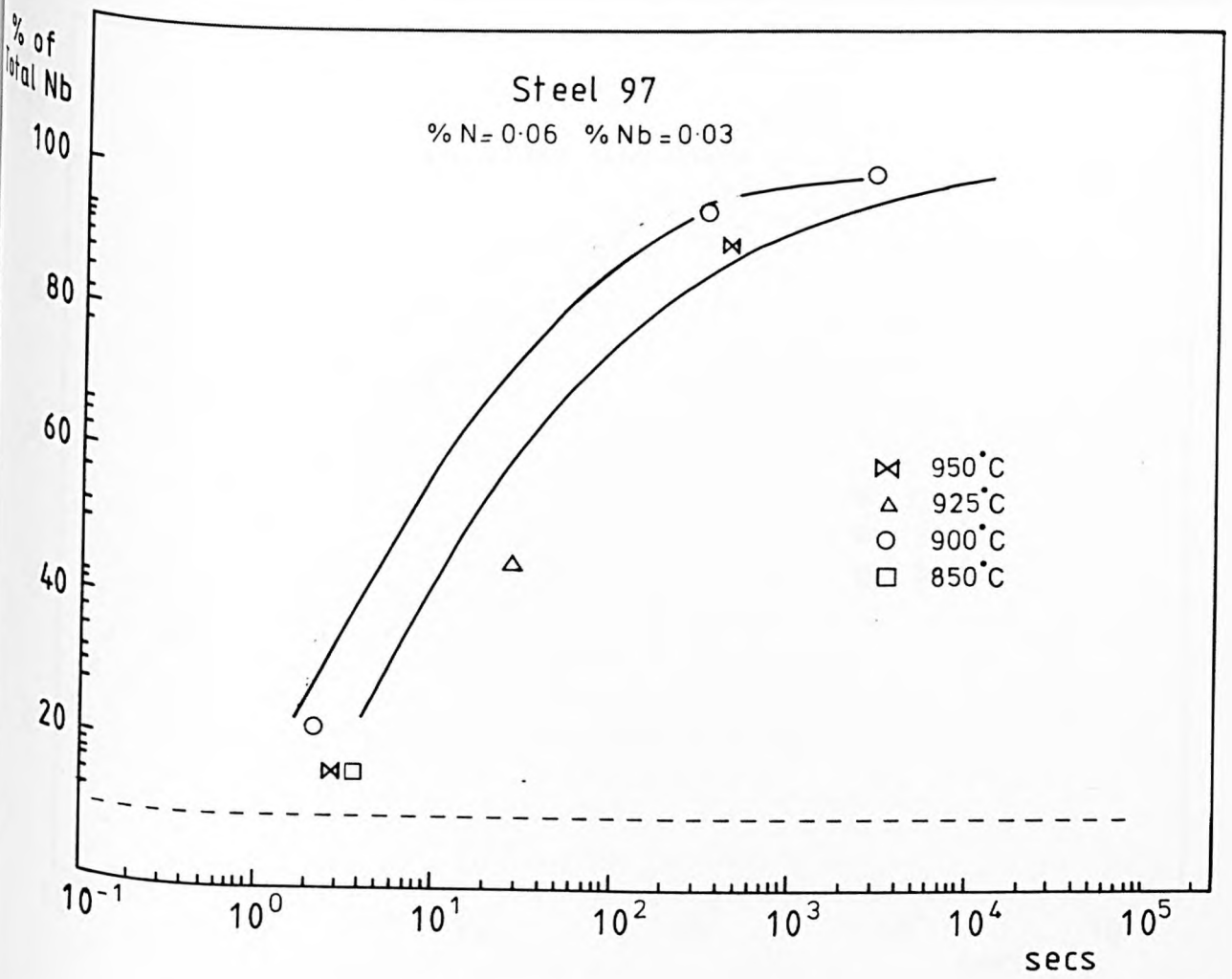
Fig. 6.22 Weight Fraction of Niobium Precipitating During Annealing.
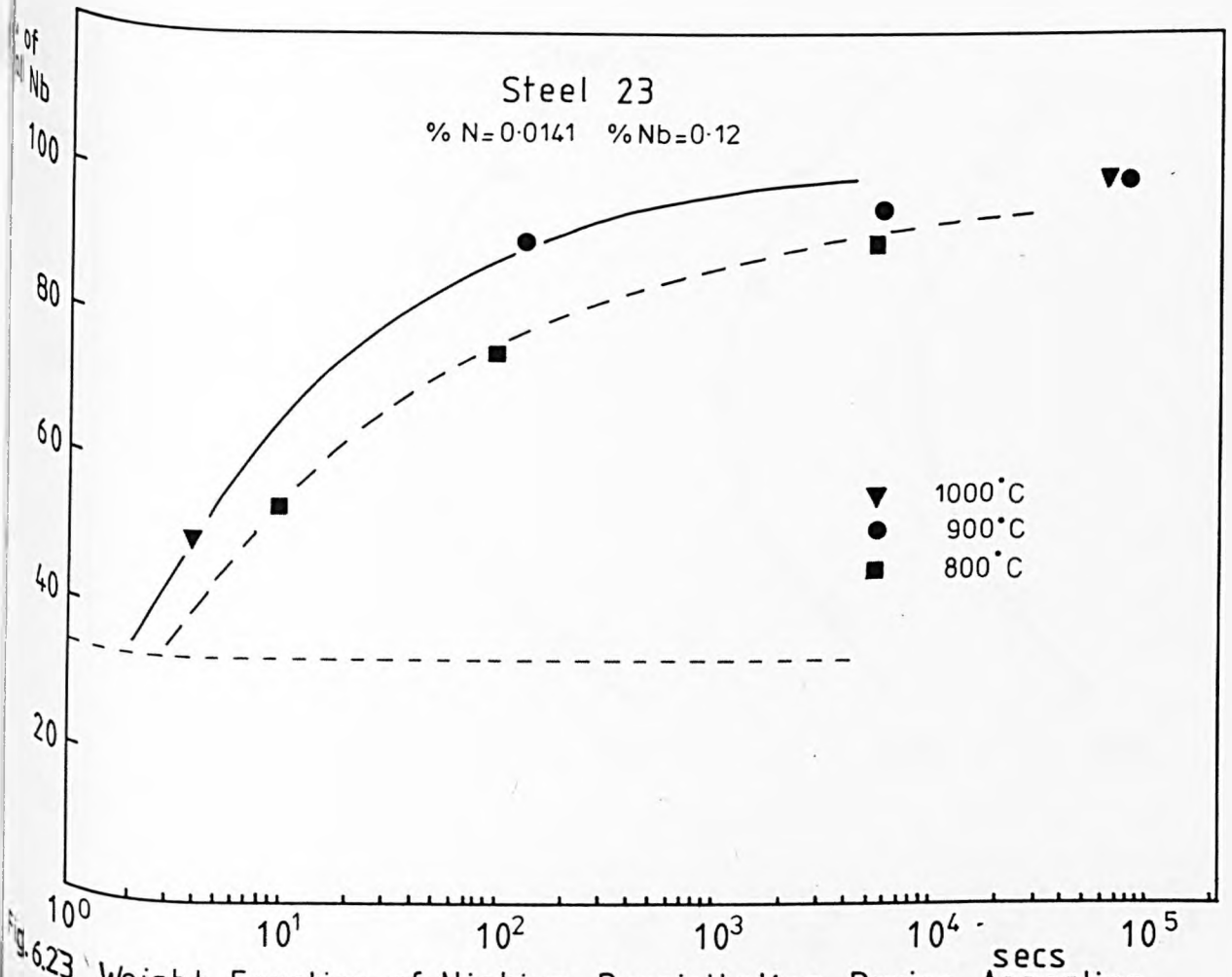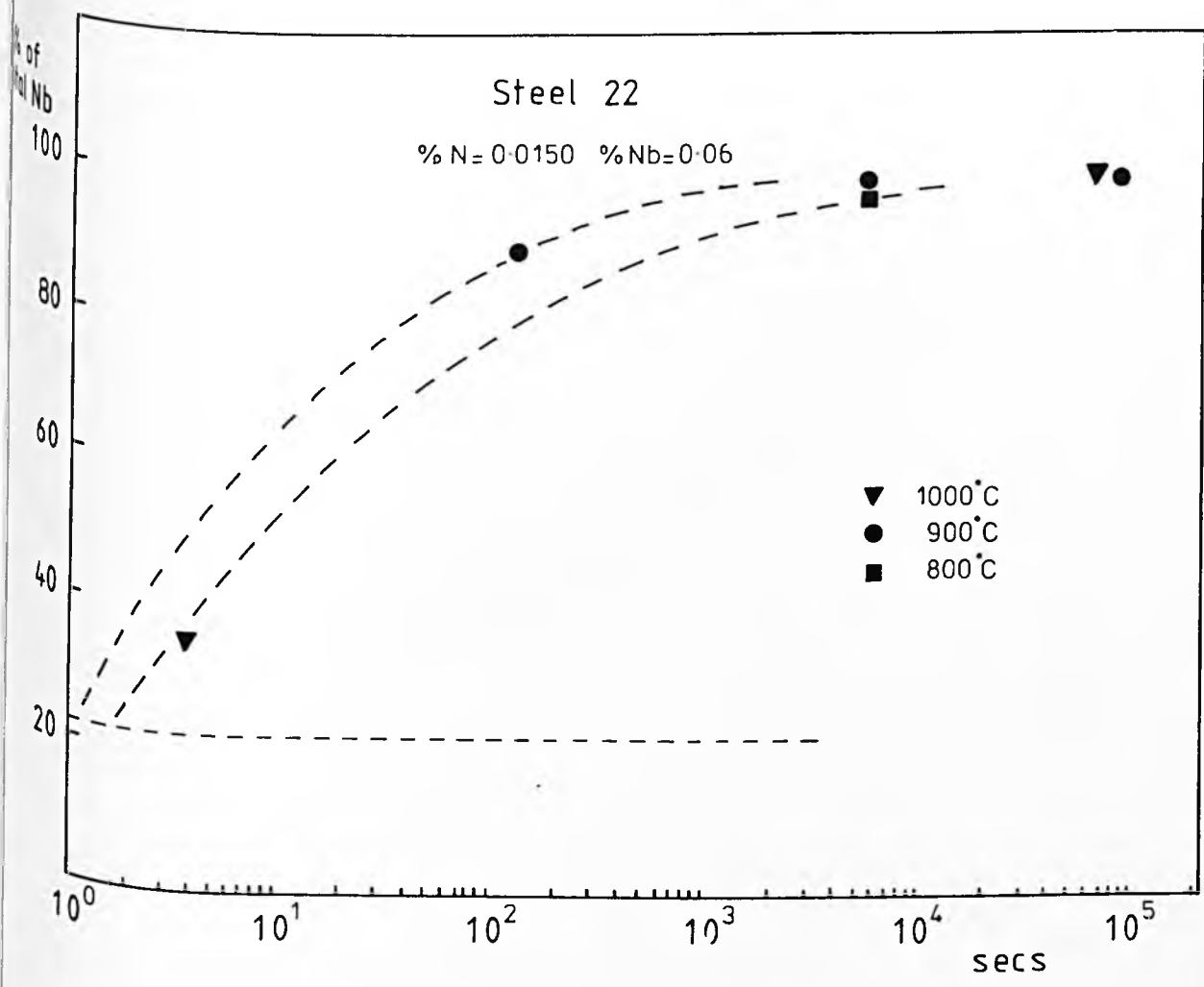
Fig. 6.23 Weight Fraction of Niobium Precipitating During Annealing.
Steels 22 and 23
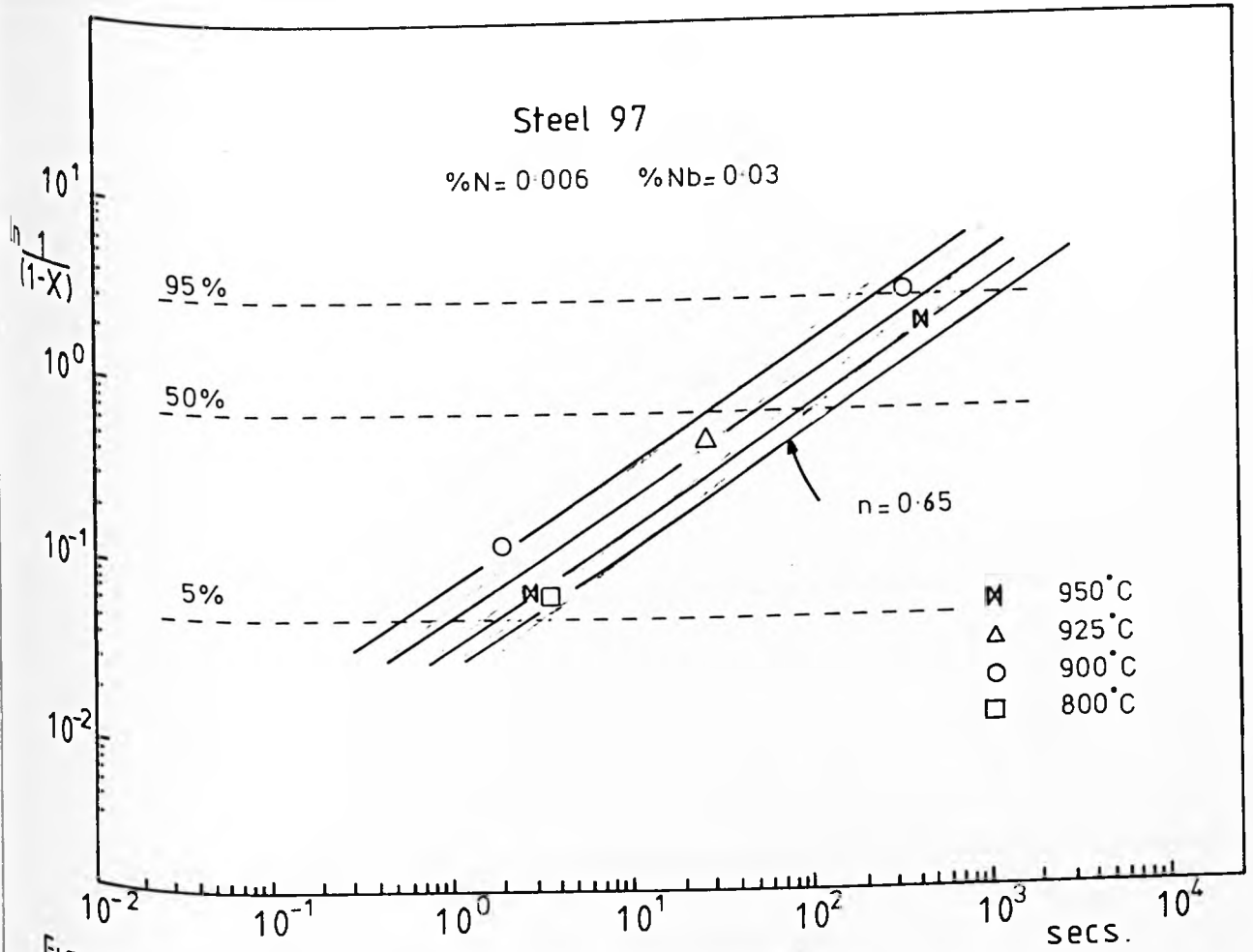
Fig. 6.24.a   Avrami Type Plot for Precipitation.
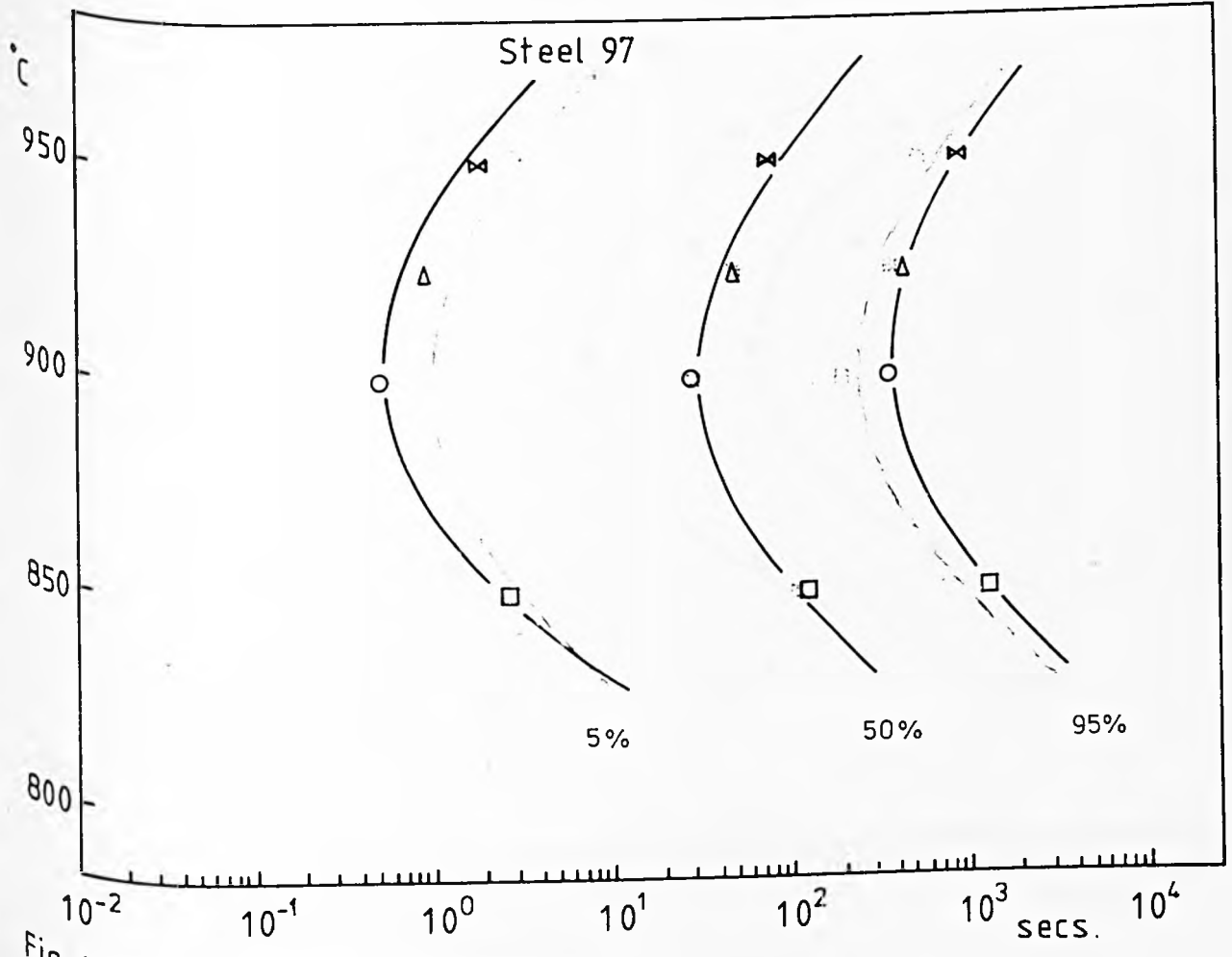
Fig. 6.24.b   Precipitation Kinetics.
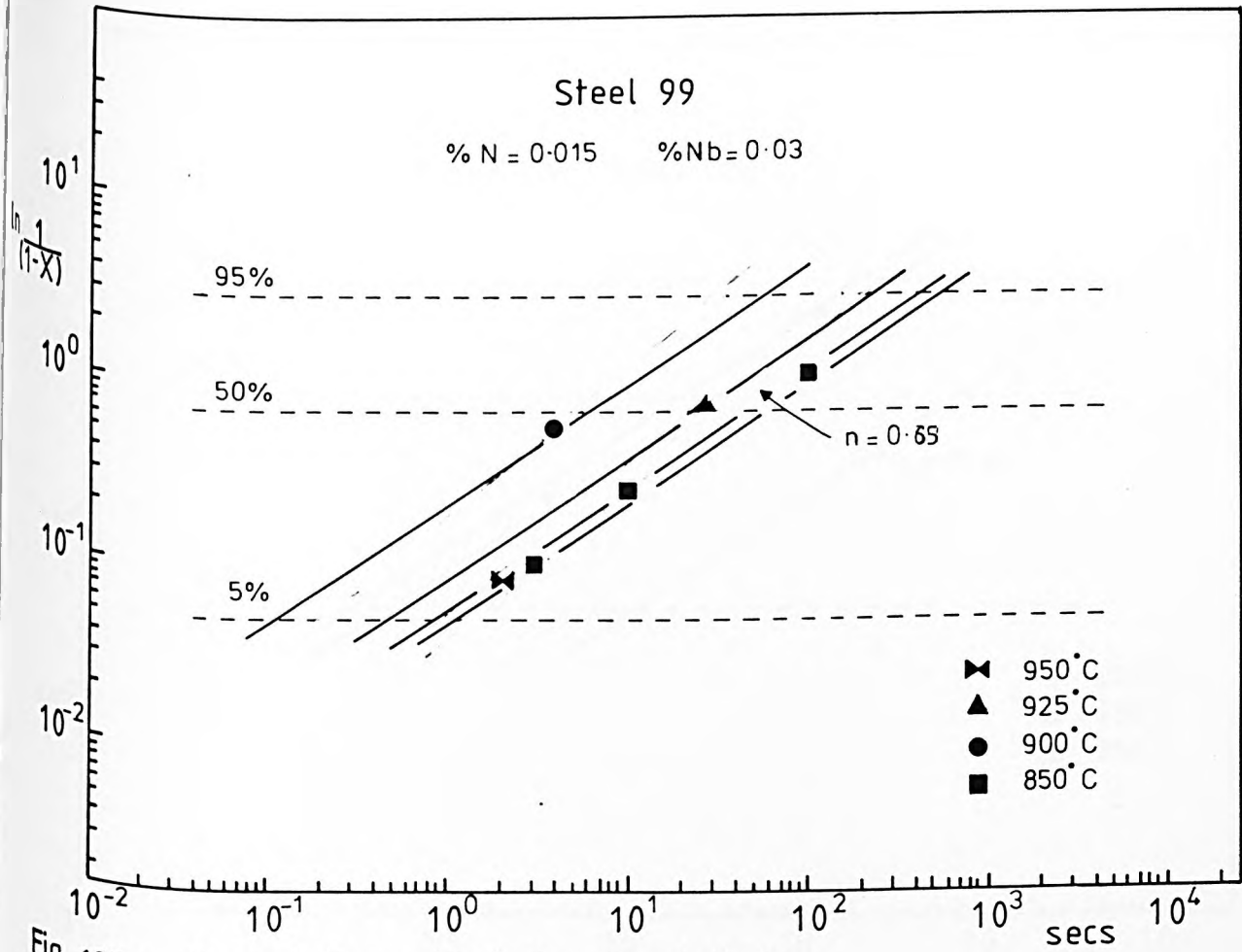
Fig. 6.25.a   Avrami Type Plot for Precipitation.
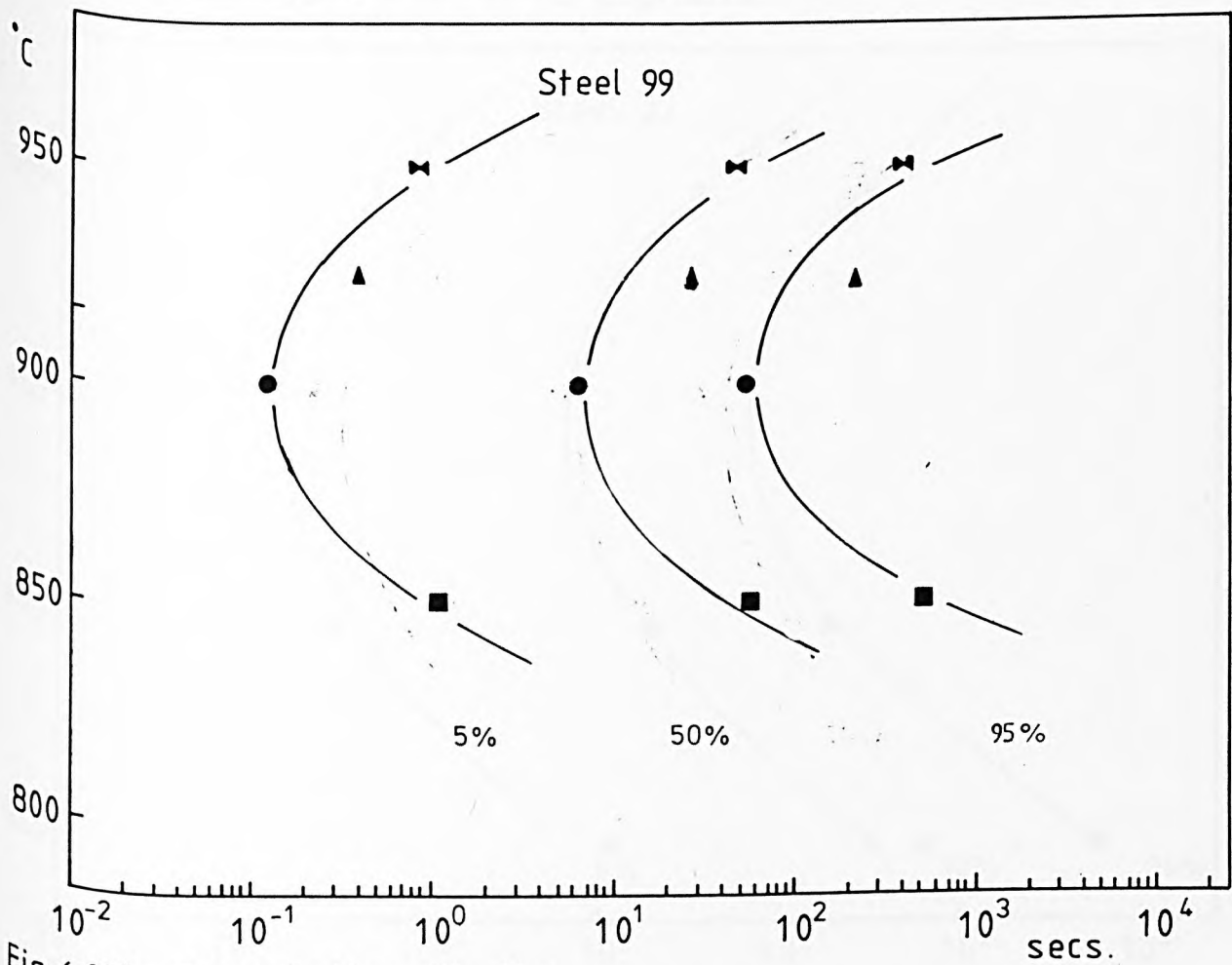
Fig. 6.25.b   Precipitation Kinetics.
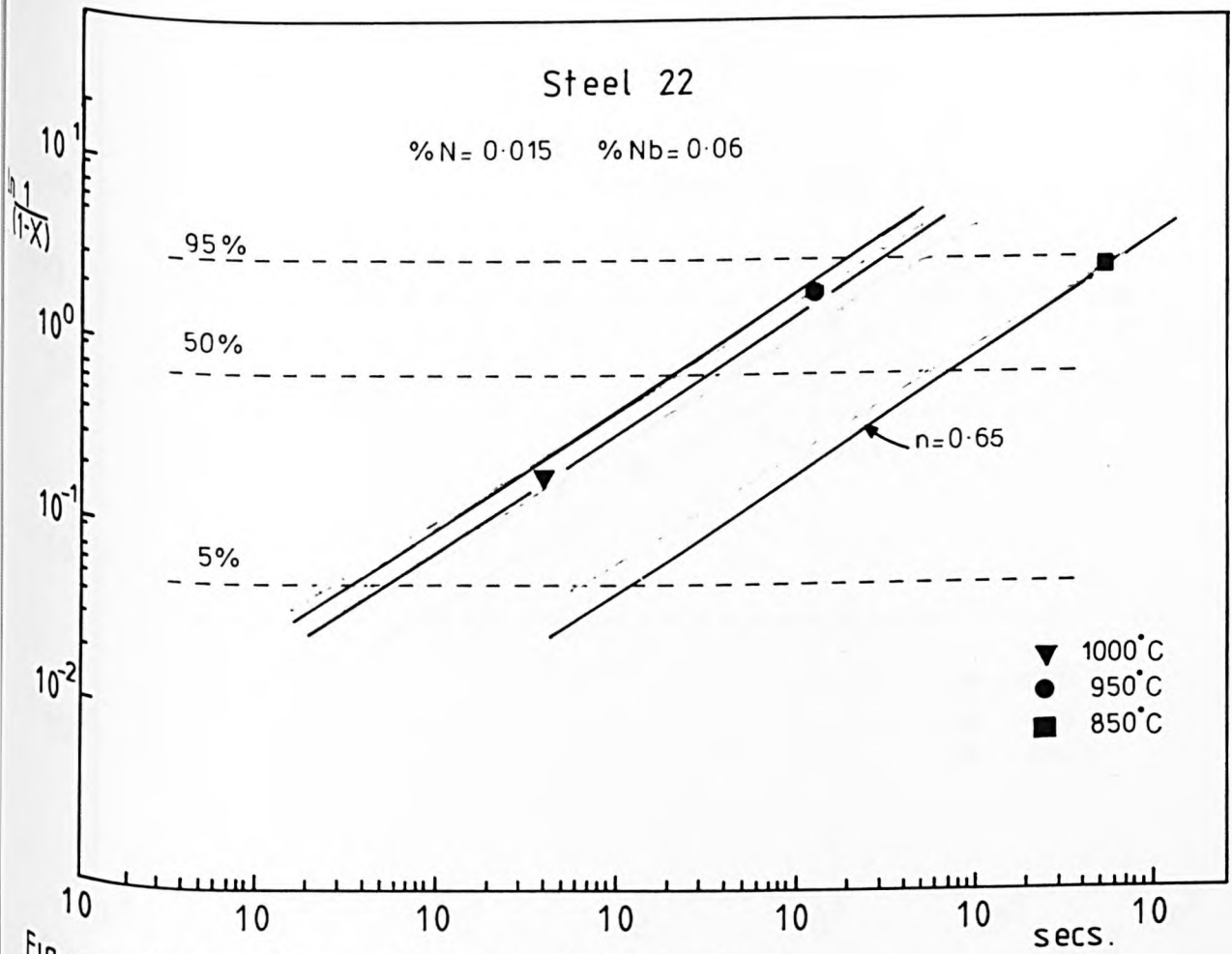
Fig.6.26a Avrami Type Plot for Precipitation.
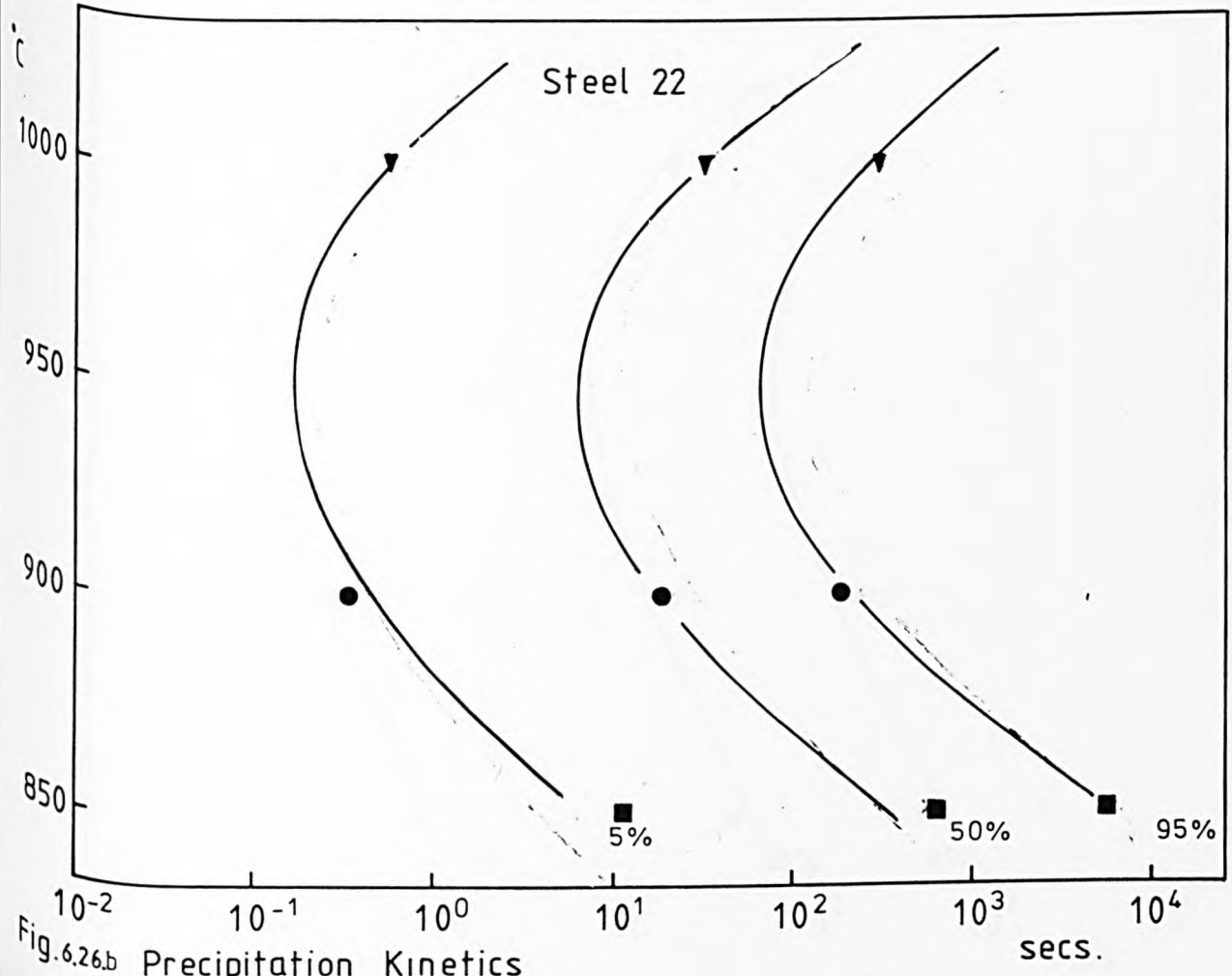
Fig.6.26.b Precipitation Kinetics
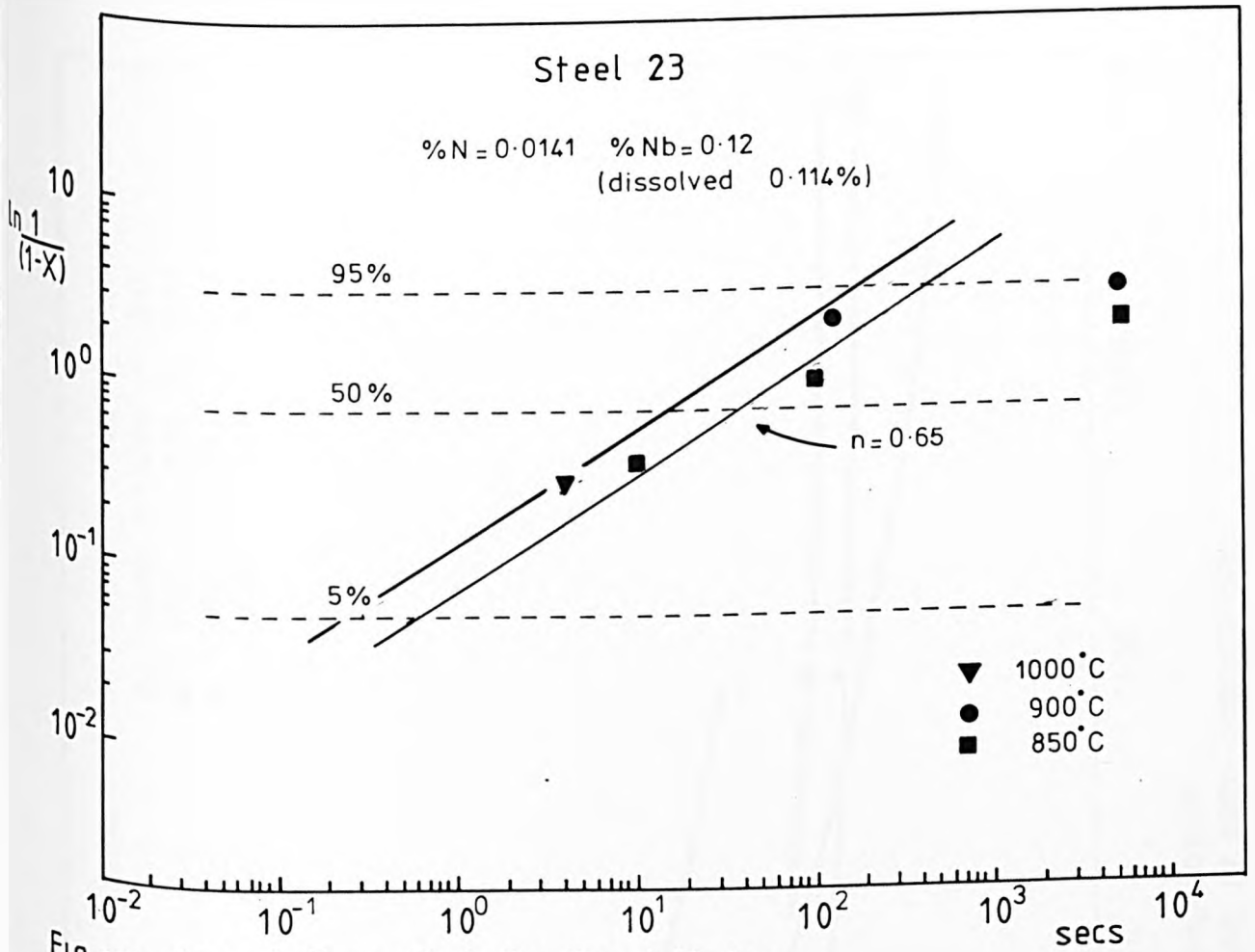
Fig. 6.27.a Avrami Type Plot for Precipitates.
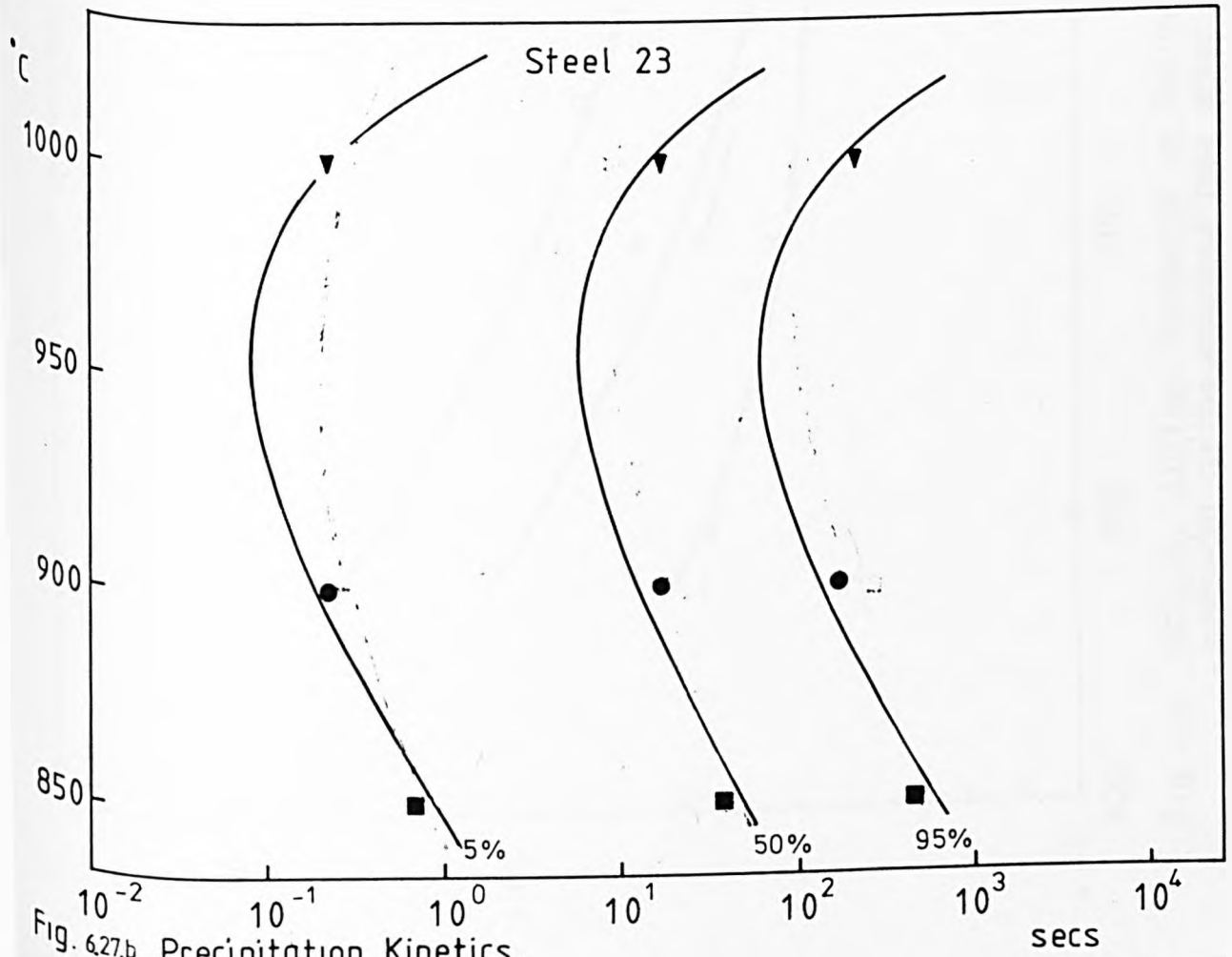
Fig. 6.27.b Precipitation Kinetics.

Steel		%N	%C	%Nb
97	○	0.006	0.84	0·03
99	●	0.015	0.80	0·03
22	■	0.015	0.84	0·06
23	▲	0.014	0.81	0·12
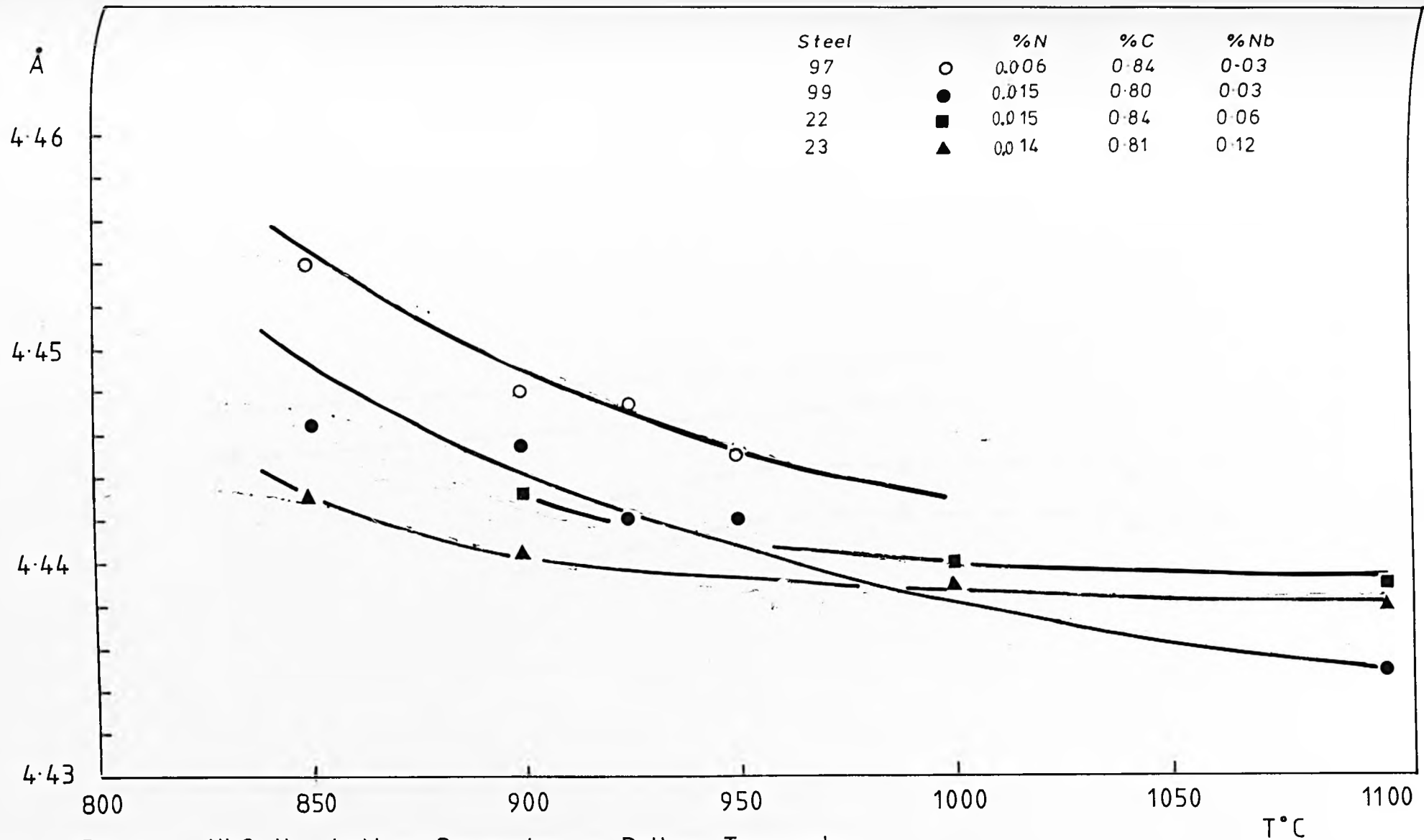
Fig. 6.28 $NbC_x N_y$ Lattice Parameter vs Rolling Temperature
— measured at the shortest time after rolling at each temperature.
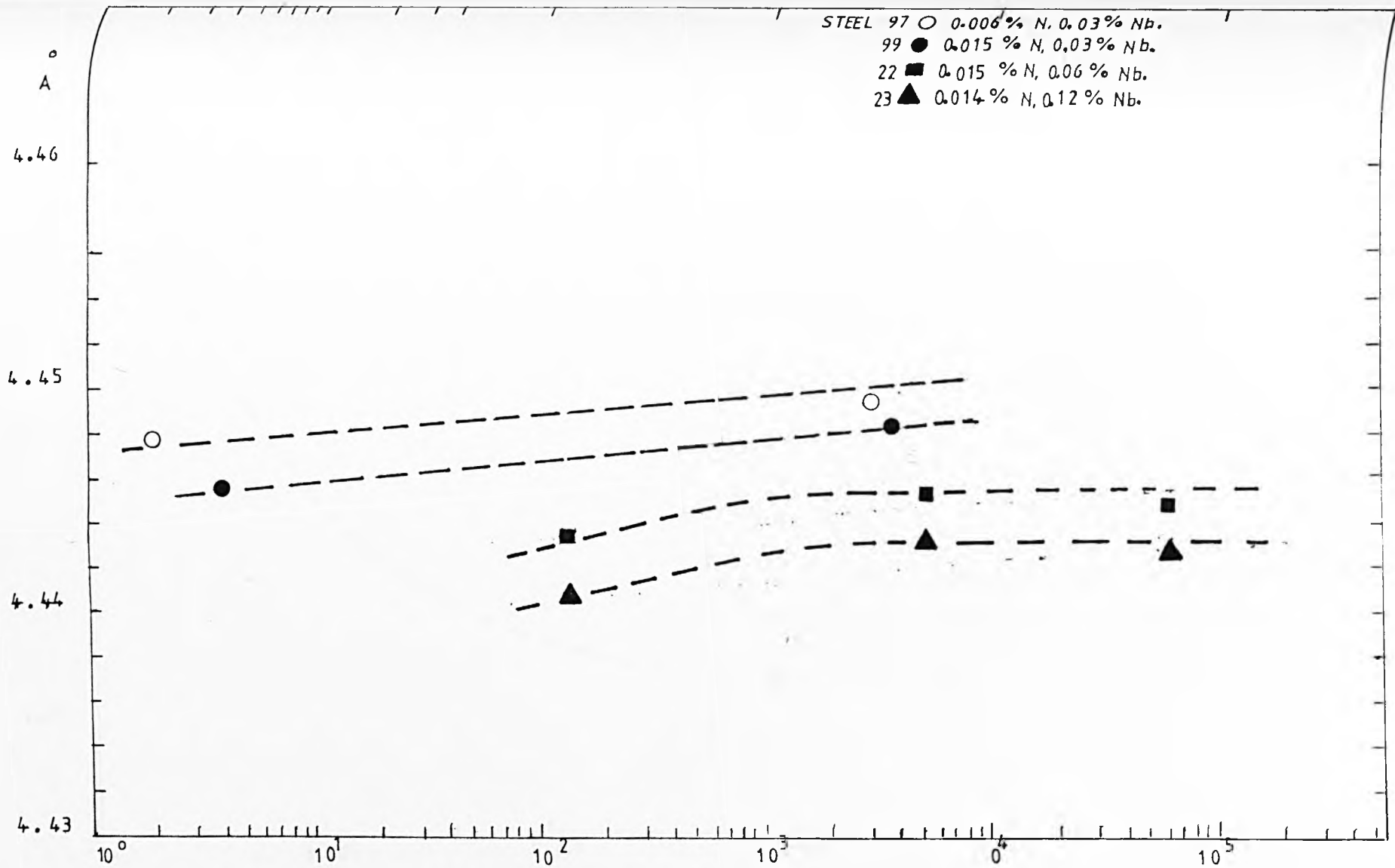
FIG. 6.29   Nb C$_x$N$_y$ LATTICE PARAMETER VS ANNEALING TIME AT 900°C.
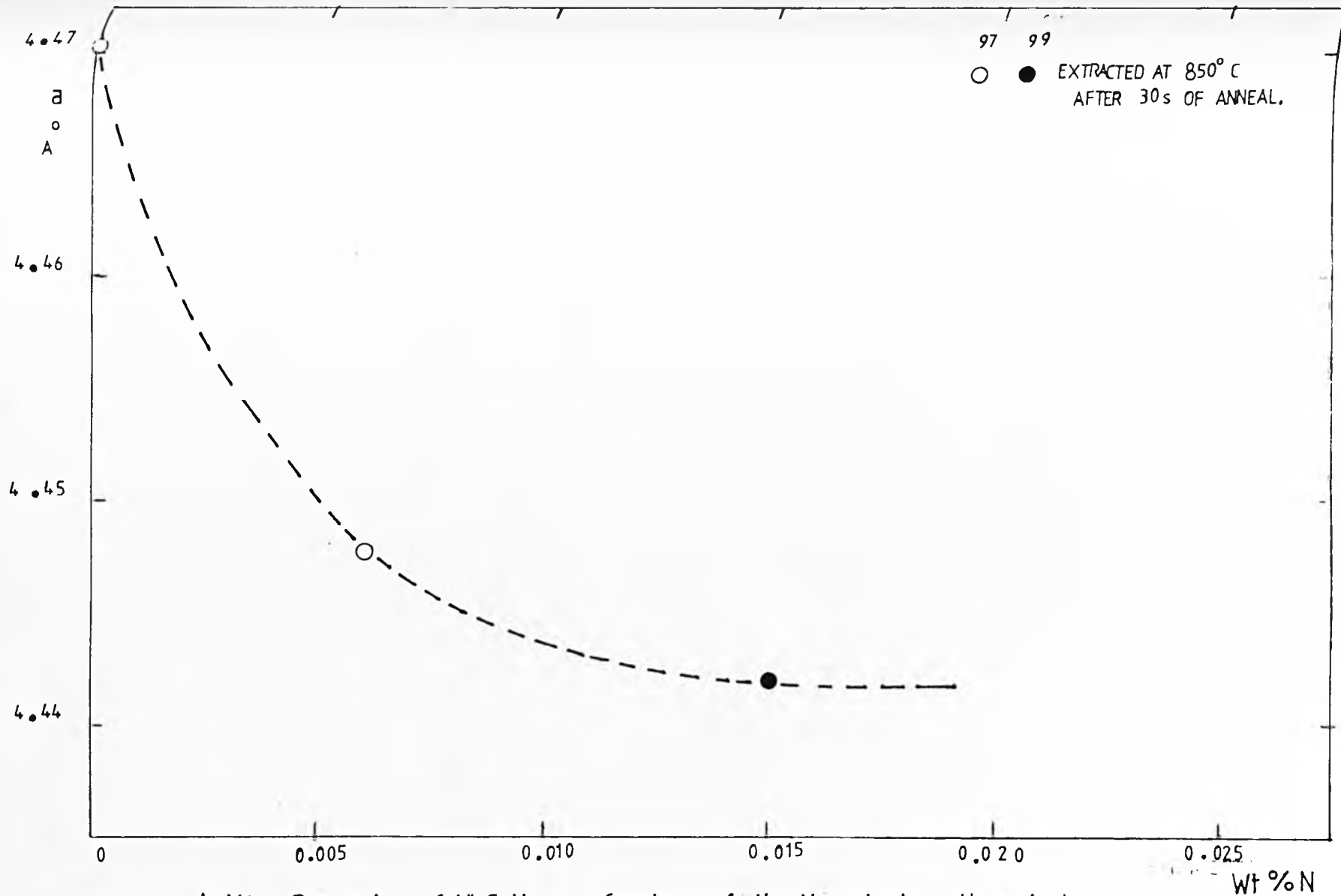
FIG. 6.30 Lattice Parameter of NbC_xN_y as a function of the N content in the steel
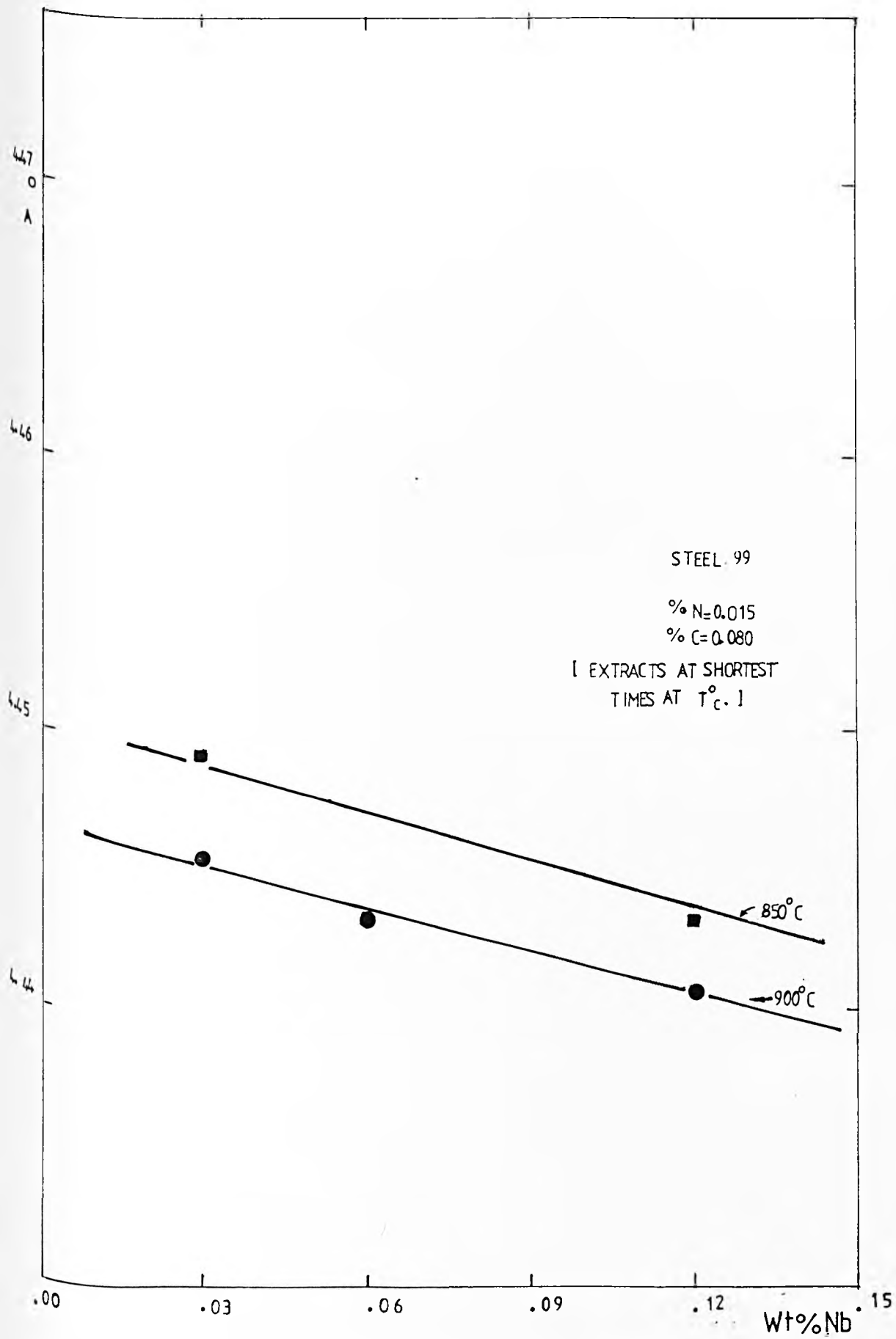
FIG. 6.31   NbC$_x$ N$_y$ LATTICE PARAMETER VS %Nb IN STEEL.

1. Steel 97   x 28K

2. Steel 22   x 6K

3. Magnified area of 2, x 17K. Microanalysis given in Table 6.10.

Fig. 6.32.a. Replicas from quenched slabs after rolling at 1100°C. Note Nb(C,N) precipitates on prior austenite grain boundaries.
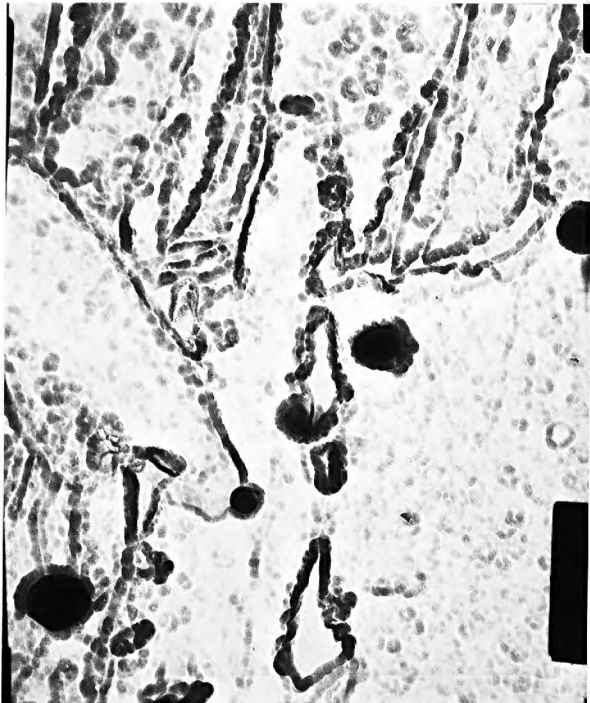
1. Steel 99, Rolled at $1100^{\circ}C \rightarrow WQ$.
    x 36 K

2. Steel 23, Rolled at $1100/850^{\circ}C$
    + 5000s at $850^{\circ}C \rightarrow WQ$.
    x 22K

Fig. 6.32.b.   Bright field micrographs of foils

Fig. 6.33 Precipitate-Size Frequency Distribution for Steel 23.
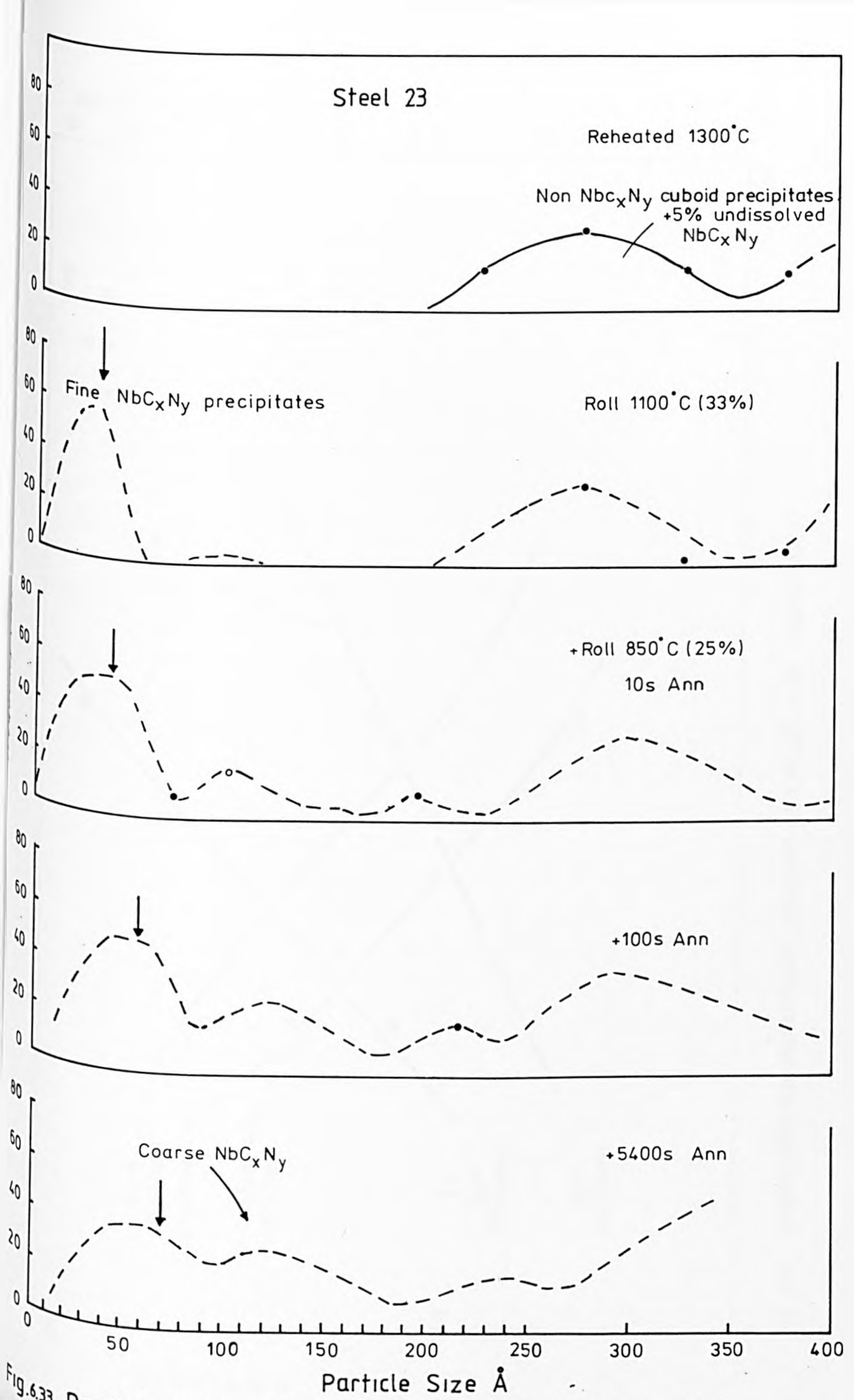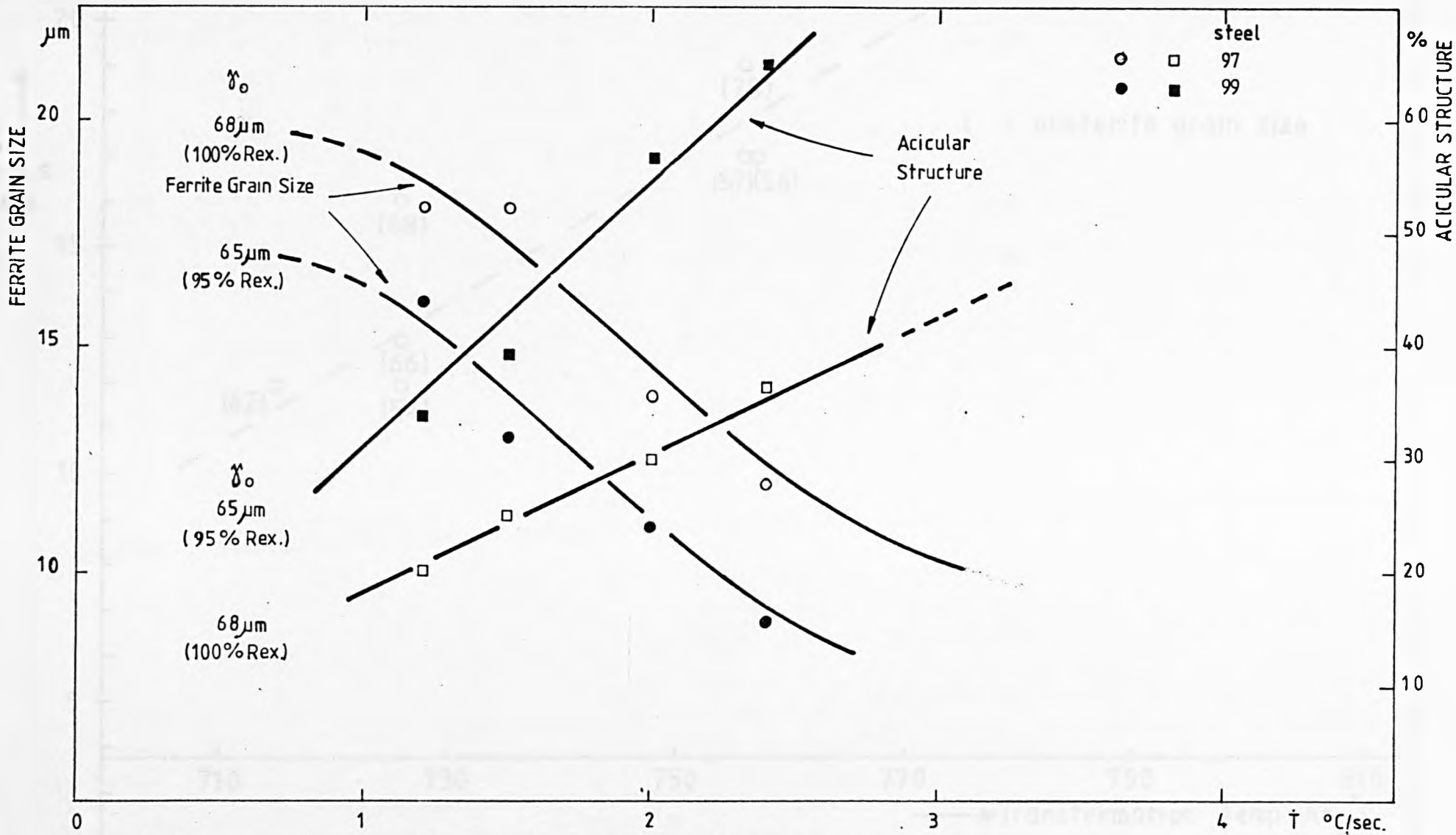
FIG. 6.34   FERRITE GRAIN SIZE AND ACICULAR STRUCTURE AS A FUNCTION OF COOLING RATE, $\dot{T}$
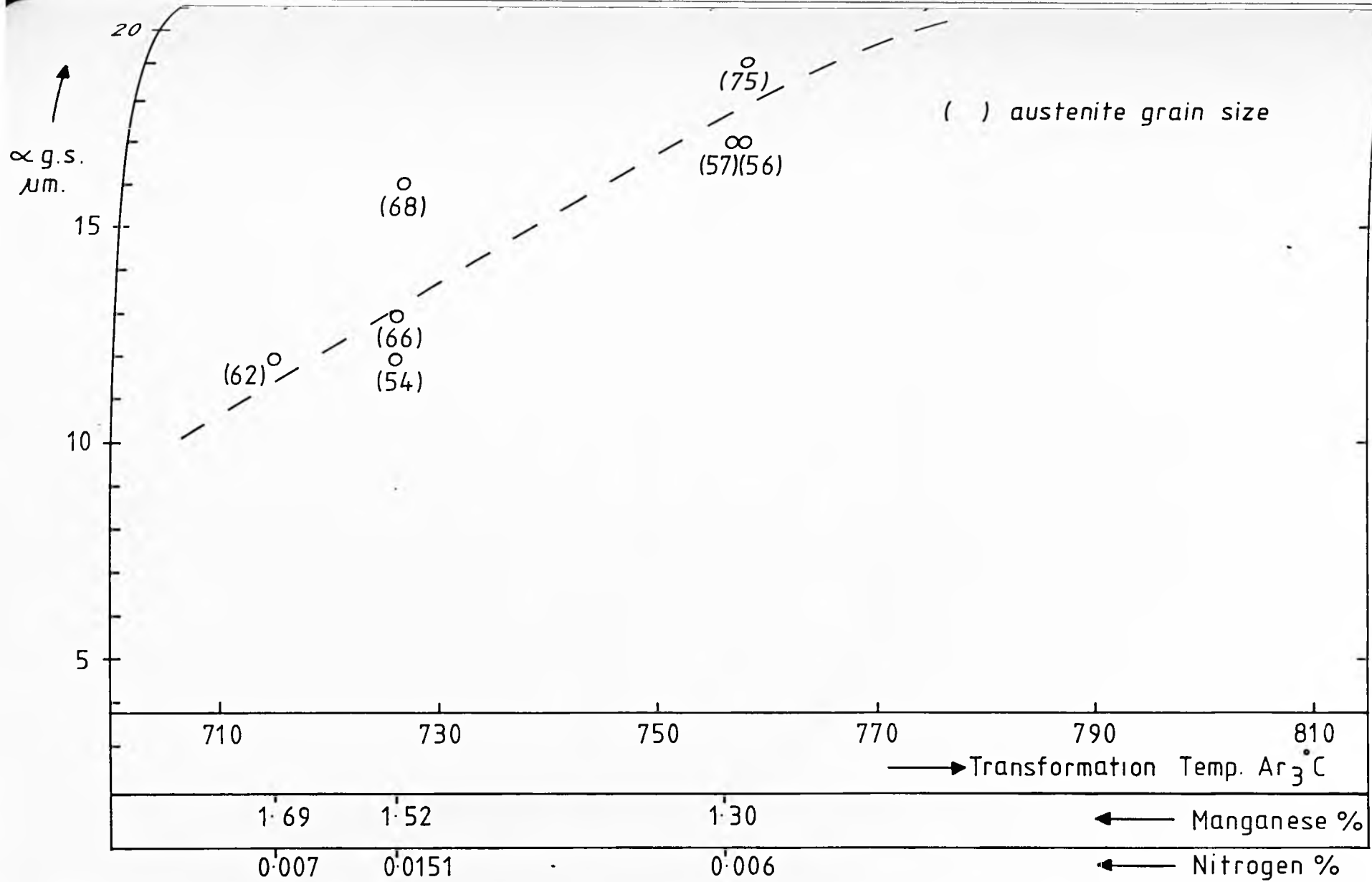
Fig.635 Influence of the Transformation Temperature,%Manganese and % Nitrogen on the Ferrite Grain Size – Cooling Rate ~1-2°C/Sec.
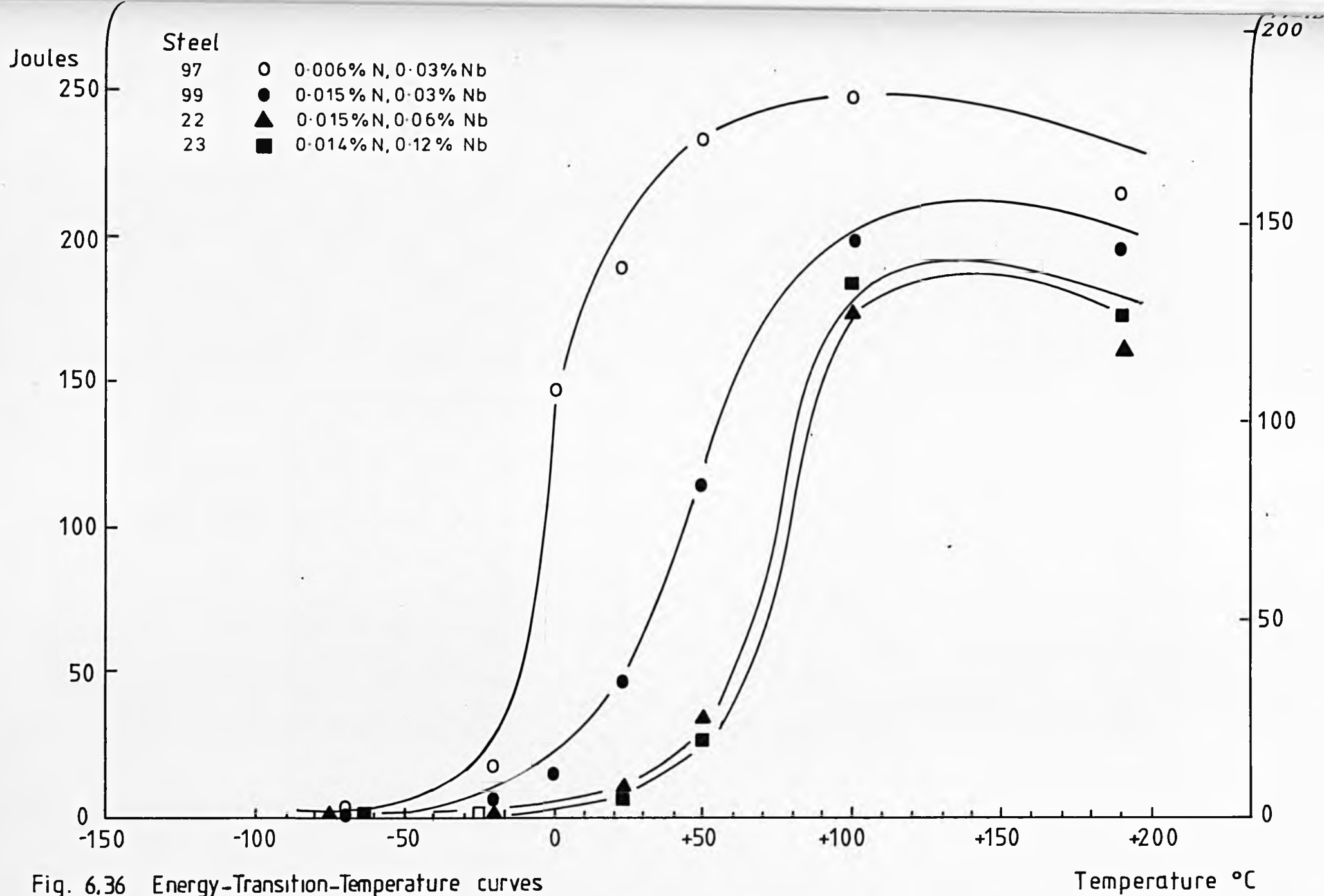
Fig. 6.36 Energy-Transition-Temperature curves

a. Fully recrystallized austenite
   after rolling at 1100°C.
   x 200

b. Non recrystallized austenite
   after rolling at 900°C, 25%
   reduction. Water quenched
   after 4 seconds.
   x 200

Fig. 7.1. Typical microstructures of fully recrystallized, after roughing at 1100°C, and
          non recrystallized after finishing at 900°C for all steels. Photographs, from
           steel 99.
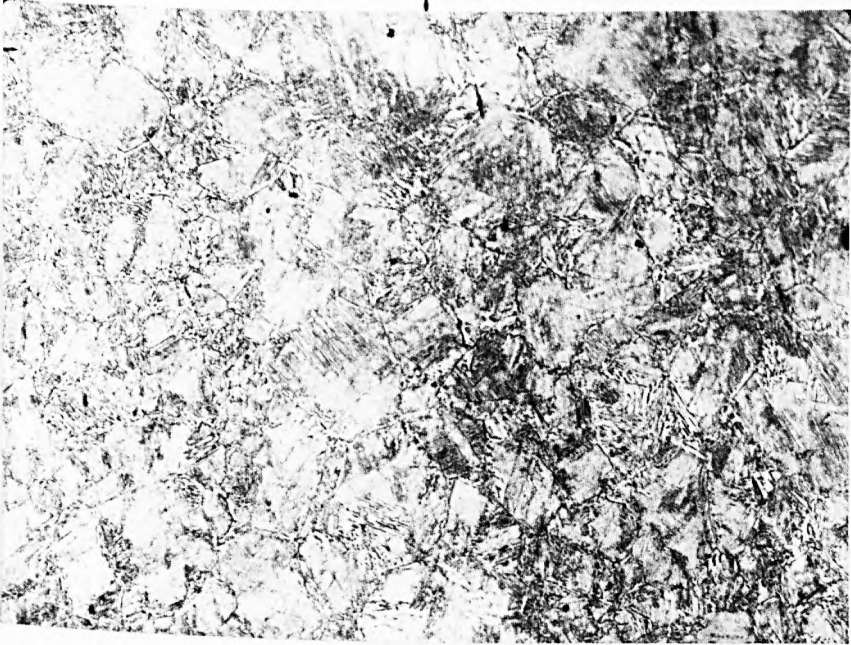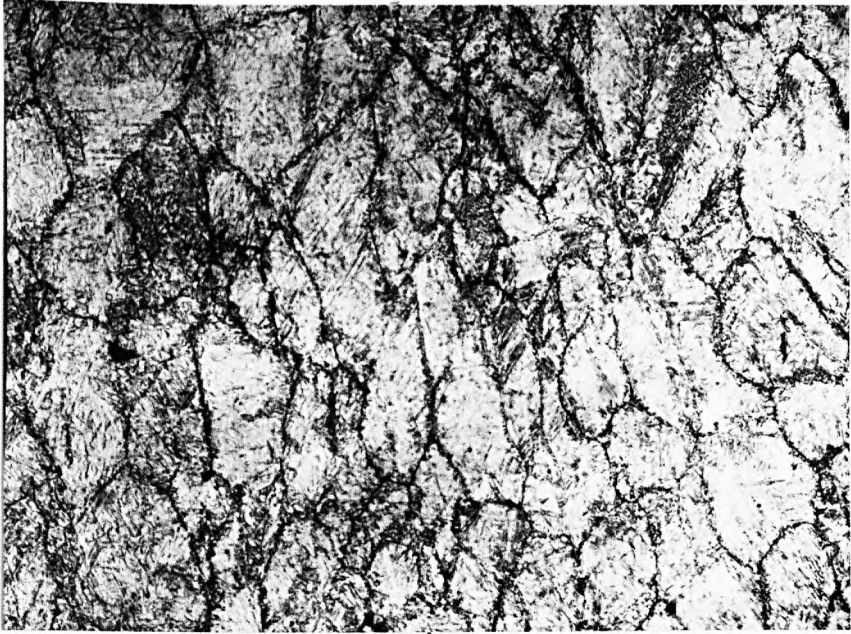
a. Non recrystallized   b.   ~ 20%

c. ~ 70%   d.   ~ 95%

Fig. 7.2. Kinetics of Recrystallization after finishing at 900°C. Note the non uniform
           nucleation of recrystallization. Steel 99.
             x 200

Fig. 7.3. Ferrite nucleation precedes austenite
recrystallization. After roughing,
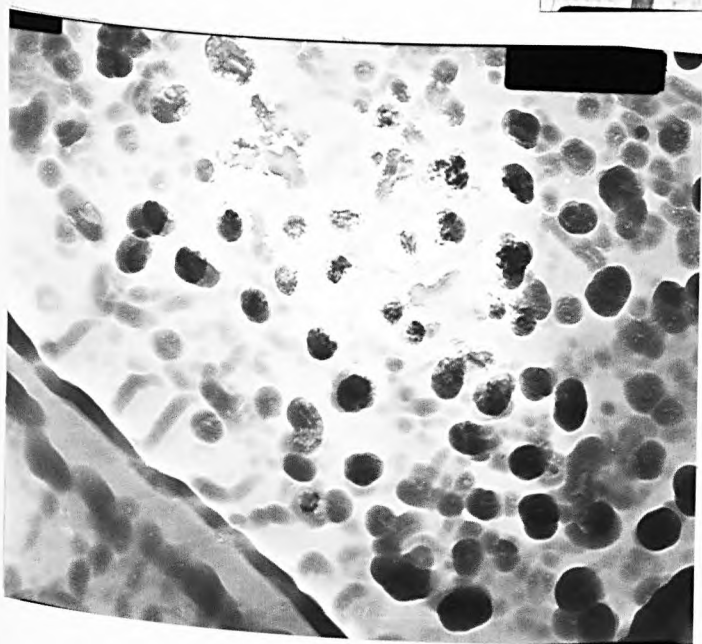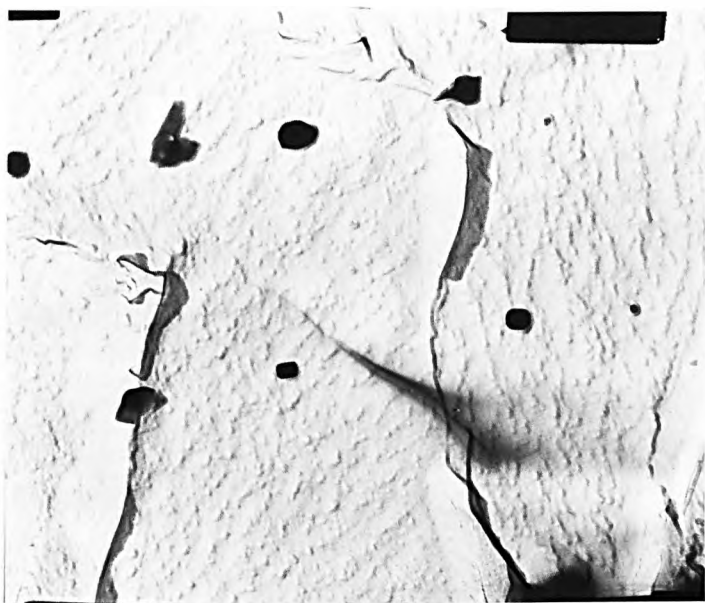finished at 850°C and annealed at this
temperature for $\sim$ 400s. Steel 97.
x 200
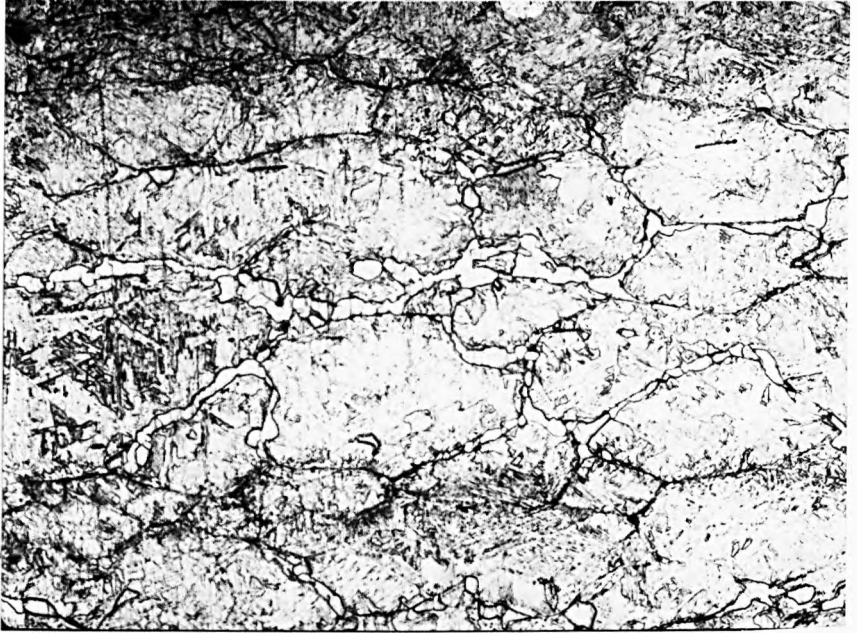
a. 28K

b. 43K

c. 18K

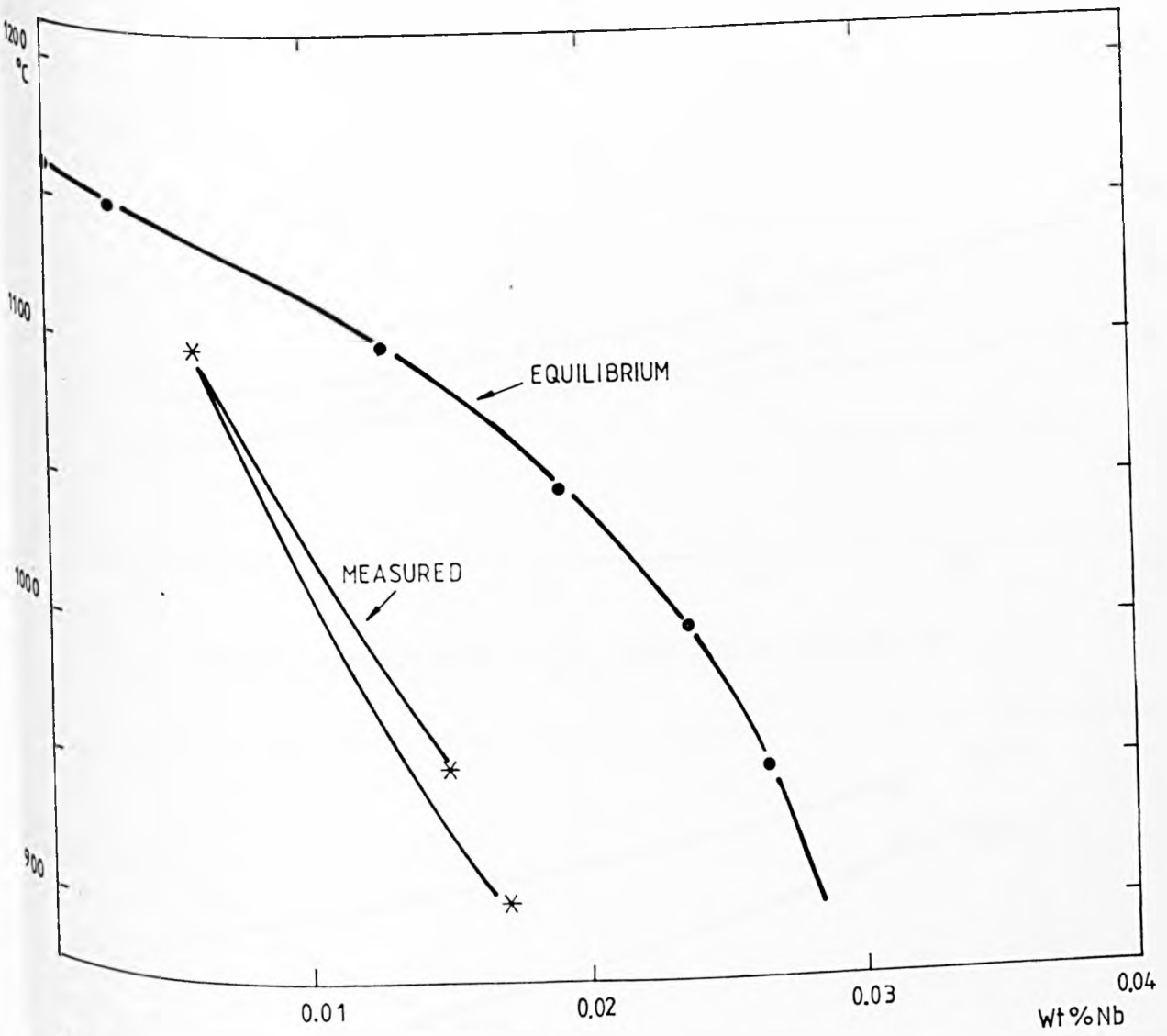Fig. 7.4. Precipitation after roughing, at 1100°C. Mostly following prior austenite grain boundaries.
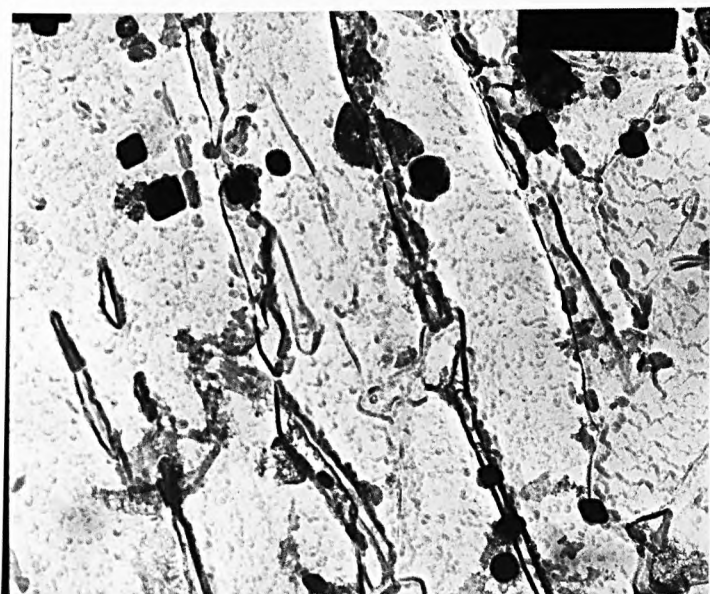
FIG. 7.5 PRECIPITATION OF Nb AS NbC$_x$N$_{(.87-x)}$ AT EQUILIBRIUM, PREDICTED BY THE MODEL, AND AFTER ROLLING, MEASURED. Steel 99
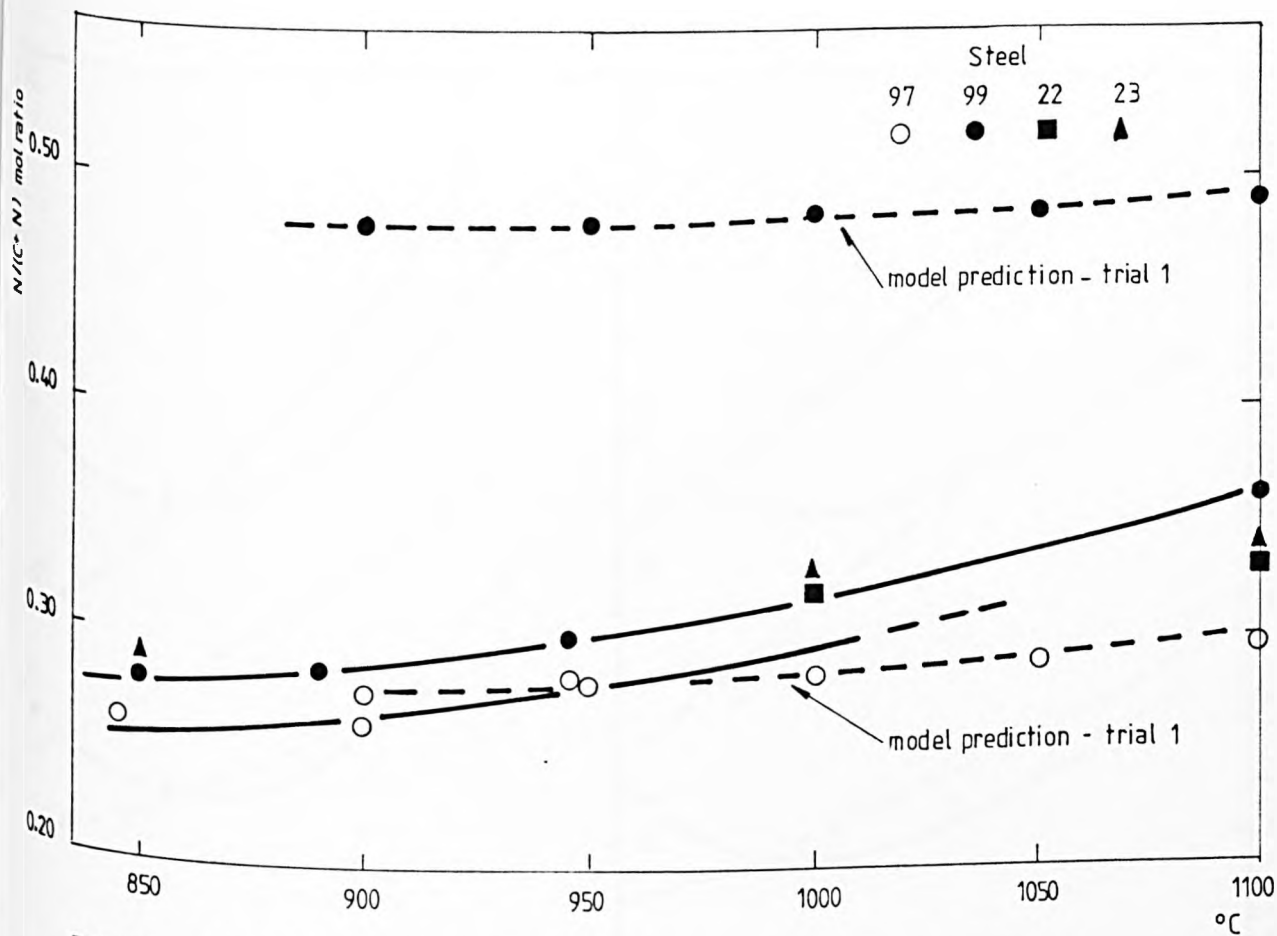
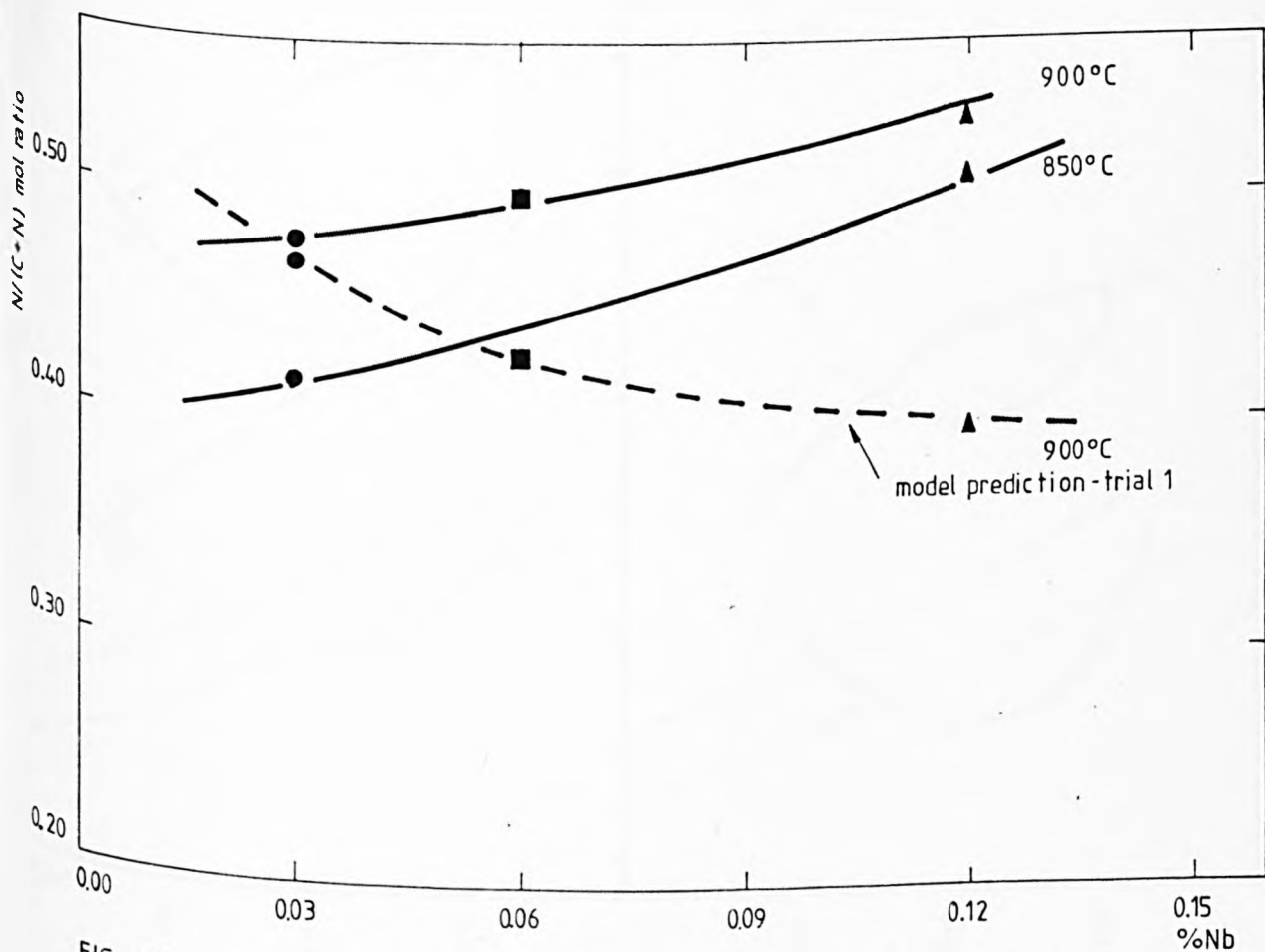FIG. 7.6   CHANGE IN COMPOSITION OF NbC_xN_y WITH ROLLING TEMPERATURE

FIG. 7.7   CHANGE IN NbC_xN_y COMPOSITION WITH THE Nb CONTENT IN THE STEEL

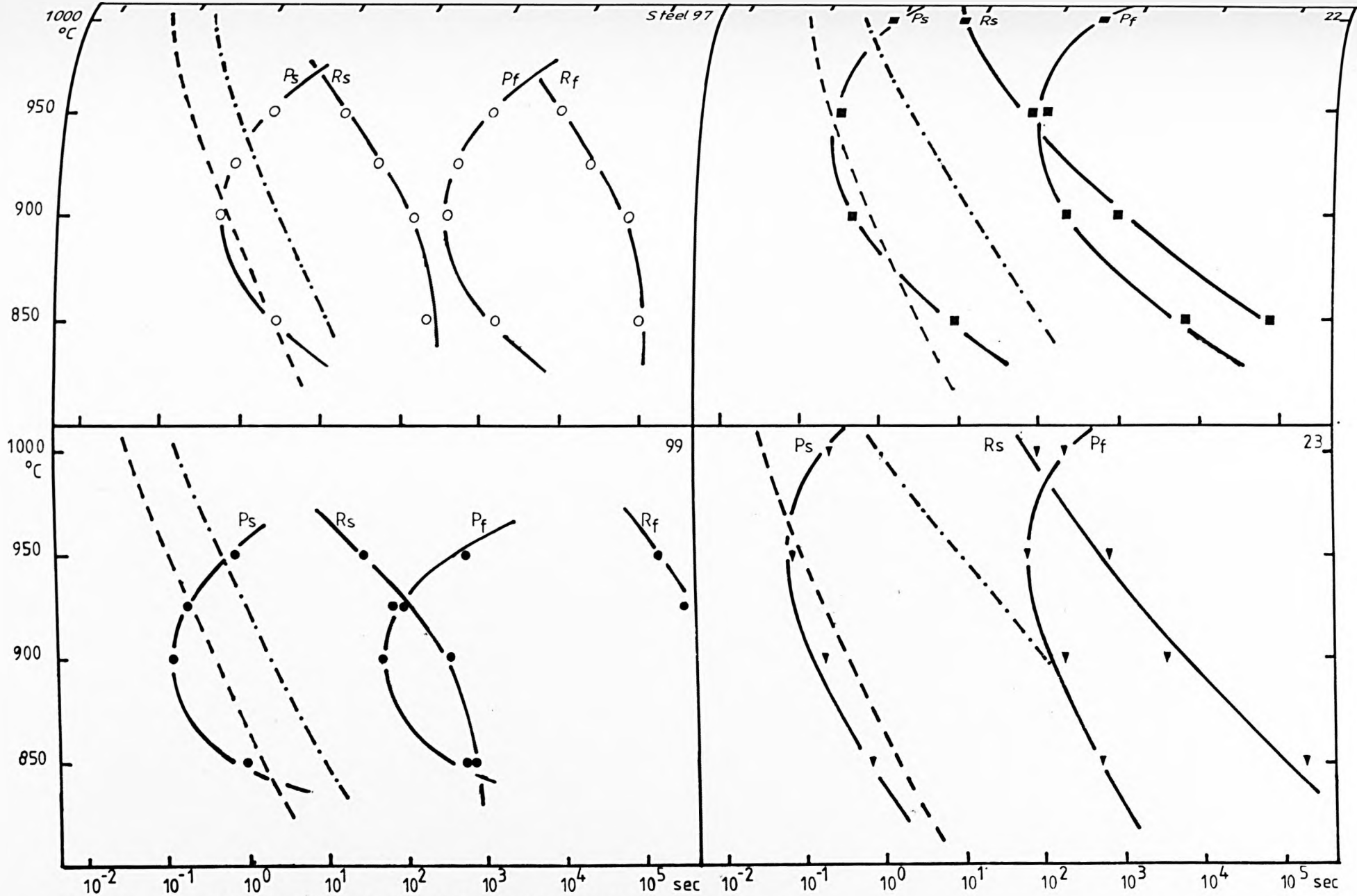FIG. 7.8   SOLID SOLUTE - PRECIPITATION - RECRYSTALLIZATION INTERACTION

Steel 97   Steel 99

Steel 22   Steel 23

Fig. 7.9. Room Temperature microstructures of the
           experimental steels. Finished rolled at
           900°C, 25% Red., air cooled.
           x 200